Evidence-Based Complementary and Alternative Medicine

Molecular Approaches Evaluating the Antioxidant Activity of Flavonoids in Health and Disease

Lead Guest Editor: Lucian Hritcu
Guest Editors: Oana Cioanca and Omayma Eldahshan

Molecular Approaches Evaluating the Antioxidant Activity of Flavonoids in Health and Disease

Evidence-Based Complementary and Alternative Medicine

Molecular Approaches Evaluating the Antioxidant Activity of Flavonoids in Health and Disease

Lead Guest Editor: Lucian Hritcu
Guest Editors: Oana Cioanca and Omayma Eldahshan

Contents

Hindawi
Evidence-Based Complementary and Alternative Medicine
Volume 2021, Article ID 6458265, 6 pages
https://doi.org/10.1155/2021/6458265

Research Article

The Cytotoxicity and Nephroprotective Activity of the Ethanol Extracts of *Angelica keiskei* Koidzumi Stems and Leaves against the NAPQI-Induced Human Embryonic Kidney (HEK293) Cell Line

Riezki Amalia,[1] **Diah Lia Aulifa**,[2] **Dichy Nuryadin Zain**,[1,3] **Anisa Pebiansyah**,[1,3] **and Jutti Levita**[1]

[1]*Department of Pharmacology and Clinical Pharmacy, Faculty of Pharmacy, Universitas Padjadjaran, Sumedang, Bandung 45363, Indonesia*
[2]*Department of Pharmaceutical Analysis and Medicinal Chemistry, Faculty of Pharmacy, Universitas Padjadjaran, Sumedang, Bandung 45363, Indonesia*
[3]*Bakti Tunas Husada School of Health Sciences, Tasikmalaya 461152, Indonesia*

Correspondence should be addressed to Jutti Levita; jutti.levita@unpad.ac.id

Received 2 August 2021; Revised 24 August 2021; Accepted 29 October 2021; Published 23 November 2021

Academic Editor: Oana Cioanca

Ethnopharmacological Relevance. In Indonesia, *Angelica keiskei* Koidzumi (ashitaba or Japanese celery) has been traditionally used to maintain health and to achieve longevity. Previously, the chlorophyll-rich extract of *A. keiskei* planted in Korea exhibited a strong antioxidant activity. The objective of the present study was to investigate the cytotoxicity and nephroprotective activity of the ethanol extract of *A. keiskei* Koidzumi on the N-acetyl-*p*-benzoquinone imine (NAPQI) induced human embryonic kidney (HEK293) cell line. *Materials and Methods*. *A. keiskei* Koidzumi plant was collected from Mount Rinjani, Lombok, Indonesia, and was identified at the School of Biology Sciences and Technology, Bandung Institute of Technology, Indonesia. Extraction of the stems (ASE) and leaves (ALE) was performed by employing ethanol 70% for 3×24 h at 26°C. The cytotoxicity study of the extracts was assessed using the water-soluble tetrazolium salt-8 (WST-8) reagent on the HEK293 cell line, while the nephroprotective activity assay was determined on the NAPQI-induced HEK293 cell line. *Results*. The WST-8 assay showed that the cytotoxicity IC_{50} of ASE = 2322 μg/mL and IC_{50} of ALE = 2283 μg/mL. The nephroprotective activity assay revealed that ASE possesses nephroprotective activity against the NAPQI-induced HEK293 cell line at 1161 μg/mL, while ALE does not show the nephroprotective activity. *Conclusion*. Taken together, lower concentrations of ASE and ALE (<2000 μg/mL) are not toxic to the HEK293 cell line, and only ASE indicates the activity to protect the HEK293 cell line against NAPQI damage. This Japanese celery could be further explored for its potential as a plant-based nephroprotective drug.

1. Introduction

Kidney injury arises when its physiological functions, detoxification, and excretion do not perform properly. This dysfunction is usually caused by exogenous, e.g., drugs (anti-inflammatories, antibiotics, and chemotherapeutics), or endogenous toxicants (oxidative stress products such as reactive oxygen species due to intracellular catabolism and activation of oxidative enzymes, e.g., superoxide dismutase) [1–4]. Acetaminophen, an anti-inflammatory drug, when taken in excess, can lead to hepatotoxicity and nephrotoxicity due to glutathione (GSH) depletion in the liver; hence, the reactive metabolite of acetaminophen, N-acetyl-p-benzoquinone imine (NAPQI), is not conjugated [5]. Nephrotoxicity is indicated by changes in glomerular filtration rate (normal GFR in young adults is 120 mL/minute), proximal tubular cell toxicity, inflammation, etc., and the enzymes present in tubular epithelial cells leak into the urine

and can be determined as nephrotoxic biomarkers [1]. Such biomarkers, e.g., neutrophil gelatinase-associated lipocalin (NGAL), kidney injury molecule-1 (KIM-1), and calprotectin, are used as an early diagnosis of acute and chronic kidney injury [6, 7].

Many natural products with antioxidant properties have been reported to have advantageous effects in the remedy of nephrotoxicity [8]. *Angelica keiskei* Koidzumi or ashitaba (a Japanese word which means tomorrow leaf) has been believed in improving health, particularly protecting the liver and kidney system, and achieving longevity. This plant has shown many pharmacology activities; among them is as antioxidants [9–11].

In this study, we investigated the cytotoxicity and nephroprotective activity of the ethanol extract of *A. keiskei* Koidzumi on the N-acetyl-p-benzoquinone imine (NAPQI) induced human embryonic kidney (HEK293) cell line. NAPQI was chosen as the kidney injury inducer because this reactive metabolite of acetaminophen binds covalently to the sulfhydryl groups of renal proteins and leads to the damage of proximal tubules. It also initiates the apoptosis process involving the activation of caspase-9 and caspase-3 by generating free radicals [12].

2. Materials and Methods

2.1. Plant Materials. The *A. keiskei* Koidzumi plant (Figure 1) was collected from Mount Rinjani, Lombok, and was taxonomically identified at the School of Biology Sciences and Technology, Bandung Institute of Technology, Indonesia. The stems and leaves were washed under tap water to remove dirt and soil and were dried in the glasshouse for 2 days. The dried plants were ground to pass a mesh-60 sieve and kept for further use.

2.2. Materials and Chemicals. The materials used were HEK293 cell line (ATCC® CRL-1573™), a collection of the Cell and Molecular Biology Laboratory, Faculty of Pharmacy, Universitas Padjadjaran. Chemicals were N-acetyl-p-benzoquinone imine (NAPQI) (CAS reg. no. 50700-49-7, Cayman Chemical, Ann Arbor, USA), quercetin (CAS reg. no. 117-39-5, Sigma-Aldrich, Saint Louis, USA), Cell Counting Kit-8: WST (product code: CK04-11, Dojindo Europe), Dulbecco's Modified Eagle Medium (Gibco), and penicillin-streptomycin (Gibco™ 670087).

2.3. Instruments. Instruments used were an evaporator Rotavapor RV 10 Digital V connected to heating bath HB digital and RV 10.1 set of glassware vertical (IKA Id. no. 0010004799), chemical glassware (Iwaki Pyrex), autoclave (all American type 75X), Biological Safety Cabinet (BSC) type-2, microplate reader (Infinite M200 Pro, Tecan), microplate reader filter 450–490 nm, inverted microscope (Zeiss), sterilized 96-well microplates, multichannel pipettes (8 or 12 channels: 10–100 μL), CO_2 incubator (Heracell VIOS 250i, Thermo Scientific), and hemocytometer (cell counter).

2.4. Extraction. Extraction of the stems (ASE) and leaves (ALE) was performed by employing ethanol 70% for 3×24 h at 26°C. The extracts were then evaporated at 60°C to remove the solvent, freeze-dried to obtain the dry extracts, and were stored at 4°C until used.

2.5. Cytotoxicity Assay of the Extracts. The cytotoxicity of ASE and ALE towards the HEK293 cell line was assessed using the water-soluble tetrazolium salt-8 (WST-8) reagent. WST-8 (2-(2-methoxy-4-nitrophenyl)-3-(4-nitrophenyl)-5-(2,4-disulfophenyl)-2H tetrazolium, monosodium salt) is highly stable and utilized in Cell Counting Kit-8 (CCK-8) [13]. ASE and ALE solutions were prepared by dissolving 32 mg extract in 1 mL of 1% DMSO in a culture medium. The solution was serial-diluted to concentrations of 160 μg/mL, 320 μg/mL, 640 μg/mL, 1280 μg/mL, 2560 μg/mL, and 5120 μg/mL in DMSO 1%. The percentage growth inhibition was calculated using the following formula [14]:

$$\text{growth inhibition}\,(\%) = \left(1 - \frac{\text{absorbance sample}}{\text{absorbance control}}\right) \times 100\%. \quad (1)$$

IC_{50} was calculated using GraphPad Prism 8.0.2.

The cytotoxicity of quercetin and NAPQI was assessed using the same procedure. Quercetin and NAPQI solutions were prepared as follows: accurately weighed quercetin (605 μg) and NAPQI (500 μg) were each dissolved in 1 mL of 1% DMSO in the culture medium. The solution was serial-diluted to concentrations of 15.13 μg/mL, 30.25 μg/mL, 60.5 μg/mL, 121 μg/mL, and 242 μg/mL for quercetin and 15.63 μg/mL, 31.25 μg/mL, 62.5 μg/mL, 125 μg/mL, and 250 μg/mL for NAPQI, respectively, in DMSO 1%.

2.6. Nephroprotective Activity Assay. The nephroprotective activity assay was determined on the NAPQI-induced HEK293 cell line by adopting the method of Nafiu and coworkers [14] with modifications. The assay was performed on six groups for each ASE and ALE, which were (1) normal control; (2) negative control (NAPQI: 75.00 μg/mL); (3) positive control (quercetin: 45.68 μg/mL); (4) positive control II (quercetin: 91.36 μg/mL); (5) ASE or ALE concentration I; and (6) ASE or ALE concentration II. To each well of the microplate, 50 μL of diluted HEK293 cells (approximately 5×10^3 cells) was added. Cultures were maintained at 37°C in a humidified atmosphere of a 5% CO_2 incubator. After 24 h, the supernatant was discarded, and the monolayer of cells was washed with DMEM, and 50 μL of ASE in 1% DMSO (1161 μg/mL and 2322 μg/mL, respectively, in three replicates) and ALE (1141 μg/mL and 2283 μg/mL, respectively, in three replicates) was added. The microplate was incubated at 37°C in 5% CO_2 for 1 h, followed by the addition of 50 μL of NAPQI 75 μg/mL solution. After 24 h of incubation, the medium was flicked off, and 10 μL of WST-8 reagent was added. The mixture in the microplate was incubated for 2 h at 37°C in 5% CO_2. Following this, a volume of 100 μL HCl was added to each well to stop the reaction, and the absorbance of the mixture was measured at 450 nm using a microplate reader.

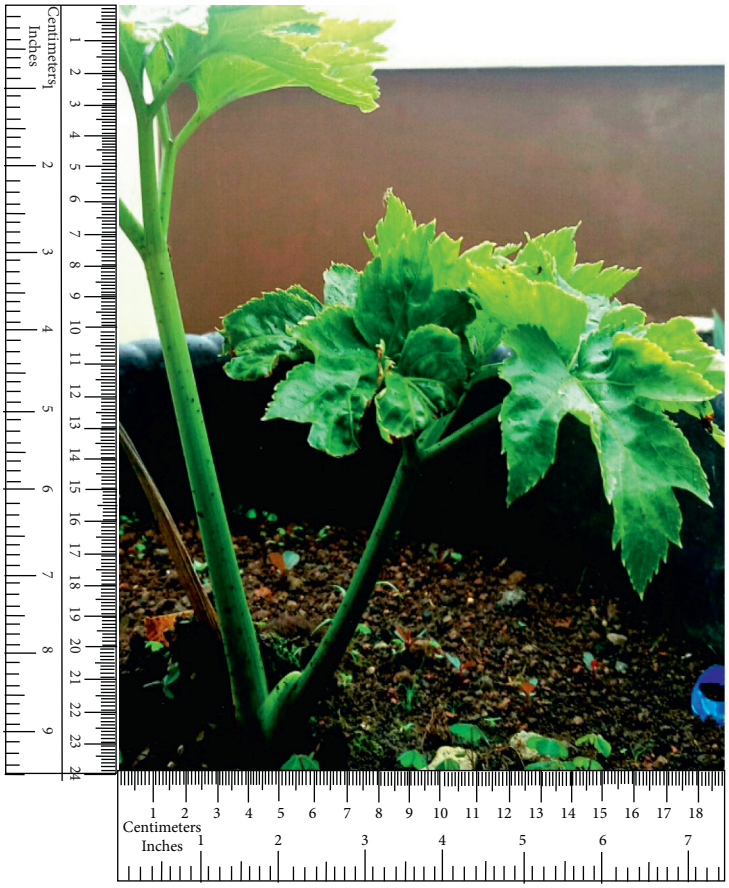

Figure 1: *Angelica keiskei* Koidzumi or Japanese celery.

2.7. Statistical Analysis. Results are presented as the mean and standard deviation of replicate experiments. One-way ANOVA and Duncan's multiple range tests were used to determine significant differences ($p < 0.05$ was considered statistically significant).

3. Results

As depicted in the photomicrographs (Figure 2), the untreated HEK293 and the *A. keiskei*-treated HEK293 cell lines show only slight differences. The untreated cells could be seen located in a wider space, and some indicated dendritic processes to reach their neighboring cells. Some of the cells are binucleate that indicated proliferation. The *A. keiskei*-treated HEK293 cells revealed lesser dendritic processes and the absence of binucleate.

Furthermore, the nephroprotective activity assay (Figure 3) reveals that ASE possesses nephroprotective activity on the NAPQI-induced HEK293 cell line at 1161 μg/mL, while ALE does not.

4. Discussion

N-Acetyl-p-benzoquinone imine (NAPQI) is a reactive metabolite of acetaminophen (paracetamol), which has been confirmed for its damage effect on the liver and kidney due to glutathione depletion. NAPQI cytotoxicity has been studied in lymphoblastoid cell lines derived from Caucasian-American, African-American, and Han Chinese-American healthy subjects. Average NAPQI IC_{50} for those cell lines was $6.5 \pm 4.5\,\mu$M. Lower concentrations of NAPQI resulted in a proliferation increase in many of the cell lines [5]. In the body, NAPQI binds to selenium protein and glutamine synthetase at the S3 segment of the proximal tubule, which causes an increase of xanthine oxidase (XOD) activity; thus, the production of reactive oxygen species (ROS) is also enhanced [14, 15]. Excess ROS production and its exposure to the kidney leads to oxidative stress and is followed by nephropathy and eventually kidney failure [8, 16]. In this study, we investigated the cytotoxicity and nephroprotective activity of the ethanol extract of *A. keiskei* Koidzumi on the NAPQI-induced HEK293 cell line.

In the NAPQI-induced HEK293 cell line (the negative control group), only approximately 82% of the cells were viable (Figure 3), compared to the extract-treated groups (Figure 3). The result obtained in our study is comparable with the previously reported result given by Kwon and coworkers. The chlorophyll-rich methanol extract of *A. keiskei* planted in Korea possesses a strong antioxidant activity [11]. The radical scavenging effect of the leaf extract was stronger than that of the extract of the stem [17]. This antioxidant activity is predicted caused by certain phytoconstituents contained in the plant. However, various secondary metabolites, e.g., flavonoids, chalcones, coumarins, phenolics, acetylenes, and terpenes, have been identified in

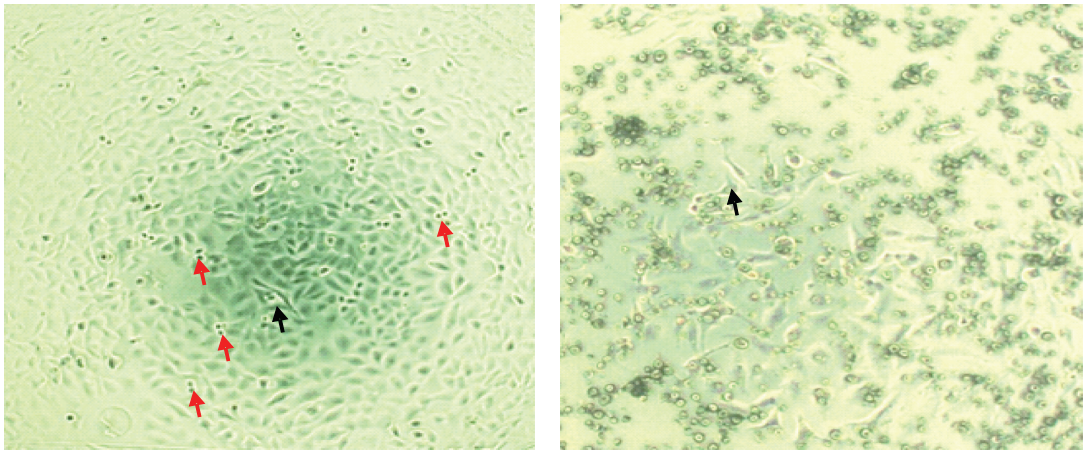

Figure 2: Microphotograph of (a) untreated HEK293 cell line and (b) *A. keiskei*-treated HEK293 cell line. Magnification: 200x. The black arrow indicates the dendritic process, and the red arrow indicates binucleate cells.

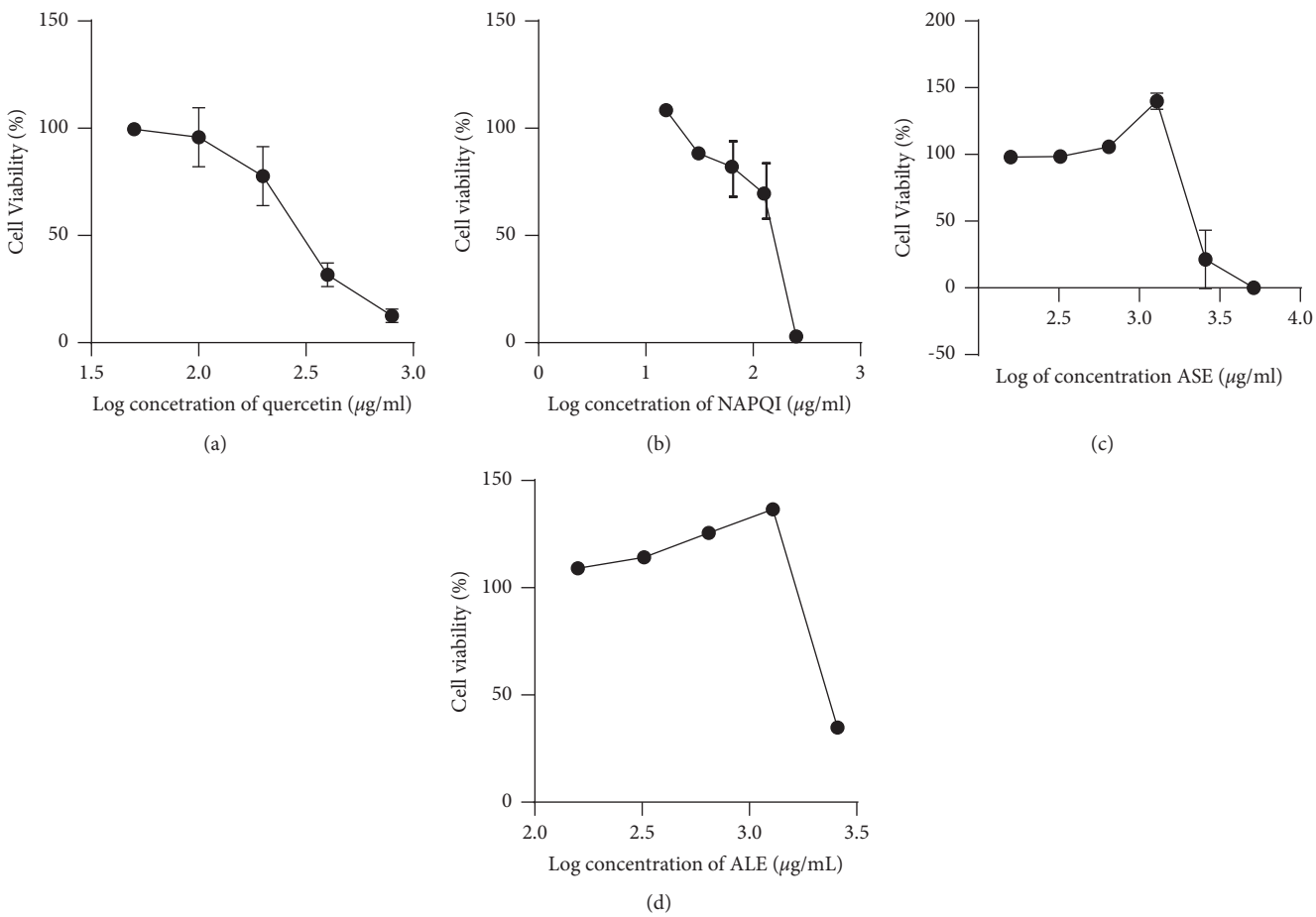

Figure 3: Cytotoxicity of quercetin (a) ($IC_{50} = 91.35\,\mu g/mL$ or 0.302 mM), NAPQI (b) ($IC_{50} = 163.19\,\mu g/mL$ or 1.093 mM), the ethanol extract of (c) *A. keiskei* stem (ASE; $IC_{50} = 2322\,\mu g/mL$), and (d) *A. keiskei* leaves (ALE; $IC_{50} = 2283\,\mu g/mL$) on HEK293 cell lines.

different parts of *A. keiskei* [18, 19]. Unexpectedly, quercetin ($IC_{50} = 91.35\,\mu g/mL$ or 0.302 mM), a well-known flavonoid, in the concentration of 45.68 μg/mL and 91.36 μg/mL reduced the viability of the HEK293 cell line (Figures 4 and 3).

Our result is in accordance with that of Dugan [16]. Dugan had pretreated HEK293 cells with 10–100 μM concentrations of quercetin. Then, the cells were 24-hour toxicity-induced with 30 μM of cadmium chloride. It was

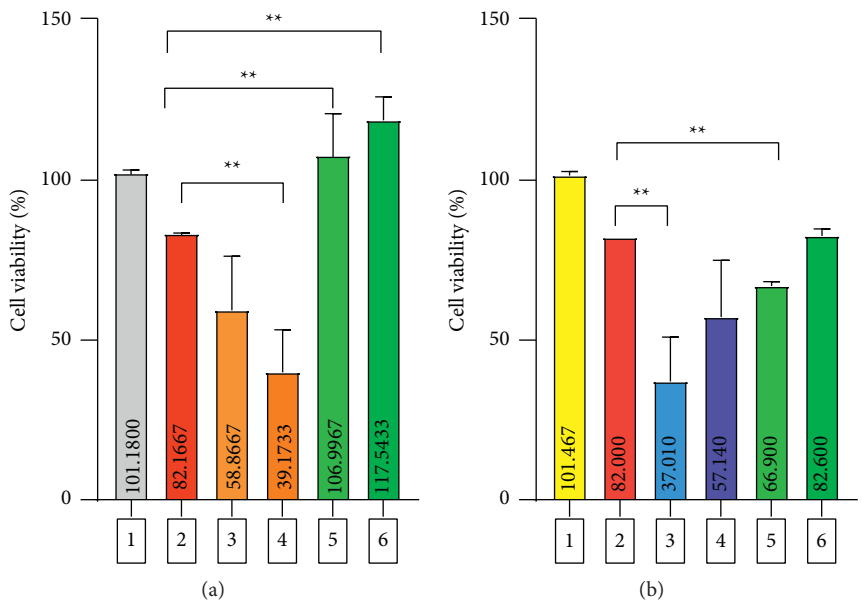

Figure 4: The nephroprotective activity of ASE (a) and ALE (b) on the NAPQI-induced HEK293 cell line. 1: normal control group; 2: negative control group; 3-4: positive control group (quercetin: 45.68 μg/mL and 91.36 μg/mL); 5-6: assayed extract group. ** indicates a significant difference with the negative control group ($p < 0.05$).

suggested that higher concentrations of quercetin (>10 μM) could stimulate an increase in cell death. In higher concentrations, quercetin was predicted to enhance the toxic effect of cadmium in HEK293 cells through JNK phosphorylation [16]. Nevertheless, in another study on cultured granulosa cells from chicken ovarian follicles, quercetin confirmed the potential in preventing cadmium-induced cytotoxicity. This protective activity of quercetin was predicted by diminishing lipid peroxidation, enhancing the antioxidant status within the cells, and inhibiting apoptosis [20].

A study on the effect of chalcone derivatives on D-galactosamine/lipopolysaccharide-induced liver failure in mice has confirmed a strong hepatoprotective activity of those compounds [21]. Chalcones have been disclosed as inhibitors of the synthesis of triglycerides. These open-ring flavonoids also work as activating factors of hepatic stellate cells and extracellular matrix deposition; thus, they could be used as liver-protective drugs [22]. Moreover, several flavonoids have revealed kidney-protective activities against many nephrotoxic agents, such as lipopolysaccharide, gentamycin, lead, or cadmium. In studies in murine models of chronic kidney disease, flavonoids significantly impaired kidney function [23]. A chalcone derivate has been reported which could significantly decrease the key markers for renal and cardiac dysfunction in diabetic mice [24].

5. Conclusions

The lower concentration of the ethanol extract of *Angelica keiskei* Koidzumi stems and leaves is not toxic to the human embryonic kidney (HEK)293 cell line, and only the stem extract protects the HEK293 cell line against N-acetyl-*p*-benzoquinone imine (NAPQI) damage. Chalcones and flavonoids contained in the stem extract might play a key role in this protective activity by scavenging the reactive oxygen species. This Japanese celery could be further explored for its potential as a plant-based nephroprotective drug.

Data Availability

The data used to support the findings are available on request from the corresponding author.

Conflicts of Interest

The authors declare that there are no conflicts of interest regarding the publication of this paper.

Acknowledgments

The authors thank the Rector of Universitas Padjadjaran via the Directorate of Research and Community Engagement (DRPM) for facilitating the research and publication fee in the scheme of Academic Leadership Grant of Prof. Dr. Jutti Levita. This research was funded by Universitas Padjadjaran Academic Leadership Grant 2020 (no. 1427/UN6.3/LT/2020). The publication fee was funded by Universitas Padjadjaran via the Directorate of Research and Community Engagement.

References

[1] S. Y. Kim and A. R. Moon, "Drug-induced nephrotoxicity and its biomarkers," *Biomolecules and Therapeutics*, vol. 20, no. 3, pp. 268–272, 2012.

[2] J. B. Patel and A. Sapra, *Nephrotoxic Medications*, StatPearls [Internet], Treasure Island, FL, USA, 2021, https://www.ncbi.nlm.nih.gov/books/NBK553144/.

[3] G. T. M. Sales and R. D. Foresto, "Drug-induced nephrotoxicity," *Revista da Associação Médica Brasileira*, vol. 66, no. 1, 2020.

[4] D. Singh, W. C. Cho, and G. Upadhyay, "Drug-induced liver toxicity and prevention by herbal antioxidants: an overview," *Frontiers in Physiology*, vol. 6, p. 363, 2016.

[5] A. M. Moyer, B. L. Fridley, G. D. Jenkins et al., "Acetaminophen-NAPQI hepatotoxicity: a cell line model system genome-wide association study," *Toxicological Sciences*, vol. 120, no. 1, pp. 33–41, 2011.

[6] F. S. Seibert, M. Sitz, J. Passfall et al., "Prognostic value of urinary calprotectin, NGAL and KIM-1 in chronic kidney disease," *Kidney and Blood Pressure Research*, vol. 43, no. 4, pp. 1255–1262, 2018.

[7] A. R. Syadiah, E. Febrina, and J. Levita, "Review neutrophil gelatinase-associated lipocalin (NGAL): perannya sebagai biomarker pada kerusakan ginjal akut," *Jurnal Sains Farmasi & Klinis*, vol. 8, no. 1, pp. 35–42, 2021.

[8] E. Molaei, A. Molaei, F. Abedi, A. W. Hayes, and G. Karimi, "Nephroprotective activity of natural products against chemical toxicants: the role of Nrf2/ARE signaling pathway," *Food Science & Nutrition*, vol. 9, no. 6, pp. 3362–3384, 2021.

[9] M. Kweon, H. Lee, C. Park, Y. H. Choi, and J.-H. Ryu, "A chalcone from Ashitaba (*Angelica keiskei*) stimulates myoblast differentiation and inhibits dexamethasone-induced muscle atrophy," *Nutrients*, vol. 11, no. 10, p. 2419, 2019.

[10] L. Zhang, Y. Jiang, X. Pang et al., "Simultaneous optimization of ultrasound-assisted extraction for flavonoids and antioxidant activity of *Angelica keiskei* using response surface methodology (RSM)," *Molecules*, vol. 24, no. 19, p. 3461, 2019.

[11] D. Kwon, S. Yoon, O. Carter, G. S. Bailey, and R. H. Dashwood, "Antioxidant and antigenotoxic activities of *Angelica keiskei*, Oenanthe javanica and *Brassica oleraceain* the *Salmonella* mutagenicity assay and in HCT116 human colon cancer cells," *Biofactors*, vol. 26, no. 4, pp. 231–244, 2006.

[12] M. Ściskalska, M. Śliwińska-Mossoń, M. Podawacz, W. Sajewicz, and H. Milnerowicz, "Mechanisms of interaction of the N-acetyl-p-aminophenol metabolites in terms of nephrotoxicity," *Drug and Chemical Toxicology*, vol. 38, no. 2, pp. 121–125, 2015.

[13] Ö. S. Aslantürk, "In vitro cytotoxicity and cell viability assays: principles, advantages, and disadvantages," *Genotoxicity—a Predictable Risk to our Actual World*, 2017.

[14] M. O. Nafiu, A. Omotayo, T. Ashafa, and S. Sabiu, "Anti-nephrolithiatic potential and the protective role of saponin-rich extract of Dianthus basuticus against acetaminophen-induced damage in HEK293 cells," *Indian Journal of Natural Product and Resources*, vol. 9, pp. 117–125, 2018.

[15] A. Ijaz, I. Javed, B. Aslam et al., "Nephroprotective and antioxidant effects of *Moringa oleifera* (Sohanjna) in paracetamol induced nephrotoxic albino rabbits," *Pakistan Veterinary Journal*, vol. 36, no. 3, pp. 292–296, 2016.

[16] E. Dugan, "Determining the effects of quercetin on cadmium toxicity in kidney cells," Thesis of the Bellarmine University Honors Program, Louisville, KY, USA, 2018.

[17] L. Q. Qin, S. Y. Luo, Z. H. Zhan, X. X. Liu, and K. Wang, "Determination of antioxidant compounds from leaf and stem of *Angelica keiskei* by gas chromatography-mass spectrometry," *Asian Journal of Chemistry*, vol. 26, no. 16, pp. 5097–5099, 2014.

[18] D. L. Aulifa, I. K. Adnyana, J. Levita, and S. Sukrasno, "4-Hydroxyderricin isolated from the sap of *Angelica keiskei* koidzumi: evaluation of its inhibitory activity towards dipeptidyl peptidase-IV," *Scientia Pharmaceutica*, vol. 87, no. 4, p. 30, 2019.

[19] Y. S. Kil, S. T. Pham, E. K. Seo, and M. Jafari, "*Angelica keiskei*, an emerging medicinal herb with various bioactive constituents and biological activities," *Archives of Pharmacal Research*, vol. 40, no. 6, pp. 655–675, 2017.

[20] Y. Jia, J. Lin, Y. Mi, and C. Zhang, "Quercetin attenuates cadmium-induced oxidative damage and apoptosis in granulosa cells from chicken ovarian follicles," *Reproductive Toxicology*, vol. 31, no. 4, pp. 477–485, 2011.

[21] L. P. Guan, J. X. Nan, X. J. Jin et al., "Protective effects of chalcone derivatives for acute liver injury in mice," *Archives of Pharmacal Research*, vol. 28, no. 1, pp. 81–86, 2005.

[22] E. Karimi-Sales, G. Mohaddes, and M. R. Alipour, "Chalcones as putative hepatoprotective agents: preclinical evidence and molecular mechanisms," *Pharmacological Research*, vol. 129, pp. 177–187, 2018.

[23] F. Vargas, P. Romecín, A. I. García-Guillén et al., "Flavonoids in kidney health and disease," *Frontiers in Physiology*, vol. 9, p. 394, 2018.

[24] Q. Fang, J. Wang, L. Wang et al., "Attenuation of inflammatory response by a novel chalcone protects kidney and heart from hyperglycemia-induced injuries in type 1 diabetic mice," *Toxicology and Applied Pharmacology*, vol. 288, no. 2, pp. 179–191, 2015.

Hindawi
Evidence-Based Complementary and Alternative Medicine
Volume 2021, Article ID 1718709, 12 pages
https://doi.org/10.1155/2021/1718709

Research Article

Luteolin Improves Cyclophosphamide-Induced Cystitis through TXNIP/NLRP3 and NF-κB Pathways

Hengshuai Zhang, Jiang Zhao, Qudong Lu, Bishao Sun, Xin Liu, Chengfei Yang, Shuai Li, Longkun Li, Shanhong Yi, Zhenxing Yang, and Jie Xu

Department of Urology, Second Affiliated Hospital, Army Medical University, Chongqing 400037, China

Correspondence should be addressed to Zhenxing Yang; yangzx88@tmmu.edu.cn and Jie Xu; xujie1981@tmmu.edu.cn

Received 5 August 2021; Revised 5 October 2021; Accepted 18 October 2021; Published 11 November 2021

Academic Editor: Lucian Hritcu

Hemorrhagic cystitis is an important complication of cyclophosphamide chemotherapy, and current therapies for the disease are limited. The natural flavonoid luteolin (LUT) has significant anti-inflammatory and antioxidant properties, but its protective effect on cyclophosphamide (CYP)-induced bladder toxicity has yet to be evaluated. This study aims to explore the protective effect of LUT on CYP-induced acute cystitis in rats. Female Sprague-Dawley rats were randomly assigned to the control (CON) group, CON + LUT group, CYP group, and CYP + LUT group. A single intraperitoneal injection of CYP was administered to establish an acute hemorrhagic cystitis model. HE staining was performed to detect the degree of bladder tissue damage, and TUNEL staining was performed to count apoptotic cells. Oxidative stress indicators were measured using commercial kits, and bladder surgery was performed to assess urinary function. The levels of inflammatory cytokines, apoptosis-related indicators, TXNIP/NLRP3 pathway, and NF-κB pathway were detected by western blot. We found that LUT treatment reduced bladder bleeding, congestion, and edema caused by CYP. Compared with the CYP + LUT group, the level of apoptosis was more highly expressed in the CYP group. We also found that caspase-3, caspase-8, and Bax were significantly upregulated and Bcl-2 was downregulated after LUT treatment. In addition, LUT inhibited the activation of NF-κB signal pathway in the rat bladder tissue after CYP exposure. LUT treatment can also reduce the NLRP3 inflammasome (NLRP3, ASC, and caspase-1) and TXNIP in the bladder. Finally, LUT can reduce the increase in the urination frequency and maximum urination pressure caused by cystitis. These results indicate that LUT displays effective anti-inflammatory, antioxidant, and antiapoptotic properties in CYP-induced acute hemorrhagic cystitis rats by inhibiting the TXNIP/NLRP3 and NF-κB pathways. LUT may be a potent therapeutic agent for the prevention and treatment of hemorrhagic cystitis.

1. Introduction

Cyclophosphamide (CYP) is a commonly used drug for chemotherapy of tumors and autoimmune diseases, but it has side effects on organs such as the bladder, liver, and kidneys [1]. High-dose CYP often causes chemical cystitis, also known as hemorrhagic cystitis, which is specifically manifested as bladder mucosal damage, pelvic pain, and bladder dysfunction [2]. A recent study showed that nearly one-quarter of patients using high-dose CYP suffer from hemorrhagic cystitis [3]. The pathological mechanism of CYP-induced hemorrhagic cystitis is related to its metabolite acrolein. Acrolein is a product of CYP metabolism in the liver, and it accumulates in the bladder after being excreted by the kidneys. Acrolein can induce the production of reactive oxygen species (ROS) and nitric oxide (NO) to promote oxidative stress and inflammation and ultimately induce hemorrhagic cystitis through a variety of cascade reactions [4]. At present, mesna is the preferred drug for the prevention and treatment of hemorrhagic cystitis, but it is not ideal due to adverse reactions and instability of treatment [5]. Therefore, exploring new drugs for the prevention or treatment of hemorrhagic cystitis has important clinical significance.

Thioredoxin interacting protein (TXNIP) is a regulatory protein involved in oxidative stress [6], which can inhibit the thioredoxin (TRX) antioxidant system and participate in the occurrence of oxidative stress in many diseases such as ischemia-reperfusion injury [7], acute lung injury [8], and atherosclerosis [9]. Inhibition of TXNIP expression in ketamine-induced chemical cystitis can reverse apoptosis and oxidative stress [10]. TXNIP acts as a bridge between ROS and the NLRP3 inflammasome, linking oxidative stress and inflammation. Many studies have shown that the NOD-like receptor protein 3 (NLRP3) inflammasome is involved in the occurrence of bladder inflammation, and inhibiting the expression of NLRP3 can effectively improve bladder injury [11]. Nuclear factor-κB (NF-κB), as a proinflammatory transcription factor widely involved in a variety of inflammatory reactions, is activated during inflammation and amplifies the inflammatory response by regulating the release of proinflammatory factors such as TNF-α [12]. Activated NF-κB has also been shown to increase the transcription of NLRP3 and promote the formation of inflammasome [13]. Therefore, TXNIP/NLRP3 and NF-κB may be potentially effective targets for hemorrhagic cystitis.

Luteolin (LUT) (Figure 1(a)) is a natural flavonoid compound widely found in honeysuckle, chrysanthemum, green pepper, celery, and other plants. LUT has many beneficial properties, including anti-inflammatory, antioxidant, wound-healing, nerve protection, and antitumor properties [14]. LUT has an excellent therapeutic effect on the chemical damage caused by the poison to the tissue. Recent studies have shown that LUT can reduce the damage caused by heavy metal cobalt to the hearts and kidneys of rats through its anti-inflammatory and antioxidant effects mediated by the NF-κB/Kim-1 pathway [15]. Wang et al. found that LUT can reduce inflammation, cell necrosis, and oxidative stress caused by lipopolysaccharide through the TXNIP-NLRP3 axis [16] and achieve a protective effect on the liver. In lower urinary tract diseases, LUT also shows a certain therapeutic effect. According to reports, luteolin can improve bladder dysfunction caused by diabetic bladder disease by downregulating SCF/c-kit and PI3K [17]. LUT can also protect the bladder epithelium from *E. coli* infection by inhibiting cAMP-phosphodiesterase [18]. The therapeutic effect of LUT on chemical toxicity injury and lower urinary tract disease indicates that it may have a protective effect on CYP-induced hemorrhagic cystitis. Therefore, this study aims to verify the therapeutic effect of LUT on acute hemorrhagic cystitis in rats and to further determine whether the NF-κB signal pathway and the TXNIP/NLRP3 axis are the therapeutic targets of LUT against bladder injury.

2. Materials and Methods

2.1. Animals. The female SD rats (200–240 g, 10–16 weeks old) used in this experiment were purchased from the Experimental Animal Center of Army Medical University. The experimental animals were kept at 20–23°C in a standard environment with the same length of day and night, and they were given unlimited food and water. All animal research was authorized by the Laboratory Animal Welfare and Ethics Committee of the Army Military Medical University (project identification code: AMUWEC2019416), and the study complied with the Animal Welfare Guidelines and the Declaration of Helsinki.

2.2. Animal Groupings and Administered Treatments. Before the experiment, the rats were randomly divided into the CON (control), CON + LUT, CYP, and CYP + LUT groups. During the one-week experimental period, the CON + LUT group and CYP + LUT group were given LUT 100 mg/kg (T2682, TCI, Japan) via daily gavage for 7 days [19]. The CON group and CYP group were treated with an equivalent volume of saline by gavage. On the fifth day of the experiment, the CYP group and CYP + LUT group were injected with CYP (150 mg/kg) (HY17420, MCE, USA) by intraperitoneal injection to induce acute hemorrhagic cystitis [20], and the CON group and CON + LUT group received normal saline solution intraperitoneally. The experiment was terminated on day 7. Some rats were sacrificed for tissue collection, and the remaining rats were used for continuous cystometry experiments.

2.3. Tissue Sections and HE Staining. The bladder tissue was collected through a midline incision in the lower abdomen 48 hours after intraperitoneal injection of CYP or saline. The harvested bladder was divided into two parts longitudinally; one part was used for histological research, and the other part was used for western blotting or oxidative stress measurement. The fixed bladder was cut into 5 μm thick sections and adhered to a glass slide. The hematoxylin-eosin (HE) staining was carried out as described previously [21]. Four visual fields (400×) were randomly selected from the HE stained sections, and the inflammation score was measured according to the standards reported in the literature [22].

2.4. TUNEL Staining. According to the manufacturer's protocol, bladder sections were analyzed by TUNEL assay using a Tunel Cell Apoptosis Detection Kit (G1507, Servicebio, China). In brief, bladder sections were deparaffinized and permeabilized with proteinase K. Membrane breaking working liquid was then used to rupture the membrane. PBS containing 0.3% hydrogen peroxide was used to block endogenous peroxidase for 30 minutes. After washing three times with PBS, the bladder sections were dripped with recombinant TdT enzyme and incubated in a 37°C incubator for 1 hour for the end labeling reaction. After washing again, the bladder sections were treated with streptavidin-HRP reaction solution and incubated at 37°C for 30 min. The DAB solution was added to the section, and the color development was monitored under an optical microscope. The reaction was stopped by washing with deionized water for 3 min. Finally, bladder sections were counterstained with hematoxylin, dehydrated, and mounted. Five fields in the TUNEL-stained section were randomly selected under a 400X microscope to determine the apoptotic index (the proportion of apoptotic cells in the total cells).

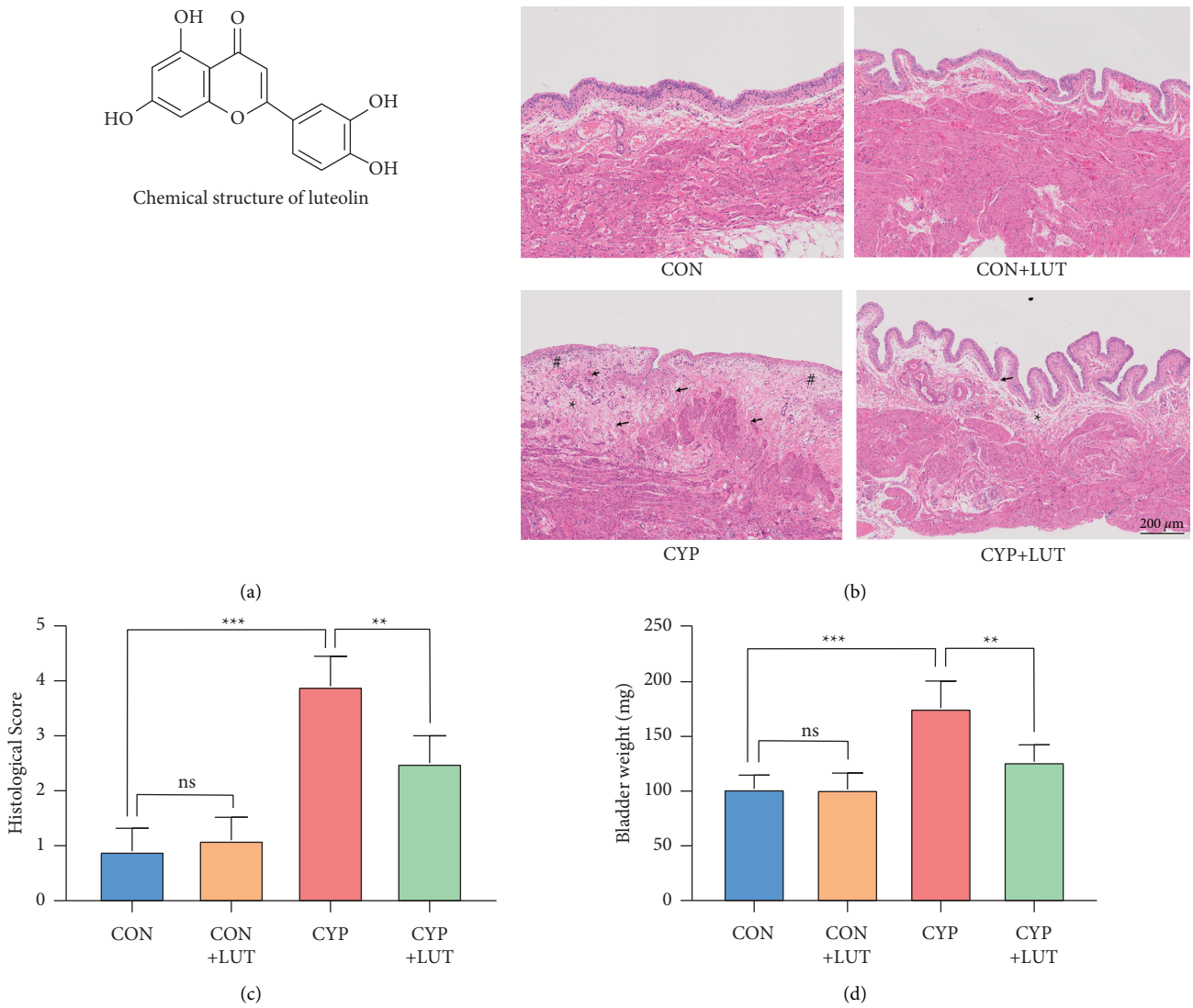

Figure 1: Effect of LUT on the pathological morphology of the bladder tissue in CYP-induced cystitis. (a) The chemical structure of LUT (3,4,5,7-hydroxyl-flavone). (b) Bladder microstructure from four groups of rats. In the CYP group, the bladder structure was severely damaged, with obvious bleeding, edema, and inflammatory cell infiltration. The shape of the bladder in the CYP + LUT group was close to normal. Arrows indicate bleeding, ∗ indicates edema, and # indicates infiltration of inflammatory cells. (c) Inflammation score under HE staining of the bladder in each group ($n = 5$). (d) The difference in the wet bladder weight between different groups ($n = 6$). $^{**}P < 0.01$ and $^{***}P < 0.001$; NS: not significant.

2.5. Estimation of Bladder Oxidative Stress Indicators. The harvested bladder was treated with physiological saline at a ratio of 1 : 10 and then polished into a homogenate. The tissue homogenate was centrifuged at 3000 rpm for 12 minutes, and the supernatant was extracted. According to the manufacturer's instructions, the levels of malondialdehyde (MDA), total superoxide dismutase (SOD), and glutathione (GSH) in the bladder were measured using commercial kits (A003, A001, and A006) obtained from the Nanjing Jiancheng Institute of Bioengineering.

2.6. Western Blot. The protein in the bladder tissue was extracted with RIPA buffer, and its concentration was measured with BCA Protein Assay Reagent (P0012, Beyotime, China). 30 μg of protein in each sample was loaded onto the SDS-PAGE gel for electrophoresis and then transferred to the PVDF membranes (ISEQ00010, Merck Millipore, Germany). After being blocked for one hour, the membranes were incubated overnight at 4°C with the following primary antibodies: NLRP3 (1 : 500, ab270449, Abcam, UK), TXNIP (1 : 1000, ab188865, Abcam, UK), Bcl-2 (1 : 1000, ab196495, Abcam, UK), IL-6 (1 : 500, P620, Thermo Fisher, USA), p–NF–κB (1 : 1000, 3033, CST, USA), NF-κB (1 : 1000, 8242, CST, USA), IL-1β (1 : 1000, sc12742, Santa, USA), caspase-3 (1 : 1000, 66470, Proteintech, China), caspase-8 (1 : 1000, 13426, Proteintech, China), Bax (1 : 1000, 60267, Proteintech, China), TNF-α (1 : 1000, 17590, Proteintech, China), TRX (1 : 1000, 14999, Proteintech, China), IκBα (1 : 1000, 4814, CST, USA), p-IκBα (1 : 1000, 2859, CST, USA), caspase-1(1 : 1000,

22915, Proteintech, China), ASC (1 : 1000, sc514414, Santa, USA), and GAPDH (1 : 1000, 60004, Proteintech, China). The membranes were rinsed in TBST the next day before being incubated with goat anti-rabbit secondary antibody (1 : 2000, G6120, Thermo Fisher, USA) or goat anti-mouse secondary antibody (1 : 2000, G21040, Thermo Fisher, USA). Finally, ECL Substrate (VK312464, Thermo Fisher, USA) and a bioanalytical imaging system (C300, Azure Biosystems, USA) were used to detect protein bands.

2.7. Continuous Cystometry. Five rats in each group were taken for cystometry measurement to evaluate the urodynamic contraction pressure and time as previously described [23]. In brief, rat bladders were exposed through an abdominal incision after they were anesthetized with urethane. Then, a tiny incision was made on the top of the bladder; the PE-50 catheter was connected to the bladder cavity and secured with sutures. The tube was connected to a microperfusion pump (YPJ01, Smiths Medical, USA) and received saline infusion (10 ml/h). The bladder function reached a stable state about 30 minutes after the start of the experiment. At this time, the urination waveform data were recorded using a data acquisition system (RM6240, Chengdu Instrument Factory, China), and the maximum bladder pressure (MBP) and intercontractile interval (ICI) between the different groups were measured and compared.

2.8. Statistical Analysis. Statistical analysis was performed using SPSS statistics 26 (SPSS Inc, USA). All data are presented as the mean ± standard error of the mean (mean ± SEM). The histological scores and apoptotic index scores were statistically compared between groups by Kruskal–Wallis multiple comparison tests. The other data were assessed with two-way ANOVA, and Bonferroni correction was followed. $P < 0.05$ indicated statistical significance (NS: not significant; $^{*}P < 0.05$, $^{**}P < 0.01$, and $^{***}P < 0.001$).

3. Results

3.1. LUT Treatment Improves the Histopathology of CYP-Induced Cystitis. We first performed a histological examination of the bladder to preliminarily judge the therapeutic effect of LUT. The bladder structure was normal in the CON group and CON + LUT group. The epithelial structure was complete without obvious pathological changes. In the CYP group, the bladder mucosa and lamina propria showed obvious congestion, bleeding, edema, ulcers, and inflammatory cell infiltration 48 hours after the induction of cystitis. LUT treatment reduced the pathological damage caused by CYP to the bladder tissue, and the phenomenon of edema and bleeding was improved (Figure 1(b)). The histological score also showed that the degree of tissue damage in the CYP + LUT group was better than that in the CYP group (Figure 1(c)). A general examination of the bladder revealed that CYP caused a significant increase in wet bladder weight, while LUT improved bladder edema and reduced bladder weight (Figure 1(d)).

3.2. Effect of LUT on Oxidative Stress Indexes and Inflammatory Cytokine Levels in CYP-Induced Cystitis. To further clarify the potential mechanism of LUT, we measured GSH, SOD, and MDA levels in the bladder to assess the level of bladder oxidative stress. Compared with the CON group, there was no significant difference in the abovementioned indicators in the CON + LUT group. Compared with those of normal rats, the activities of SOD and GSH in the CYP group were significantly reduced and the level of MDA was significantly increased. However, LUT treatment inhibited the increase of MDA in the bladder and partially restored GSH and SOD activity (Figures 2(a)–2(c)). In addition, we measured bladder proinflammatory cytokines with western blot. The results showed that the levels of IL-6, IL-1β, and TNF-α in the bladder of the CYP group were significantly increased. LUT treatment significantly reduced the inflammatory cytokines, while the expression of these inflammatory proteins did not change in normal rats after using LUT (Figure 2(d)).

3.3. LUT Decreases the Apoptosis Level in CYP-Induced Cystitis. Subsequently, we further detected the apoptosis level of bladder tissue by TUNEL staining and western blotting. Apoptosis was not obvious in the CON group and the CON + LUT group, while the number of apoptotic cells increased significantly in the CYP group, especially in the bladder mucosa. However, LUT treatment reduced the high levels of apoptosis induced by CYP (Figures 3(a) and 3(b)). Western blot results showed that the expression of Bax, caspase-3, and caspase-8 in the bladder of the CYP group was significantly upregulated while Bcl-2 was inhibited. Compared with the CYP group, the disorder of these apoptosis-related proteins in the CYP + LUT group was significantly improved (Figures 3(c)–3(g)), further proving that LUT can reduce CYP-induced bladder cell apoptosis.

3.4. Effect of LUT on the TXNIP/NLRP3 Axis in CYP-Induced Cystitis. The regulating effect of the TXNIP/NLRP3 axis on oxidative stress has been widely reported [16]. In order to study the mechanism of LUT improving CYP-induced cystitis, we used western blot to study the expression changes of TXNIP/NLRP3 before and after LUT treatment. Figure 4 shows that the expression of TXNIP, NLRP3, ASC, and caspase-1 protein in the CYP group was significantly increased compared to those of the CON group. However, the expression levels of TXNIP, NLRP3, ASC, and caspase-1 proteins in the CYP + LUT group decreased, and the expression of TRX increased. In conclusion, our results indicate that the activation of the TXNIP/NLRP3 pathway was suppressed by LUT.

3.5. LUT Inhibits the Activation of NF-κB Signal Pathway Caused by CYP. The role of inflammation in CYP-induced cystitis cannot be ignored. We further studied the changes of the inflammatory NF-κB pathway in these four groups. The expression of p-IκBα and p-NF-κB in the CYP group was significantly increased compared with that of the CON

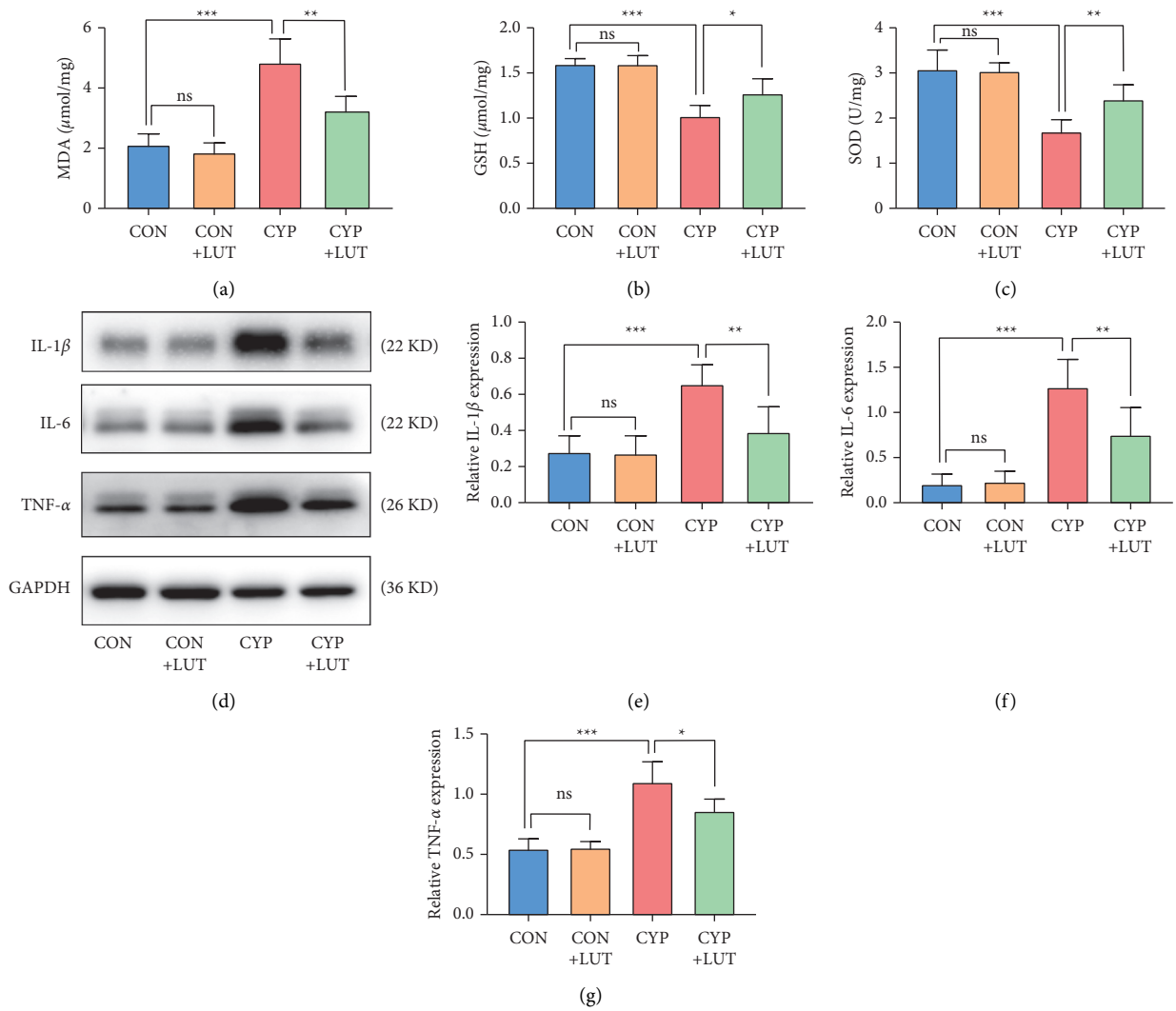

Figure 2: LUT inhibits the increase in oxidative stress and inflammatory cytokine levels in the bladder tissue caused by CYP. The measurement results of MDA (a), GSH (b), and SOD (c) levels in the bladder of each group. LUT treatment reduced the disorder of bladder oxidative stress-related molecules caused by CYP. (d) The expressions of IL-1β, IL-6, and TNF-α in the bladder of four groups were detected by western blot. LUT inhibited the upregulation of inflammatory factors induced by CYP. The expression analysis of IL-1β (e), IL-6 (f), and TNF-α (g) protein in the bladder of four groups ($n = 6$). $*P < 0.05$, $^{**}P < 0.01$, and $^{***}P < 0.001$; NS: not significant.

group (Figure 5). The LUT treatment inhibited the phosphorylation of NF-κB and IκBα.

3.6. LUT Improves Bladder Dysfunction in Hemorrhagic Cystitis. To evaluate the effect of LUT treatment on bladder function, we performed cystometry to measure the bladder voiding time and contraction of the four groups of rats. The maximum bladder pressure (MBP) of the CYP group was higher than that of normal rats, and the pressure showed greater fluctuation. The MBP of rats treated with LUT decreased significantly, and the urination pressure was more stable (Figures 6(a) and 6(b)). In addition, we observed that CYP shortened intercontractile intervals (ICIs), corresponding to an increase in the urination frequency. The ICI of the LUT + CYP group was significantly increased, but it was shorter than that of the CON group and the CON + LUT group (Figure 6(c)).

4. Discussion

Hemorrhagic cystitis, as a serious complication caused by the chemotherapy drug CYP, has brought great trouble to the use of CYP in tumor and rheumatic diseases. Preventive use of urinary tract protectors is currently the main method to solve this problem, but the search for a more effective and safer treatment of hemorrhagic cystitis is still widely underway [5]. LUT is a natural flavonoid compound found in many edible plants. It has been shown to play a protective role in a variety of diseases, such as acute lung injury caused by sepsis [8] and myocardial ischemia-reperfusion injury [24]. In this study, we verified the protective effect of LUT on CYP-induced cystitis. We found that LUT treatment can inhibit the level of bladder inflammation, oxidative stress, and apoptosis. In addition, we found that LUT may mediate anti-inflammatory and antioxidant effects by inhibiting NK-κB activity and TXNIP/NLRP3 axis activation. Finally, the

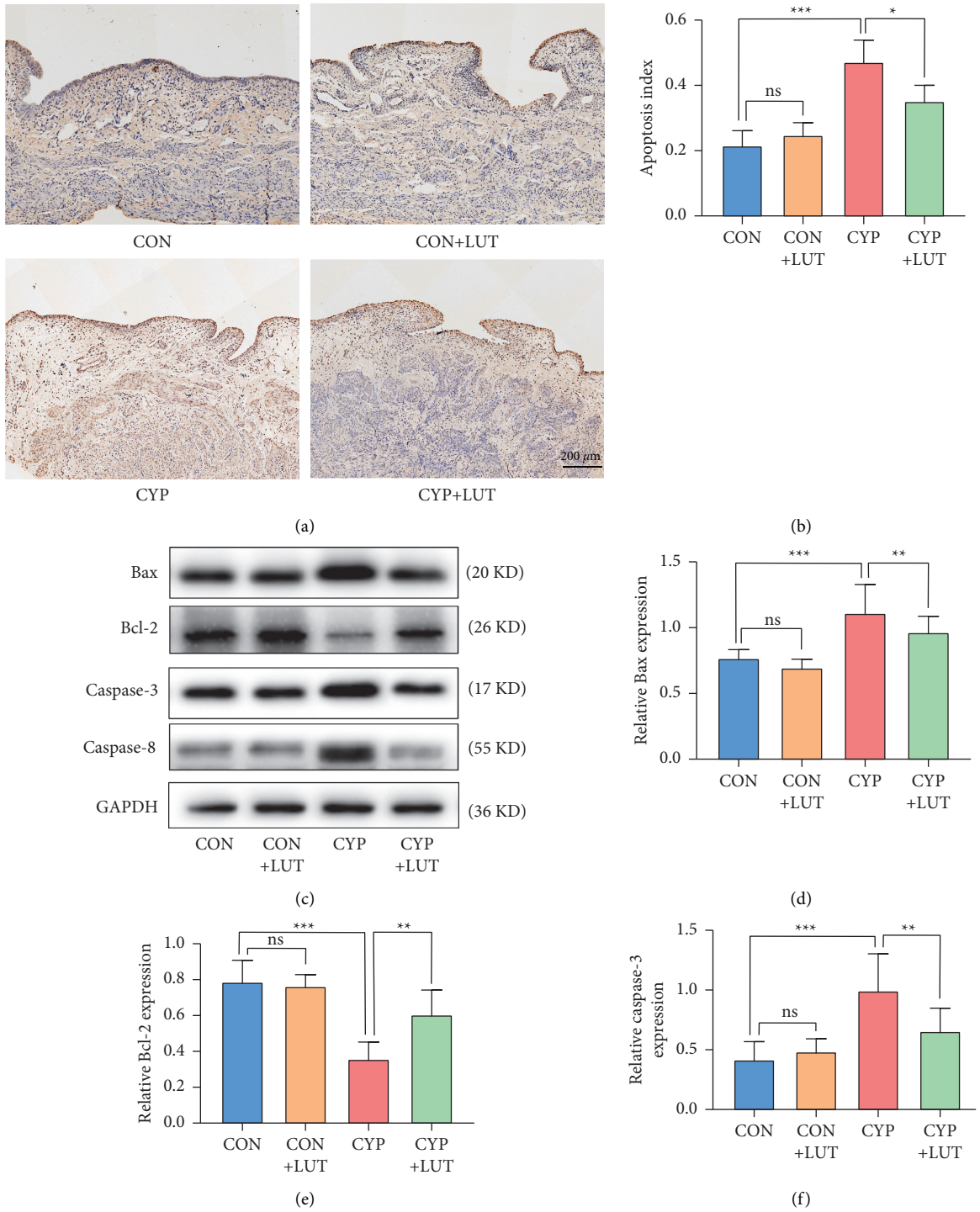

Figure 3: Continued.

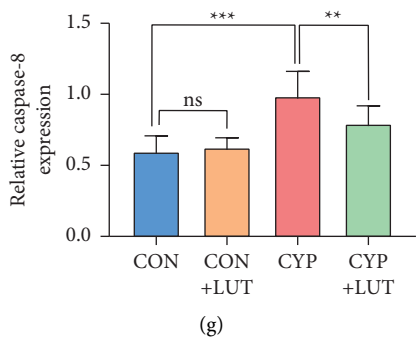

Figure 3: LUT reduces apoptosis in CYP-induced cystitis. (a) TUNEL staining of bladder slices in each group. Apoptotic cells were stained dark brown and nonapoptotic cells were stained blue. (b) Statistics of apoptotic index from TUNEL staining in each group ($n = 5$). LUT reduced the number of TUNEL staining positive cells in the bladder. (c) The expression of Bax, Bcl-2, caspase-3, and caspase-8 in the bladder of each group was detected by western blot. LUT treatment ameliorated the disorder of apoptosis-related proteins in CYP-induced cystitis. The expression analysis of Bax (d), Bcl-2 (e), caspase-3 (f), and caspase-8 (g) proteins in the bladder of each group ($n = 6$). $^{*}P < 0.05$, $^{**}P < 0.01$, and $^{***}P < 0.001$; NS: not significant.

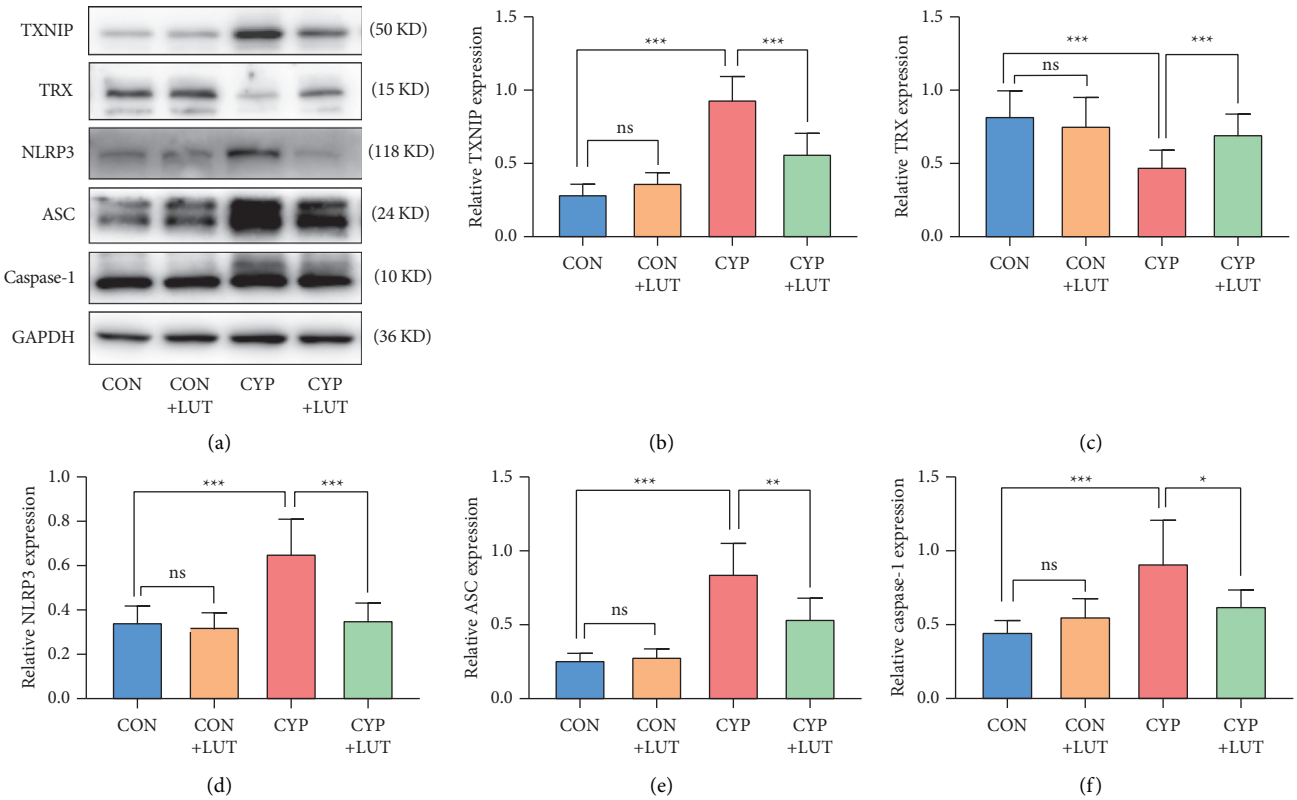

Figure 4: LUT inhibits the TXNIP/NLRP3 pathway in CYP-induced cystitis. (a) The expression of TXNIP, TRX, NLRP3, ASC, and caspase-1 in each test group was detected by western blot. LUT inhibited the upregulation of TXNIP, NLRP3, ASC, and caspase-1 in CYP-induced cystitis and increased the expression of TRX. The expression analysis of TXNIP (b), TRX (c), NLRP3 (d), ASC (e), and caspase-1 (f) protein in the bladder of each group ($n = 6$). $^{*}P < 0.05$, $^{**}P < 0.01$, and $^{***}P < 0.001$; NS: not significant.

urodynamic parameters we collected proved that LUT treatment improved the abnormal bladder function caused by hemorrhagic cystitis.

The typical pathological manifestation of hemorrhagic cystitis includes edema, ulcers, submucosal hemorrhage, epithelial injury, and inflammatory cell infiltration [25]. Consistently, we found that CYP-treated rats showed these typical characteristics. The increase in bladder weight may be due to inflammation damage, which leads to increased microvascular permeability and thus to tissue edema. Cystometry is an effective method to assess bladder function. Previous studies have found that bladder compliance decreases and urination frequency increases after CYP treatment [26]. Similarly, bladder neuropathy caused by diabetes has been shown to increase the maximum bladder capacity and residual urine volume. LUT restores bladder function by

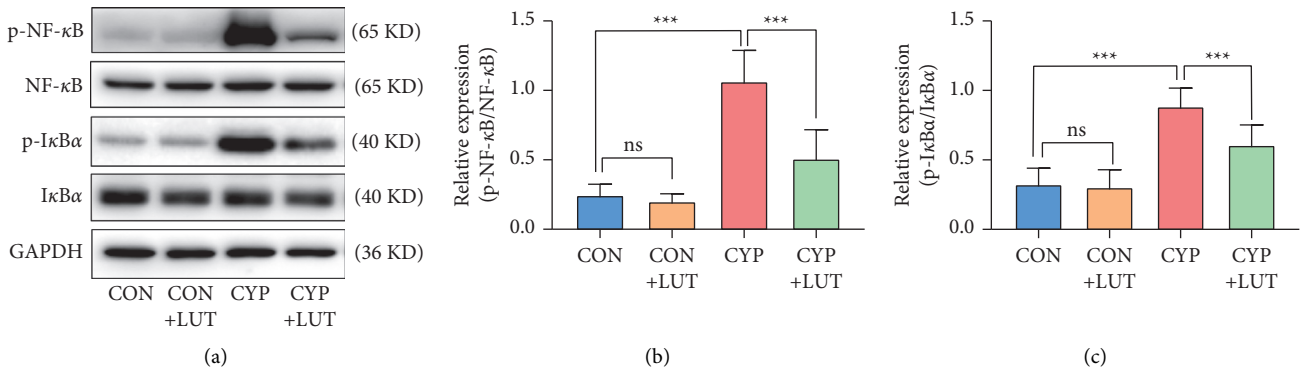

Figure 5: LUT inactivates the NF-κB pathway in CYP-induced cystitis. (a) The expression of p-NF-κB, NF-κB, p-IκB, and IκB in the bladder of each group was detected by western blot. LUT inhibited the phosphorylation of NF-κB and IκBα in the bladder caused by CYP. Analysis of the levels of NF-κB (b) phosphorylation and IκBα (c) phosphorylation in each group ($n = 6$). $^{***}P < 0.001$; NS: not significant.

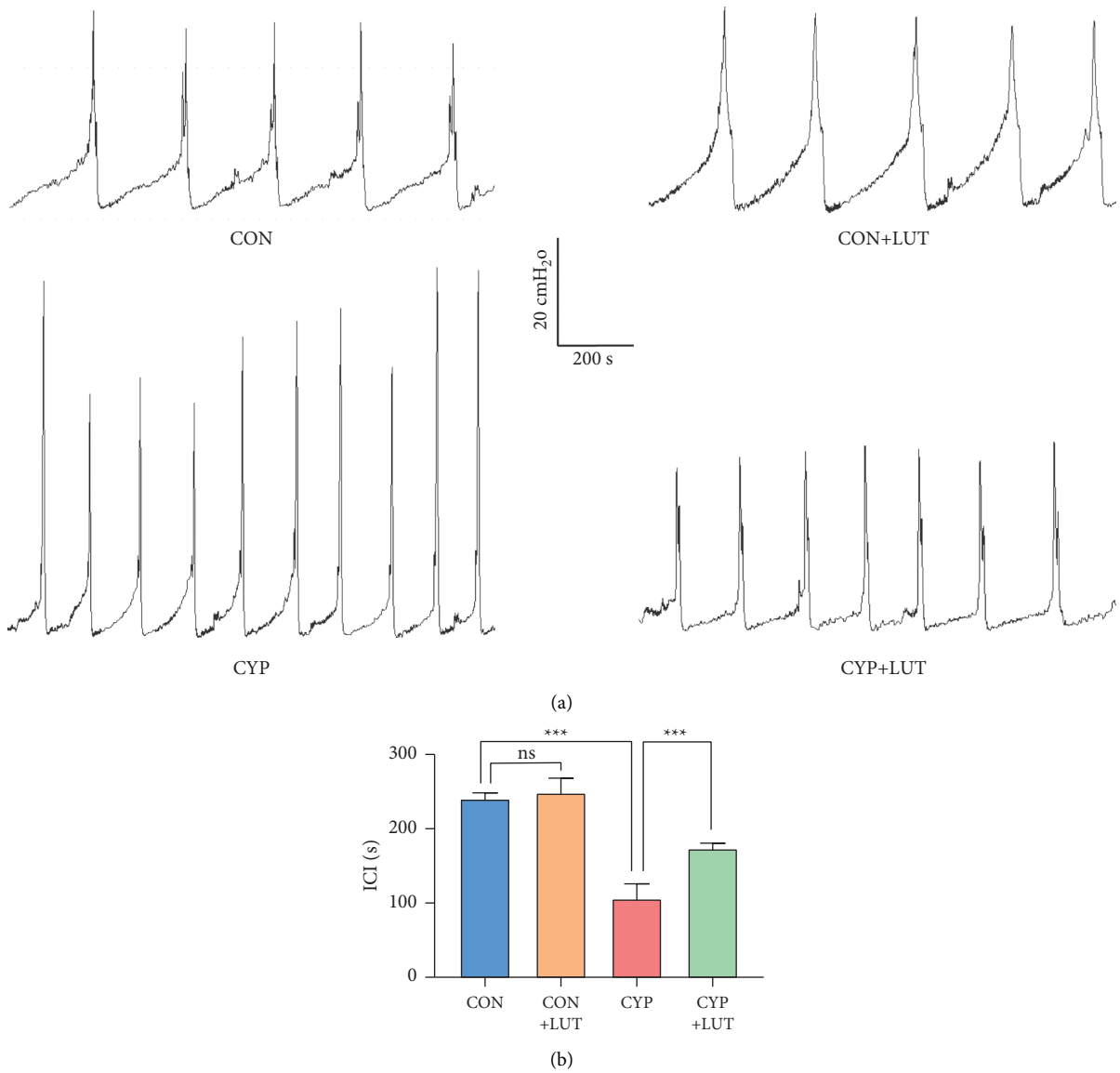

Figure 6: Continued.

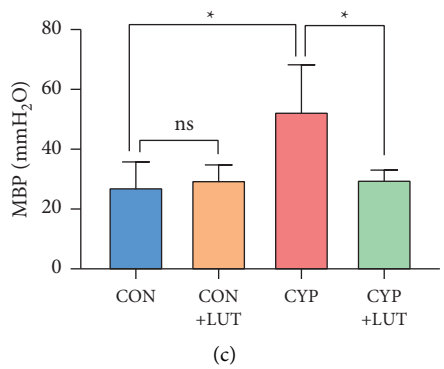

Figure 6: LUT improves bladder dysfunction induced by CYP. (a) Pressure waveform during urination of the CON group, CON + LUT group, CYP group, and CYP + LUT group. LUT improves abnormal urination patterns caused by CYP. Comparison of maximum bladder pressure (b) and intercontractile interval (c) in each group ($n = 5$). $^{*}P < 0.05$ and $^{***}P < 0.001$; NS: not significant.

inhibiting the activity of SCF and c-Kit [17]. In our study, LUT treatment significantly improved the pathological damage and urination abnormalities caused by CYP, proving the protective effect of LUT on the bladder.

It is generally believed that oxidative stress plays a leading role in the pathogenesis of CYP-induced cystitis [27]. Under normal physiological conditions, the antioxidant system composed of SOD and GSH can promptly remove ROS and other free radicals generated by oxidation reactions and maintain a balanced state [28]. A large amount of ROS induced by acrolein disrupts the oxidative balance of the bladder epithelium, further leads to the destruction of DNA structure, and induces lipid peroxidation to form MDA [29], accompanied by a decrease in GSH and SOD levels [30]. As an excellent antioxidant, LUT can effectively reduce the ROS production of macrophages under the stimulation of LPS [31]. Also, in a study of a mouse model of liver failure, LUT treatment increased the glutathione content of the tissues and decreased lipid peroxidation [32]. Our results also prove that LUT treatment can effectively improve the disorder of bladder oxidative stress indicators. Therefore, it can be concluded that LUT improves hemorrhagic cystitis by maintaining SOD and GSH activity and suppressing MDA production.

As we all know, TXNIP and TRX are important components in the thioredoxin system that regulates oxidative stress in the body [33]. TRX is a key antioxidant protein that exists in the cytoplasm to protect proteins and nucleic acids from oxidative damage. TXNIP, as a negative regulator of TRX, increases the sensitivity of tissues to oxidative stress [6]. The occurrence of oxidative damage in ketamine-induced cystitis resulted in high expression of TXNIP in the bladder [10], and consistent results were also found in CYP-induced cystitis. In addition, we also observed a significant decrease in the expression of TRX, which may be related to the inhibitory effect of TXNIP on TRX and the inhibitory effect of cyclophosphamide on the activity of thioredoxin reductase [34]. ROS leads to the dissociation of TXNIP from the TXNIP/TRX complex. Subsequently, TXNIP binds to NLRP3 and promotes the activation of inflammasome [35]. It has been proved that abnormal or excessive activation of NLRP3 contributes to the development of bladder inflammation [36]. Recent studies have shown that the use of drugs to inhibit the activation of NLRP3 alleviates the pyrolysis in acute interstitial cystitis [11]. Our results showed that LUT treatment significantly inhibited the expression of TXNIP and the NLRP3 inflammasome constituent proteins (NLRP3, caspase-1, and ASC). This is consistent with similar results by Wang et al. [16]. This illustrates that LUT exerts bladder-protective effects by inhibiting the TXNIP/NLRP3 axis.

Tissue damage caused by oxidative stress is usually accompanied by inflammation; the NF-κB signal is the main signal pathway that mediates the production of inflammatory factors [12]. Under normal conditions, NF-κB usually binds to its inhibitor IκBα in the form of dimers and is in an inactive state. The oxidative stress induced by CYP leads to the activation of IκB kinases (IKKs) and the degradation and phosphorylation of IκBα. At the same time, NF-κB dissociates and transfers to the nucleus to induce the production of inflammatory factors [12]. Increasing inflammatory mediators such as TNF-α, IL-6, and IL-1β in hemorrhagic cystitis will further aggravate the inflammatory response [37]. According to reports, LUT can prevent the activation of NF-κB in the colon tissue stimulated by ammonium thiosulfate through the HMGB1-TLR pathway [38]. In this study, LUT can inhibit the activation of the NF-κB signal induced by CYP. In addition, the increased inflammatory factors such as TNF-α caused by CYP were reversed by LUT treatment. This illustrates that LUT exerts anti-inflammatory effects by inhibiting the NF-κB pathway.

Apoptosis is the key mechanism of CYP-induced bladder toxicity [39], which can be triggered by inflammatory factors and oxidative stress [40]. Chronic intermittent hypoxia-induced mitochondrial dysfunction mediates endothelial injury via the TXNIP/NLRP3/IL-1β pathway. Antiapoptotic Bcl-2 can inhibit the permeability changes of the outer mitochondrial membrane caused by Bax to prevent the release of cytochrome C into the cytoplasm, thereby inhibiting the occurrence of apoptosis [41]. In previous studies, it was found that CYP can cause urothelial cell apoptosis by upregulating the ratio of Bax/Bcl-2 [42]. Caspase-8 participates in apoptosis induced by the death receptor pathway [43]. As a key mediator of the executive

function of the terminal stage of apoptosis, caspase-3 can be activated by death receptors and mitochondrial pathways to induce the occurrence of apoptosis [44]. In previous studies, it was found that LUT treatment can counteract cell apoptosis, which is achieved by regulating the apoptosis markers Bcl-2, Bax, and caspase-3 [45]. In addition, the caspase inhibitory effect of LUT may be related to its antiapoptotic effect [46]. In accordance with these reports, our findings revealed that LUT therapy can improve bladder injury in rats with hemorrhagic cystitis by controlling cell apoptosis.

Previous studies have shown that the TXNIP/NLRP3/IL-1β pathway is involved in cell apoptosis under hypoxia. In addition, the knockdown of NLRP3 can protect cells from apoptosis [47]. This finding indicates that LUT can inhibit CYP-induced bladder cell apoptosis through the TXNIP/NLRP3 axis. NF-κB activation is also involved in the initiation of apoptosis in inflammatory diseases [48]. Existing reports have shown that the nuclear translocation of NF-κB and the significant increase in Bax expression in the bladder tissue are related to bladder cell apoptosis [48]. NF-κB activation mediates the process of oxidative stress-induced apoptosis by reducing Bcl-2 protein activation and Bax protein translocation and enhancing p53 function [49]. NF-κB also promotes apoptosis by upregulating the expression of death receptors [50]. Although the effect of NF-κB is not direct, our results also indicate that luteolin can protect the bladder from apoptosis and inflammation by inhibiting NF-κB.

5. Conclusions

In summary, we found that LUT can inhibit oxidative stress, inflammation, and apoptosis through TXNIP/NLRP3 and NF-κB, which then produces protection against CYP-induced hemorrhagic cystitis and effectively improves bladder voiding dysfunction. Therefore, our results indicate that LUT may be a promising candidate for the prevention and treatment of hemorrhagic cystitis.

Data Availability

The research data used to support the findings of this study are included within the article.

Conflicts of Interest

The authors declare that there are no conflicts of interest regarding the publication of this paper.

Acknowledgments

This work was supported by the National Natural Science Foundation of China (grant numbers: 81974101 and 81873628).

References

[1] G. B. McDonald, J. T. Slattery, M. E. Bouvier et al., "Cyclophosphamide metabolism, liver toxicity, and mortality following hematopoietic stem cell transplantation," *Blood*, vol. 101, no. 5, pp. 2043–2048, 2003.

[2] M. M. Morais, J. N. Belarmino-Filho, G. A. C. Brito, and R. A. Ribeiro, "Pharmacological and histopathological study of cyclophosphamide-induced hemorrhagic cystitis-comparison of the effects of dexamethasone and Mesna," *Brazilian Journal of Medical and Biological Research*, vol. 32, no. 10, pp. 1211–1215, 1999.

[3] R.-C. Petca, R.-I. Popescu, C. Toma et al., "Chemical hemorrhagic cystitis: diagnostic and therapeutic pitfalls (review)," *Experimental and Therapeutic Medicine*, vol. 21, no. 6, p. 624, 2021.

[4] D. N. Tripathi and G. B. Jena, "Effect of melatonin on the expression of Nrf2 and NF-κB during cyclophosphamide-induced urinary bladder injury in rat," *Journal of Pineal Research*, vol. 48, no. 4, pp. 324–331, 2010.

[5] E. L. Matz and M. H. Hsieh, "Review of advances in uroprotective agents for cyclophosphamide- and ifosfamide-induced hemorrhagic cystitis," *Urology*, vol. 100, pp. 16–19, 2017.

[6] E. Yoshihara, S. Masaki, Y. Matsuo, Z. Chen, H. Tian, and J. Yodoi, "Thioredoxin/Txnip: redoxisome, as a redox switch for the pathogenesis of diseases," *Frontiers in Immunology*, vol. 4, p. 514, 2014.

[7] Y. Jia, R. Cui, C. Wang et al., "Metformin protects against intestinal ischemia-reperfusion injury and cell pyroptosis via TXNIP-NLRP3-GSDMD pathway," *Redox Biology*, vol. 32, Article ID 101534, 2020.

[8] S. Rungsung, T. U. Singh, D. J. Rabha et al., "Luteolin attenuates acute lung injury in experimental mouse model of sepsis," *Cytokine*, vol. 110, pp. 333–343, 2018.

[9] J. B. Nyandwi, Y. S. Ko, H. Jin, S. P. Yun, S. W. Park, and H. J. Kim, "Rosmarinic acid inhibits oxLDL-induced inflammasome activation under high-glucose conditions through downregulating the p38-FOXO1-TXNIP pathway," *Biochemical Pharmacology*, vol. 182, Article ID 114246, 2020.

[10] L. Cui, X. Jiang, C. Zhang et al., "Ketamine induces endoplasmic reticulum stress in rats and SV-HUC-1 human uroepithelial cells by activating NLRP3/TXNIP aix," *Bioscience Reports*, vol. 39, no. 10, 2019.

[11] X. Wang, H. Yin, L. Fan et al., "Shionone alleviates NLRP3 inflammasome mediated pyroptosis in interstitial cystitis injury," *International Immunopharmacology*, vol. 90, Article ID 107132, 2021.

[12] T. Liu, L. Zhang, D. Joo, and S.-C. Sun, "NF-kappaB signaling in inflammation," *Signal Transduction and Targeted Therapy*, vol. 2, 2017.

[13] A. Shao, H. Wu, Y. Hong et al., "Hydrogen-rich saline attenuated subarachnoid hemorrhage-induced early brain injury in rats by suppressing inflammatory response: possible involvement of NF-κB pathway and NLRP3 inflammasome," *Molecular Neurobiology*, vol. 53, no. 5, pp. 3462–3476, 2016.

[14] G. Seelinger, I. Merfort, and C. Schempp, "Anti-oxidant, anti-inflammatory and anti-allergic activities of luteolin," *Planta Medica*, vol. 74, no. 14, pp. 1667–1677, 2008.

[15] A. A. Oyagbemi, A. S. Akinrinde, O. E. Adebiyi et al., "Luteolin supplementation ameliorates cobalt-induced oxidative stress and inflammation by suppressing NF-κB/Kim-1 signaling in the heart and kidney of rats," *Environmental Toxicology and Pharmacology*, vol. 80, Article ID 103488, 2020.

[16] X. Wang, L. Wang, R. Dong et al., "Luteolin ameliorates LPS-induced acute liver injury by inhibiting TXNIP-NLRP3

inflammasome in mice," *Phytomedicine*, vol. 87, Article ID 153586, 2021.

[17] J. Xu, H. Xu, Y. Yu, Y. He, Q. Liu, and B. Yang, "Combination of luteolin and solifenacin improves urinary dysfunction induced by diabetic cystopathy in rats," *Medical Science Monitor*, vol. 24, pp. 1441–1448, 2018.

[18] X.-F. Shen, Y. Teng, K.-H. Sha et al., "Dietary flavonoid luteolin attenuates uropathogenic Escherichia. Coliinvasion of the urinary bladder," *BioFactors*, vol. 42, no. 6, pp. 674–685, 2016.

[19] X. Zhang, Q. Du, Y. Yang et al., "The protective effect of luteolin on myocardial ischemia/reperfusion (I/R) injury through TLR4/NF-κB/NLRP3 inflammasome pathway," *Biomedicine & Pharmacotherapy*, vol. 91, pp. 1042–1052, 2017.

[20] B. Chen, H. Zhang, L. Liu, J. Wang, and Z. Ye, "PK2/PKR1 signaling regulates bladder function and sensation in rats with cyclophosphamide-induced cystitis," *Mediators of Inflammation*, vol. 2015, Article ID 289519, 9 pages, 2015.

[21] J. Luo, C. Yang, X. Luo et al., "Chlorogenic acid attenuates cyclophosphamide-induced rat interstitial cystitis," *Life Sciences*, vol. 254, Article ID 117590, 2020.

[22] J. S. Starkman, M. Martinez-Ferrer, J. M. Iturregui, C. Uwamariya, R. R. Dmochowski, and N. A. Bhowmick, "Nicotinic signaling ameliorates acute bladder inflammation induced by protamine sulfate or cyclophosphamide," *The Journal of Urology*, vol. 179, no. 6, pp. 2440–2446, 2008.

[23] Y. Yang, H. Zhang, Q. Lu et al., "Suppression of adenosine A2a receptors alleviates bladder overactivity and hyperalgesia in cyclophosphamide-induced cystitis by inhibiting TRPV1," *Biochemical Pharmacology*, vol. 183, Article ID 114340, 2021.

[24] B. Wei, Q. Lin, Y.-G. Ji et al., "Luteolin ameliorates rat myocardial ischaemia-reperfusion injury through activation of peroxiredoxin II," *British Journal of Pharmacology*, vol. 175, no. 16, pp. 3315–3332, 2018.

[25] M. Sucic, K. Luetic, I. Jandric et al., "Therapy of the rat hemorrhagic cystitis induced by cyclophosphamide. Stable gastric pentadecapeptide BPC 157, L-arginine, L-NAME," *European Journal of Pharmacology*, vol. 861, Article ID 172593, 2019.

[26] A. Wróbel, Ł. Zapała, T. Kluz et al., "The potential of asiatic acid in the reversion of cyclophosphamide-induced hemorrhagic cystitis in rats," *International Journal of Molecular Sciences*, vol. 22, no. 11, 2021.

[27] S. Haldar, C. Dru, and N. A. Bhowmick, "Mechanisms of hemorrhagic cystitis," *American Journal of Clinical and Experimental Urology*, vol. 2, no. 3, pp. 199–208, 2014.

[28] A. Korkmaz, T. Topal, and S. Oter, "Pathophysiological aspects of cyclophosphamide and ifosfamide induced hemorrhagic cystitis; implication of reactive oxygen and nitrogen species as well as PARP activation," *Cell Biology and Toxicology*, vol. 23, no. 5, pp. 303–312, 2007.

[29] E. Beshay and S. Carrier, "Oxidative stress plays a role in diabetes-induced bladder dysfunction in a rat model," *Urology*, vol. 64, no. 5, pp. 1062–1067, 2004.

[30] I. O. Sherif, Z. M. Nakshabandi, M. A. Mohamed, and O. M. Sarhan, "Uroprotective effect of oleuropein in a rat model of hemorrhagic cystitis," *The International Journal of Biochemistry & Cell Biology*, vol. 74, pp. 12–17, 2016.

[31] B. C. Zhang, Z. Li, W. Xu, C. H. Xiang, and Y. F. Ma, "Luteolin alleviates NLRP3 inflammasome activation and directs macrophage polarization in lipopolysaccharide-stimulated RAW264.7 cells," *American Journal of Tourism Research*, vol. 10, no. 1, pp. 265–273, 2018.

[32] M. Tai, J. Zhang, S. Song et al., "Protective effects of luteolin against acetaminophen-induced acute liver failure in mouse," *International Immunopharmacology*, vol. 27, no. 1, pp. 164–170, 2015.

[33] J. Lu and A. Holmgren, "The thioredoxin antioxidant system," *Free Radical Biology and Medicine*, vol. 66, pp. 75–87, 2014.

[34] J. Zhang, K. Ma, and H. Wang, "Cyclophosphamide suppresses thioredoxin reductase in bladder tissue and its adaptive response via inductions of thioredoxin reductase and glutathione peroxidase," *Chemico-Biological Interactions*, vol. 162, no. 1, pp. 24–30, 2006.

[35] R. Zhou, A. Tardivel, B. Thorens, I. Choi, and J. Tschopp, "Thioredoxin-interacting protein links oxidative stress to inflammasome activation," *Nature Immunology*, vol. 11, no. 2, pp. 136–140, 2010.

[36] K. B. Tudrej, T. Piecha, and M. Kozłowska-Wojciechowska, "Role of NLRP3 inflammasome in the development of bladder pain syndrome interstitial cystitis," *Therapeutic advances in urology*, vol. 11, 2019.

[37] R. A. Ribeiro, H. C. Freitas, M. C. Campos et al., "Tumor necrosis factor-α and interleukin-1β mediate the production of nitric oxide involved in the pathogenesis of ifosfamide induced hemorrhagic cystitis in mice," *The Journal of Urology*, vol. 167, no. 5, pp. 2229–2234, 2002.

[38] T. Zuo, Y. Yue, X. Wang, H. Li, and S. Yan, "Luteolin relieved DSS-induced colitis in mice via HMGB1-TLR-NF-κb signaling pathway," *Inflammation*, vol. 44, no. 2, pp. 570–579, 2021.

[39] A. Ayhanci, D. T. Tanriverdi, V. Sahinturk, M. Cengiz, S. Appak-Baskoy, and I. K. Sahin, "Protective effects of boron on cyclophosphamide-induced bladder damage and oxidative stress in rats," *Biological Trace Element Research*, vol. 197, no. 1, pp. 184–191, 2020.

[40] K.-M. Liu, S.-M. Chuang, C.-Y. Long et al., "Ketamine-induced ulcerative cystitis and bladder apoptosis involve oxidative stress mediated by mitochondria and the endoplasmic reticulum," *American Journal of Physiology-Renal Physiology*, vol. 309, no. 4, pp. F318–F331, 2015.

[41] T. T. Renault, L. M. Dejean, and S. Manon, "A brewing understanding of the regulation of Bax function by Bcl-xL and Bcl-2," *Mechanism of Ageing and Development*, vol. 161, pp. 201–210, 2017.

[42] I.-G. Ko, J.-J. Jin, L. Hwang et al., "Adenosine A2A receptor agonist polydeoxyribonucleotide alleviates interstitial cystitis-induced voiding dysfunction by suppressing inflammation and apoptosis in rats," *Journal of Inflammation Research*, vol. 14, pp. 367–378, 2021.

[43] M. Lam, D. A. Lawrence, A. Ashkenazi, and P. Walter, "Confirming a critical role for death receptor 5 and caspase-8 in apoptosis induction by endoplasmic reticulum stress," *Cell Death & Differentiation*, vol. 25, no. 8, pp. 1530-1531, 2018.

[44] X. Li, F. Fang, Y. Gao et al., "ROS induced by killer red targeting mitochondria (mtKR) enhances apoptosis caused by radiation via cyt c/caspase-3 pathway," *Oxidative Medicine and Cellular Longevity*, vol. 2019, Article ID 4528616, 11 pages, 2019.

[45] Y. Zhang, C. Ma, C. Liu, and F. Wei, "Luteolin attenuates doxorubicin-induced cardiotoxicity by modulating the PHLPP1/AKT/Bcl-2 signalling pathway," *PeerJ*, vol. 8, p. e8845, 2020.

[46] B. Wu, H. Song, M. Fan et al., "Luteolin attenuates sepsis induced myocardial injury by enhancing autophagy in mice," *International Journal of Molecular Medicine*, vol. 45, no. 5, pp. 1477–1487, 2020.

[47] B. Cao, T. Wang, Q. Qu, T. Kang, and Q. Yang, "Long noncoding RNA SNHG1 promotes neuroinflammation in Parkinson's disease via regulating miR-7/NLRP3 pathway," *Neuroscience*, vol. 388, pp. 118–127, 2018.

[48] W. J. Li, M. K. Shin, and S. J. Oh, "Poly(ADP-ribose) polymerase is involved in the development of diabetic cystopathy via regulation of nuclear factor kappa B," *Urology*, vol. 77, no. 5, pp. 1265–1268, 2011.

[49] M. Aoki, T. Nata, R. Morishita et al., "Endothelial apoptosis induced by oxidative stress through activation of NF-κB," *Hypertension*, vol. 38, no. 1, pp. 48–55, 2001.

[50] P. P. Tak and G. S. Firestein, "NF-κB: a key role in inflammatory diseases," *Journal of Clinical Investigation*, vol. 107, no. 1, pp. 7–11, 2001.

Hindawi
Evidence-Based Complementary and Alternative Medicine
Volume 2021, Article ID 2898995, 14 pages
https://doi.org/10.1155/2021/2898995

Research Article

Quercetin Reduces Oxidative Stress and Apoptosis by Inhibiting HMGB1 and Its Translocation, Thereby Alleviating Liver Injury in ACLF Rats

Peng Fang,[1] Bo Dou,[2] Jiajun Liang,[2] Weixin Hou,[2] Chongyang Ma,[2] and Qiuyun Zhang[2]

[1]*Department of Infectious Diseases, The First Affiliated Hospital of Zhejiang Chinese Medical University, Hangzhou 310006, Zhejiang Province, China*
[2]*Beijing Key Lab of TCM Collateral Disease Theory Research, School of Traditional Chinese Medicine, Capital Medical University, Beijing 100069, China*

Correspondence should be addressed to Qiuyun Zhang; zhangqiuyun8202@aliyun.com

Received 12 June 2021; Accepted 5 October 2021; Published 25 October 2021

Academic Editor: Omayma Eldahshan

Background. Acute on chronic liver failure (ACLF) is a syndrome of acute liver failure that occurs on the basis of chronic liver disease, which is characterized by a rapid deterioration in a short period and high mortality. High mobility group box 1 (HMGB1) may be involved in the pathological process of ACLF; its specific role remains to be further elucidated. Our previous studies have shown that quercetin (Que) exerts anti-oxidant and anti-apoptotic effects by inhibiting HMGB1 in vitro. The present study aimed to investigate the effect of Que on liver injury in ACLF rats. *Methods*. The contents of ALT, AST, TBiL, and PT time of rats in each group were observed. HE staining was used to detect liver pathology. The levels of oxidative stress indicators such as MDA, GSH, and 4-HNE in the rat liver were detected. TUNEL assay was used to detect apoptosis in rat hepatocytes. Immunofluorescence and western blot analysis were performed to explore the protective effect of Que on ACLF rats and the underlying mechanism. *Results*. The results showed that Que could reduce the increase of serum biochemical indices, improve liver pathology, and reduce liver damage in ACLF rats. Further results confirmed that Que reduced the occurrence of oxidative stress and apoptosis of hepatocytes, and these reactions may aggravate the progress of ACLF. Meanwhile, the results of immunofluorescence and western blotting also confirmed that the expression of HMGB1 and extranuclear translocation in ACLF rat hepatocytes were significantly increased, which was alleviated by the treatment of Que. In addition, when cotreated with glycyrrhizin (Gly), an inhibitor of HMGB1, the inhibition of Que on HMGB1 and its translocation, apoptosis and oxidative stress, and the related proteins of HMGB1-mediated cellular pathway have been significantly enhanced. *Conclusion*. Thus, Que alleviates liver injury in ACLF rats, and its mechanism may be related to oxidative stress and apoptosis caused by HMGB1 and its translocation.

1. Introduction

Acute on chronic liver failure (ACLF) refers to a syndrome of liver failure caused by various factors on the basis of chronic liver disease, which is manifested by acute jaundice deepening and coagulopathy [1]. It can be complicated by various symptoms such as hepatic encephalopathy, ascites, infection, and extrahepatic organ failure [2]. ACLF is accompanied by rapid deterioration and high mortality in the short term. In Western countries, ACLF is mainly caused by alcoholic liver injury, improper drug use, and infection. In Asia, the main cause is hepatitis virus, and about 80% of patients are caused by acute exacerbation of HBV infection, followed by damage from drugs and hepatotoxic substances [3]. A study on hospitalized patients with liver cirrhosis in the United States showed that the incidence of ACLF among hospitalized patients with cirrhosis was 26.39%, and the 90-day mortality rate was 40.02% [4, 5]. Another 10-year cohort study conducted in China showed that the 60-day mortality rate of ACLF patients who did not undergo liver

transplantation was 37.4% [6]. Even though the East and West have different understanding and definitions of ACLF, the mortality rate of ACLF is extremely high in both parties [7].

Although the pathogenesis of ACLF is poorly understood, however, the release of damage-associated molecular patterns (DAMPs) caused by immune system imbalance and inflammatory response has been confirmed to aggravate the pathological process of ACLF [8]. High mobility group box 1 (HMGB1), an evolutionarily conserved nuclear DNA binding protein, is widely present in eukaryotic cells and has important biological activities both inside and outside the cell [9, 10]. Once released outside the cell membrane, it can also act as DAMP. Many convincing evidence indicate that the pathological process of ACLF is affected by HMGB1 [11, 12].

Quercetin (3,3′,4′,5,7-pentahydroxyflavone, Que), a typical flavonol-type flavonoid, is also considered as a potential inhibitor of HMGB1 [13]. Several research suggest that Que has a wide range of biological effects such as anti-oxidant, anti-inflammatory, and anti-apoptosis [14, 15]. Supplementing the diet with Que has beneficial effects on many liver diseases [16]. Que improves liver cell damage by inhibiting inflammation, oxidative stress, and cell apoptosis, thereby reducing liver damage caused by various hepatoxins in vivo [17–19]. As an effective phytochemical component for the treatment of various liver diseases, it has been studied in hepatitis, acute liver failure, and fibrosis [13, 20, 21]. Our previous studies have shown that Que exerts anti-oxidant and anti-apoptotic effects via inhibiting HMGB1, thereby protecting the liver cell from damage caused by D-GaLN in vitro [22]. In the present ACLF rat model, the application of D-GaLN is the main stimulating factor for acute liver injury. However, whether Que can reduce liver injury in ACLF rats has not yet been adequately studied. In the present study, we investigated the protective effect of Que on liver injury in ACLF rats, following the research method of the hepatoprotective effect of flavonoids [23]. In addition, an exact inhibitor of HMGB1 was combined to further verify the hypothesis that HMGB1 plays an important role in the disease process of ACLF and the beneficial therapeutic effect of its inhibition.

2. Materials and Methods

2.1. Chemicals and Regents. Que was obtained from Sigma-Aldrich (St. Louis, USA; cat: Q4951); its purity is ≥95%. Human serum albumin (HSA; cat: A9731), D-galactosamine (D-GaLN; cat:G1639), and lipopolysaccharides (LPS; cat:L3012) were also obtained from Sigma-Aldrich (St. Louis, USA). Anti-Bcl-2 (cat: ab19645), anti-Bax (cat: ab32503), anti-HMGB1 (cat:ab79823), anti-iNOS (cat: ab49999), anti-COX-2 (cat:ab15191), and anti-4HNE (cat: ab48506) were obtained from Abcam (Shanghai, China). Anti-TLR-4 (cat: SC-293072) was obtained from Santa Cruz Biotechnology (Santa Cruz, USA). Anti-caspase-9 (cat: #9508), anti-caspase-3 (cat: #9662), anti-NF-κB p65 (cat:#8242) were obtained from Cell Signaling Technology (Boston, USA).

2.2. Experimental Animals. Ninety male Wistar rats weighing 200 to 240 g were purchased from Vital River Laboratory Animal Technology Co. Ltd. (Beijing, China). The animals were housed in a specific pathogen-free environment under constant temperature (25 ± 3°C) and humidity (60 ± 10%), with a 12 h light/dark cycle. All animals were acclimated to the environment for 5 days before the experiments. All of the procedures were performed according to the Institutional Guidelines for the Care and Use of Laboratory Animals and were authorized by the Animal Ethics Committee of Capital Medical University (NO.AEEI-2019-067).

2.3. Animal Treatment. The ACLF rat model was established as we described previously [24]. Briefly, acute liver failure was induced on the basis of chronic immune liver fibrosis. As shown in (Figure 1), except for the normal control group ($n = 10$), the remaining 80 rats were injected with HSA to induce immune liver injury. After 6 weeks, 50 survived rats with liver fibrosis confirmed by Masson's trichrome staining [25] were selected, and then the rats were injected intraperitoneally with 400 mg/kg D-GaLN and 100 μg/kg LPS to establish the ACLF model. Then the rats were randomly divided into 5 groups: (1) ACLF group, rats were intragastric administration of an equal volume of normal saline solution and intraperitoneal injection of an equal amount of vehicle; (2) low-dose Que treatment group (Que-25), rats were intragastric administration of 25 mg/kg Que for 7 consecutive days and intraperitoneal injection of an equal amount of vehicle; (3) middle dose of Que treatment group (Que-50), treatment was the same as the Que-25 group, while the dose of Que was 50 mg/kg; (4) high dose of Que treatment group (Que-100), treatment was the same as the Que-25 group, while the dose of Que was 100 mg/kg; and (5) HMGB1 inhibitor intervention group (Que-100 + Gly), rats were intragastric administration of 100 mg/kg Que and intraperitoneal injection of 50 mg/kg glycyrrhizin (Gly) for 7 consecutive days. Gly is a direct inhibitor of HMGB1, which can bind to HMGB1 directly, interacting with two shallow concave surfaces formed by the two arms of both HMG boxes [26, 27]. At the end of the experiment, there were 10 survivors in the normal control group, 5 in the ACLF group, 6 in Que-25 group, 6 in the Que-50 group, 7 in the Que-100 group, and 7 in the Que-100 + Gly group. Before tissue collection, rats were deeply anesthetized by intraperitoneal injection of 1% pentobarbital sodium (40 mg/kg). After the anesthesia was stable, blood was collected from the abdominal aorta, and the serum collected by centrifugation was stored at −80°C. The liver tissue was quickly collected and weighed, frozen in liquid nitrogen, and stored at −80°C. Then the rats were euthanized by cervical dislocation.

2.4. Determination of Serum Biochemical Indices. Blood samples were collected in tubes and centrifuged for 15 min at 3,000 rpm (Sigma-Aldrich, USA) to collect serum. The levels of alanine aminotransferase, aspartate aminotransferase (AST), and total bilirubin (TBiL) in serum were detected

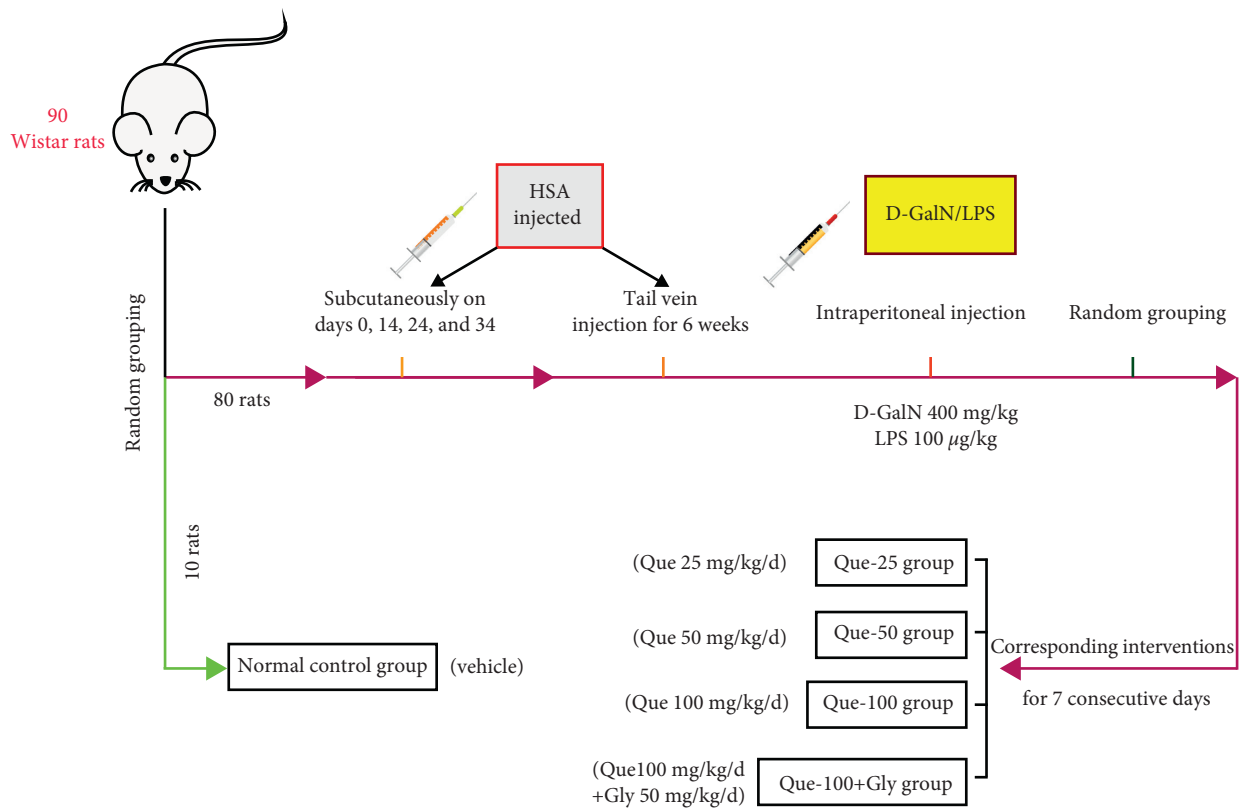

Figure 1: Establishment of ACLF rat model and experimental intervention. The rats were injected with HSA to induce immune hepatic fibrosis. At first stage, rats were sensitized by subcutaneous injection of HSA solution (0.5 ml, HSA 4 mg) for a total of 4 injections (days 0, 14, 24, and 34). Subsequently, tail vein injection was performed twice a week for 6 weeks (0.5 ml, gradually increased the HSA dose, 2.5 mg⟶3 mg⟶3.5 mg⟶4 mg⟶4.5 mg, and then maintained at 4.5 mg), and the normal group was injected with the same amount of normal saline. And then, intraperitoneal injection of 400 mg/kg D-GaLN and 100 μg/kg LPS caused acute liver injury to establish the ACLF model. Finally, the rats were randomly divided into 5 intervention groups: receiving Que and/or glycyrrhizin, or vehicle treatment for 7 consecutive days. The normal control group underwent the same procedures without therapeutic intervention.

with an automatic analyzer (Hitachi, Inc., Japan) using commercial kits following the manufacturer's instructions.

2.5. Determination of Prothrombin Times. Blood samples were collected in anti-coagulant tubes containing sodium citrate solution and centrifuged for 15 min at 3,000 rpm (Sigma-Aldrich, USA) to collect plasma. Prothrombin times (PTs) were measured using a kit (Nanjing, China) according to the manufacturer's instructions.

2.6. Liver Histological Observation. Left lobes of liver tissues were isolated and fixed immediately with 10% neutral buffered formalin. The paraffin-embedded liver tissue samples were cut into 5 μm thick sections for hematoxylin and eosin (H&E) staining, and then the sections were observed with a pathological section panoramic scanner (Leica Aperio AT2).

2.7. Assessment of Oxidative Stress. The content of hepatic malondialdehyde (MDA) was determined by thiobarbituric acid (TBA) reagent test using a commercial kit (Beyotime, China; cat: S0131). The liver homogenate was mixed with TBA buffer, incubated at 95°C for 1 hour, and then incubated on ice to stop the reaction. The mixture was centrifuged (4,000 rpm; 10 min), and the absorbance was measured by a microplate reader at a wavelength of 532 nm. The results were presented as nmol/mg protein.

The level of anti-oxidant enzyme-reduced glutathione (GSH) content was determined by the 5,5'-dithiobis-(2-nitrobenzoic acid) (DTNB) reactant test using a commercial kit (Beyotime, China; cat: S0053). Briefly, after mixing liver homogenate with DTNB stock solution and reacted, the absorbance was measured at a wavelength of 412 nm by a microplate reader. The GSH content in the sample was calculated according to the standard curve and presented as nmol/mg protein.

2.8. Immunofluorescence Analysis. Briefly, after dewaxing and antigen retrieval, the paraffin section was blocked by incubating with bovine serum albumin (BSA). Then the sections were individually incubated with anti-4-hydroxynonenal (4-HNE), anti-TLR-4, and anti-HMGB1 at 4°C overnight. After washing with PBS, the sections were incubated with FITC or TIRTC-labeled secondary antibody for 2 h at 37°C in the dark. Then the sections were washed 3

times with PBS for 5 min each time. Then, the tables were sealed with antifluorescence attenuation sealing solution (containing DAPI). Fluorescence images were collected by using a confocal microscope (Leica TCS SP8), and the results were analyzed using Image J software version 1.80.

2.9. Terminal Deoxynucleotidyl Transferase dUTP Nick End Labeling (TUNEL) Assays. The apoptotic response of hepatocytes was detected with paraffin-embedded sections using a TUNEL assay and Fluorescein In Situ Cell Death Assay Kit (KeyGEN BioTECH, China; cat: KGA7072) according to the manufacturer's instructions. The positive cells were counted in 10 random fields at 400X magnification, and 3 sections of each sample were analyzed.

2.10. Western Blot Analysis. Liver proteins were homogenized and then collected by using RIPA lysis buffer. Cytoplasmic and nuclear proteins were isolated using nuclear and cytoplasmic protein extraction kits (Beyotime, China; cat: P0028), according to the manufacturer's instructions. The BCA protein assay reagent kit was used to determine the concentration of total liver protein and the extracted nuclear protein and cytoplasmic protein. An equal amount of protein (30 μg) was separated by 8–12% SDS-PAGE and transferred into PVDF membranes. Next, membranes were incubated with Tris-buffered saline, containing 5% non-fat dry milk for blocking purposes at room temperature for 1 hour. Then, membranes were incubated overnight at 4°C with primary antibodies directed against HMGB1, TLR-4, caspase-3, caspase-9, Bax, Bcl-2, NF- kB p65, iNOS, and COX-2. After washing with TBST, the membrane was incubated with a secondary antibody for 1 h at room temperature. Finally, the reaction was detected with an enhanced chemiluminescent reagent (NCM Biotech, China; cat: P10100). An ImageQuantLAS4000 chemiluminescence imaging system was used to visualize the target proteins (GE Co., USA), and densitometry was performed using the Image J software version 1.80.

2.11. Statistical Analysis. All data in the present study were analyzed using Prism 8.0 and expressed as the mean ± standard deviation (SD). Differences between groups were determined by ANOVA with Tukey's post hoc test. $p < 0.05$ was regarded as statistically significant.

3. Results

3.1. Que Alleviates Hepatic Injury in ACLF Rats. As shown in Figures 2(a)–2(d), serum ALT, AST, and TBiL were significantly increased, whereas PT was significantly prolonged in the ACLF model group, and these increases were attenuated dose dependently by Que. Furthermore, H&E staining was performed to verify the extent of liver injury. In the normal control group, clear lobular structures could be observed, and hepatocytes were arranged in an orderly manner. In the ACLF group, disordered cell arrangement, inflammatory cell infiltration, hepatic sinus expansion and bleeding, and numerous necrotic liver cells were observed. However, the treatment with Que at the dose of 25 mg/kg, 50 mg/kg, and 100 mg/kg ameliorated liver pathological damage, and the dose of 100 mg/kg Que was more obvious (Figure 2(e)). On the basis of the results of liver function and pathological analysis, 100 mg/kg Que was chosen as the optimal dose for further studies. What's more, when compared with Que-100, the ALT, AST, TBiL, and PT were further decreased after addition with Gly, an inhibitor of HMGB1, and the amelioration of pathologies showed the same performance.

3.2. Que Reduces Oxidative Stress Damage in ACLF Rats. To assess the oxidative stress damage, the levels of MDA and GSH in the liver of rats were detected. The MDA level (Figure 3(a)) was significantly increased, and the GSH level (Figure 3(b)) was decreased in the ACLF group. However, the intervention of Que reduced the increase in MDA and increased the level of GSH. The level of 4-HNE accumulation, the main product of lipid peroxidation [28], was measurement by IF. Massive 4-HNE accumulation was in hepatocytes of the ACLF group, which decreased after Que intervention. What's more, the above-mentioned effects of Que were significantly enhanced by Gly (Figures 3(c) and 3(d)).

3.3. Que Inhibits Hepatocyte Apoptosis in ACLF Rats. Next, the extent of apoptosis in liver tissues was evaluated by TUNEL staining, which labels 3′-OH ends of DNA by ribonuclease that are activated during apoptosis. Our results showed that the number of TUNEL-positive cells in the ACLF group dramatically increase, while Que blocked the changes significantly (Figures 4(a) and 4(c)). Furthermore, we performed western blot to detect changes in apoptosis-related proteins. As results (Figures 4(b) and 4(d)–4(g)) shown, the upregulation of Bax, the ratio of cleaved caspase-9 and cleaved caspase-3, and the downregulation of anti-apoptotic protein Bcl-2 were observed in the ACLF group, which were reversed by Que treatment. Moreover, after addition with Gly, this anti-apoptotic effect was enhanced.

3.4. Que Decreases the Expression and Translocation of HMGB1 in Hepatocytes of ACLF Rats. On the basis of our previous research, Que could inhibit HMGB1-mediated hepatocyte damage in vitro [22]. Therefore, in order to determine whether the improvement effect of ACLF by Que is related to HMGB1, we performed IF and western blot to detect the expression of HMGB1. IF showed the increased expression and distribution in the cytoplasm of HMGB1 in the ACLF group (Figure 5(a)). Western blot also confirmed that the total amount of HMGB1 and the ratio of HMGB1 in the cytoplasm to the total were increased (Figures 5(b)–5(f)). The treatment of Que reduced the increase and translocation of HMGB1. While cotreated with Gly, the inhibition was significantly enhanced.

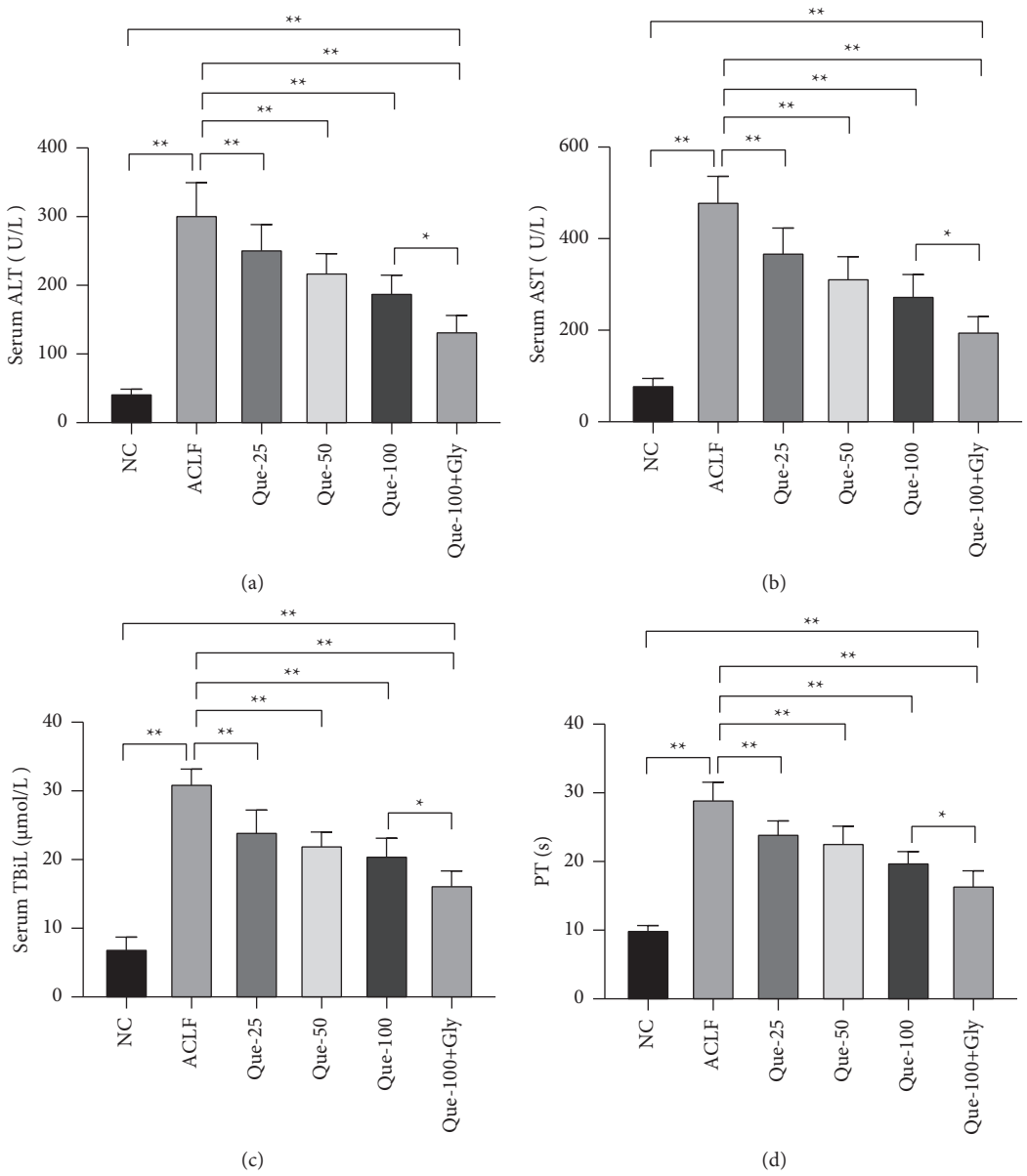

Figure 2: Continued.

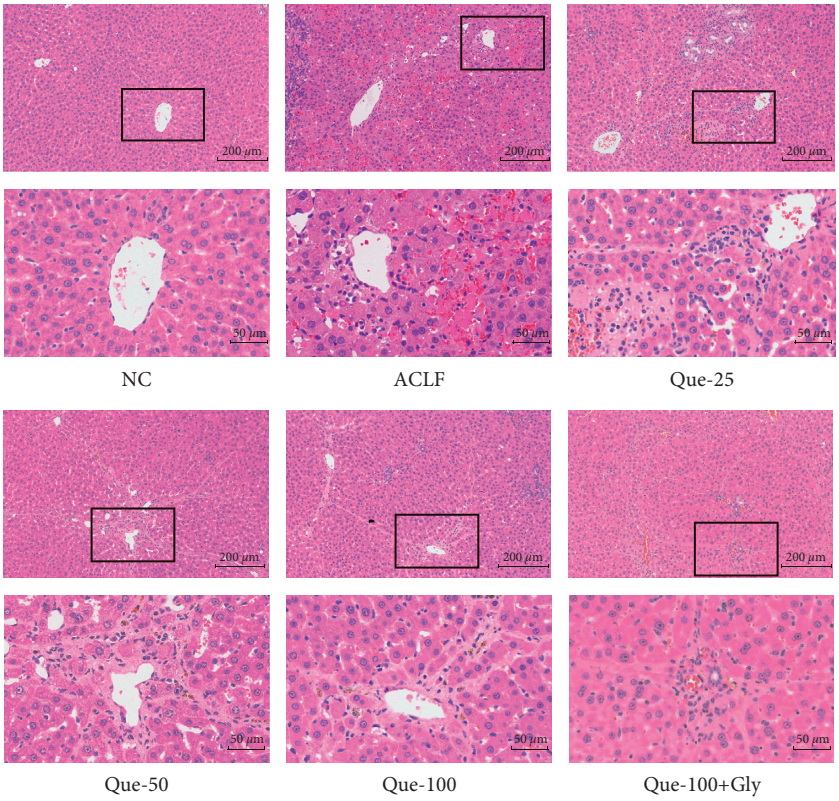

Figure 2: Effects of different doses of Que on liver function and pathology in acute on chronic liver failure (ACLF) rats: (a) the serum levels of alanine aminotransferase, (b) aspartate aminotransferase (AST), (c) total bilirubin (TBiL), (d) prothrombin times (PTs), and (e) hematoxylin and eosin (H&E) staining. Magnification 200X and 800X; scale bar: 200 μm and 50 μm; data are presented as the mean ± SD ($^{*}p < 0.05$, $^{**}p < 0.01$, representative of 5–10 rats/group).

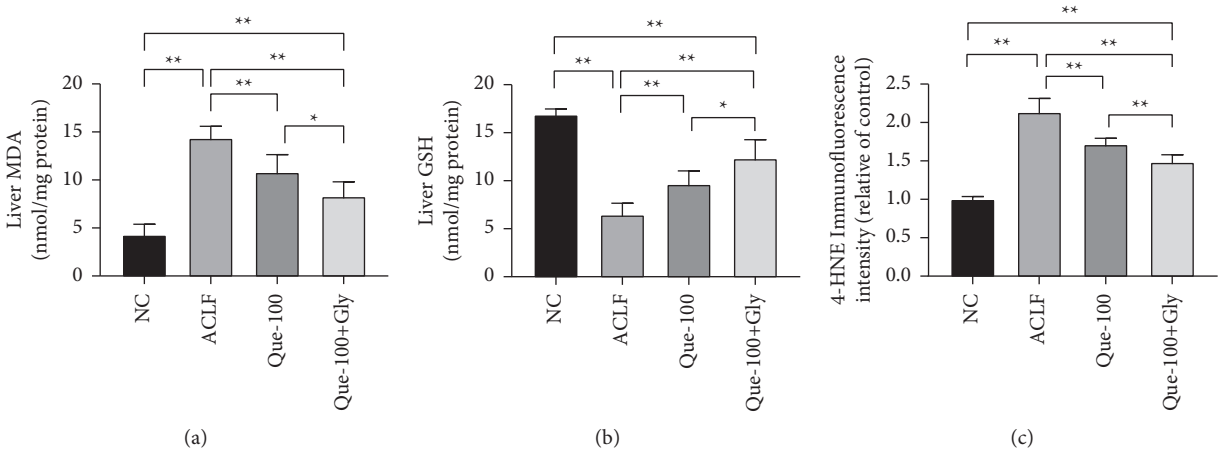

Figure 3: Continued.

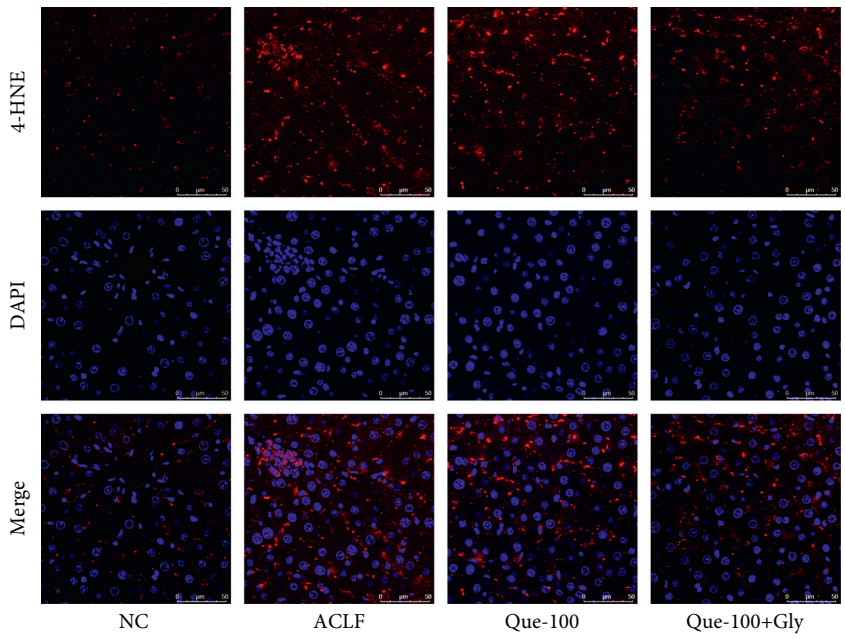

(d)

Figure 3: Effects of Que on oxidative stress damage in ACLF rats. The content of hepatic malondialdehyde (MDA); (b) glutathione (GSH); (c, d) immunofluorescence analysis of 4-hydroxynonenal (4-HNE). Magnification 400X; scale bar: 50 μm; data are presented as the mean ± SD ($^{*}p < 0.05$, $^{**}p < 0.01$, representative of 5–10 rats/group).

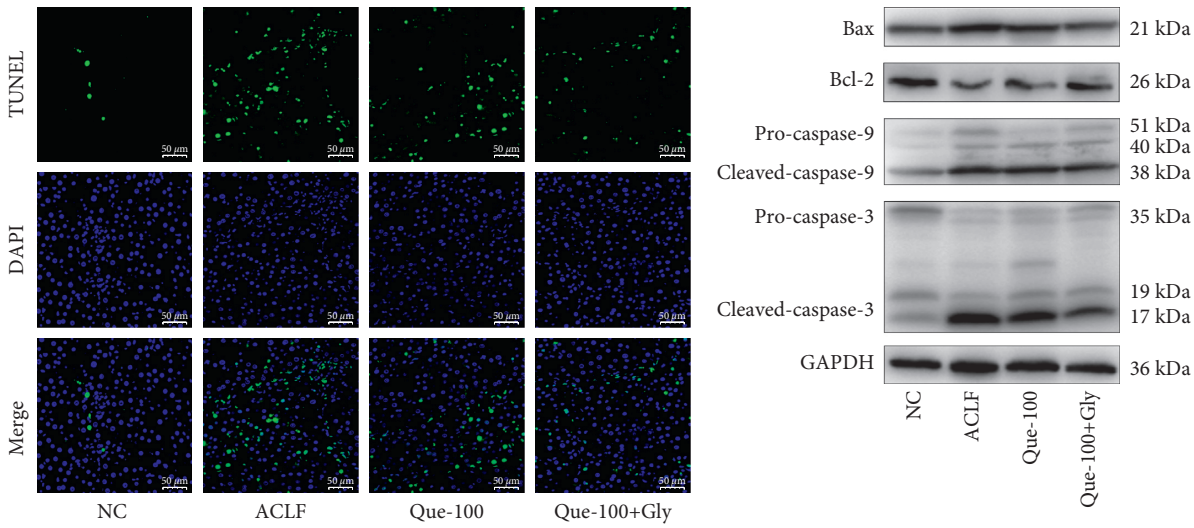

(a) (b)

Figure 4: Continued.

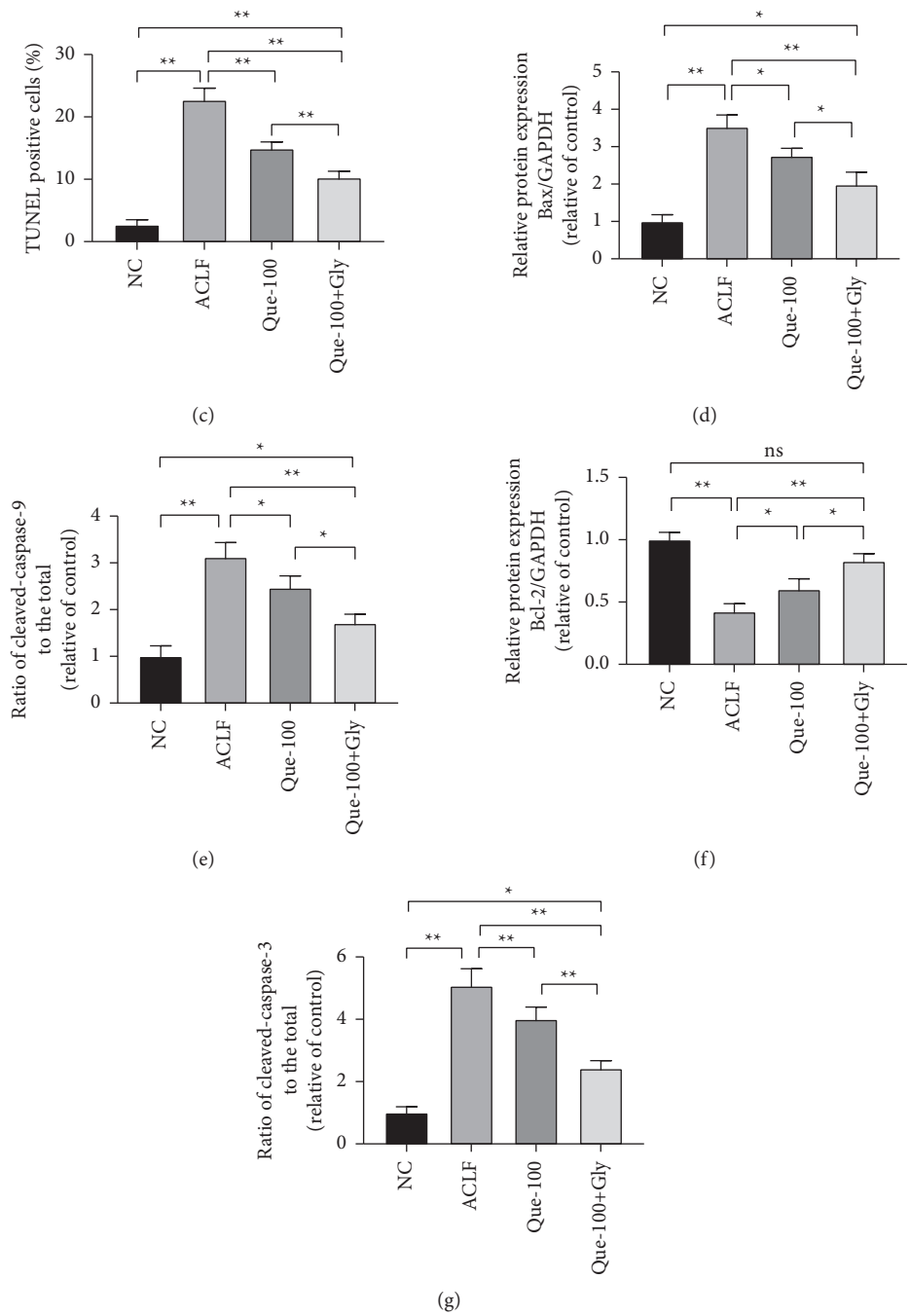

Figure 4: Effects of Que on apoptosis in ACLF rats. (a, c) Representative stainings and positive cells of TUNEL assays. The positive cells were counted in 10 random fields at 400X magnification, and 3 sections of each sample were analyzed, representative of 5–10 rats/group, scale bar: 50 μm. (b, d, e, f) Representative western blot analyses of apoptosis-related proteins (Bax, Bcl-2, Pro-caspase-9, caspase-9, Pro-caspase-3, and caspase-3). Data are presented as the mean ± SD ($^{*}p < 0.05$, $^{**}p < 0.01$). The blots shown are representative of 3 independent experiments.

3.5. Que Inhibits HMGB1-Mediated Signaling Pathway. Next, to investigate the molecular mechanism of Que on HMGB1-mediated oxidative stress and apoptosis in ACLF, we analyzed changes in proteins expression of related pathways. The expression of TLR-4, an HMGB1 receptor, was significantly increased (Figures 6(b) and 6(c)), and IF showed the extensive expression of TLR-4 in the cytoplasm of damaged hepatocytes. The treatment of Que reduced this kind of expression (Figure 6(a)). Moreover, the expressions of related pathway proteins NF-kB-p65, iNOS, and Cox-2 were also increased in the ACLF group, and the treatment of Que reduced this increase of expression. What's more, the cotreatment of Gly, the inhibition effect on the expression of TLR-4, and related pathway proteins were significantly enhanced over that of Que alone (Figures 6(b) and 6(d)–6(f)).

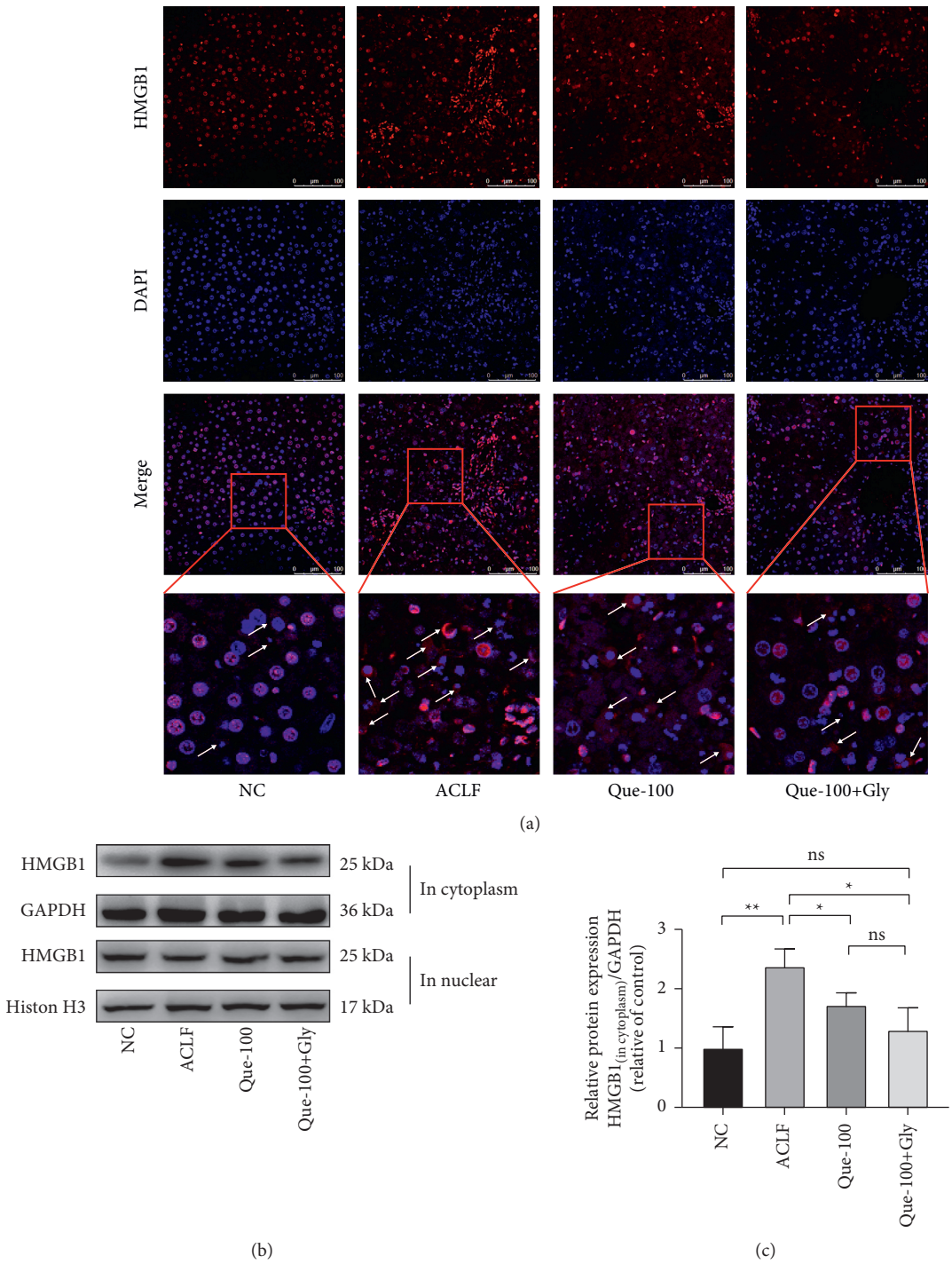

Figure 5: Continued.

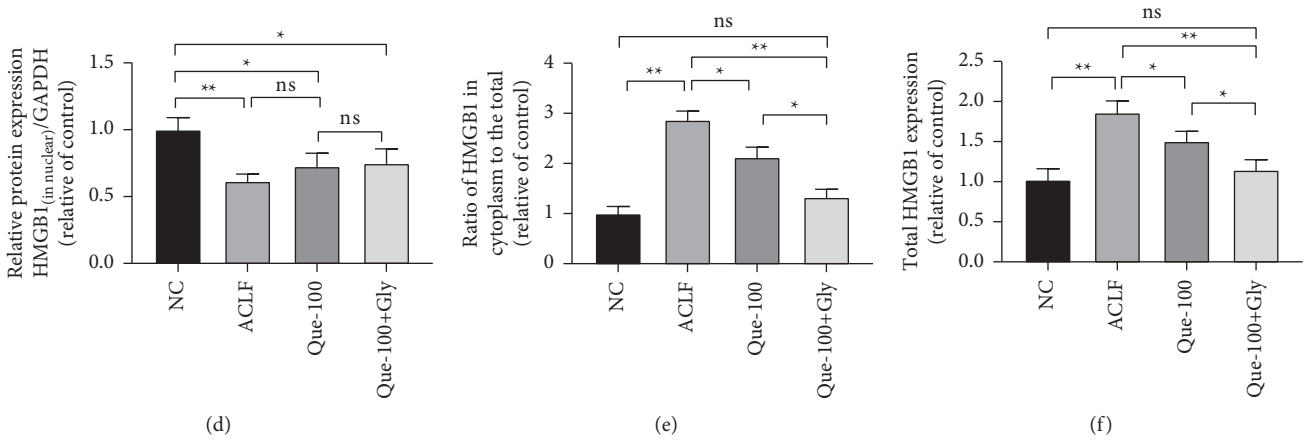

Figure 5: Effects of Que on the expression and translocation of HMGB1 in ACLF rats. (a) Immunofluorescence staining of HMGB1 expression and translocation. Arrows indicate the HMGB1 in cytoplasm. Magnification 400 (X); scale bar: 100 μm. (b) Representative immunoblots for the HMGB1 in the nucleus; HMGB1 in the cytoplasm. (c, d) HMGB1 in the cytoplasm and nucleus under different treatments under different treatment by western blot assay. (e, f) Calculated results of the ratio of HMGB1 in the cytoplasm and the total expression of HMGB1. According to the different positions of HMGB1 expressed in the cytoplasm and nucleus, GAPDH and histone H3 were selected as housekeeping proteins. Data are presented as the mean ± SD ($^{*}p < 0.05$, $^{**}p < 0.01$). The blots shown are representative of 3 independent experiments.

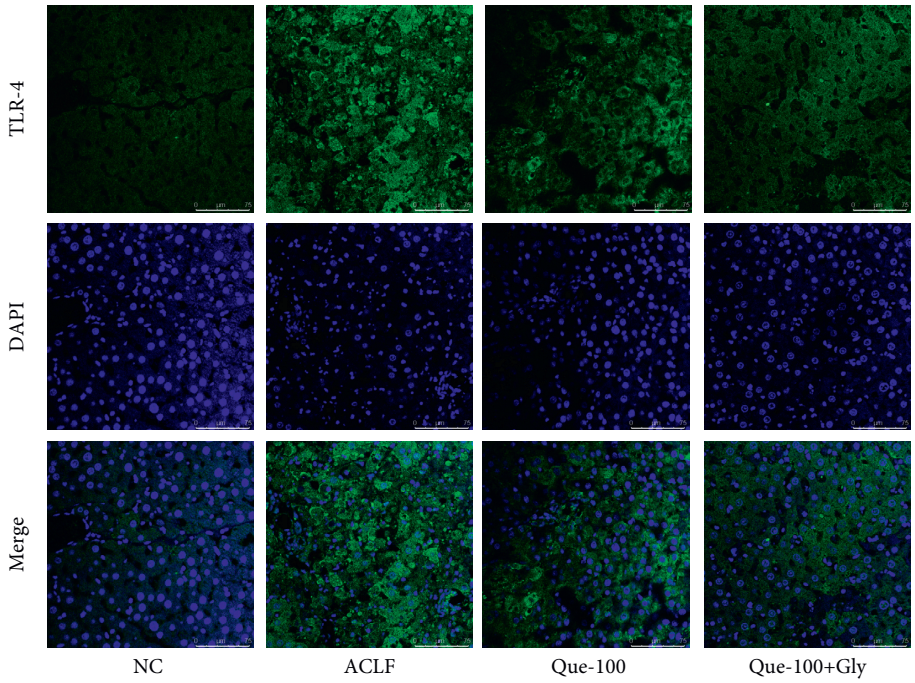

(a)

Figure 6: Continued.

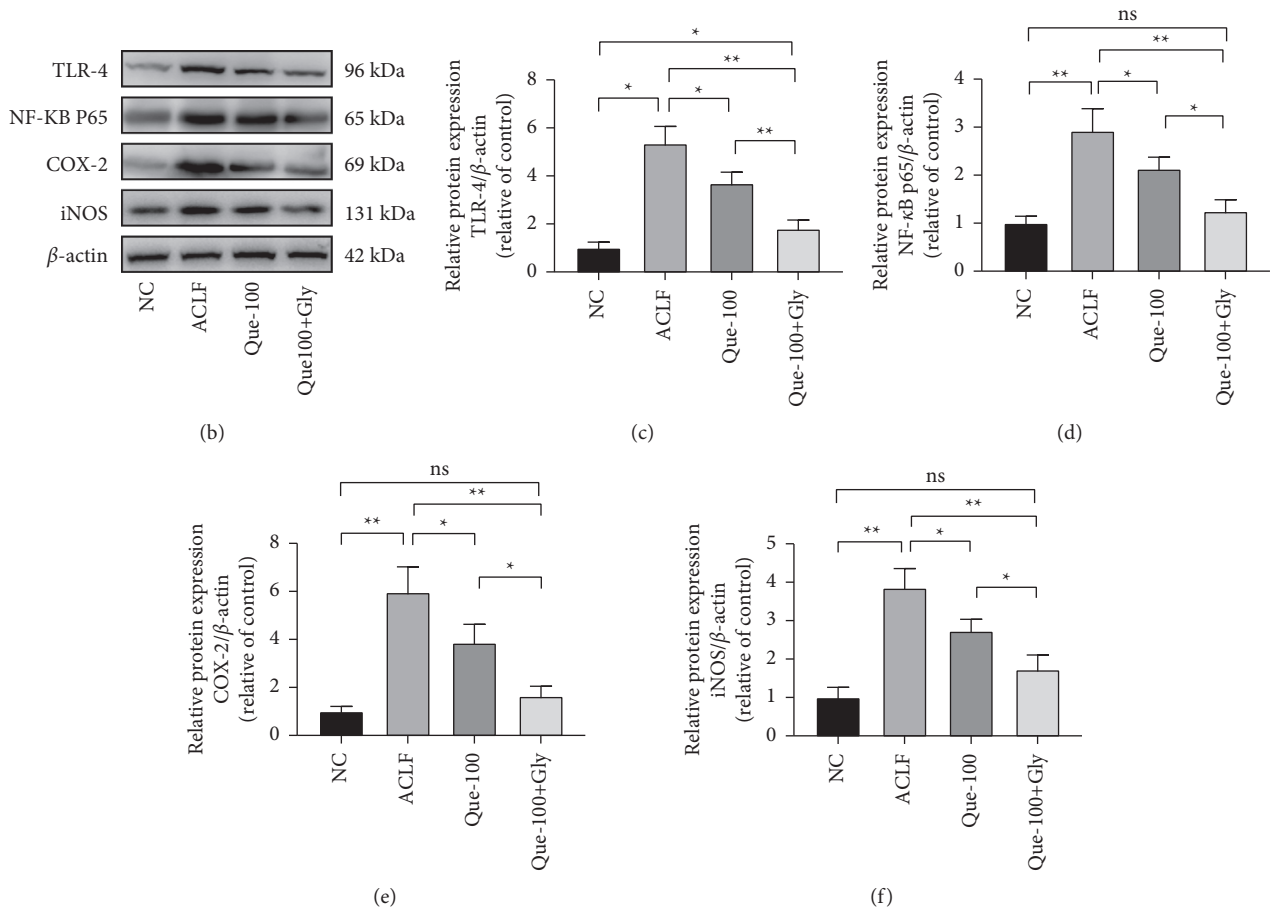

Figure 6: Effects of Que on the HMGB1 signaling pathway. (a) Immunofluorescence staining of TLR-4 receptor expression under different treatment conditions. Magnification 400X; scale bar: 75 μm. (b–f) The TLR-4, NF-κB P65, iNOS, and COX-2 proteins expression levels were evaluated by western blot assay. Data are presented as the mean ± SD ($^{*}p < 0.05$, $^{**}p < 0.01$). The blots shown are representative of 3 independent experiments.

4. Discussion

At present, the pathophysiology of ACLF remains poorly understood, and pharmacological approaches to reduce mortality from ACLF are still lacking. However, increasing evidence indicate that HMGB1 may be involved in the pathological progress of liver failure [11, 29]. A study on the detection of hepatocyte death biomarkers in patients with hepatitis B virus-related ACLF (HBV-ACLF) finds that the serum HMGB1 level of HBV-ACLF patients is significantly higher than that of healthy controls and chronic hepatitis B (CHB) patients [30]. Moreover, the increased expression of HMGB1 is significantly correlated with the occurrence of ACLF [31]. A meta-analysis also indicates that HMGB1 may be a useful therapeutic target for severe hepatitis B and ACLF [32]. Meanwhile, the translocation of HMGB1 to extranuclear does not exist in hepatocytes of healthy people and CHB patients. But, in ACLF patients, even in their non-necrotic hepatocytes, a lot of extranuclear translocations occurred. The nucleus-to-cytoplasm translocation of HMGB1 is a key process prior to its extracellular secretion [33].

The extracellular HMGB1, which acts as a DAMP factor, plays an important role in various liver injuries. Especially in severe liver injury, the level of HMGB1 is significantly increased [34]. However, previous studies have focused more on the proinflammatory effects of HMGB1. The increasing credible evidence confirms that HMGB1 is also essential to mediate the occurrence of oxidative stress [35]. In vitro, recombinant HMGB1 caused oxidative stress with TLR-4-dependent activation of NADPH oxidase [36]. What's more, HMGB1 activates the TLR-4 signal transduction pathway and induces the translocation of NF-κB-p65 subunits to the nucleus, thereby increasing its transcriptional activity [37]. Thus, the activation of COX-2 and iNOS is induced, leading to the accumulation of 4-HNE, causing lipid peroxidation and oxidative stress [38, 39].

For liver failure, excessive apoptosis is also one of the main ways of cell death, which is also confirmed in our current experiment. And, the release of HMGB1 is also present in apoptotic cells. HMGB1 can be released in late apoptotic cells by binding to DNA [40]. Macrophages are also activated by apoptotic cells to release HMGB1 [41]. After being released, caspase-3 dependent apoptosis can be

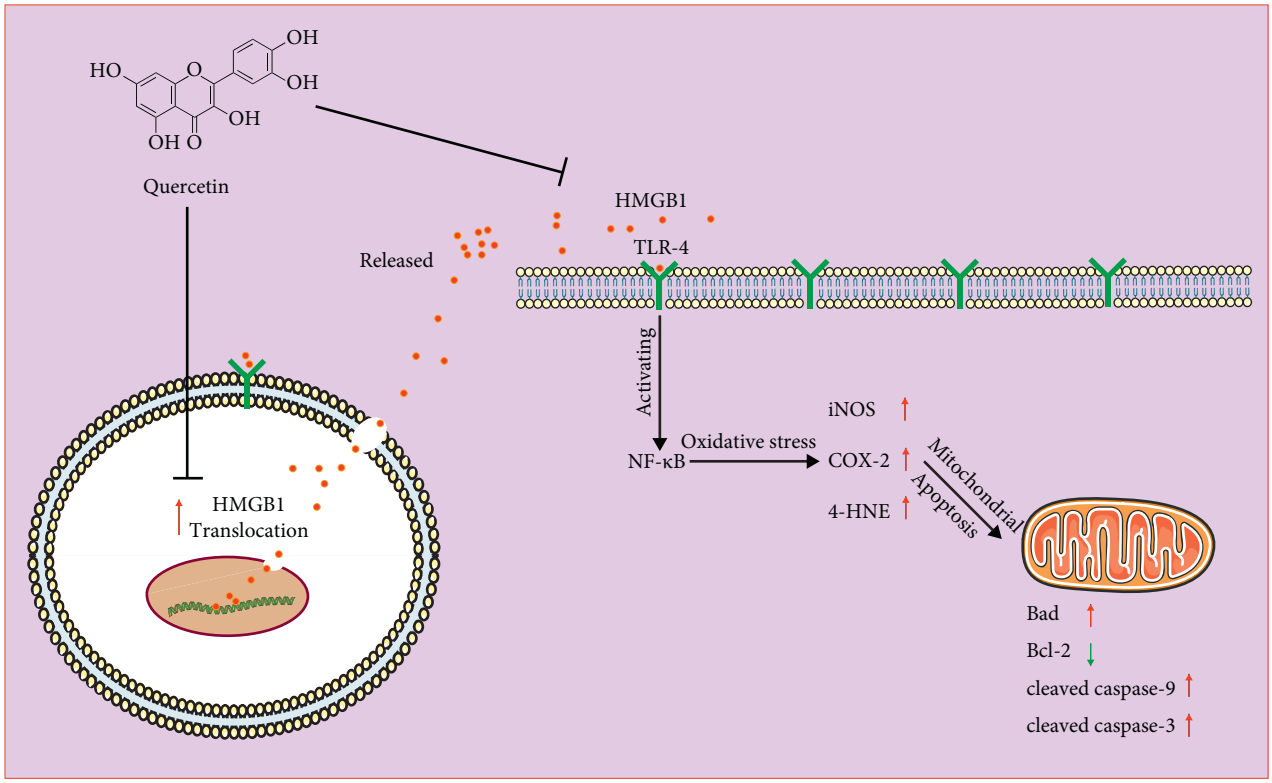

Figure 7: The mechanism of Que attenuating liver injury in ACLF rats by inhibiting HMGB1 and its translocation.

activated by HMGB1 through the TLR-4 pathway [42]. Moreover, it has been confirmed that blocking HMGB1 can inhibit caspase-3 activation, thereby reducing cell apoptosis [43]. Oxidative stress regulates the mitochondrial membrane potential, leading to the initiation of apoptosis in the mitochondrial pathway [44]. Mitochondria plays an important role in apoptosis by relocating intermembrane mitochondrial proteins, such as Bcl-2 and Bax [45]. Here, in the present study, we found that HMGB1 may play a regulatory role in hepatocyte apoptosis and oxidative stress in ACLF rats. Therefore, we hypothesize that HMGB1-mediated apoptosis is caused by the mitochondrial release of apoptotic proteins caused by oxidative stress. To our best knowledge, this mechanism by which HMGB1 is involved in ACLF pathological progression is confirmed for the first time.

Que, as an effective phytochemical ingredient for the treatment of various liver diseases, has been proved to have hepatocellular protection in vivo and in vitro [46]. Que inhibits the production of oxidative markers and the activation of NF-κB and MAPK signaling pathways; thus, the expression of apoptosis-related proteins has been induced in acute liver failure (ALF) mice induced by LPS/D-GalN [21]. Que also inhibits the translocation and release of HMGB1 in macrophages induced by LPS and protects mice from immune liver injury induced by Con-A by inhibiting the HMGB1-TLR2/TLR4-NF-κB pathway [20]. Our previous research shows that Que inhibits HMGB1-mediated oxidative stress and apoptosis, thereby protecting L02 cells from D-GaLN mediated damage in vitro [22]. In the present study, we confirmed that Que could reduce the pathological damage, the occurrence of oxidative stress, and apoptosis in ACLF rats for the first time. The treatment of Que also reduced the translocation and overexpression of HMGB1, and its signaling pathway proteins mediated by it. The cotreatment with Gly, a direct HMGB1 inhibitor, further inhibited HMGB1 and its translocation, as well as the oxidative stress and apoptosis mediated by it, when compared with Que alone. Therefore, part of the mechanism of Que attenuating ACLF may be related to inhibiting HMGB1 and its translocation, thereby the oxidative stress and apoptosis mediated by it (Figure 7). However, there are some limitations in current research, such as the effect of Que on ACLF rats after HMGB1 overexpression or activation was not observed, and also the lack of a group with Gly alone. These should be considered in our future research.

5. Conclusion

In conclusion, our present study confirmed that HMGB1 and its translocation were involved in ACLF, and the specific mechanism may be related to the oxidative stress and apoptosis mediated by it. Thus, this provides further evidence for ACLF treatment with intervention HMGB1 as the target. And also Que may provide a new pharmacological intervention option for ACLF.

Data Availability

The data used to support the findings of this study are available from the corresponding author on reasonable request.

Conflicts of Interest

The authors declare that there are no conflicts of interest.

Authors' Contributions

P.F. and Q.Z. conceived and designed the experiments; X.F., J.L., X.W., and C.M. were involved in the experimental study design, preparation, and review of this manuscript. All the authors have reviewed and approved the final version of the manuscript.

Acknowledgments

This research was funded by Natural Science Foundation of Beijing Municipality (Grant no. 7192024).

References

[1] S. K. Sarin, A. Choudhury, M. K. Sharma et al., "Acute-on-chronic liver failure: consensus recommendations of the Asian Pacific association for the study of the liver (APASL): an update," *Hepatology international*, vol. 13, no. 4, pp. 353–390, 2019.

[2] R. Hernaez, E. Solà, R. Moreau, and P. Ginès, "Acute-on-chronic liver failure: an update," *Gut*, vol. 66, no. 3, pp. 541–553, 2017.

[3] J. S. Bajaj, R. Moreau, P. S. Kamath et al., "Acute-on-Chronic liver failure: getting ready for prime time?" *Hepatology*, vol. 68, no. 4, pp. 1621–1632, 2018.

[4] R. Hernaez, J. R. Kramer, Y. Liu et al., "Prevalence and short-term mortality of acute-on-chronic liver failure: a national cohort study from the USA," *Journal of Hepatology*, vol. 70, no. 4, pp. 639–647, 2019.

[5] E. Levesque, A. Winter, Z. Noorah et al., "Impact of acute-on-chronic liver failure on 90-day mortality following a first liver transplantation," *Liver International*, vol. 37, no. 5, pp. 684–693, 2017.

[6] C. Huang, K. K. Yu, J. M. Zheng, and N. Li, "Steroid treatment in patients with acute-on-chronic liver failure precipitated by hepatitis B: a 10-year cohort study in a university hospital in East China," *Journal of Digestive Diseases*, vol. 20, no. 1, pp. 38–44, 2019.

[7] V. Arroyo, R. Moreau, P. S. Kamath et al., "Acute-on-chronic liver failure in cirrhosis," *Nature Reviews Disease Primers*, vol. 2, no. 1, Article ID 16041, 2016.

[8] X. X. Du, Y. Shi, Y. Yang et al., "DAMP molecular IL-33 augments monocytic inflammatory storm in hepatitis B-precipitated acute-on-chronic liver failure," *Liver International*, vol. 38, no. 2, pp. 229–238, 2018.

[9] H. Wang, O. Bloom, and M. Zhang, "HMG-1 as a late mediator of endotoxin lethality in mice," *Science*, vol. 285, no. 5425, pp. 248–251, 1999.

[10] H. Yang, D. J. Antoine, U. Andersson, and K. J. Tracey, "The many faces of HMGB1: molecular structure-functional activity in inflammation, apoptosis, and chemotaxis," *Journal of Leukocyte Biology*, vol. 93, no. 6, pp. 865–873, 2013.

[11] T. Yamamoto and Y. Tajima, "HMGB1 is a promising therapeutic target for acute liver failure," *Expert Review of Gastroenterology & Hepatology*, vol. 11, no. 7, pp. 673–682, 2017.

[12] H. Yang, H. Wang, S. S. Chavan, and U. Andersson, "High mobility group box protein 1 (HMGB1): the prototypical endogenous danger molecule," *Molecular Medicine*, vol. 21, no. Suppl 1, pp. S6–S12, 2015.

[13] X. Li, Q. Jin, Q. Yao, B. Xu, Z. Li, and C. Tu, "Quercetin attenuates the activation of hepatic stellate cells and liver fibrosis in mice through modulation of HMGB1-TLR2/4-NF-κB signaling pathways," *Toxicology Letters*, vol. 261, pp. 1–12, 2016.

[14] L. G. Costa, J. M. Garrick, P. J. Roquè, and C. Pellacani, "Mechanisms of neuroprotection by quercetin: counteracting oxidative stress and more," *Oxidative Medicine and Cellular Longevity*, vol. 2016, Article ID 2986796, 10 pages, 2016.

[15] Y. Li, J. Yao, C. Han et al., "Quercetin, inflammation and immunity," *Nutrients*, vol. 8, no. 3, p. 167, 2016.

[16] G. D'Andrea, "Quercetin: a flavonol with multifaceted therapeutic applications?" *Fitoterapia*, vol. 106, pp. 256–271, 2015.

[17] M. Abdelhalim, S. Moussa, and H. Qaid, "The protective role of quercetin and arginine on gold nanoparticles induced hepatotoxicity in rats," *International Journal of Nanomedicine*, vol. 13, pp. 2821–2825, 2018.

[18] A. Eftekhari, E. Ahmadian, V. Panahi-Azar, H. Hosseini, M. Tabibiazar, and S. Maleki Dizaj, "Hepatoprotective and free radical scavenging actions of quercetin nanoparticles on aflatoxin B1-induced liver damage: in vitro/in vivo studies," *Artificial Cells, Nanomedicine, and Biotechnology*, vol. 46, no. 2, pp. 411–420, 2018.

[19] D. Tang, R. Kang, W. Xiao et al., "Quercetin prevents LPS-induced high-mobility group box 1 release and proinflammatory function," *American Journal of Respiratory Cell and Molecular Biology*, vol. 41, no. 6, pp. 651–660, 2009.

[20] X. Li, H.-C. Liu, Q.-Y. Yao, B.-L. Xu, S.-C. Zhang, and C.-T. Tu, "Quercetin protects mice from ConA-induced hepatitis by inhibiting HMGB1-TLR expression and down-regulating the nuclear factor kappa B pathway," *Inflammation*, vol. 39, no. 1, pp. 96–106, 2016.

[21] Z. Peng, X. Gong, Y. Yang et al., "Hepatoprotective effect of quercetin against LPS/d -GalN induced acute liver injury in mice by inhibiting the IKK/NF-κB and MAPK signal pathways," *International Immunopharmacology*, vol. 52, pp. 281–289, 2017.

[22] P. Fang, J. Liang, X. Jiang et al., "Quercetin attenuates d-GaLN-induced L02 cell damage by suppressing oxidative stress and mitochondrial apoptosis via inhibition of HMGB1," *Frontiers in Pharmacology*, vol. 11, p. 608, 2020.

[23] J. Yang, D. Xiang, D. Xiang et al., "Baicalin protects against 17α-ethinylestradiol-induced cholestasis via the sirtuin 1/hepatic nuclear receptor-1α/farnesoid X receptor pathway," *Frontiers in Pharmacology*, vol. 10, p. 1685, 2019.

[24] W. Yang, Y. Hao, W. Hou et al., "Jieduan-niwan formula reduces liver apoptosis in a rat model of acute-on-chronic liver failure by regulating the E2F1-mediated intrinsic apoptosis pathway," *Evidence-Based Complementary and Alternative Medicine*, vol. 2019, Article ID 8108503, 11 pages, 2019.

[25] J. C. Iezzoni, "Diagnostic histochemistry in hepatic pathology," *Seminars in Diagnostic Pathology*, vol. 35, no. 6, pp. 381–389, 2018.

[26] L. Mollica, F. De Marchis, A. Spitaleri et al., "Glycyrrhizin binds to high-mobility group box 1 protein and inhibits its

cytokine activities," *Chemistry & Biology*, vol. 14, no. 4, pp. 431–441, 2007.

[27] R. Smolarczyk, T. Cichoń, S. Matuszczak et al., "The role of Glycyrrhizin, an inhibitor of HMGB1 protein, in anticancer therapy," *Archivum Immunologiae et Therapiae Experimentalis*, vol. 60, no. 5, pp. 391–399, 2012.

[28] A. Ayala, M. F. Muñoz, and S. Argüelles, "Lipid peroxidation: production, metabolism, and signaling mechanisms of malondialdehyde and 4-hydroxy-2-nonenal," *Oxidative Medicine and Cellular Longevity*, vol. 2014, Article ID 360438, 31 pages, 2014.

[29] R. Yang, X. Zou, J. Tenhunen, and T. I. Tonnessen, "HMGB1 and extracellular histones significantly contribute to systemic inflammation and multiple organ failure in acute liver failure," *Mediators of Inflammation*, vol. 2017, Article ID 5928078, 6 pages, 2017.

[30] Z. Cao, F. Li, X. Xiang et al., "Circulating cell death biomarker: good candidates of prognostic indicator for patients with hepatitis B virus related acute-on-chronic liver failure," *Scientific Reports*, vol. 5, no. 1, Article ID 14240, 2015.

[31] H. Xu, H. Li, Y. Qu, J. Zheng, and J. Lu, "High mobility group box 1 release from cholangiocytes in patients with acute-on-chronic liver failure," *Experimental and Therapeutic Medicine*, vol. 8, no. 4, pp. 1178–1184, 2014.

[32] Y. B. Hu, D. P. Hu, and R. Q. Fu, "Correlation between high mobility group box-1 protein and chronic hepatitis B infection with severe hepatitis B and acute-on-chronic liver failure: a meta-analysis," *Minerva Medica*, vol. 108, no. 3, pp. 268–276, 2017.

[33] R.-R. Zhou, S.-S. Zhao, M.-X. Zou et al., "HMGB1 cytoplasmic translocation in patients with acute liver failure," *BMC Gastroenterology*, vol. 11, no. 1, p. 21, 2011.

[34] B. Khambu, S. Yan, N. Huda, and X. M. Yin, "Role of high-mobility group box-1 in liver pathogenesis," *International Journal of Molecular Sciences*, vol. 20, no. 21, 2019.

[35] D. Tang, R. Kang, H. J. Zeh, and M. T. Lotze, "High-mobility group box 1, oxidative stress, and disease," *Antioxidants and Redox Signaling*, vol. 14, no. 7, pp. 1315–1335, 2011.

[36] Y. Zhang, R. Karki, and O. J. Igwe, "Toll-like receptor 4 signaling: a common pathway for interactions between prooxidants and extracellular disulfide high mobility group box 1 (HMGB1) protein-coupled activation," *Biochemical Pharmacology*, vol. 98, no. 1, pp. 132–143, 2015.

[37] Y. Chen, Z. Wu, B. Yuan, Y. Dong, L. Zhang, and Z. Zeng, "MicroRNA-146a-5p attenuates irradiation-induced and LPS-induced hepatic stellate cell activation and hepatocyte apoptosis through inhibition of TLR4 pathway," *Cell Death & Disease*, vol. 9, no. 2, p. 22, 2018.

[38] S. M. Chuang, J. H. Lu, K. L. Lin et al., "Epigenetic regulation of COX-2 expression by DNA hypomethylation via NF-κB activation in ketamine-induced ulcerative cystitis," *International Journal of Molecular Medicine*, vol. 44, no. 3, pp. 797–812, 2019.

[39] S. S. Singhal, S. P. Singh, P. Singhal, D. Horne, J. Singhal, and S. Awasthi, "Antioxidant role of glutathione S-transferases: 4-Hydroxynonenal, a key molecule in stress-mediated signaling," *Toxicology and Applied Pharmacology*, vol. 289, no. 3, pp. 361–370, 2015.

[40] Y. Shi, X. Guo, J. Zhang, H. Zhou, B. Sun, and J. Feng, "DNA binding protein HMGB1 secreted by activated microglia promotes the apoptosis of hippocampal neurons in diabetes complicated with OSA," *Brain, Behavior, and Immunity*, vol. 73, pp. 482–492, 2018.

[41] M. Velegraki, E. Papakonstanti, I. Mavroudi et al., "Impaired clearance of apoptotic cells leads to HMGB1 release in the bone marrow of patients with myelodysplastic syndromes and induces TLR4-mediated cytokine production," *Haematologica*, vol. 98, no. 8, pp. 1206–1215, 2013.

[42] Y. Zhang, H. Zhang, Z. Zhang et al., "LncRNA MALAT1 cessation antagonizes hypoxia/reoxygenation injury in hepatocytes by inhibiting apoptosis and inflammation via the HMGB1-TLR4 axis," *Molecular Immunology*, vol. 112, pp. 22–29, 2019.

[43] J. Y. Tan, F. Zhao, S. X. Deng, H. C. Zhu, Y. Gong, and W. Wang, "Glycyrrhizin affects monocyte migration and apoptosis by blocking HMGB1 signaling," *Molecular Medicine Reports*, vol. 17, no. 4, pp. 5970–5975, 2018.

[44] K. Sinha, J. Das, P. B. Pal, and P. C. Sil, "Oxidative stress: the mitochondria-dependent and mitochondria-independent pathways of apoptosis," *Archives of Toxicology*, vol. 87, no. 7, pp. 1157–1180, 2013.

[45] P. D. Bhola and A. Letai, "Mitochondria-judges and executioners of cell death sentences," *Molecular Cell*, vol. 61, no. 5, pp. 695–704, 2016.

[46] S. Miltonprabu, M. Tomczyk, K. Skalicka-Woźniak et al., "Hepatoprotective effect of quercetin: from chemistry to medicine," *Food and Chemical Toxicology*, vol. 108, no. Pt B, pp. 365–374, 2017.

Hindawi
Evidence-Based Complementary and Alternative Medicine
Volume 2021, Article ID 6421122, 12 pages
https://doi.org/10.1155/2021/6421122

Research Article

Network Pharmacology Integrated with Molecular Docking Explores the Mechanisms of Naringin against Osteoporotic Fracture by Regulating Oxidative Stress

Xiang Yu,[1] Peng Zhang,[2,3] Kai Tang,[2,3] Gengyang Shen,[1] Honglin Chen,[1,2,3] Zhida Zhang,[1,3] Wenhua Zhao,[2,3] Qi Shang,[2,3] Guangye Zhu,[2] Riwei Tan,[2] Yanchi Gan,[2] You Zhang,[2] De Liang,[1] Hui Ren ,[1,3] Xiaobing Jiang ,[1,3] and Bengen Zhou [1]

[1]*The First Affiliated Hospital of Guangzhou University of Chinese Medicine, Guangzhou 510405, China*
[2]*Guangzhou University of Chinese Medicine, Guangzhou 510405, China*
[3]*Lingnan Medical Research Center of Guangzhou University of Chinese Medicine, Guangzhou 510405, China*

Correspondence should be addressed to Hui Ren; renhuispine@163.com, Xiaobing Jiang; spinedrjxb@sina.com, and Bengen Zhou; zhbg810@sina.com

Received 27 July 2021; Accepted 3 September 2021; Published 20 September 2021

Academic Editor: Lucian Hritcu

Naringin (NG), as the most abundant component of *Drynariae Rhizoma* (Chinese name: Gusuibu), has been proved to be an antioxidant flavonoid on promoting osteoporotic fracture (OF) healing, but relevant research is scanty on the underlying mechanisms. We adopted target prediction, protein-protein interaction (PPI) analysis, Gene Ontology (GO) analysis, Kyoto Encyclopedia of Genes and Genomes (KEGG) analysis, and molecular docking to establish a system pharmacology database of NG against OF. Totally 105 targets of naringin were obtained, including 26 common targets with OF. A total of 415 entries were obtained through GO Biological Process enrichment analysis ($P < 0.05$), and 37 entries were obtained through KEGG pathway enrichment analysis with seven signaling pathways included ($P < 0.05$), which were primarily concerned with p53, IL-17, TNF, estrogen, and PPAR signaling pathways. According to the results of molecular docking, naringin is all bound in the active pockets of the core targets with 3–9 hydrogen bonds through some connections such as hydrophobic interactions, Pi-Pi stacked interactions, and salt bridge, demonstrating that naringin binds tightly to the core targets. In general, naringin may treat OF through multiple targets and multiple pathways via regulating oxidative stress, etc. Notably, it is first reported that NG may regulate osteoclast differentiation and oxidative stress through the expression of the core targets so as to treat OF.

1. Introduction

Osteoporosis (OP) is a bone disease that often results in severe consequences such as fracture [1, 2]. Osteoporotic fracture (OF) is one of the most serious outcomes and clinical endpoints of OP because the lifetime risk of any OF is very high, ranging from 40 to 50 percent for women and 13 to 22 percent for men [3]. In accordance with a Chinese report in 2015, there were about 2.69 million cases of OF happening mainly in the wrists, hips, and vertebral body. OF seriously endangers the life and health of the elderly and increases the burden on families and society. OF is mainly treated using drugs for inhibition of bone resorption in clinics, but the clinical application of these drugs is limited due to some complications for long-term use [4]. Recently, traditional Chinese medicine has been gradually proved to have a functional effect on treating OF, which has attracted increasing attention from more and more scholars [5].

Drynariae Rhizoma (Chinese name: Gusuibu) is widely used to prevent and treat OF and OF-related bone diseases, whose isolated active constituents are composed of flavonoids, phenolic acids, triterpenes, and their glycosides [6]. Among them, flavonoids are the hot spots of current research on the active constituents of *Drynariae Rhizoma*. It has been reported that total flavonoids of *Drynariae Rhizoma* can reduce the production of reactive oxygen species

(ROS) to alleviate osteoporosis [7]. Naringin (PubChem CID: 442428), the main ingredient of the flavonoids from *Drynariae Rhizoma*, has the curative effect of treating osteoporosis and promoting fracture healing, so it has a good application prospect in clinics [6]. Current studies have revealed that NG can promote osteoblast proliferation [8]. Moreover, NG can promote osteogenic differentiation and fracture healing by inducing the expression of bone morphogenetic protein-2 (BMP-2) [9]. However, multiple targets and pathways are involved in the process of NG treating OF, and it is hard for traditional pharmacology to carry out systematic analysis about its complex underlying mechanism.

Oxidative stress (OS) is considered to be one of the most critical pathogenic factors of age-related bone loss, which is a primary factor in OF; oxidative stress and bone loss increase with aging, thus leading to OF [10]. Studies have reported that NG has a protective effect against bone loss through relieving oxidative stress [11, 12]. To our knowledge, data on NG treating OF through relieving oxidative stress are scanty, so the correlation between oxidative stress and NG in treating OF is worth further exploring.

For better understanding the potential mechanism of NG treatment on OF, we adopted an integrative strategy of network pharmacology and molecular docking [13], which would provide a profound theoretical basis for NG application in treating OF.

2. Materials and Methods

2.1. Network Pharmacological Data Screening

2.1.1. Naringin-Related Structure and Target Proteins. Naringin-related structure and targets were obtained in 3 steps. Step 1: Data retrieval was performed with the TCMSP database (https://tcmsp-e.com/) [14]. NG was retrieved from the "Chemical name" search box in the TCMSP database to obtain the structure and target information. The advantage of this approach is that the TCMSP database provides a comprehensive study for naringin. Step 2: The structure of naringin was exported as an "SDF" file by retrieving the PubChem database (https://pubchem.ncbi.nlm.nih.gov/), which was input into the SwissTargetPrediction database (http://new.swisstargetprediction.ch/) [15] to obtain the naringin-related targets. Step 3: The target proteins of naringin obtained from the two databases were imported into the UniProt database (http://www.uniprot.org/uniprot/), and the "popular organisms" search field was set to humans, so that target proteins of naringin were obtained, which were referred to as gene symbols.

2.1.2. OF-Related Genes and Corresponding Proteins. Genes of OF were obtained from 2 databases (GeneCards and Online Mendelian Inheritance in Man). GeneCards, a human gene database (https://www.genecards.org/) [16], includes more than 190 data sources about genes, diseases, pathways, and compounds. Online Mendelian Inheritance in Man (OMIM, https://omim.org/) [17] contains information on all known Mendelian disorders and over 15,000 genes. The same key word "Osteoporotic Fracture" was searched in the two databases, and the species was limited to "*Homo sapiens*." The proteins corresponding to OF-related genes were standardized using the UniProt database for subsequent analysis.

2.1.3. Intersection Target Proteins (ITPs). We used R (v3.6.1) software (Statistics Department of the University of Auckland, New Zealand) to take the intersection between OF-related proteins and the target proteins of NG to obtain ITPs.

2.2. Network Pharmacological Data Analysis

2.2.1. Protein-Protein Interaction (PPI) Analysis. To explore the interaction between ITPs, we adopted the STRING database (https://string-db.org/) [18] to obtain the PPI data, which was exported as a .tsv file for further analysis. Next, the PPI information of intersection target proteins was used for the following work by using Cytoscape (v3.7.2) software (Institute for Systems Biology, Seattle, Washington, USA; http://www.cytoscape.org/) [19]. Briefly, the NG-intersection target-OF network was generated. Afterward, we constructed the PPI network of ITPs and performed a network topology analysis by using the Cytoscape plugin NetworkAnalyzer to count the degrees. The target proteins, whose degrees were above average, were considered core target proteins.

2.2.2. GO Enrichment Analysis and KEGG Pathway Analysis. GO and KEGG analyses of the intersection targets were performed using clusterProfiler package (R3.6.1). The enrichment results with $P < 0.05$ were extracted.

2.3. Molecular Docking between Core Targets and Naringin. AutoDock Vina (v1.1.2) software (Department of Molecular Biology, The Scripps Research Institute, La Jolla, California, USA) [20] was utilized to conduct molecular docking simulations on naringin and its core targets to verify its interaction activity. The 3D structure of naringin was downloaded from the PubChem database (https://pubchem.ncbi.nlm.nih.gov/). AutoDockTools (v1.5.6; Department of Molecular Biology, The Scripps Research Institute, La Jolla, California, USA) was used to combine nonpolar hydrogen and distribute charge for naringin, the results of which were converted into a PDBQT file. The crystal structures of proteins were obtained from the RCSB PDB website (http://www.rcsb.org/), and the selection of proteins should satisfy the following three principles: (i) it should be a human protein; (ii) the protein owns one or more eutectic ligands, and the eutectic ligand having higher structural similarity with naringin is preferred; and (iii) the crystal structure with smaller "resolution" value is selected. Molecular docking simulations were not conducted, when the eutectic ligand structure of the protein could not be found in the PDB database or its specific active sites could not be obtained through literature search. We used AutoDockTools to separate the target protein from its ligand, add polar

hydrogen and distribute charge, and then output the results to a PDBQT file. AutoDockTools was also used to determine the size and center of the docking box. The specific process of docking is as follows: First, the eutectic ligand of target protein was used to obtain the affinity of the docked protein as the comparison of the docking results of naringin. Then, naringin was successively docked with the target proteins and every affinity was calculated. Finally, the docking results of naringin were plotted and analyzed using PyMOL software (DeLano Scientific Limited Liability Company, South San Francisco, USA).

3. Results

3.1. The Structure and Target Proteins of Naringin. Finally, 105 targets of naringin were obtained from TCMSP and SwissTargetPrediction databases. After input into the UniProt database, target proteins of naringin were obtained, which were referred to as gene symbols. The structure and target information of naringin are shown in Supplementary Tables S1 and S2.

3.2. OF-Related Target Proteins and ITPs. Totally 840 target proteins of OF were retrieved in GeneCards and OMIM databases. After they were mapped with the target proteins of naringin, ITPS were obtained including 26 intersection targets, which are shown in Figure 1(a) and Table 1.

3.3. PPI Network Plotting and Core Target Protein Identification. We input ITPs into the STRING database, hiding the targets with no interactive relationship with others. And then, the data of protein-protein interaction (PPI) were obtained, which was imported into Cytoscape (v 3.7.2) to plot the PPI network in Figure 1(b). There were 11 target proteins whose degrees were higher than the average degree (7.91), which were predicted as the core target proteins (Table 2).

3.4. NG-Intersection Target-OF Network Construction. Figure 1(c) shows the NG-intersection target-OF network, which involved 28 nodes and 52 edges, including one NG node, one OF node, and twenty-six target nodes. In Figure 1(c), the blue diamond nodes represent the intersection target proteins. The red polygon node represents "naringin." The orange oval node represents "osteoporotic fracture." The edges represent the corresponding relationship among naringin, osteoporotic fracture, and the intersection targets.

3.5. GO Enrichment Analysis. We obtained 415 items of biological process (BP). Figure 2(a) shows the top 20 items. Notably, we have screened 20 items mainly related to oxidative stress, osteoclast differentiation, and NF-κB signaling regulations, which are shown in Figure 2(b). In addition, 26 interaction targets were imported into Cytoscape (v3.7.2) for GO.BP enrichment analysis. The GO.BP results are mainly related to the following aspects shown in Figure 2(c): (i) inflammation-related activities, such as nuclear receptor activity and extracellular matrix disassembly, which are closely associated with oxidative stress; (ii) cell cycle, such as execution phase of apoptosis; (iii) hormone metabolism, such as estrogen metabolism process; and (iv) lipid metabolism, such as long-chain fatty acid transportation.

3.6. KEGG Pathway Analysis. The KEGG pathway analysis of 26 target genes was performed using R software. A total of 37 items were obtained, and Table 3 lists 7 key signaling pathways. Cytoscape (v3.7.2) was used for network visualization, as shown in Figure 2(d).

3.7. Molecular Docking Analysis. Among 11 core targets, a total of 8 proteins suitable for molecular docking were obtained after screening, including ESR1, CASP3, ACE, TNF, PPARG, SERPINE1, CYP19A1, and MMP1. To verify how naringin binds to core targets as previously referred, molecular docking using AutoDock Vina was developed in this section. We predicted whether naringin could enter the active pocket of target proteins successfully or not and calculated the affinities between them. The relevant information of the eight proteins and the docking results of eutectic ligands are shown in Supplementary Table S3, and the affinity and hydrogen bond information of naringin with each target protein are shown in Table 4.

As presented in Table 4 and Figure 3(a), the binding affinity of this combination is −7.1 kcal/mol. Naringin was bound with ESR1 by forming 2 hydrogen bonds with Thr-347, while one hydrogen bond with Leu-525. In addition, there are hydrophobic contacts between naringin and Ala-350 and Leu-525.

As presented in Table 4 and Figure 3(b), the binding affinity of naringin upon CASP3 is −5.4 kcal/mol. The residues including Arg-179, Gln-283, Tyr-338, Arg-341, and Ser-343 interact with naringin by forming 9 hydrogen bonds, which provide a powerful electrostatic force for the combination of naringin and CASP3.

As presented in Table 4 and Figure 3(c), the binding affinity of naringin upon ACE was −9.4 kcal/mol. There were 8 hydrogen bonds provided by Glu-162, Gln-281, His-383, His-513, Lys-449, Lys-454, and Ala-354 residues in the interaction with naringin. Naringin was located in the hydrophobic pocket comprising Glu-376, Val-379, Val-380, and Phe-457 residues. Interestingly, naringin interacts with the His-353 residue by salt bridge.

As presented in Table 4 and Figure 3(d), the binding affinity of naringin upon TNF was −6.5 kcal/mol. There were hydrogen bonds provided by Gly-121, Gly-148, and Gln-149 residues in the interaction with naringin. Naringin was located in the hydrophobic pocket comprising Tyr-59, Gln-61, and Tyr-119 residues. Interestingly, naringin interacts with Tyr-59 and Tyr-151 residues by Pi-Pi stacked interactions.

As presented in Table 4 and Figure 3(e), the binding affinity of naringin upon PPARG was −9.1 kcal/mol. There were 6 hydrogen bonds provided by Ala-278, Ile-281, Gln-286, Ser-289, and Glu-343 residues in the interaction with

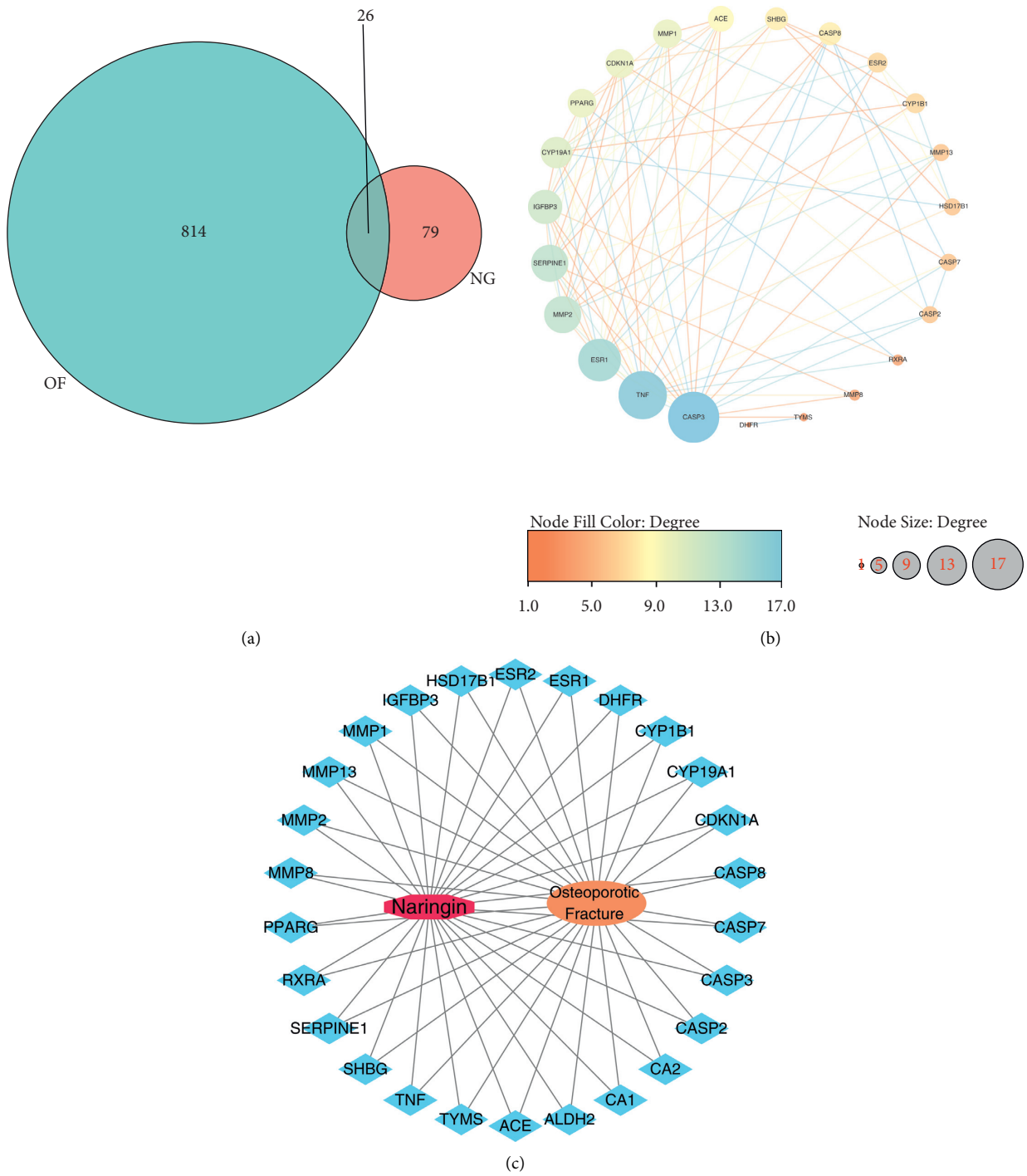

Figure 1: Venn diagram of NG-OF intersection targets: (a), PPI network of potential targets (b), and NG-intersection target-OF network (c).

Table 1: Potential target genes of NG in the treatment of OF.

Number	Gene	Number	Gene
1	CDKN1A	14	ALDH2
2	TNF	15	CASP3
3	CYP19A1	16	ACE
4	CA2	17	PPARG
5	CA1	18	IGFBP3
6	MMP1	19	CASP7

Table 1: Continued.

Number	Gene	Number	Gene
7	MMP8	20	CASP8
8	MMP13	21	CASP2
9	CYP1B1	22	RXRA
10	HSD17B1	23	SERPINE1
11	SHBG	24	DHFR
12	ESR1	25	MMP2
13	ESR2	26	TYMS

Table 2: Core targets of NG in the treatment of OF.

Number	Core targets	Degree
1	CASP3	17
2	TNF	16
3	ESR1	14
4	MMP2	12
5	SERPINE1	12
6	IGFBP3	11
7	CYP19A1	10
8	PPARG	9
9	CDKN1A	9
10	MMP1	9
11	ACE	8

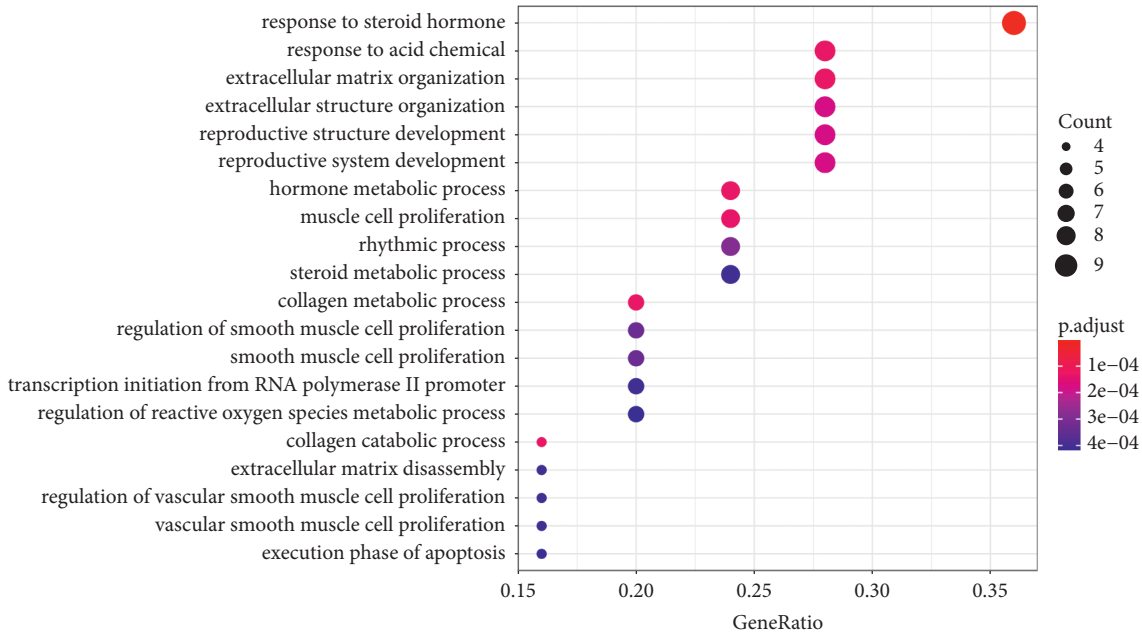

(a)

Figure 2: Continued.

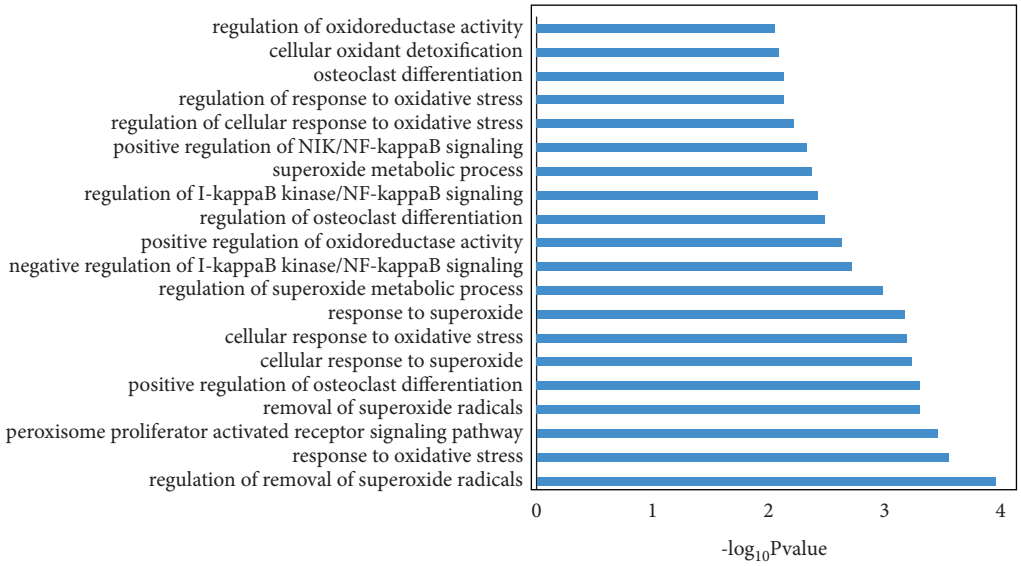

(b)

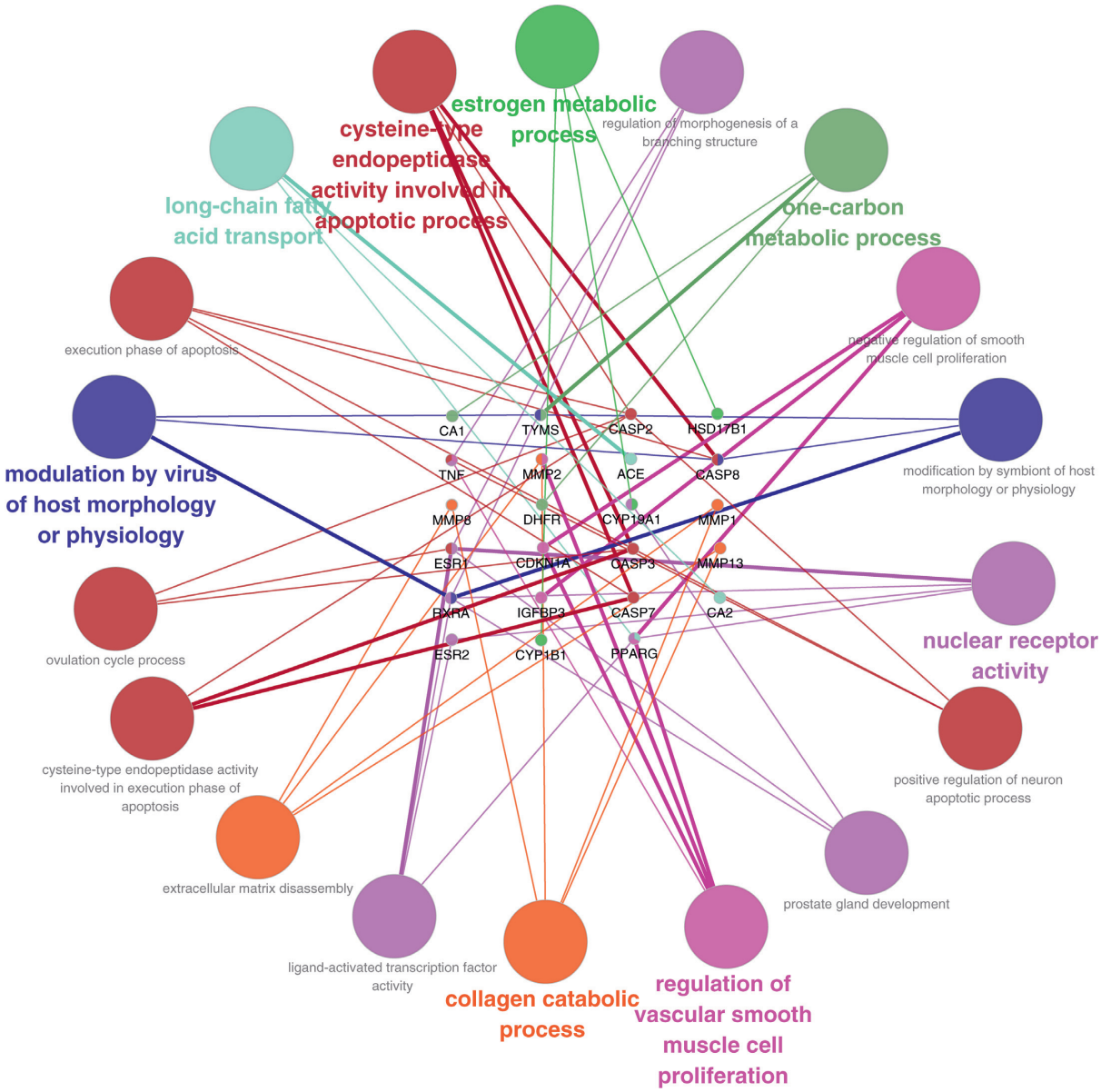

(c)

Figure 2: Continued.

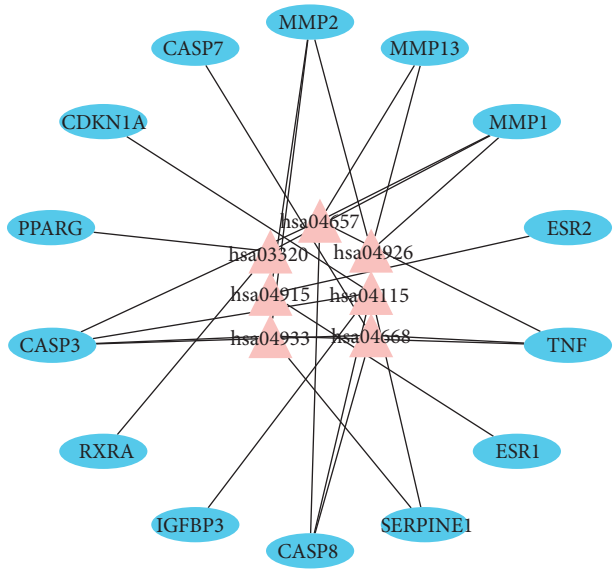

(d)

Figure 2: GO.BP enrichment analysis (a, b, c) and pathway-target network (d).

Table 3: KEGG pathway enrichment analysis.

ID	Signaling Pathway	Enriched Gene Number	*P* value
hsa04115	p53 Signaling Pathway	5	0.000271
hsa04657	IL-17 Signaling Pathway	5	0.000508
hsa04933	AGE-RAGE Signaling Pathway	4	0.002583
hsa04668	TNF Signaling Pathway	4	0.00296
hsa03320	PPAR Signaling Pathway	3	0.009397
hsa04926	Relaxin Signaling Pathway	3	0.028958
hsa04915	Estrogen Signaling Pathway	3	0.032836

Table 4: Molecular interactions of core targets and naringin.

Compound	Target	Affinity (kcal/mol)	Number of hydrogen bonds	Hydrogen bonds interacting residues
Naringin	ESR1	−7.1	3	Thr-347(2), Leu-525
Naringin	CASP3	−5.4	9	Arg-179, Gln-283, Tyr-338(2), Arg-341(4), Ser-343
Naringin	ACE	−9.4	8	Glu-162, Gln-281, Ala-354(2), His-383, Lys-449, Lys-454, His-513
Naringin	TNF	−6.5	3	Gly-121, Gly-148, Gln-149
Naringin	PPARG	−9.1	6	Ala-278, Ile-281, Gln-286, Ser-289(2), Glu-343
Naringin	SERPINE1	−7.2	5	Tyr-37, Arg-76, Tyr-79, Asp-95, Arg-118
Naringin	CYP19A1	−9.0	7	Arg-115(2), Thr-310, Ser-314, Leu-372, Phe-430, Gly-439
Naringin	MMP1	−9.5	5	Asn-180, Leu-181, Ala-182(2), Glu-219

naringin. Naringin was located in the hydrophobic pocket of PPARG. Interestingly, naringin interacts with the His-449 residue by salt bridge.

As presented in Table 4 and Figure 3(f), the binding affinity of naringin upon SERPINE1 was −7.2 kcal/mol. There were hydrogen bonds provided by Tyr-37, Arg-76, Tyr-79, Asp-95, and Arg-118 residues in the interaction with naringin. Tyr-79, Thr-93, and Arg-118 residues interact with naringin by hydrophobic interaction.

As presented in Table 4 and Figure 3(g), the binding affinity of naringin on CYP19A1 was −9.0 kcal/mol. There were 7 hydrogen bonds provided by Thr-310, Ser-314, Leu-372, Phe-430, Gly-439, and Arg-115 residues in the interaction with naringin. In addition, naringin interacts with the Phe-430 residue by T-type Pi-Pi stacked interaction.

As presented in Table 4 and Figure 3(h), the binding affinity of naringin upon MMP1 was −9.5 kcal/mol. The residues including Asn-180, Leu-181, Glu-219, and Ala-182 interact with naringin by forming 5 hydrogen bonds, which provide a powerful electrostatic force for the combination of naringin and MMP1. Interestingly, naringin interacts with the His-228 residue by salt bridge.

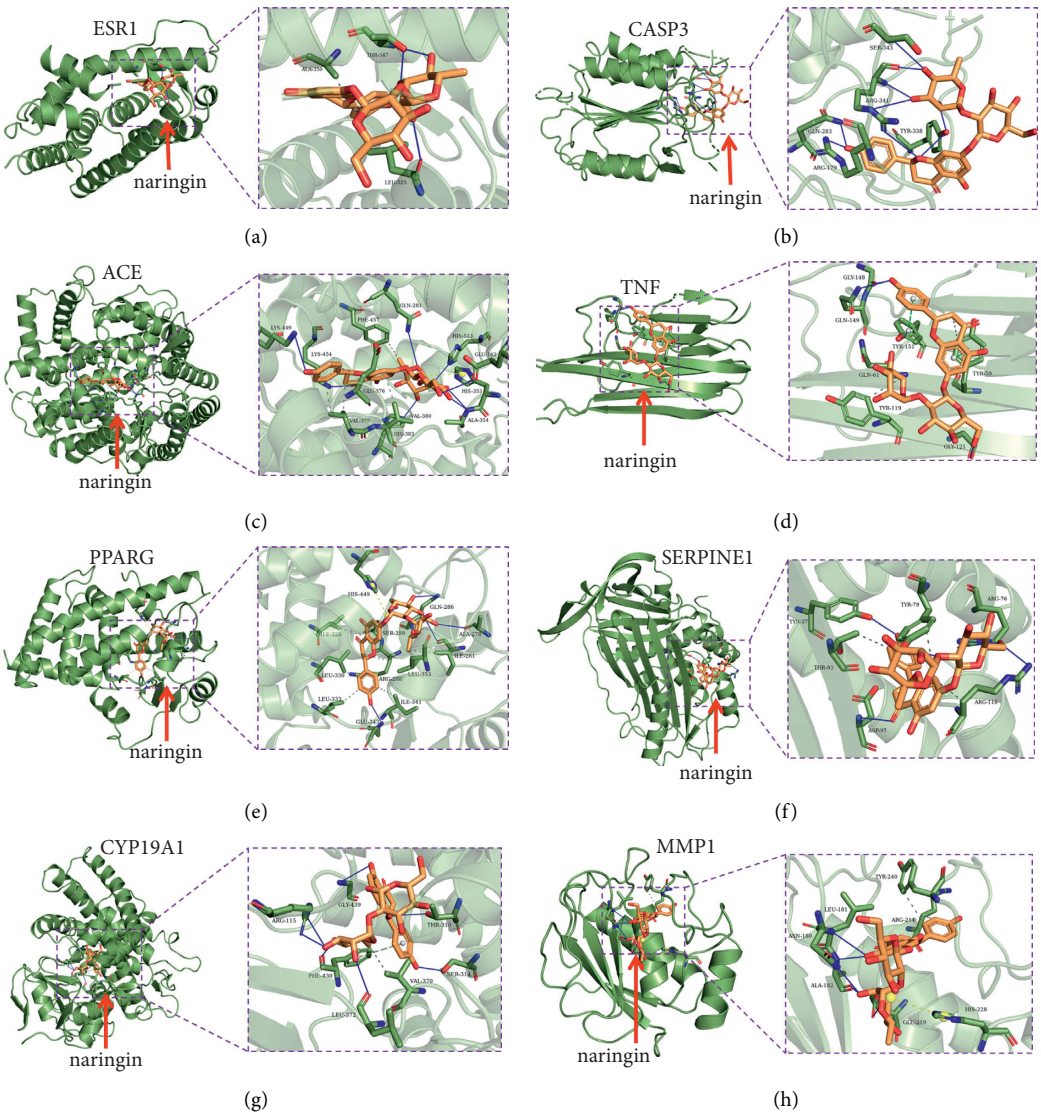

Figure 3: Simulated molecular docking of naringin on ESR1: (a), CASP3 (b), ACE (c), TNF (d), PPARG (e), SERPINE1 (f), CYP19A1 (g), and MMP1 (h).

4. Discussion

Chinese traditional medicine *Drynariae Rhizoma* has been widely applied in treating osteoporosis and osteoporotic fracture clinically for many years. Naringin is one of the most abundant flavonoids in *Drynariae Rhizoma*, which is also found in citrus fruits and many other Chinese medicines [6]. Studies have revealed that flavonoids have the therapeutic effect on OF by regulating estrogen receptor, OPG/RANK/RANKL, enzyme inhibition, or signal transduction pathways [21, 22].

In this study, there were 26 common targets obtained between NG and OF, among which 11 core targets were identified, namely CASP3, TNF, ESR1, MMP2, MMP1, SERPINE1, IGFBP3, CYP19A1, PPARG, CDKN1A, and ACE. PPI network topology analysis suggested that the targets were mainly characterized by oxidative stress, inflammation, cell cycle, and lipid and hormone metabolism-related proteins. The top three targets in terms of degree are TNF, CASP3, and ESR1, indicating that they may be the key targets of NG in the treatment of OF.

TNF (tumor necrosis factor), known as TNF-α, which is the earliest inflammatory medium produced in oxidative stress response, can promote the generation of inflammatory mediators and induce macrophage colony-stimulating factor (M-CSF) expression [23]. TNF can increase bone absorption and thus influence the healing of OF through activating NF-κB and promoting RANKL-induced osteoclast differentiation [24]. TNF-α can promote oxidative stress and regulate bone homeostasis and bone reconstruction [25, 26]. Moreover, it has been reported that NG could decrease the TNF-α expression [27]. Therefore, we speculated that NG could reduce oxidative stress by downregulating TNF expression in OF patients, so as to anti-OF.

CASP3 (caspase-3) affects the apoptosis of osteoclasts [28]. Some studies have proved that the upregulation of

CASP3 mRNA can promote OF healing [29]. Further studies have shown that the upregulation of CASP3 can activate the p53 signaling pathway, destroy the maturation of osteoblasts, and inhibit chondrocyte differentiation, thus promoting fracture healing [30].

ESR1 (estrogen receptor 1) has a close relationship with bone formation [31]. When ESR1 is combined with estrogen, it can up- or downregulate cytokines to affect relevant signaling pathways. ESR1 affects the proliferation, differentiation, and maturation of chondrocytes, regulates the process of endochondral osteogenesis, and maintains chondrocyte phenotype, which promotes the maintenance of cartilage thickness, bone growth balance, and fracture healing [32]. The lack of estrogen results in the acceleration of bone mass loss in postmenopausal women, which could easily give rise to OF [33]. Estrogen exerts physiological activities in cells through ESR1, which are mainly manifested in cell growth, differentiation, senescence, and apoptosis [34]. Guo et al. [35] reported that naringin from *Drynariae Rhizoma* revealed a double directional adjusting function of estrogenic and antiestrogenic activities. Pang et al. [6] also demonstrated that naringin might mediate ligand-independent activation of ESR1 in osteoblastic cells to protect against ovariectomy-induced bone loss in mice. However, studies are needed to determine whether naringin could prevent and treat OF via exerting estrogen-like protective actions in bone.

MMP2 (matrix metalloproteinase 2) and MMP1 (matrix metalloproteinase 1) are all members of the family of matrix metalloproteinases (MMPs). MMP2 is expressed in the cytoplasm of osteoblasts and some osteoclasts, which can regulate the dissolution of bone matrix, inhibit bone resorption, and contribute to bone reconstruction [36], which promotes fracture healing. MMP1 is closely related to the repair of cartilage tissue. It has been shown that the expression of MMP1 can inhibit the degradation of cartilage matrix and promote the repair of cartilage [37]. Nevertheless, there is no research revealing the regulatory function of NG on MMP2 or MMP1 in OF, which is needed to be further studied in the next step study.

PPARG (peroxisome proliferator-activated receptor gamma), which is related to the regulation of cell differentiation, inflammatory response, and oxidative stress, mainly affects the catabolism of lipids and plays a key role in the process of adipocyte differentiation [38]. It can promote lipid formation and inhibit osteogenesis through different regulatory pathways like PPARγ2 signaling pathway [39, 40]. A study [41] reported that naringin can protect against steroid-induced avascular necrosis of the femoral head (SANFH) through upregulation of PPARγ2 and activation of the Notch signaling pathway in a rabbit model.

CDKN1A (cyclin-dependent kinase inhibitor 1), also known as p21, is a negative regulator of cell cycle that regulates cell proliferation, differentiation, and senescence [42]. The number of osteoblasts is closely related to cell proliferation, and the process of cell proliferation cycle is mainly regulated by cycle-regulating proteins, of which the regulation of $G1$ phase is the most important [43]. In this process, the combination of cyclin $D1$ and CDK4 (cyclin-dependent kinase 4) forms the CDK4-cyclin complex to promote the $G1$ phase [44]. CDKN1A (p21), as a $G1$ phase regulatory protein, inactivates the CDK4-cyclin complex by binding to it, leading to cell cycle stagnation in the $G1$ phase [45]. An animal experiment [46] has proved that the expression of p21 in osteoblasts was significantly increased in rats after ovariectomy ($P < 0.01$). It is also reported that the downregulation of p21 protein expression can promote the proliferation of osteoblasts [45]. Thus, p21 plays a key role in the proliferation of osteoblasts and NG might treat OF by upregulating the p21 expression, which is expected to be demonstrated in the future research.

In addition, CASP2, CASP3, CASP7, and CASP8 in Table 3 are members of the cysteine protease family, which can promote osteoclast apoptosis and thus promote fracture healing [47, 48]. ESR2 is also a receptor of estrogen, which is associated with postmenopausal OF [33].

The results of GO enrichment analysis are similar to those of PPI network analysis. Notably, GO.BP enrichment analysis reveals that the regulation of oxidative stress and osteoclast differentiation play a critical role in NG treating OF, as shown in Figure 2(b). In recent years, relevant reports have confirmed that oxidative stress plays a key role in the pathogenesis of OF [49]. Studies have also revealed that oxidative stress (OS) is one of the important factors that trigger OF [50, 51]. OS is due to the generation of excess reactive oxygen species (ROS), which cannot be cleared by endogenous antioxidants, exceeding the normal physiological threshold and triggering a series of cell toxic reactions, thus further causing tissue damage [52]. Oxidative stress induced by ROS can cause changes in bone homeostasis, increase bone resorption, and decrease bone formation, leading to the occurrence of OF [53]. Some scholars have reported that miR-320a can increase the OS level, reduce osteoblast function, and result in the occurrence of OF [54]. Liu et al. [55] found that the reduction of ROS can increase bone mass and prevent ovariectomized osteoporosis. And some studies have revealed the protective effects of naringin against H2O2-induced inhibition of osteogenic differentiation, which suggests that naringin is a natural antioxidant [56]. Based on our study, naringin may be a promising antioxidant, which would help relieve oxidative stress and ameliorate OF. Moreover, numerous studies have demonstrated that the expression of core targets including TNF [57], CASP3 [58], ESR1 [59], MMP2 [60], MMP1 [61], PPARG [62], CDKN1A [63], ACE [64], etc., plays an important part in regulating oxidative stress. Therefore, we speculated that NG could regulate core targets' expressions and osteoclast differentiation by oxidative stress in OF patients, so as to anti-OF.

KEGG pathway enrichment analysis demonstrated that p53, IL-17, TNF, estrogen, and PPAR signaling pathways may play a key role in naringin treating OF. Similarly, the results of KEGG analysis are consistent with those of PPI and GO analysis.

Some studies have verified that the activation of p53 signaling pathway can destroy the maturation of osteoblasts and inhibit chondrocyte differentiation [30]. Studies have shown that NG could inhibit inflammation and apoptosis

mediated by p53, NF-κB, and TNF pathways [65, 66]. However, whether NG could regulate the p53 signaling pathway to treat OF is still unclear, which needs further identification in the future research.

The IL-17 signaling pathway can stimulate the synthesis of TNF-α, IL-6, and NF-κB, thus promoting osteoclast differentiation induced by RANKL [67]. Moreover, studies have shown that the TNF signaling pathway plays a critical role in the occurrence of postmenopausal OF through promoting the expression of RANKL and inducing osteoclast differentiation [23]. So, IL-17 [68] and TNF signaling pathways [69] have close connection with osteoclast differentiation.

The estrogen signaling pathway can regulate the proliferation, differentiation, and apoptosis of osteoblasts and osteoclasts [70]. It has also been proved that the PPAR pathway can inhibit the lipogenesis of bone marrow, promote the generation of osteoblasts, and improve bone formation and bone mass [40], which promotes fracture healing.

Collectively, the results in our study predicted some pathways and targets that may be potentially therapeutic targets and provide reference for future research on NG treating OF. Nevertheless, a limitation of this study is that further experiments are necessary to demonstrate our findings.

5. Conclusion

In summary, for the first time, our results revealed that naringin may treat OF possibly by regulating numerous signaling pathways and targets related to oxidative stress and osteoclast differentiation. These results will provide a theoretical basis for the treatment of OF. However, these predicted altered signaling pathways or target genes still need to be further verified in the future study.

Data Availability

The data used to support the study's results came from the first author.

Conflicts of Interest

The authors declare no conflicts of interest.

Authors' Contributions

All the authors have actively participated in the planning of the work, data gathering and analyzing, and writing the manuscript. All the authors have read and confirmed their participation in the manuscript. The authors Xiang Yu, Peng Zhang, and Kai Tang contributed equally to this work.

Acknowledgments

The project was generously supported by the grants from Guangdong Province Universities and Colleges Pearl River Scholar Funded Scheme (GDUPS 2018), the National Natural Science Foundation of China (81674000, 81774338, and 81904225), the Medical Research Foundation of Guangdong Province (A2021320 and A2019167), and the Guangdong Provincial Department of Education Project (2018KTSCX041).

Supplementary Materials

Supplementary Table S1: the structure of naringin. Supplementary Table S2: targets of naringin. Supplementary Table S3: target protein information and original ligand docking results. (*Supplementary Materials*)

References

[1] B. J. Gates and S. Das, "Management of osteoporosis in elderly men," *Maturitas*, vol. 69, no. 2, pp. 113–119, 2011.

[2] J. E. Compston, M. R. McClung, and W. D. Leslie, "Osteoporosis," *The Lancet*, vol. 393, no. 10169, pp. 364–376, 2019.

[3] O. Johnell and J. Kanis, "Epidemiology of osteoporotic fractures," *Osteoporosis International*, vol. 16, no. Suppl 2, pp. S3–S7, 2005.

[4] M. Gambacciani and M. Levancini, "Management of postmenopausal osteoporosis and the prevention of fractures," *Panminerva Medica*, vol. 56, no. 2, pp. 115–131, 2014.

[5] Y.-C. Wang, J.-H. Chiang, H.-C. Hsu, and C.-H. Tsai, "Decreased fracture incidence with traditional Chinese medicine therapy in patients with osteoporosis: a nationwide population-based cohort study," *BMC Complementary and Alternative Medicine*, vol. 19, no. 1, p. 42, 2019.

[6] W.-Y. Pang, X.-L. Wang, S.-K. Mok et al., "Naringin improves bone properties in ovariectomized mice and exerts oestrogen-like activities in rat osteoblast-like (UMR-106) cells," *British Journal of Pharmacology*, vol. 159, no. 8, pp. 1693–1703, 2010.

[7] P. Mu, Y. Hu, X. Ma, J. Shi, Z. Zhong, and L. Huang, "Total flavonoids of Rhizoma Drynariae combined with calcium attenuate osteoporosis by reducing reactive oxygen species generation," *Experimental and Therapeutic Medicine*, vol. 21, no. 6, p. 618, 2021.

[8] N. Li, Y. Jiang, P. H. Wooley, Z. Xu, and S. Y. Yang, "Naringin promotes osteoblast differentiation and effectively reverses ovariectomy-associated osteoporosis," *Journal of Orthopaedic Science: Official Journal of the Japanese Orthopaedic Association*, vol. 18, no. 3, pp. 478–485, 2013.

[9] X. Zhou, P. Zhang, C. Zhang, and Z. A. Zhu, "Promotion of bone formation by naringin in a titanium particle-induced diabetic murine calvarial osteolysis model," *Journal of Orthopaedic Research*, vol. 28, no. 4, pp. 451–456, 2010.

[10] Y.-B. Zhang, Z.-M. Zhong, G. Hou, H. Jiang, and J.-T. Chen, "Involvement of oxidative stress in age-related bone loss," *Journal of Surgical Research*, vol. 169, no. 1, pp. e37–e42, 2011.

[11] O. A. Adebiyi, O. O. Adebiyi, and P. M. O. Owira, "Naringin reduces hyperglycemia-induced cardiac fibrosis by relieving oxidative stress," *PLoS One*, vol. 11, no. 3, Article ID e0149890, 2016.

[12] C. Li, J. Zhang, F. Lv, X. Ge, and G. Li, "Naringin protects against bone loss in steroid-treated inflammatory bowel disease in a rat model," *Archives of Biochemistry and Biophysics*, vol. 650, pp. 22–29, 2018.

[13] X. Qi, H. Xu, P. Zhang et al., "Investigating the mechanism of scutellariae barbata herba in the treatment of colorectal cancer by network pharmacology and molecular docking," *Evidence-*

Based Complementary and Alternative Medicine, vol. 2021, Article ID 3905367, 18 pages, 2021.

[14] J. Ru, P. Li, J. Wang et al., "TCMSP: a database of systems pharmacology for drug discovery from herbal medicines," *Journal of Cheminformatics*, vol. 6, no. 1, p. 13, 2014.

[15] D. Gfeller, A. Grosdidier, M. Wirth, A. Daina, O. Michielin, and V. Zoete, "SwissTargetPrediction: a web server for target prediction of bioactive small molecules," *Nucleic Acids Research*, vol. 42, no. W1, pp. W32–W38, 2014.

[16] G. Stelzer, N. Rosen, I. Plaschkes et al., "The GeneCards suite: from gene data mining to disease genome sequence analyses," *Current Protocols in Bioinformatics*, vol. 54, no. 1, pp. 1–33, 2016.

[17] J. S. Amberger and A. Hamosh, "Searching online mendelian inheritance in man (OMIM): a knowledgebase of human genes and genetic phenotypes," *Current Protocols in Bioinformatics*, vol. 58, no. 1, pp. 1–12, 2017.

[18] C. v. Mering, M. Huynen, D. Jaeggi, S. Schmidt, P. Bork, and B. Snel, "STRING: a database of predicted functional associations between proteins," *Nucleic Acids Research*, vol. 31, no. 1, pp. 258–261, 2003.

[19] P. Shannon, A. Markiel, O. Ozier et al., "Cytoscape: a software environment for integrated models of biomolecular interaction networks," *Genome Research*, vol. 13, no. 11, pp. 2498–2504, 2003.

[20] O. Trott and A. J. Olson, "AutoDock Vina: improving the speed and accuracy of docking with a new scoring function, efficient optimization, and multithreading," *Journal of Computational Chemistry*, vol. 31, no. 2, pp. 455–461, 2009.

[21] D. Choudhary, P. Kushwaha, J. Gautam et al., "Fast and long acting neoflavonoids dalbergin isolated from Dalbergia sissoo heartwood is osteoprotective in ovariectomized model of osteoporosis: osteoprotective effect of Dalbergin," *Biomedicine & Pharmacotherapy*, vol. 83, pp. 942–957, 2016.

[22] M. Satué, M. d. M. Arriero, M. Monjo, and J. M. Ramis, "Quercitrin and taxifolin stimulate osteoblast differentiation in MC3T3-E1 cells and inhibit osteoclastogenesis in RAW 264.7 cells," *Biochemical Pharmacology*, vol. 86, no. 10, pp. 1476–1486, 2013.

[23] H. Kitaura, P. Zhou, H. J. Kim, D. V. Novack, F. P. Ross, and S. L. Teitelbaum, "M-CSF mediates TNF-induced inflammatory osteolysis," *Journal of Clinical Investigation*, vol. 115, no. 12, pp. 3418–3427, 2005.

[24] R. C. Schulman, A. J. Weiss, and J. I. Mechanick, "Nutrition, bone, and aging: an integrative physiology approach," *Current Osteoporosis Reports*, vol. 9, no. 4, pp. 184–195, 2011.

[25] B. A. Abdel-Wahab and M. E. Metwally, "Clozapine-induced cardiotoxicity: role of oxidative stress, tumour necrosis factor Alpha and NF-$\kappa\beta$," *Cardiovascular Toxicology*, vol. 15, no. 4, pp. 355–365, 2015.

[26] C. Sang, Y. Zhang, F. Chen et al., "Tumor necrosis factor alpha suppresses osteogenic differentiation of MSCs by inhibiting semaphorin 3B via Wnt/β-catenin signaling in estrogen-deficiency induced osteoporosis," *Bone*, vol. 84, pp. 78–87, 2016.

[27] O. M. Oladapo, B. Ben-Azu, A. M. Ajayi et al., "Naringin confers protection against psychosocial defeat stress-induced neurobehavioral deficits in mice: involvement of glutamic acid decarboxylase isoform-67, oxido-nitrergic stress, and neuroinflammatory mechanisms," *Journal of Molecular Neuroscience*, vol. 71, no. 3, pp. 431–445, 2021.

[28] S. A. Lakhani, A. Masud, K. Kuida et al., "Caspases 3 and 7: key mediators of mitochondrial events of apoptosis," *Science*, vol. 311, no. 5762, pp. 847–851, 2006.

[29] W.-J. Liu, Z.-M. Jiang, Y. Chen et al., "Network pharmacology approach to elucidate possible action mechanisms of Sinomenii Caulis for treating osteoporosis," *Journal of Ethnopharmacology*, vol. 257, Article ID 112871, 2020.

[30] J. Wu, Y. Yang, Y. He et al., "EFTUD2 gene deficiency disrupts osteoblast maturation and inhibits chondrocyte differentiation via activation of the p53 signaling pathway," *Human Genomics*, vol. 13, no. 1, p. 63, 2019.

[31] C. Yang, J. Ren, B. Li et al., "Identification of gene biomarkers in patients with postmenopausal osteoporosis," *Molecular Medicine Reports*, vol. 19, no. 2, pp. 1065–1073, 2018.

[32] M. Liu, W. Xie, W. Zheng, D. Yin, R. Luo, and F. Guo, "[Targeted binding of estradiol with ESR1 promotes proliferation of human chondrocytes in vitro by inhibiting activation of ERK signaling pathway]," *Nan Fang Yi Ke Da Xue Xue Bao*, vol. 39, no. 2, pp. 134–143, 2021.

[33] T. Mitek, Ł. Nagraba, J. Deszczyński, M. Stolarczyk, E. Kuchar, and A. Stolarczyk, "Genetic predisposition for osteoporosis and fractures in postmenopausal women," *Advances in Experimental Medicine & Biology*, vol. 1211, pp. 17–24, 2019.

[34] A. Basudan, N. Priedigkeit, R. J. Hartmaier et al., "Frequent ESR1 and CDK pathway copy-number alterations in metastatic breast cancer," *Molecular Cancer Research*, vol. 17, no. 2, pp. 457–468, 2019.

[35] D. Guo, J. Wang, X. Wang et al., "Double directional adjusting estrogenic effect of naringin from Rhizoma drynariae (Gusuibu)," *Journal of Ethnopharmacology*, vol. 138, no. 2, pp. 451–457, 2011.

[36] V. Parikka, A. Väänänen, J. Risteli et al., "Human mesenchymal stem cell derived osteoblasts degrade organic bone matrix in vitro by matrix metalloproteinases," *Matrix Biology*, vol. 24, no. 6, pp. 438–447, 2005.

[37] S.-Y. Sheu, W.-S. Chen, J.-S. Sun, F.-H. Lin, and T. Wu, "Biological characterization of oxidized hyaluronic acid/resveratrol hydrogel for cartilage tissue engineering," *Journal of Biomedical Materials Research Part A*, vol. 101, no. 12, pp. 3457–3466, 2013.

[38] M. Folwaczny, V. Manolis, C. Markus, and J. Glas, "Variants of the human PPARG locus and the susceptibility to chronic periodontitis," *Innate Immunity*, vol. 17, no. 6, pp. 541–547, 2011.

[39] M. Herlin, F. E. McGuigan, H. Luthman, and K. Åkesson, "Polymorphisms in inflammation associated genes ALOX15 and IL-6 are associated with bone properties in young women and fracture in elderly," *Bone*, vol. 79, pp. 105–109, 2015.

[40] J.-H. Kim, D. Y. Jung, A. Nagappan, and M. H. Jung, "Histone H3K9 demethylase JMJD2B induces hepatic steatosis through upregulation of PPARγ2," *Scientific Reports*, vol. 8, no. 1, Article ID 13734, 2018.

[41] D. Huang, Z. Li, B. Chen et al., "Naringin protects against steroidinduced avascular necrosis of the femoral head through upregulation of PPAR gamma and activation of the Notch signaling pathway," *Molecular Medicine Reports*, vol. 17, no. 2, pp. 3328–3335, 2017.

[42] A. Karimian, Y. Ahmadi, and B. Yousefi, "Multiple functions of p21 in cell cycle, apoptosis and transcriptional regulation after DNA damage," *DNA Repair*, vol. 42, pp. 63–71, 2016.

[43] S. Dalton, "Linking the cell cycle to cell fate decisions," *Trends in Cell Biology*, vol. 25, no. 10, pp. 592–600, 2015.

[44] H. Matsushime, M. F. Roussel, R. A. Ashmun, and C. J. Sherr, "Colony-stimulating factor 1 regulates novel cyclins during the *G*1 phase of the cell cycle," *Cell*, vol. 65, no. 4, pp. 701–713, 1991.

[45] B. He, L. Dai, X. Zhang et al., "The HDAC inhibitor quisinostat (JNJ-26481585) supresses hepatocellular carcinoma alone and synergistically in combination with sorafenib by *G*0/*G*1 phase arrest and apoptosis induction," *International Journal of Biological Sciences*, vol. 14, no. 13, pp. 1845–1858, 2018.

[46] K. Asano, T. Okawa, I. Matsuoka, Y. Suzuki, and A. Sato, "Effects of sex steroids on expression of adenylyl cyclase messenger RNA in rat uterus," *Journal of Endocrinological Investigation*, vol. 28, no. 4, pp. 357–362, 2005.

[47] M. Reyes-Becerril, C. Angulo, V. Sanchez, A. Cuesta, and A. Cruz, "Methylmercury, cadmium and arsenic (III)-induced toxicity, oxidative stress and apoptosis in Pacific red snapper leukocytes," *Aquatic Toxicology*, vol. 213, Article ID 105223, 2019.

[48] N. Tisch, A. Freire-Valls, R. Yerbes et al., "Caspase-8 modulates physiological and pathological angiogenesis during retina development," *Journal of Clinical Investigation*, vol. 129, no. 12, pp. 5092–5107, 2019.

[49] S. Zhu, W. Wei, Z. Liu, Y. Yang, and H. Jia, "TanshinoneIIA attenuates the deleterious effects of oxidative stress in osteoporosis through the NFkappaB signaling pathway," *Molecular Medicine Reports*, vol. 17, no. 5, pp. 6969–6976, 2018.

[50] J. Kular, J. Tickner, S. M. Chim, and J. Xu, "An overview of the regulation of bone remodelling at the cellular level," *Clinical Biochemistry*, vol. 45, no. 12, pp. 863–873, 2012.

[51] V. Domazetovic, G. Marcucci, T. Iantomasi, M. L. Brandi, and M. T. Vincenzini, "Oxidative stress in bone remodeling: role of antioxidants," *Clinical Cases in Mineral and Bone Metabolism*, vol. 14, no. 2, pp. 209–216, 2017.

[52] R. Li, Z. Jia, and M. A. Trush, "Defining ROS in Biology and medicine," *Reactive Oxygen Species (Apex, N.C.)*, vol. 1, no. 1, pp. 9–21, 2016.

[53] Y. Zhang, Y. Jiang, Y. Luo, and Y. Zeng, "Interference of miR-212 and miR-384 promotes osteogenic differentiation via targeting RUNX2 in osteoporosis," *Experimental and Molecular Pathology*, vol. 113, Article ID 104366, 2020.

[54] L. De-Ugarte, S. Balcells, X. Nogues, D. Grinberg, A. Diez-Perez, and N. Garcia-Giralt, "Pro-osteoporotic miR-320a impairs osteoblast function and induces oxidative stress," *PLoS One*, vol. 13, no. 11, Article ID e0208131, 2018.

[55] Y. Liu, C. Wang, G. Wang et al., "Loureirin B suppresses RANKL-induced osteoclastogenesis and ovariectomized osteoporosis via attenuating NFATc1 and ROS activities," *Theranostics*, vol. 9, no. 16, pp. 4648–4662, 2019.

[56] L. Wang, Y.-G. Zhang, X.-M. Wang, L.-F. Ma, and Y.-M. Zhang, "Naringin protects human adipose-derived mesenchymal stem cells against hydrogen peroxide-induced inhibition of osteogenic differentiation," *Chemico-Biological Interactions*, vol. 242, pp. 255–261, 2015.

[57] T. H. Khan, M. A. Ganaie, K. M. Alharthy, H. Madkhali, B. L. Jan, and I. A. Sheikh, "Naringenin prevents doxorubicin-induced toxicity in kidney tissues by regulating the oxidative and inflammatory insult in Wistar rats," *Archives of Physiology and Biochemistry*, vol. 126, no. 4, pp. 300–307, 2020.

[58] P. M. Costa, C. Miguel, S. Caeiro et al., "Transcriptomic analyses in a benthic fish exposed to contaminated estuarine sediments through laboratory and in situ bioassays," *Ecotoxicology*, vol. 20, no. 8, pp. 1749–1764, 2011.

[59] P. Fan, O. L. Griffith, F. A. Agboke et al., "c-Src modulates estrogen-induced stress and apoptosis in estrogen-deprived breast cancer cells," *Cancer Research*, vol. 73, no. 14, pp. 4510–4520, 2013.

[60] D. A. Siwik, P. J. Pagano, and W. S. Colucci, "Oxidative stress regulates collagen synthesis and matrix metalloproteinase activity in cardiac fibroblasts," *American Journal of Physiology-Cell Physiology*, vol. 280, no. 1, pp. C53–C60, 2001.

[61] E. J. Nam, G. Yoo, J. Y. Lee et al., "Glycosyl flavones from Humulus japonicus suppress MMP-1 production via decreasing oxidative stress in UVB irradiated human dermal fibroblasts," *BMB Reports*, vol. 53, no. 7, pp. 379–384, 2020.

[62] L. Liu, T. Zheng, F. Wang et al., "Pro12Ala polymorphism in the PPARG gene contributes to the development of diabetic nephropathy in Chinese type 2 diabetic patients," *Diabetes Care*, vol. 33, no. 1, pp. 144–149, 2010.

[63] C. Giovannini, P. Chieco, A. Bertaccini, L. Gramantieri, M. Lacchini, and G. Martorana, "Checkpoint effectors CDKN1A and Gadd45 correlate with oxidative DNA damage in human prostate carcinoma," *Anticancer Research*, vol. 24, no. 6, pp. 3955–3960, 2004.

[64] S. Zahler, C. Kupatt, J. Möbert, B. F. Becker, and E. Gerlach, "Effects of ACE-inhibition on redox status and expression of P-selectin of endothelial cells subjected to oxidative stress," *Journal of Molecular and Cellular Cardiology*, vol. 29, no. 11, pp. 2953–2960, 1997.

[65] Y. Chtourou, B. Aouey, S. Aroui, M. Kebieche, and H. Fetoui, "Anti-apoptotic and anti-inflammatory effects of naringin on cisplatin-induced renal injury in the rat," *Chemico-Biological Interactions*, vol. 243, pp. 1–9, 2016.

[66] Y. Chtourou, B. Aouey, M. Kebieche, and H. Fetoui, "Protective role of naringin against cisplatin induced oxidative stress, inflammatory response and apoptosis in rat striatum via suppressing ROS-mediated NF-κB and P53 signaling pathways," *Chemico-Biological Interactions*, vol. 239, pp. 76–86, 2015.

[67] Y. Wang, J. Xu, X. Zhang et al., "TNF-α-induced LRG1 promotes angiogenesis and mesenchymal stem cell migration in the subchondral bone during osteoarthritis," *Cell Death & Disease*, vol. 8, no. 3, Article ID e2715, 2017.

[68] D. Daoussis, A. P. Andonopoulos, and S.-N. C. Liossis, "Wnt pathway and IL-17: novel regulators of joint remodeling in rheumatic diseases. Looking beyond the RANK-RANKL-OPG axis," *Seminars in Arthritis and Rheumatism*, vol. 39, no. 5, pp. 369–383, 2010.

[69] M. P. Whyte, "Paget's disease of bone and genetic disorders of RANKL/OPG/RANK/NF-B signaling," *Annals of the New York Academy of Sciences*, vol. 1068, no. 1, pp. 143–164, 2006.

[70] R. Y. Kim, H. J. Yang, Y. M. Song, I. S. Kim, and S. J. Hwang, "Estrogen modulates bone morphogenetic protein-induced sclerostin expression through the wnt signaling pathway," *Tissue Engineering. Part A*, vol. 21, no. 13-14, pp. 2076–2088, 2015.

Hindawi
Evidence-Based Complementary and Alternative Medicine
Volume 2021, Article ID 2444839, 10 pages
https://doi.org/10.1155/2021/2444839

Research Article

Bioflavonoid *Galangin* Suppresses Hypertrophic Scar Formation by the TGF-β/Smad Signaling Pathway

Zha Ru,[1] **Ying Hu**,[1] **Shenghua Huang**,[1] **Li Bai**,[1] **Kun Zhang**,[2] **and Yue Li**[2]

[1]*Department of Plastic Surgery, The Third Affiliated Hospital of Sun Yat-Sen University, Guangzhou 510630, China*
[2]*Department of Traditional Chinese Medicine, The Third Affiliated Hospital of Sun Yat-Sen University, Guangzhou 510630, China*

Correspondence should be addressed to Kun Zhang; zhangk58@mail.sysu.edu.cn and Yue Li; liyue48@mail.sysu.edu.cn

Received 28 April 2021; Revised 10 August 2021; Accepted 20 August 2021; Published 4 September 2021

Academic Editor: Amjad Iqbal

Background. Hypertrophic scar (HS) is a benign fibroproliferative skin disease resulting from an aberrant wound healing process and can cause aesthetic and functional damage to patients. Currently, there is no ideal treatment to treat this disease. *Galangin*, a natural active bioflavonoid compound, is suggested to inhibit fibrosis and proliferation in certain cells. *Methods*. In this study, we found *Galangin* could attenuate abnormal scar formation in an HS rabbit ear model. Additionally, the HE staining shows *Galangin* reduced scar elevation index (SEI) and Masson's trichrome staining changed collagen deposition. *Results*. The expressions of type I collagen, type III collagen, and TGF-β1 were much lower under a proper dose of *Galangin* treatment, and Smad7 expression was also enhanced, which are examined by real-time PCR, immunohistochemistry, and western blot. *Conclusion*. Our data indicated that *Galangin* can alleviate dermal scarring via the TGF-β/Smad signaling pathway probably by upregulating Smad 7 expression and, thus, suppressing the expression of type I and type III collagens and TGF-β1.

1. Background

Scarring is an inevitable natural process during wound healing. The wound healing progress is a complex one which involves many types of cells, mediators, and three sequential steps: inflammation, new tissue formation, and remodeling [1, 2]. Besides, the remodeling phase comes with scar formation to some extent. However, in some cases, hypertrophic scar (HS) is formed, which is defined as an excessive scar tissue within the original wound. Despite the yet unknown detailed mechanism of HS, some factors are considered to be related to HS formation, such as age, bacterial colonization, and skin stretch [3, 4]. Collagen is overdeposited in the extracellular matrix (ECM), and the fibroblasts become overproliferated during the remodeling phase of wound healing [5]. As a result, wound healing ends up with HS formation, which may cause dysfunction, pain, aesthetic problem, etc. [6]. Although several decades have been spent to searching optimal treatments for HS, it remains an unmet challenge.

However, unlike the scar formation in adults, wound healing of fetal tissue is scarless [7]. The expression of cytokines, growth factors, and ECM deposition in the injured tissue differs significantly, among which transforming growth factor-β (TGF-β) is considered to play the key role [8]. TGF-β, activated by Smad proteins in fibroblasts, interacts with TGF-β receptor and leads to an increase in the production of collagen in the ECM and cell proliferation [9]. Smad 7, as the particularly negative feedback regulator of the TGF-β/Smad signal path, can prevent receptor-regulated Smads (*R*-Smads) phosphorylation by integrating with the activated TGF-β1 receptors. Therefore, an overexpression of Smad 7 may possibly attenuate TGF-β1 excretion and inhibit fibrinolysis [10].

Galangin is a flavonoid compound extracted from Chinese galangal root and used as herbal treatment in traditional medicine, which is also used in modern clinical treatment because of its antioxidant, anti-inflammatory, and proapoptosis effects [11–13]. Also, the bioflavonoid had been reported of its alleviating fibrosis effect in the kidney

and renal organs [14, 15]. Considering the bioactivity and pharmacological effects of *Galangin*, we wondered whether it can be used to inhibit HS formation in vivo. Besides, among a large amount of studies to investigate the therapeutic effect of bioflavonoid, little is known about its effect in HS formation.

In this study, HS models were established in rabbits' ears. The effect of bioflavonoid on HS was investigated, and its unique role in regulating the expression of key factors in the TGF-β/Smad signaling pathway was studied.

2. Materials and Methods

2.1. Animals. All procedures of this experiment were approved by the Ethics Committee of the First Affiliated Hospital of Xinjiang Medical University. Also, our researchers observed the Animal Welfare Act. Twenty female New Zealand white rabbits (weighing 2.0 to 2.8 kg, cleaning I grade) were single-housed under the same standard in the Laboratory Animal Center of Xinjiang Medical University (License No. 20170214-71).

2.2. Preparation of Rabbit Ear HS Models, Treatment, and Sampling. On day 0, rabbits were anesthetized by intramuscular injection with 0.15 mL/kg Zoletil 50 (tiletamine hydrochloride and zolazepam hydrochloride) and 0.1 mL/kg ketamine, respectively. Under sterile conditions, six 8 mm diameter round full-thickness dermal wounds were excised down to the bare cartilage on the ventral surface of each ear [16]. The bare cartilages, from the epidermis to perichondrium, were all removed under a surgical operating microscope [17]. During the excision, visible vessels were avoided and bleeding was treated by manually pressing with gauze. All of the wounds were then banded with sterile adhesive dressings. A total of 240 wounds were created in 20 rabbits. On day 15, successfully established HS models were divided into four groups along the vertical axis of each ear from left to right in 19 rabbits (one rabbit died on day 2 probably due to the anesthetization side effects) (Figure 1). Subsequently, 219 HSs (9 scars were excluded because of invagination) were treated by intralesional injection of either normal saline (group *A*, $n = 55$) or different doses of *Galangin* solution (group *B*, $n = 54$, 2 mg/mL; group *C*, $n = 56$, 1 mg/mL; and group *D*, $n = 54$, 0.5 mg/mL), which were purchased from Shanxi Guanchen Biotechnology Co., Ltd., China (GC-01-398, Purity: $\geq 98\%$ (HPLC)) and ultrasonic dissolved with normal saline [16, 18]. The injection was performed every three days and four times in total. In addition, since day 15 after wounding, photographs of ears and scarring areas were taken before each time of injection for qualitative changes in scar morphology [19]. On day 27, rabbits were sacrificed and 207 HS tissue (a rabbit died after the second injection) were harvested with a 3 mm unwounded margin (Figure 1(e)). From each group, 45 HSs were randomly collected.

2.3. Histopathological Analysis. The 60 HSs (15 in each group) were fixed with formaldehyde, embedded in paraffin, cut into 4 μm sections, and stained for histopathological analysis. After haematoxylin and eosin (HE) stain, the protuberant degrees were measured as scar elevation index (SEI), which represents the ratio of the scar area to the estimated area below the protuberant portion that had the neogenesis with the same height as the surrounding non-wounded dermis [16]. To analyze collagen deposition and arrangement, Masson's trichrome staining was carried out using a quick staining kit (Njjcbio, China) as the manufacturer's instruction recommended. For immunohistochemistry, the endogenous peroxidase was inactivated by 3% H_2O_2 incubation for 10 minutes at around 25°C, and then, the sections were incubated with 1% citric acid for 10 minutes in a microwave for antigen retrieval. After that, the sections were blocked with normal goat serum (ZSGB-Bio, China) for 15 minutes at 37°C and then incubated with primary antibodies of collagen I (Cat# ab90395; 1 : 1000dilution; Abcam), collagen III (Cat# ab7778; 1 : 5000 dilution; Abcam), TGF-β1 (Cat# sc-146; 1 : 500 dilution; Santa Cruz Biotechnology), and Smad-7 (Cat#sc-365846; 1 : 500 dilution; Santa Cruz Biotechnology) at 4°C overnight. Finally, sections were incubated with goat anti-rabbit secondary antibody (Boster, China) or goat anti-mouse secondary antibody (Boster, China) for 30 minutes at 37°C, followed by DAB (Boster, China) coloration for 5 minutes and haematoxylin staining. All histological images were obtained with an optical microscope connected to cellSens software (Olympus, Japan), and the quantification of positive cells in immunohistochemistry was carried out using Image J software (1.52 v).

2.4. Real-Time PCR. Sixty (15 for each group) HS samples were ground into powders in liquid nitrogen, and then, total RNA was extracted using TRIzol® (Invitrogen) following the manufacturer's instructions. RNA was reverse-transcripted into cDNA with a RevetAid First Strand cDNA Synthesis Kit (Thermo Scientific, USA). Real-time PCR was operated using the Maxima SYBR Green qPCR Master Mix (Thermo Scientific, USA) on the iQCycler thermocycler (Bio-Rad). The primer sequences (synthesized by Sangon Biotech, China) are listed in Table 1. Real-time PCR was carried out as follows: initial denaturation for 10 minutes at 95°C and 40 cycles of 15 seconds at 95°C and 60 seconds at 60°C. Quantification was always normalized to the internal control GAPDH, and each template was repeated three times under the same condition.

2.5. Western Blot. Briefly, 60 HS tissue samples (15 each group) were lysed with Pierce® RIPA buffer (Thermo Scientific, USA) and PMSF (100 : 1). The extracted proteins were measured by using the Pierce® BCA Protein Assay Kit (Thermo Scientific, USA). Proteins were isolated on 12% SDS-PAGE and transferred to polyvinylidene fluoride (PVDF) membranes (Millipore, Bedford, USA). Then, the membranes were incubated with primary antibodies of collagen I (Cat# ab90395; 1 : 500 dilution; Abcam), collagen III (Cat# ab7778; 1 : 1000 dilution; Abcam), TGF-β1 (Cat# sc-146; 1 : 200 dilution; Abcam), Smad-7 (Cat# sc-365846; 1 : 200 dilution; Abcam), and β-actin (Cat# sc-47778; 1 : 500 dilution; Santa Cruz Biotechnology) overnight at 4°C, respectively. After PBS washing, HRP-conjugated goat anti-

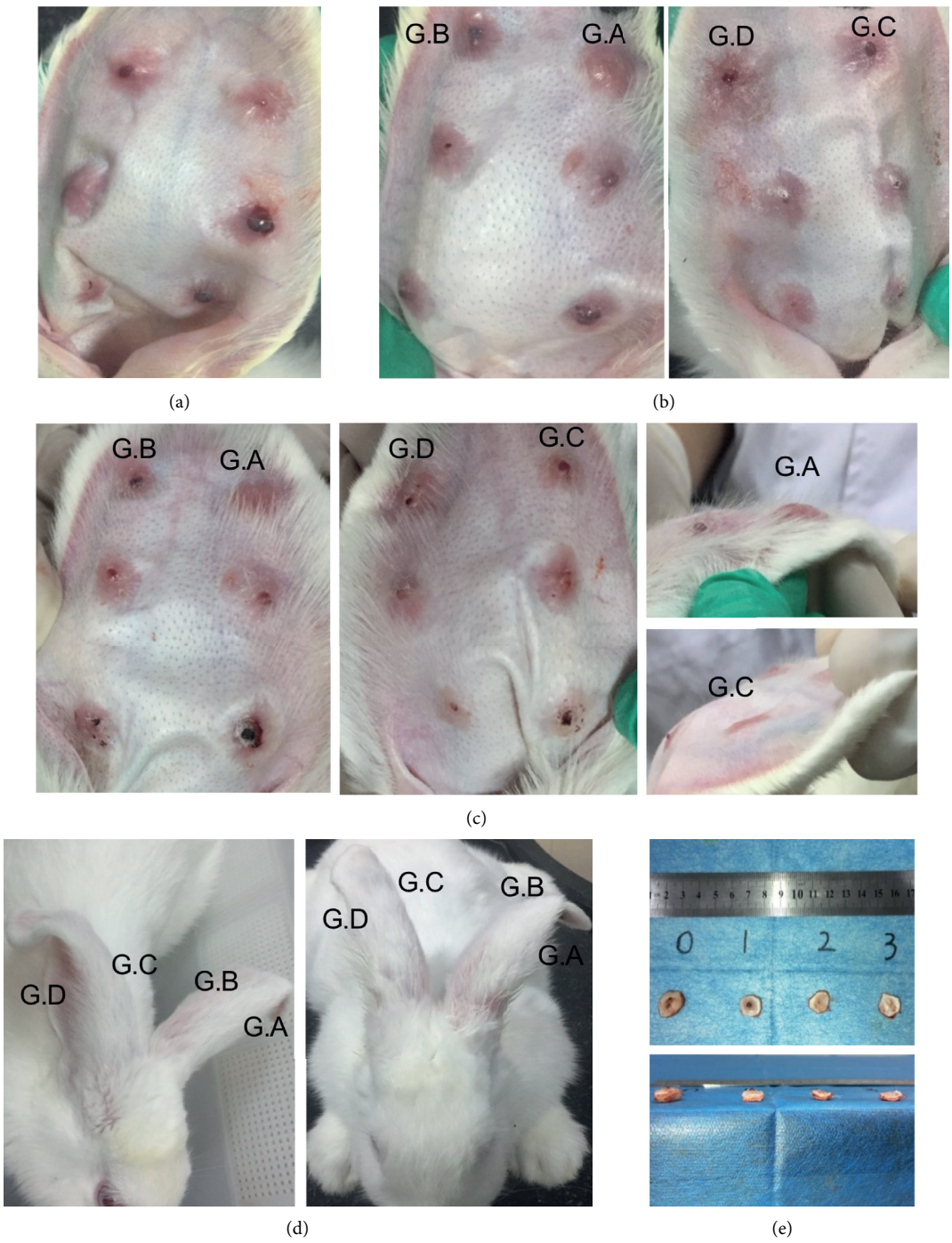

Figure 1: Gross images of representative scarring samples. (a) On day 15 after wounding, the epithelialization was completed and the HS model was accomplished. (b) After the second injection (day 20), the HSs in group *C* and *D* were more softened and had lower protuberant heights. (c) At the end of the injection (day 27), a much more significant effect in the *Galangin* injection groups was observed. G. A : group *A*; G. B : group *B*; G. C : group *C*; and G. D : group *D*. (d) A special phenomenon was noticed; after the third injection (day 24), the rabbit ear of group *A* and group *B* was slouched (left) and the rabbit ear of group *C* and *D* became erected again (right). (e) On day 27, after the injection procedure, the HSs were harvested for further experiments. The numbers 0 to 3 represent group *A* to *D*, respectively.

Table 1: Primer sequences for PCR amplification.

Gene		Sequence (5′-3′)
Collagen I	Forward:	AAG GAG ACA CTG GTG CCA AG
	Reverse:	AGT AGG TCC GGG TTC ACC TC
Collagen III	Forward:	TGG GAA GCC AGG AGT TAA TG
	Reverse:	ATC CAG GGT TTC CGT CTC TT
TGF-β1	Forward:	CCA GGA ATA CAG CAA CGA TTC C
	Reverse:	CCA CTG CCT CAC AAC TCC A
Smad 7	Forward:	GTG GCA TAC TGG GAG GAG AA
	Reverse:	TTG TTG TCC GAA TTG AGC TG
GAPDH	Forward:	ATT TGA AGG GCG GAG CCA AA
	Reverse:	TCA TGA GCC CCT CCA CAA TG

rabbit or goat anti-mouse secondary antibody (Abbkine, USA) was added and incubated at around 25°C for 2 hours. The protein bands were visualized using the ECL Kit (Thermo Scientific, USA), and the densities of the bands were compared with that of β-actin as reference.

2.6. Statistical Analysis. All statistic data were analyzed with SPSS version 22 and were demonstreated as mean ± standard deviation (SD). Intergroup comparisons were analyzed by Student's *t*-test. One-way ANOVA was used to compare the mean values of four groups simultaneously, followed by Tukey's test or Tamhane's method while the variance was not homogenous. P value less than 0.05 was considered as statistically significant.

3. Results

3.1. Effect of Galangin on Gross Scar Formation. To dynamically observe the scar-forming progress and the effect of *Galangin* on scar formation since day 15 after wounding (Figure 1(a)), the scars were observed every day and photographed before each injection. The intralesional *Galangin* injection groups showed obvious softness after the second injection compared with the control group (Figure 1(b)). Some HSs in group *C* and *D* almost resembled the normal skin, which had lower protuberant heights (Figure 1(c)). Some vulnerable epidermis samples were observed in group *B*, in the form of bleeding or ulceration. In addition, a rabbit showed slouched ears because of the scar contracture, but the sides of rabbit ears in group *C* and *D* became erected again after the third injection (Figure 1(d)). These results indicate that *Galangin* may soften the scar and delay the wound healing.

3.2. Effect of Galangin on SEI and Collagen. To evaluate the effects of *Galangin* on cell morphology, HE staining was performed. Many spindle-shaped cells of the control group were observed, while most of them in the *Galangin* injection groups were round. The number of fibroblasts was the lowest in group *C* (Figure 2(a)). Furthermore, the quantitative analysis of SEI decreased from 1.75 ± 0.13 to 1.68 ± 0.08, 1.57 ± 0.10, and 1.58 ± 0.86 (Figure 2(b)). These results suggest that treatment with a proper dose of *Galangin* may restrain the proliferation of fibroblasts and less decrease the protuberant degree of HSs. The HS tissues were subjected to Masson staining to examine the effect of *Galangin* on collagen arrangement. It showed that the collagen was sparsely distributed and arranged as a net-like shape resembling to the surrounding unwounded tissues in the *Galangin*-treated groups, especially in group *C* and *D*, while the collagen of the control group was densely arranged, parallel to the epithelium and less mature with more fibroblasts (Figure 2(c)). Therefore, treatment with a proper dose of *Galangin* may lead to collagen arranging and depositing in a beneficial direction.

3.3. The Effect of Galangin on the Protein Expressions of Type I Collagens, Type III Collagens, TGF-β1, and Smad 7. In order to observe the expression of type I collagens, type III collagens, TGF-β1, and Smad 7 of HS tissues, immunohistochemical staining was performed. There was less type I collagen deposition in the cellular mesenchyme after *Galangin* treatment from 10.97 ± 0.53 to 6.24 ± 0.60, 4.12 ± 0.65, and 4.21 ± 0.54 (Figure 3(a), *E*, $P < 0.05$), and type III collagen deposition also decreased from 16.84 ± 0.42 to 13.71 ± 0.47, 11.79 ± 0.60, and 8.83 ± 0.56 (Figure 3(b), *F*, $P < 0.05$). Besides, expressions of TGF-β1 were 15.14 ± 0.71, 17.10 ± 0.36, 12.34 ± 0.73, and 10.88 ± 0.63 (Figure 3(c), *G*, $P < 0.05$), and a higher expression was detected in group B. Also, Smad 7 increased in the *Galangin*-treated groups, from 4.33 ± 0.26 to 5.47 ± 0.41, 6.81 ± 0.46, and 11.45 ± 0.56 (Figure 3(d), *H*, $P < 0.05$). To further verify the influence of *Galangin* treatment on the protein expressions of type I collagens, type III collagens, TGF-β1, and Smad 7, western blot was performed. The results demonstrated that type I collagens and type III collagen expressions remarkably reduced in the *Galangin*-treated groups from 1.32 ± 0.09 to 0.83 ± 0.21, 0.27 ± 0.12, and 0.34 ± 0.16 and from 1.27 ± 0.02 to 0.90 ± 0.09, 0.65 ± 0.11, and 0.34 ± 0.09, respectively (Figures 4(b) and 4(c), $P < 0.05$). The TGF-β1 protein expressions were 1.13 ± 0.27, 1.56 ± 0.09, 0.36 ± 0.07, and 0.16 ± 0.05, which were effectively suppressed in group *C* and *D*, while a higher expression was detected in group *B* (Figure 4(d) $P < 0.05$). By contrast, the Smad 7 protein expression significantly increased after *Galangin* treatment, from 0.18 ± 0.08 to 0.46 ± 0.25, 0.81 ± 0.13, and 1.21 ± 0.11 (Figure 4(d), $P < 0.05$). Thus, it is assumed that *Galangin* might reduce collagen deposition and TGF-β1 expression, while promoting Smad 7 expression.

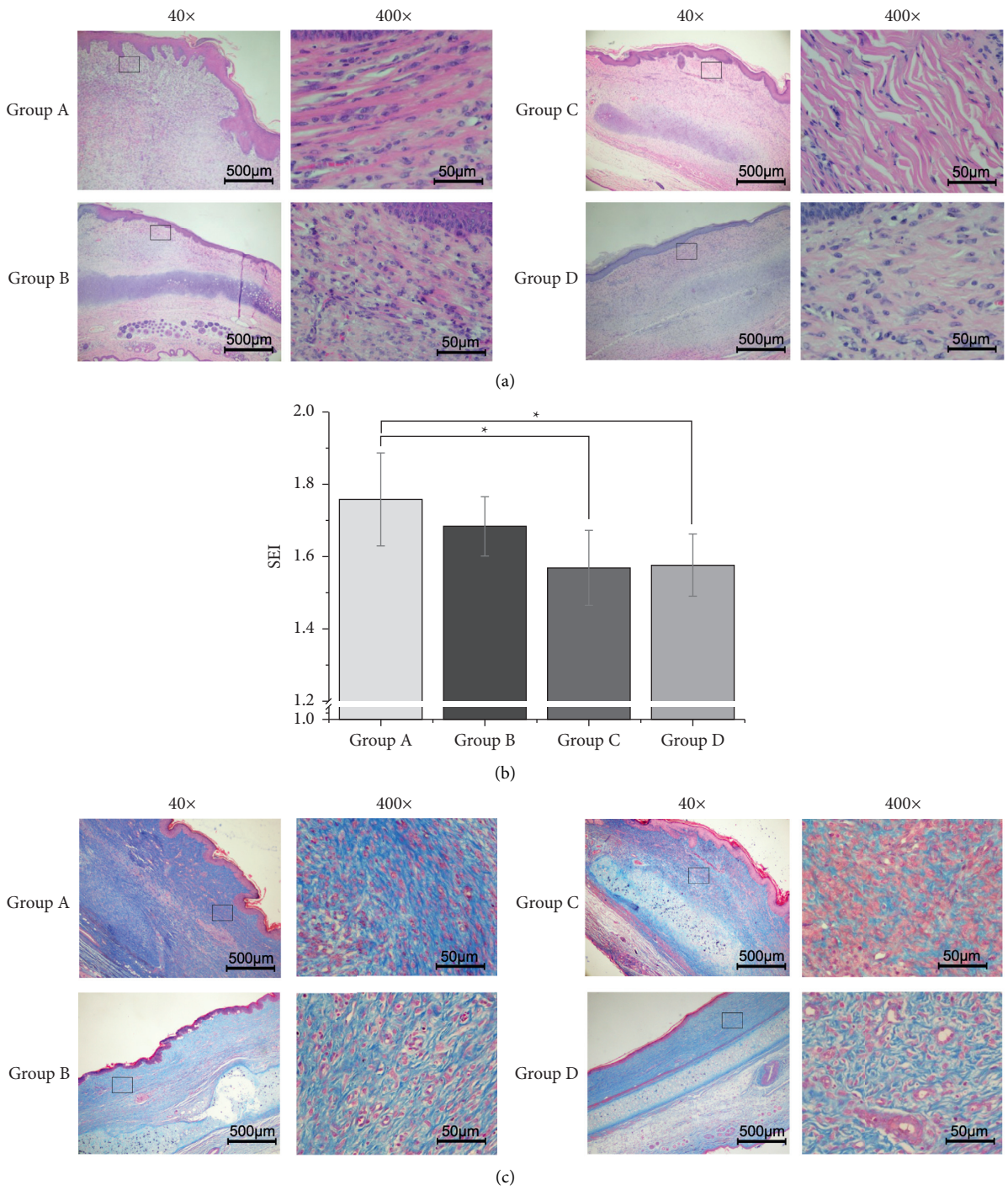

Figure 2: Morphology analysis of hypertrophic scars after *Galangin* injection. (a) HE staining showed different protuberant degrees among these groups. (b) The SEI was measured according to the observation of HE staining. The SEI significantly decreased in group *C* and *D*. $^{*}P < 0.05$, compared with the control group (saline injection). (c) Masson staining revealed the collagen and arrangement in the HS tissues.

3.4. The Effect of Galangin on the mRNA Expressions of Type I Collagens and Type III Collagens, TGF-β1, and Smad 7. To test the mRNA expressions of type I collagens and type III collagens, TGF-β1, and Smad 7, quantitative RT-PCR was carried out. The results demonstrated that the type I collagen mRNA expression was suppressed in all the *Galangin*-treated groups (Figure 5(a), $P < 0.05$), especially in group *C* (*Galangin*, 1 mg/mL). The mRNA expressing of type III collagen and TGF-β1 was inhibited in the *Galangin*-treated groups, among which the effect in group *D* (*Galangin*, 0.5 mg/mL) was the most significant (Figures 5(b) and 5(c), $P < 0.05$). In contrast, the mRNA expression of Smad 7, which is considered as a unique inhibitor of the TGF-β/Smad signal pathway, in the *Galangin*-treated groups was

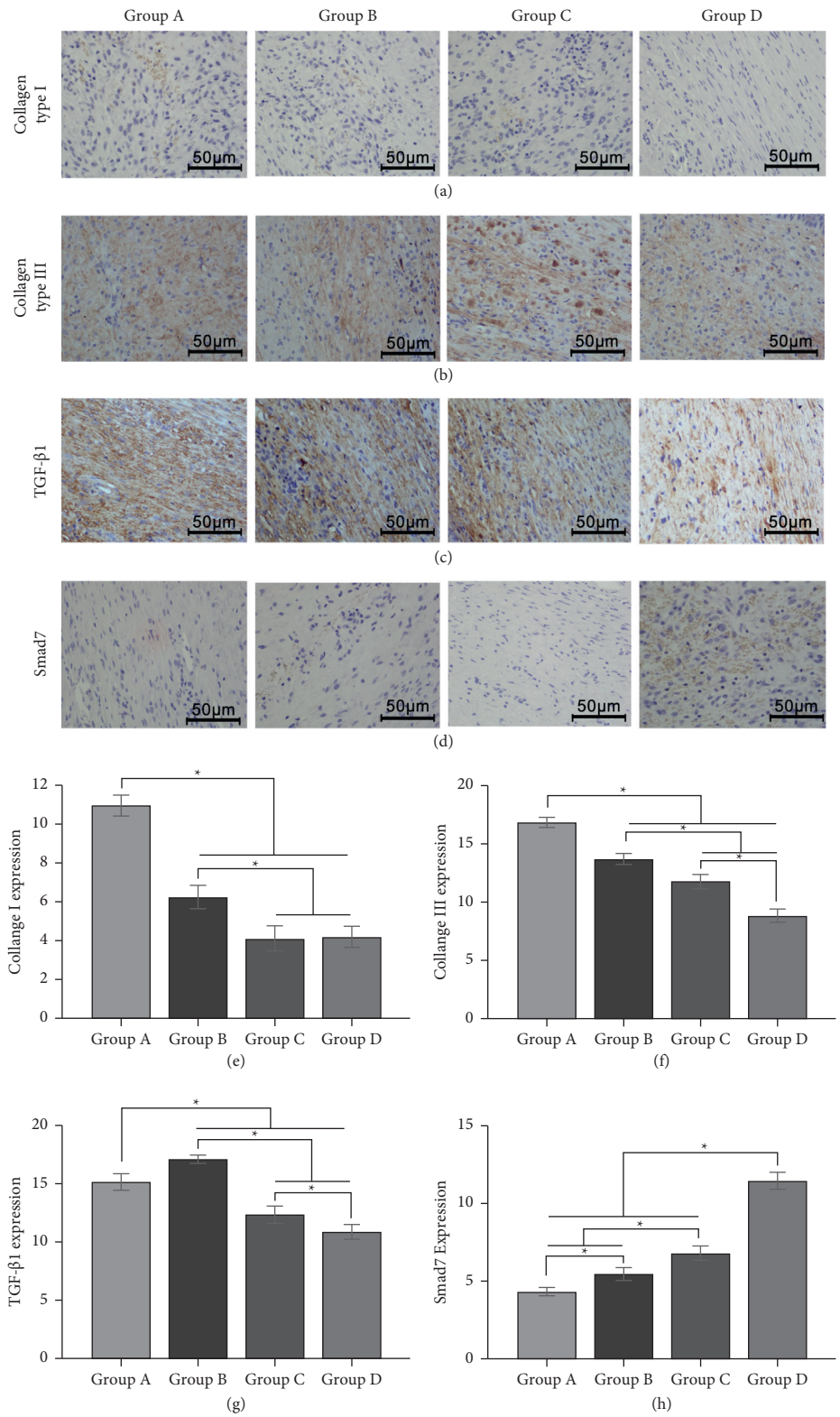

Figure 3: Representative immunohistochemical staining of (a) type I and (b) type III collagens, (c) TGF-β1, and (d) Smad 7 in each group.

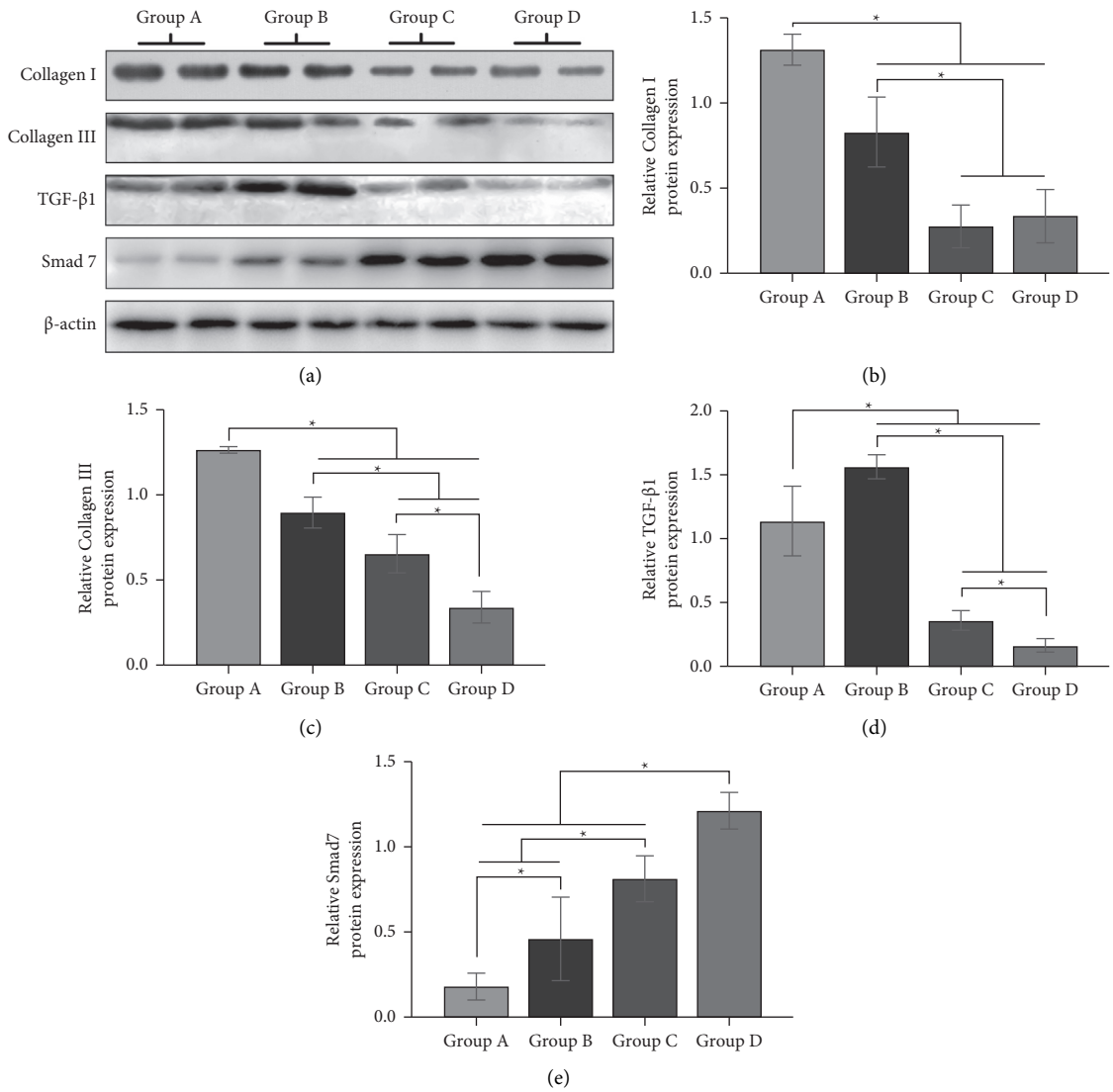

Figure 4: The protein expression levels of type I and type III collagens, TGF-β1, and Smad 7. The protein levels were analyzed by western blot, and β-actin was used as an internal control. The representative and quantitative results of (a) type I and (b) type III collagens, (c) TGF-β1, and (d) Smad7 are shown. $^{*}P < 0.05$, compared to the control group.

much higher than that of the control group (Figure 5(d), $P < 0.05$). These results suggest that the mRNA levels of type I collagen and type III collagen and TGF-β1 were down-regulated after a proper dose of *Galangin* treatment, while the Smad 7 level was upregulated.

4. Discussion

Scar formation is the normal consequence of skin injury, which is thin and resembles normal skin under correct regulation. However, prolonged inflammation, local mechanical tension, and chronic stimulation may cause excessive deposition of collagen and proliferation of fibroblasts, eventually leading to HS formation [9, 10, 20]. Moreover, because of the overproliferated and overactivated fibroblasts, HS also is considered as a benign skin tumor [21]. So far, although the treatment for HS is still unsatisfying, surgical operation to reduce local force and anti-inflammatory and anti-angiogenesis treatment are applicable strategies [22]. *Galangin*, a kind of bioflavonoid, is found to have antiproliferative property to certain cells [11, 23, 24]. Besides, bioflavonoid has also been proved to alleviate fibrosis in the liver [15]. Thus, based on the abovementioned study, we assumed that *Galangin* could suppress HS formation, and this assumption is proved in our further investigation which shows that *Galangin* could soften the HSs and decrease the SEI of the rabbit ear model in vivo.

Previous studies have suggested that wound healing and scarring are closely related to TGF-β family members, which also participate in regulations of a wide spectrum of cellular functions such as proliferation, differentiation, migration, and apoptosis [25, 26]. Increased amounts of TGF-β have been found in HS, and the scar-free healing in human fetus is

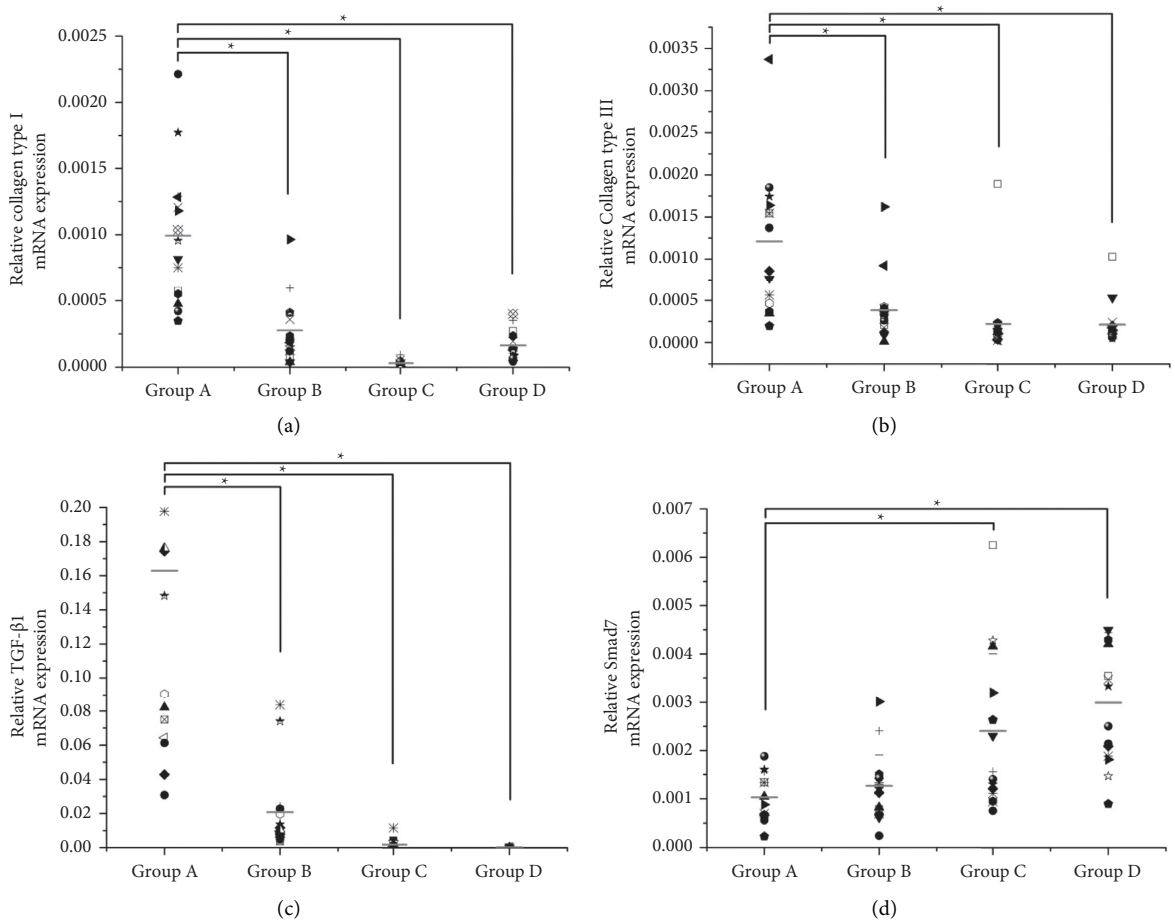

Figure 5: The effect of *Galangin* on the mRNA expression of (a) type I collagen, (b) type III collagen, (c) TGF-β1, and (d) Smad 7. The mRNA expression was detected with real-time PCR and normalized to that of GADPH. The horizontal bar indicates the mean of the measurements in each group. $^{*}P < 0.05$, compared to the control group.

considered as a consequence of TGF-β deficiency [8, 27]. Besides, it has been reported that TGF-β mediates the fibroblast proliferation, angiogenesis, ECM synthesis, and reepithelialization during the wound healing course [28, 29]. Overexpression of TGF-β1 and TGF-β2 was detected in HSs, whereas TGF-β3 was reported to have antifibrotic effects [10]. Particularly, TGF-β1 regulates various fibrosis-related proteins transcriptionally, including type I collagen and type III collagen [30, 31]. A previous study showed that bioflavonoid can attenuate TGF-β-induced fibrosis in human tubular epithelial cells [14]. Also, our preliminary study in vitro shows that bioflavonoid dose-dependently decreased cell viability in fibroblast cells [32], and the high expression of TGF-β1 protein in group *B* (*Galangin*, 2 mg/mL) might be due to the high dose of bioflavonoid which may cause tissue damage, though no visible wounds were observed on rabbit ears; thus, the proper dose of *Galangin* in vivo and toxicity study for epidermal cells need further tests. It can also accelerate the transformation of fibroblasts to myofibroblasts, which are considered as major cells in HS formation and characterized as an improved propensity to synthesize collagen and upregulation of cytokines [33, 34]. Therefore, it is speculated that attenuation of TGF-β1 activities would have potential advantages in inhibiting HS formation.

Despite the limited varieties of TGF-β receptors and Smads, there may be a greater variety of the signal possibilities than we used to expect. Combinatorial interactions between TGF-β receptors and Smads in oligomeric complexes allow substantial diversity and are complemented by various sequence transcription factors cooperating with Smads, leading to context-dependent transcriptional regulation [35–37]. Additionally, other signaling pathways may also help to define the responses to TGF-β, and it is evidently shown that TGF-β-related protein activation is not a linear signaling transduction pathway. These pathways not only involve Smad-dependent responses but also the Smad-independent responses [38]. On the one hand, the TGF-β1-activated Smad-dependent pathways can cause cellular changes such as the collagen synthesis and secretion, leading to the aggravated scar formation. However, Smad-independent signaling paths may improve healing. Therefore, inhibition of TGF-β1 transcription may reduce scarring but delay wound healing [39–41]. In the current study, it was observed that treatment with a proper dose of *Galangin* could lessen scarring and delay healing. Meanwhile, the Smad 7 expression was upregulated and that of TGF-β1 was decreased.

There are three distinct Smad subfamilies: receptor-regulated Smads (*R*-Smads), common-partner Smads (Co-Smads), and inhibitory Smads (I-Smads). Smad 7, which acts as the I-Smads of TGF-β family signaling, can bind with TGF-β receptor, thus preventing the recruitment and phosphorylation of effector Smads and inhibiting TGF-β/Smads signaling [10, 38, 42]. The TGF-β/Smad signal path is an autoinhibitory loop to control the intensity and duration of TGF-β signaling response. TGF-β stimulation could cause the export of Smad 7 from the nucleus [37]. Therefore, the expression level of Smad 7 will influence TGF-β transcriptional responses. Cells with a higher level of Smad 7 are more inclined to resist the profibrotic activities of TGF-β. As this study indicated, *Galangin* treatment blocked the TGF-β/Smad signaling via increasing the expression of Smad 7, and thus, the stimulation effect of TGF-β1 on collagen deposition in ECM was inhibited.

5. Conclusions

The rabbit ear HS model was established successfully. A proper dose of *Galangin* could negatively regulate the expression of type I collagens and type III collagens and the collagen deposition. TGF-β1 transcription was downregulated, which might be partially due to Smad 7 upregulation. This study suggests that *Galangin* may have potential to prevent HS formation.

Data Availability

The data used to support the findings of this study are available from the corresponding author upon request.

Conflicts of Interest

The authors declare no conflicts of interest.

Authors' Contributions

Zha Ru and Ying Hu contributed equally to this work.

References

[1] G. C. Gurtner, S. Werner, Y. Barrandon, and M. T. Longaker, "Wound repair and regeneration," *Nature*, vol. 453, no. 7193, pp. 314–321, 2008.

[2] H. Sorg, D. J. Tilkorn, S. Hager, J. Hauser, and U. Mirastschijski, "Skin wound healing: an update on the current knowledge and concepts," *European Surgical Research*, vol. 58, no. 1-2, pp. 81–94, 2016.

[3] L. Butzelaar, M. M. W. Ulrich, A. B. Mink van der Molen, F. B. Niessen, and R. H. J. Beelen, "Currently known risk factors for hypertrophic skin scarring: a review," *Journal of Plastic, Reconstructive & Aesthetic Surgery*, vol. 69, no. 2, pp. 163–169, 2016.

[4] E. Y. Rha, Y. H. Kim, T.-J. Kim et al., "Topical application of a silicone gel sheet with verapamil microparticles in a rabbit model of hypertrophic scar," *Plastic and Reconstructive Surgery*, vol. 137, no. 1, pp. 144–151, 2016.

[5] E. E. Tredget, B. Levi, and M. B. Donelan, "Biology and principles of scar management and burn reconstruction," *Surgical Clinics of North America*, vol. 94, no. 4, pp. 793–815, 2014.

[6] C. C. Finnerty, M. G. Jeschke, L. K. Branski, J. P. Barret, P. Dziewulski, and D. N. Herndon, "Hypertrophic scarring: the greatest unmet challenge after burn injury," *The Lancet*, vol. 388, no. 10052, pp. 1427–1436, 2016.

[7] K. Kishi, K. Okabe, R. Shimizu, and Y. Kubota, "Fetal skin possesses the ability to regenerate completely: complete regeneration of skin," *Keio Journal of Medicine*, vol. 61, no. 4, pp. 101–108, 2012.

[8] A. L. Rippa, E. P. Kalabusheva, and E. A. Vorotelyak, "Regeneration of dermis: scarring and cells involved," *Cells*, vol. 8, no. 6, 2019.

[9] A. Armour, P. G. Scott, and E. E. Tredget, "Cellular and molecular pathology of HTS: basis for treatment," *Wound Repair and Regeneration*, vol. 15, no. s1, pp. S6–S17, 2007.

[10] W. M. van der Veer, M. C. T. Bloemen, M. M. W. Ulrich et al., "Potential cellular and molecular causes of hypertrophic scar formation," *Burns*, vol. 35, no. 1, pp. 15–29, 2009.

[11] S. Yu, L.-S. Gong, N.-F. Li, Y.-F. Pan, and L. Zhang, "Galangin (GG) combined with cisplatin (DDP) to suppress human lung cancer by inhibition of STAT3-regulated NF-κB and Bcl-2/Bax signaling pathways," *Biomedicine & Pharmacotherapy*, vol. 97, pp. 213–224, 2018.

[12] Z. Yang, X. Li, W. Han et al., "Galangin suppresses human osteosarcoma cells: an exploration of its underlying mechanism," *Oncology Reports*, vol. 37, no. 1, pp. 435–441, 2017.

[13] R. Capasso and N. Mascolo, "Inhibitory effect of the plant flavonoid galangin on rat vas deferens in vitro," *Life Sciences*, vol. 72, no. 26, pp. 2993–3001, 2003.

[14] Y. Cao, J. Hu, and J. Sui, "Quercetin is able to alleviate TGF-beta-induced fibrosis in renal tubular epithelial cells by suppressing miR-21," *Experimental and Therapeutic Medicine*, vol. 16, no. 3, pp. 2442–2448, 2018.

[15] X. Wang, G. Gong, W. Yang, Y. Li, M. Jiang, and L. Li, "Antifibrotic activity of galangin, a novel function evaluated in animal liver fibrosis model," *Environmental Toxicology and Pharmacology*, vol. 36, no. 2, pp. 288–295, 2013.

[16] L. W. D. E. Morris, "Acute and chronic animal models for excessive dermal scarring: quantative studies," *Plastic and Reconstructive Surgery*, vol. 100, no. 3, 1997.

[17] C. Yagmur, E. Guneren, M. Kefeli, and R. Ogawa, "The effect of surgical denervation on prevention of excessive dermal scarring: a study on rabbit ear hypertrophic scar model," *Journal of Plastic, Reconstructive & Aesthetic Surgery*, vol. 64, no. 10, pp. 1359–1365, 2011.

[18] M. Meuli, Y Liu, D Liggitt et al., "Efficient gene expression in skin wound sites following local plasmid injection," *Journal of Investigative Dermatology*, vol. 116, no. 1, pp. 131–5, 2001.

[19] J. H. M. Alexandrina and S. Saulis, "Effect of mederma on hypertrophic scarring in the rabbit ear model," *Plastic and Reconstructive Surgery*, vol. 110, no. 1, 2002.

[20] B. Berman, A. Maderal, and B. Raphael, "Keloids and hypertrophic scars: pathophysiology, classification, and treatment," *Dermatologic Surgery*, vol. 43, no. 1, pp. S3–S18, 2017.

[21] X. Wu, J. Li, X. Yang et al., "MiR-155 inhibits the formation of hypertrophic scar fibroblasts by targeting HIF-1α via PI3K/AKT pathway," *Journal of Molecular Histology*, vol. 49, no. 4, pp. 377–387, 2018.

[22] R. Ogawa, S. Akaishi, S. Kuribayashi, and T. Miyashita, "Keloids and hypertrophic scars can now be cured completely: recent progress in our understanding of the pathogenesis of keloids and hypertrophic scars and the most promising current therapeutic strategy," *Journal of Nippon Medical School*, vol. 83, no. 2, pp. 46–53, 2016.

[23] C.-S. Lei, Y.-C. Hou, M.-H. Pai, M.-T. Lin, and S.-L. Yeh, "Effects of quercetin combined with anticancer drugs on metastasis-associated factors of gastric cancer cells: in vitro and in vivo studies," *The Journal of Nutritional Biochemistry*, vol. 51, pp. 105–113, 2018.

[24] J. L. Johnson and E. Gonzalez de Mejia, "Interactions between dietary flavonoids apigenin or luteolin and chemotherapeutic drugs to potentiate anti-proliferative effect on human pancreatic cancer cells, in vitro," *Food and Chemical Toxicology*, vol. 60, pp. 83–91, 2013.

[25] C. Tziotzios, C. Profyris, and J. Sterling, "Cutaneous scarring: pathophysiology, molecular mechanisms, and scar reduction therapeutics," *Journal of the American Academy of Dermatology*, vol. 66, no. 1, pp. 13–24, 2012.

[26] C. Hwangbo, N. Tae, S. Lee et al., "Syntenin regulates TGF-β1-induced Smad activation and the epithelial-to-mesenchymal transition by inhibiting caveolin-mediated TGF-β type I receptor internalization," *Oncogene*, vol. 35, no. 3, pp. 389–401, 2015.

[27] Z. Zheng, X. Zhang, C. Dang et al., "Fibromodulin is essential for fetal-type scarless cutaneous wound healing," *American Journal Of Pathology*, vol. 186, no. 11, pp. 2824–2832, 2016.

[28] G. Wick, C. Grundtman, C. Mayerl et al., "The immunology of fibrosis," *Annual Review of Immunology*, vol. 31, no. 1, pp. 107–135, 2013.

[29] S. Muppala, R. Xiao, I. Krukovets, D. Verbovetsky, R. Yendamuri, and N. Habib, "Thrombospondin-4 mediates TGF-beta-induced angiogenesis," *Oncogene*, vol. 36, pp. 5189–5198, 2017.

[30] Y.-P. Hsieh, H.-M. Chen, H.-Y. Lin, H. Yang, and J. Z.-C. Chang, "Epigallocatechin-3-gallate inhibits transforming-growth-factor-β1-induced collagen synthesis by suppressing early growth response-1 in human buccal mucosal fibroblasts," *Journal of the Formosan Medical Association*, vol. 116, no. 2, pp. 107–113, 2017.

[31] M. Ide, M. Jinnin, Y. Tomizawa et al., "Transforming growth factor beta-inhibitor Repsox downregulates collagen expression of scleroderma dermal fibroblasts and prevents bleomycin-induced mice skin fibrosis," *Experimental Dermatology*, vol. 26, no. 11, pp. 1139–1143, 2017.

[32] H. Wang, W. Gao, M. Kong, N Li, and S Ma, "Preliminary study of the effect of abnormal savda munziq on TGF-β1 and Smad 7 expression in hypertrophic scar fibroblasts," *International Journal of Clinical and Experimental Medicine*, vol. 8, no. 1, pp. 519–525, 2015.

[33] F. Klingberg, B. Hinz, and E. S. White, "The myofibroblast matrix: implications for tissue repair and fibrosis," *The Journal of Pathology*, vol. 229, no. 2, pp. 298–309, 2013.

[34] B. J. Crider, G. M. Risinger, C. J. Haaksma, E. W. Howard, and J. J. Tomasek, "Myocardin-related transcription factors *A* and *B* are key regulators of TGF-β1-induced fibroblast to myofibroblast differentiation," *Journal of Investigative Dermatology*, vol. 131, no. 12, pp. 2378–2385, 2011.

[35] S. H. Qi, J.-L. Xie, S. Pan et al., "Effects of asiaticoside on the expression of Smad protein by normal skin fibroblasts and hypertrophic scar fibroblasts," *Clinical and Experimental Dermatology*, vol. 33, no. 2, pp. 171–175, 2008.

[36] S. Itoh, F. Itoh, M.-J. Goumans, and P. ten Dijke, "Signaling of transforming growth factor-β family members through Smad proteins," *European Journal of Biochemistry*, vol. 267, no. 24, pp. 6954–6967, 2000.

[37] S. Itoh, M. Landström, A. Hermansson et al., "Transforming growth factor β1 induces nuclear export of inhibitory Smad 7," *Journal of Biological Chemistry*, vol. 273, no. 44, pp. 29195–29201, 1998.

[38] Y. E. Z. Rik Derynck, "Smad-dependent and Smad-independent pathways in TGF-β family signalling," *Nature*, vol. 425, no. 9, 2003.

[39] Z. M. Altan and G Fenteany, "C-Jun *N*-terminal kinase regulates lamellipodial protrusion and cell sheet migration during epithelial wound closure by a gene expression-independent mechanism," *Biochemical and Biophysical Research Communications*, vol. 322, no. 1, pp. 56–67, 2004.

[40] X. Liu, P. Li, P. Liu et al., "The essential role for c-Ski in mediating TGF-β1-induced bi-directional effects on skin fibroblast proliferation through a feedback loop," *Biochemical Journal*, vol. 409, no. 1, pp. 289–297, 2008.

[41] L. Lu, A. S. Saulis, W. R. Liu et al., "The temporal effects of anti-TGF-β1, 2, and 3 monoclonal antibody on wound healing and hypertrophic scar formation," *Journal of the American College of Surgeons*, vol. 201, no. 3, pp. 391–397, 2005.

[42] J. Massagué, "How cells read TGF-β signals," *Nature Reviews Molecular Cell Biology*, vol. 1, 2000.

Hindawi
Evidence-Based Complementary and Alternative Medicine
Volume 2021, Article ID 8388002, 10 pages
https://doi.org/10.1155/2021/8388002

Research Article

The Antioxidant Effect of *Medicago sativa* L. (Alfalfa) Ethanolic Extract against Mercury Chloride ($HgCl_2$) Toxicity in Rat Liver and Kidney: An In Vitro and In Vivo Study

M. Raeeszadeh,[1] **M. Moradi**,[2] **P. Ayar**,[2] **and Abolfazl Akbari**[3]

[1]*Department of Basic Sciences, Sanandaj Branch, Islamic Azad University, Sanandaj, Iran*
[2]*Graduate of Faculty of Veterinary Sciences, Sanandaj Branch, Islamic Azad University, Sanandaj, Iran*
[3]*Department of Physiology, School of Veterinary Medicine, Shiraz University, Shiraz, Iran*

Correspondence should be addressed to M. Raeeszadeh; vet_mr@yahoo.com

Received 14 June 2021; Revised 4 August 2021; Accepted 14 August 2021; Published 26 August 2021

Academic Editor: Omayma Eldahshan

Heavy metals such as mercury are some of the environmental pollutants and can induce toxicity by bioaccumulation and oxidative damage. This study aimed to investigate the effect of ethanolic extract of *Medicago sativa* L. (Alfalfa) on mercury damage in the kidney and liver of rats. Thirty Wistar rats were randomly divided into five groups, the control group, S group (2 mg/kg mercury chloride), and T1, T2, and T3 groups that, in addition to mercury, received doses of 250, 500, and 750 mg/kg of the alfalfa extract. On the last day, blood samples were taken, and the serum was separated to measure biochemical and oxidative stress parameters in the kidney and liver. A part of the kidney and liver was also used for histopathological evaluation. Total phenols and flavonoids were 40.45 ± 2.12 and 14.36 ± 0.45 mg/g, respectively, whereas IC_{50} was $245.18 \pm 19.76\,\mu$g/ml. The body weight significantly decreased in the S group compared to other groups, while treatment with different doses of alfalfa extract increased the body weight. Mercury concentration in the kidney was higher than that in the liver. The serum levels of urea, creatinine, alanine aminotransferase (ALT), and alkaline phosphatase (ALP) significantly increased in the S group compared to the control group, while treatment with different doses of alfalfa extract increased their levels. Moreover, an increase in malondialdehyde (MDA) and a decrease in glutathione peroxidase (GPx), catalase (CAT), total antioxidant capacity (TAC), and superoxide dismutase (SOD) activity were observed in the S group. The level of these parameters significantly improved in the groups receiving the extract compared to the S group. Furthermore, the histopathological evaluation showed glomerular and tubular damage and hepatic necrosis in the S group and that these conditions improved in the T3 group. The findings of this study showed that the ethanolic extract of alfalfa in a dose-dependent manner has potentially unique protective effects against mercury poisoning in the kidney and liver.

1. Introduction

Mercury is a heavy metal with a dual capacity and has no biological function in the body. Exposure to it causes damage to growing and mature organisms. Mercury exposure, first, affects the central nervous system and then the kidneys and the digestive system [1]. The biological, pharmacokinetic, and clinical symptoms of mercury poisoning vary according to its chemical structure and duration of its exposure. Mercury vapors have a strong affinity for sulfhydryl groups when they enter the body and bind to sulfur-containing amino acids. Mercury dissolves in serum, attaches to the membrane of red blood cells, and is transmitted to the brain. Mineral mercury crosses the placenta and the blood-brain barrier and easily accumulates in the fetal brain [2]. In addition to the brain, mercury can accumulate in the thyroid, myocardium, muscles, adrenal glands, liver, kidneys, sweat glands, pancreas, enterocytes, salivary glands, testes, and prostate whereas impairs the function of these organs [3, 4]. Mercury has a strong tendency to revive sulfur and especially thiol-like molecules such as glutathione (GSH), cysteine, and metallothionein. The toxic effects of mercury on organs such as the liver and kidneys are due to biological reactions with metallothionein,

glutathione, and albumin [5]. Many studies showed that oxidative stress caused by mercury exposure (organic and inorganic) results from a reduction in thiol-containing groups, including glutathione. Mercury has been reported to reduce glutathione and induce lipid peroxidase and increase hydrogen peroxide formation in rat kidney tissue [6]. Several studies showed that many plants are considered rich sources of antioxidants and can be useful in preventing or treating diseases caused by an imbalance of the oxidative-antioxidative system. In consideration of the fact that oxidative stress induced by exposure to environmental pollutants such as mercury may lead to kidney and liver poisoning, researchers believe that antioxidant compounds can play a protective role against these pathological conditions [7]. Alfalfa, *Medicago sativa* L., is one of the most famous traditional medicinal plants used to cure and prevent many diseases [8]. Alfalfa contains vitamins (A, B1, B6, B12, C, D, E, and K), amino acids, sugars, proteins, minerals (Fe, Zn, Cu, Al, B, Cr, Co, Mn, Mo, Se, Si, Na, Ca, P, K, and Mg), and other nutrients. Due to its richness in vitamins and phytoestrogens, this plant is used as a food additive in several countries [8]. Phytochemical studies indicated that this plant contains a variety of secondary metabolites including flavonoids, alkaloids, phytoestrogens (coumestrol, daidzein, genistein, and pyocyanin), and coumarins as potent antioxidants [9, 10]. Now, the question is whether the consumption of this plant extract can prevent kidney and liver damage caused by exposure to mercury? Moreover, due to the lack of national and international studies as well as the importance of the toxicity of heavy metals, the subject of this study was to investigate the effect of hydroalcoholic extract of alfalfa on kidney and liver damage resulted from exposure to mercury chloride in male rats.

2. Materials and Methods

2.1. Preparation of the Alfalfa (Medicago sativa) Extract. After collection from the farmstead of Sanandaj, Iran, alfalfa plants were stored in a dry place and kept away from sunlight to dry, and then the leaves of the plant were pulverized. After that, 150 g of crushed powder with 75% ethanol were reached a volume of one liter and was immersed for 48 hours. The mixture was filtered by Whatman No. 1 filter paper and condensed by a rotary at 40°C. Finally, in order to administer the dose to the animals, concentrations of 250, 500, and 750 mg/kg of the extract were prepared by distilled water [9].

2.2. Measurement of Antioxidant Activity of the Ethanolic Extract. The measurement of antioxidant activity of the ethanolic extract was performed based on the inhibition of 2,2-diphenyl-1-picrylhydrazyl (DPPH) by extract. The concentrations of 20, 50, 100, 200, 500, 700, and 1000 μg/ml of the extract were prepared; after that, 300 μl extract was added to 2.7 ml of DPPH reagent and then read at 520 nm wavelength. IC_{50} was determined as the concentration of the extract that could inhibit 50% of DPPH radicals. This procedure was performed against vitamin C [11]. Total phenol content was measured using the Folin-Ciocalteu method. This low-cost method is the most widely used method for measuring polyphenols in plant extracts.

It is worth noting that the gallic acid was used to draw the calibration curve. The obtained results were then expressed as gallic acid equivalents (GAE) in mg/g of the extract [12].

The total flavonoid content of the extract was measured using aluminum chloride by the colorimetric method [13].

2.3. Study Design. The present study was experimental-interventional. Thirty adult male Wistar rats weighing 200 to 220 g and 6–8 weeks old were purchased from Pasteur Institute of Iran (Tehran). Animals were kept under controlled environmental conditions (18–20°C, 12 hours of light, and 12 hours of darkness) and had free access to water and chow during the study. This study was started 7 days after the adaptation of animals to environmental conditions. This study was approved by the Ethics Committee of Kurdistan University of Medical Sciences (IR.MUK.REC.1397/5004). To induce experimental poisoning, mercury chloride was administered orally at a dose of 2 mg/kg body weight daily for 30 days [14]. Rats were randomly divided into five groups:

C group: healthy animals received only distilled water

S group: the animals received mercury chloride (2 mg/kg/day) orally

T1 group: the animals received mercury chloride (2 mg/kg) + alfalfa ethanolic extract (250 mg/kg) intraperitoneally daily

T2 group: the animals received mercury chloride (2 mg/kg) + alfalfa ethanolic extract (500 mg/kg) intraperitoneally daily

T3 group: the animals received mercury chloride (2 mg/kg) + alfalfa extract (750 mg/kg) intraperitoneally daily

The duration of the study was 30 days. The basal and final body weights of the animals were measured. The doses of alfalfa ethanolic extract were selected according to earlier studies [15–17].

2.4. Sampling, Preparation, and Measurement of Biochemical Parameters. At the end of the study, the experimental groups were anesthetized by intraperitoneal injection of ketamine (100 mg/kg) and xylazine (10 mg/kg) [18]. Blood sampling was taken from the animal's heart; then samples were centrifuged and the serum was separated to measure the amount of total antioxidant capacity (TAC) by using Ferric Reducing Antioxidant Power (FRAP). Urea, creatinine, uric acid, sodium, and potassium were measured as the parameters of renal biochemistry and Alanine Aminotransferase (ALT), Aspartate transaminase (AST), and Alkaline phosphatase (ALP) concentration to assess for liver damage by standard commercial kits (Pars Test) by an autoanalyzer device (Hitachi, Japan). Further, malondialdehyde (MDA), glutathione peroxidase (GPx), catalase (CAT), and superoxide dismutase (SOD) concentration were evaluated by ZELLBIO kit, Germany. In addition, the

concentration of mercury in the kidneys and liver was measured by the atomic absorption method.

2.5. Measurement of the TAC Level Using the FRAP Method. TAC values were measured by using a standard concentration chart of 100–1000 μmol/l. In this method, the plasma's ability to regenerate the ferric iron is measured. At acidic pH, when the Fe III-TPTZ complex is regenerated to Fe II, it produces a blue color that reads at 593 wavelengths [19].

2.6. Measurement of GPx, CAT, and SOD Activity in the Liver and Kidney Tissues. After washing the liver and kidney with ice normal saline and placing it inside the microtube, the tissues were frozen in liquid nitrogen at a temperature of −80°C. At the time of the experiment, liver and kidney tissues were homogenized with a homogenizer and the supernatant obtained was used for biochemical testing. Catalase activity was measured by the Aebi method based on H_2O_2 decomposition at 240 nm [20]. Glutathione peroxidase (GSH-Px) catalyzes the oxidation of glutathione by the cumene hydroperoxide. The oxidized glutathione is then converted back to regenerative glutathione in the presence of the enzyme's glutathione reductase and nicotinamide adenine dinucleotide phosphate (NADPH). This reaction was read at 340 nm. The basis of measurement superoxide dismutase (SOD) activity was to inhibit the conversion of superoxide to H_2O_2 and O_2 at 505 nm [21].

2.7. Measurement of the MDA Level in the Liver and Kidney Tissues. Trichloroacetic acid (TBA) was added to homogenized tissue. After precipitation of proteins, TBA was added to the top solution and it was boiled in bain-marie for 30 min, the absorption of light at 532 nm wavelength was read and calculated by the standard diagram. Its level was reported as μg/g [22].

2.8. Measurement of Mercury in the Liver and Kidney Tissues by the Atomic Absorption Method. After drying the samples in an oven at 60°C, they were prepared by the wet digestion method. 0.5 g of kidney and liver tissues, 25 ml of concentrated sulfuric acid, 20 ml of 7 molar nitric acids, and 1 ml of 2% sodium molybdate solution were added. Moreover, a few welded stones were added to heat evenly. After cooling, from the top of the tube, 20 ml of nitric acid and concentrated perchloric acid was added in a ratio of 1 to 1. Then, it was heated until the white acid vapor disappeared. After cooling, 10 ml of water was added and it was heated for 100 minutes to obtain a uniform and clear solution. Finally, with standard diagram (HNO3 10% (V/V) + HCL 7% (V/V) + NaCl 0.02% (W/V)), concentrations based on the μgr/gr weight unit were read [23].

2.9. Histopathological Examination of the Liver and Kidney. Histopathological examination was performed by fixing kidney and liver tissues in 10% formaldehyde solution. Then, sections of 5 μm in diameter were prepared and stained with hematoxylin and eosin. The evaluation was performed with a light microscope and 40 magnification [24].

2.10. Statistical Methods. The study data were reported as mean ± SD. To compare the average parametric data among the groups, one-way ANOVA and Tukey's test were utilized. Liver and kidney histopathological scores were evaluated by the Kruskal–Wallis test.

3. Results

The results of the percentage of DPPH inhibition by extract and vitamin C are presented in Table 1. The results showed that the percentage of DPPH inhibition by the extract was in a dose-dependent manner. The percentage of DPPH inhibition from concentrations of 20 to 1000 μg/ml was 15.78 ± 1.10 to 68.24 ± 3.33, respectively, and for vitamin C, it increased from 27.45 ± 4.63 to 84.12 ± 2.35. IC_{50} of the extract was 245.18 ± 48.41 μg/ml. The total phenolic and flavonoid contents in Alfalfa ethanolic extract were 40.45 ± 5.19 (mg/g) and 14.36 ± 1.10 (mg/g), respectively (Table 1).

At the end of the study, the body weight decreased in the S group compared to the initial weight with other groups. There was a significant difference between the body weight in the control group and other groups ($P < 0.001$) (Table 2).

3.1. Serum Level of TAC in the Control and Treated Groups. The lowest concentration of TAC was 220 ± 15.49 μmol/L in the S group, and the highest concentration was 508.65 ± 105.31 μmol/L in the control group. There was a significant difference between the control group and other groups. The concentration of TAC significantly decreased in the S group compared with T2 and T3 groups (Figure 1).

3.2. GPx, CAT, SOD, and MDA Levels in the Liver Tissue of the Control and Treated Groups. The GPx activity in liver tissue of the S group significantly decreased compared to the control group ($P < 0.001$, Figure 2). The GPx activity significantly decreased in the S group compared to other groups (Figure 2(a)). The lowest activity of CAT was in the S group (25.9 ± 3.20) and the highest was in the control group (55.8 ± 2.04) while its activity insignificantly increased in the groups receiving the extract (Figure 2(b)). The SOD activity in the S group had a significant difference compared with other groups ($P < 0.001$) (Figure 2(c)), while its activity in T1, T2, and T3 improved compared to the S group. MDA concentration in the S group had a significant difference compared to other groups, while treatment with different doses of the extract could improve its level (Figure 2(d)).

3.3. GPx, CAT, SOD, and MDA Concentration in the Kidney Tissue of the Control and Treated Groups. The highest activity of GPx in kidney tissue was observed in the control group. The level of this enzyme in the S group had a significant difference with T1 and T2 groups (Figure 3(a)). The highest

Table 1: Total phenols, total flavonoids, and IC_{50} of the ethanolic extract of alfalfa.

Sample	Total phenolic content (mg GAE/g extract)	Total flavonoid content (mg QE/g extract)	IC_{50} (μg/ml)
Ethanolic extract	40.45 ± 5.19 mg/gr	14.36 ± 1.10	245.18 ± 48.41

Table 2: The difference between the basal and final weight of the body in the control and treated groups.

Body weight	Group				
	C	S	T1	T2	T3
Basal	210 ± 15.49	197.5 ± 15.41	205.83 ± 12.81	197.663 ± 7.52	201.66 ± 11.69
Final	237.5 ± 5.24	188.67 ± 11.31 α	217.5 ± 16.04 α, β	212.5 ± 9.54 α, β	225.65 ± 12.35 β

All values are presented as mean ± standard deviation (SD). $P < 0.001$. α and β denote comparison with C and S groups, respectively.

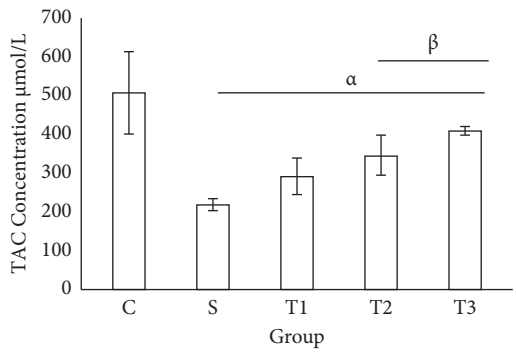

Figure 1: Evaluation of TAC concentration in serum of animals in different groups. Each column represents the mean ± standard deviation (SD). $P < 0.001$. α and β denote comparison with C and S groups.

levels of CAT and SOD were observed in the control group at which this level had a significant difference compared with other experimental groups (Figures 3(b) and 3(c)). The lowest concentration of MDA in kidney tissue was in the control group and the highest level was in the S group (Figure 3(d)). There was a significant difference between the control and the S groups compared with other experimental groups (Figure 3(d)).

3.4. Serum Levels of Liver Enzymes and Hepatic Mercury Content in the Control and Treated Groups. The serum levels of AST, ALT, and ALP significantly increased in the S group compared to other groups. The level of ALT and ALP decreased in the T3 group compared to the S group. The content of mercury significantly increased in all groups compared to the control group (Table 3).

All pathological parameters of the liver except hemorrhage under the Gleason's capsule in the T3 group had significant differences with the S group ($P < 0.01$). The content of acidophilic cytoplasm and necrosis of the nucleus in the T2 group had a significant difference with the S groups. The severity of these damages in the liver decreased by increasing the concentration of the extract (Table 4 and Figure 4).

3.5. Biochemical Parameters of the Kidney and Its Mercury Content in the Control and Treated Groups. The serum levels of urea, creatinine, and uric acid significantly increased in the S group compared to the control group (Table 5). Dose-dependent effects of alfalfa extract reduced the serum level of urea, creatinine, and uric acid in treated groups compared to the S group. The serum level of sodium had no significant change in all groups. The highest level of potassium was observed in the S group that this level had a significant with T1, T2, and control groups. Another finding of the study was a remarkable accumulation of mercury in the liver and kidney of animals in the S group compared to the C group. Prescribing the extract of alfalfa in different doses reduced the accumulation of mercury in the kidney that its lowest level was observed in the T3 group (Table 5).

3.6. Histopathological Evaluation of the Kidney of Animals in the Control and Treated Groups. The acute tubular injury significantly increased in the S and T1 groups compared to the control group. A significant difference between the S group and the control group in the interstitial nephritis was observed, while there was no significant difference with the other groups. The distinctive contrast in glomerular injury was also found in the treatment groups (T1, T2, and T3) and the S group. The hyaline casts in the kidney of the S group and the T1 group significantly increased in comparison to the control group (Table 6; Figure 5).

4. Discussion

Mercury is one of the unnecessary heavy metals that does not have any biological role in the body [25]. The body should be free of mercury in physiological conditions but exposed to diet, environmental contact, farm pesticides, and industrial activities. Almost everyone in the world has some mercury in his or her body. Mercury is known to be the third toxic metal after cadmium and lead that humans should avoid [26]. Investigation on oxidative stress indicators is one of the ways to evaluate the chronic damage of mercury to human health [27]. Plants are one of the most important sources of exogenous antioxidants that have important effects on controlling the damage of heavy metals such as mercury [28]. Polyphenols such as phenol and flavonoids are one of the most abundant antioxidant compounds in plants [29]. In this study, alfalfa extract showed a relatively high concentration of phenolic compounds. Our results showed well that reaching IC_{50} at low concentrations shows the high antioxidant activity of alfalfa extract. In this research, body

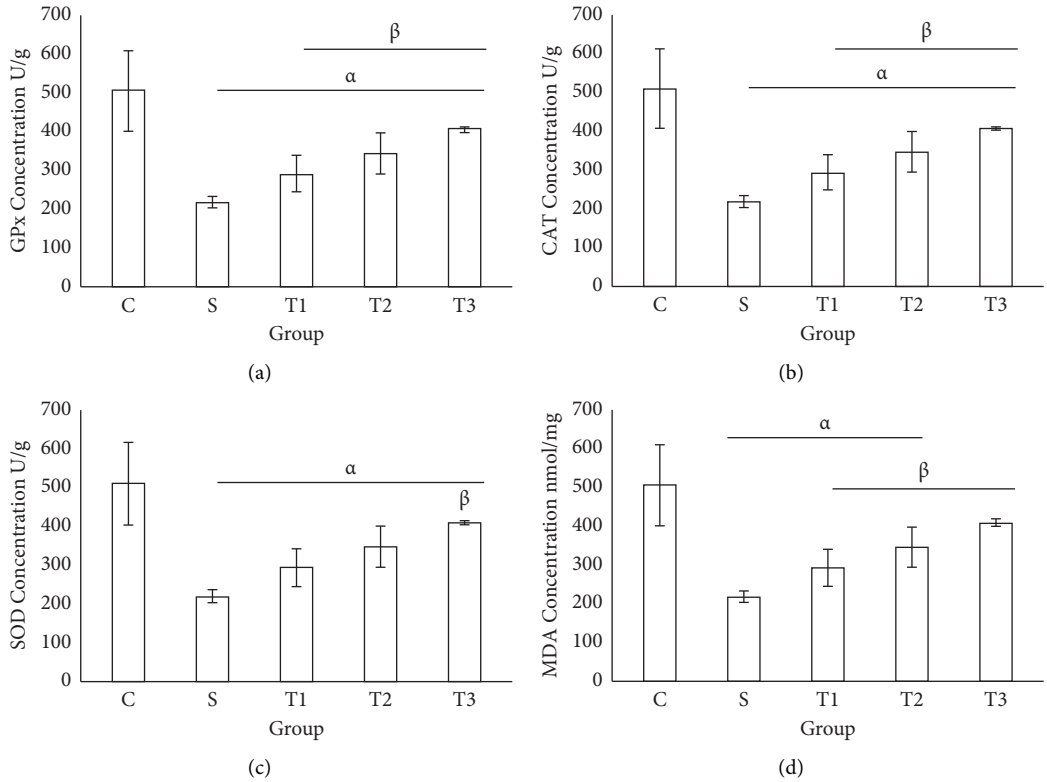

Figure 2: Determination of oxidative stress biomarker in the liver tissue of animal studied. Each column represents the mean ± standard deviation (mean ± SD). $P < 0.001$; α and β denote comparison with C and S groups.

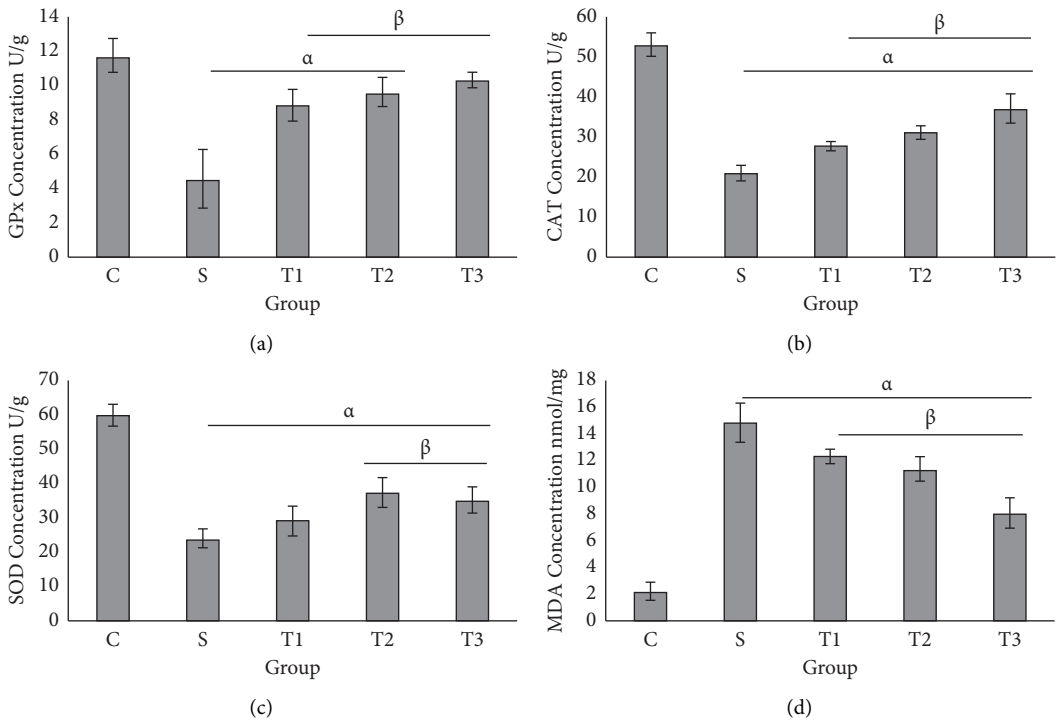

Figure 3: Determination of oxidative stress markers in the kidney tissue of animals in different groups. Each column represents the mean ± standard deviation (SD). α and β denote comparison with C and S groups.

Table 3: Serum levels of liver enzymes and hepatic mercury content in different groups.

Parameter	Group				
	C	S	T1	T2	T3
ALT (U/L)	30.5 ± 3.93	75.5 ± 8.89 α	71.33 ± 9.24 α	49.83 ± 4.62 α, β, γ	40.00 ± 5.09 β, γ
AST (U/L)	68.00 ± 5.96	152.66 ± 7.63 α	136.67 ± 6.05 α, β, γ	102.67 ± 13.76 α, β, γ	53.00 ± 5.76 α, β, γ
ALP (U/L)	186.66 ± 16.32	275.5 ± 20.03 α	256.00 ± 10.19 α	236.83 ± 9.68 α, β	187.65 ± 8.14 β, γ
Hepatic Hg content (μg/g)	5.18 ± 1.50	15.81 ± 1.68 α	13.43 ± 1.06 α	11.31 ± 1.30 α, β	8.05 ± 1.82 α, β, γ

Each row represents the mean ± standard deviation (SD). $P < 0.001$; α, β, and γ denote comparison with C, S, and T1 groups, respectively.

Table 4: Histopathological changes in the liver of animals in the control and treated groups.

Parameter	Group				
	C	S	T1	T2	T3
Central vein congestion	0.0 ± 0.3	1.7 ± 0.34 α	1.2 ± 0.75 α	0.28 ± 1.1 α	0.56 ± 0.76 β, γ
Peripheral hepatitis	0.0 ± 0.1	2.4 ± 1.20 α	1.7 ± 1.00 α	1.5 ± 0.48 α	0.47 ± 0.8 β
Hepatocyte necrosis	0.0 ± 0.0	1.27 ± 3.1 α	1.6 ± 0.48 α, β	0.5 ± 0.28 β	0.21 ± 0.3 β
Parenchymal bleeding	0.0 ± 0.0	0.6 ± 0.09 α	0.5 ± 0.02 α	0.5 ± 0.06 α	0.1 ± 0.05

All values are presented as mean ± standard deviation (SD). $P < 0.001$; α, β, and γ denote comparison with C, S, and T1 groups, respectively.

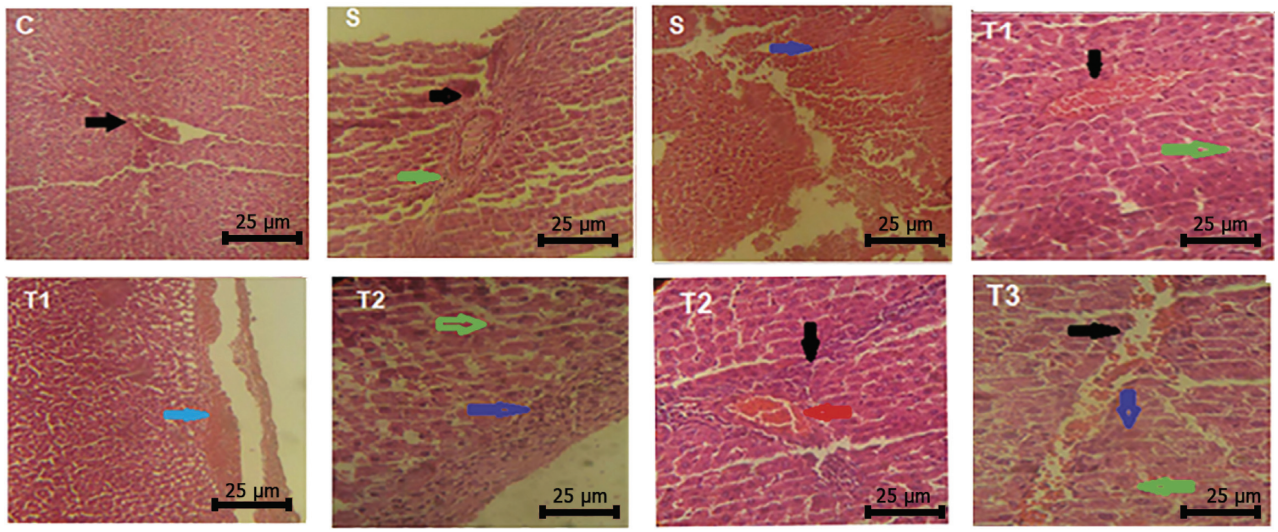

Figure 4: Histopathological changes in the liver of animals in the control and treated groups (H&E staining, 40x), scale bar = 25 μm. C represents a normal structure of healthy hepatocytes and shows no evidence of degeneration. The nucleolus is euchromatin and active. The central veins and port triads are clear (black arrow) and have a normal structure. There is no infiltration of inflammatory cells into the parenchyma, and there is no bleeding or hypertension in the liver parenchyma. S represents necrosis of liver cells, pycnotic and hyperchromic nuclear cells (green arrow), deposition of cytoplasmic proteins and eosinophilization (blue arrow), parenchymal hemorrhage, severe infiltration of mononuclear inflammatory cells into the area around the portal vein, and also the presence of fibroblasts in the preport area (black arrow). T1 represents infiltration of mononuclear inflammatory cells in the peripheral area (black arrow), central vein congestion (red arrow), acidophilic cytoplasm of hepatocellular (green arrow), and hemorrhage under the Glisson's capsule (blue arrow). T2 represents infiltration of mononuclear inflammatory cells of lymphocytes and plasma cells around the triad port (black arrow), hyperplasia of Kupffer cells, the normal nucleus of hepatocytes (green arrow), and presence of mononuclear inflammatory cells on Glisson's capsule of the liver (blue arrow). T3 represents low penetration of mononuclear inflammatory cells in the triad port (blue arrow), hepatocytes being mostly normal, nucleus having no degenerative changes (green arrow), and mild central vein congestion (red arrow).

Table 5: The levels of renal parameters in the serum of the control and treated groups.

Parameter	Groups				
	C	S	T1	T2	T3
Urea (mg/dl)	30.41 ± 2.41	46.98 ± 2.59 A	35.76 ± 2.51 α, β	37.00 ± 1.41 α, β	32.90 ± 1.68 β
Creatinine (mg/dl)	0.38 ± 0.14	1.23 ± 0.16 α, β	0.99 ± 0.09 α, β	0.83 ± 0.05 α, β	0.75 ± 0.18 α, β
Uric acid (mg/dl)	1.89 ± 0.14	5.83 ± 1.02 A	3.6 ± 0.73 α, β	2.30 ± 0.23 β	1.86 ± 0.10 β
Sodium (mmol/l)	146.66 ± 6.02	149.83 ± 2.99	142.5 ± 1.64	146.5 ± 4.59	143.5 ± 6.41
Potassium (mmol/l)	4.48 ± 0.91	5.78 ± 0.57 A	5.45 ± 0.30 α	4.83 ± 0.25 β	4.26 ± 0.23 β
Renal Hg content (μg/g)	5.46 ± 1.59	21.66 ± 3.26 A	20.00 ± 2.28 α	14.05 ± 1.04 α, β	10.25 ± 1.19 α, β

All values are presented as mean ± standard deviation (SD). $P < 0.001$; α and β, respectively, denote comparison with groups C and S.

Table 6: Evaluation of the pathological changes in the kidney of the animals in the control and treated groups.

Parameter	Groups				
	C	S	T1	T2	T3
Acute tubular necrosis	0.0 ± 0.0	2.83 ± 0.38 A	2.66 ± 0.50 α	1.33 ± 0.50 β, γ	0.83 ± 0.74 β, γ
Interstitial nephritis	0.0 ± 0.0	2.16 ± 0.74 A	1.33 ± 0.50	1.16 ± 0.38	1.16 ± 0.38
Glomerular damage	0.0 ± 0.0	2.50 ± 0.52 A	1.0 ± 0.62 β	0.83 ± 0.39 β	0.56 ± 0.43 β
Hyaline cast	0.0 ± 0.0	2.66 ± 0.79 A	2.50 ± 0.53 α	1.16 ± 0.38 β	0.83 ± 0.73 β

All values are presented as mean ± standard deviation (SD). $P < 0.01$; α, β, and γ, respectively, denote comparison with groups C, S, and T1.

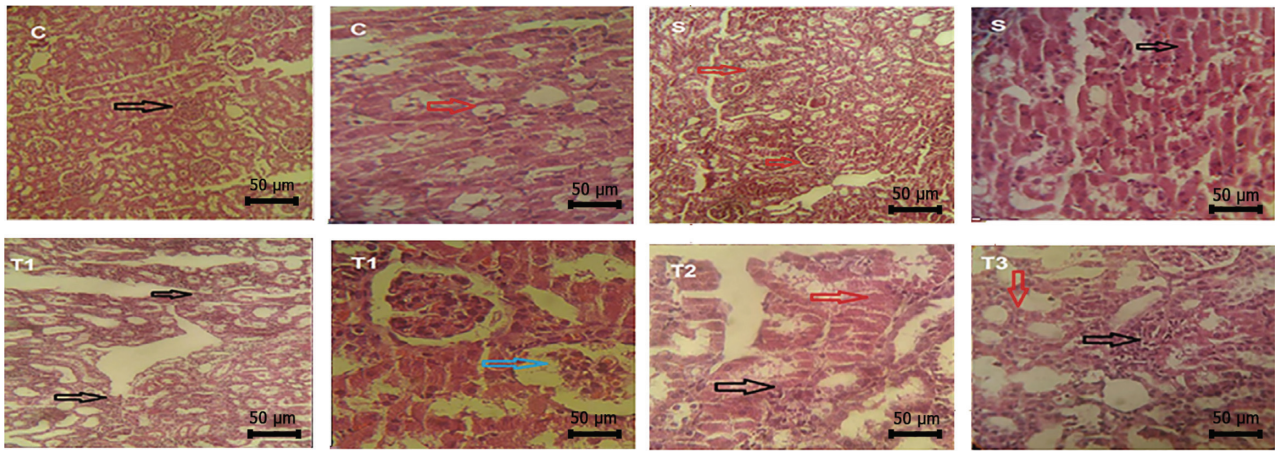

Figure 5: Histopathological changes in the kidney of animals in the control and treated groups (H&E staining, 40x), scale bar = 50 μm. C represents that the glomerular structure was normal (black arrow). There is no bleeding or hyperemia in the glomerulus. Renal tubules are normal (red arrow). Tubular cells are active, and the nucleus of tubular cells are not degenerated. S represents acute tubular damage, acidophilization of cytoplasm (black arrow), destruction of the wall of tubular cells and disintegration of epithelial cells of tubules, and interstitial nephritis (red arrow). T1 represents interstitial nephritis (black arrow), glomerular sclerosis, and increased glomerular space (space between the glomerulus and glomerular wall) (blue arrow). T2 represents extensive penetration of mononuclear inflammatory cells into the interstitial tubular and glomerular space (black arrow) and acute tubular necrosis caused by eosinophilization or acidophilization of the cytoplasm, due to the sedimentation of cytoplasmic proteins (red arrow). T3 represents that mononuclear inflammatory cells were seen in the interstitial space of the tubule (black arrow), the tubules are functional, and no acute tubular necrosis was observed (red arrow).

weight was reduced in animals receiving mercury. It was consistent with the findings of other researchers [30, 31]. Oxidative damage from mercury toxicity results in weight loss and muscle cell damage in rats (smooth and striated) [32]. In this study, the administration of alfalfa extract was associated with improving animal weight. It seems that the potential effect of alfalfa by reducing metabolic energy and increasing appetite could improve body weight in rats exposed to mercury. It also inhibits cell damages by inhibiting mercury-induced oxidative stress [33], therefore improving the weight of animals. The results of this study showed that the accumulation of mercury in kidney and liver tissue increased in groups receiving mercury. The concentration of mercury in the blood was variable and unreliable [2]. This could be due to its excellent ability to clear toxins and compounds from the kidney and increase blood flow to the kidney [34]. The kidney is the main target organ of mercury. It causes both glomerular and tubular damage, thus reducing glomerular filtration and renal tubular necrosis [35]. Collecting tubes, especially areas containing the amino acid cysteine, are the site of mercury uptake [36]. Plasma levels of urea, creatinine, and uric acid are the main indicators of kidney function. In this study, the administration of mercury was associated with a significant increase in the level of these indicators, which was consistent with the results of Boroushaki et al. and Mesquita et al. [37, 38]. Therefore, mercury could increase the level of wastewater and waste products by altering the performance of glomerular filtration and the activity of tubules in mercury-induced nephritis [39]. In confirming the nephritis induced by mercury, renal histopathological findings showed acute tubular damage, interstitial nephritis, glomerular damage, and the presence of hyaline cast which was consistent with the results of other researchers. These pathological changes appear to be due to the cell damage induced by oxidative stress [37, 40]. The liver was the second organ considered in this study due to its metabolic role. Liver lysosomes can absorb organic and inorganic mercury and be the site of accumulation of this metal. Mercury binds to glutathione in the liver, blood, and other organs and forms stable sulfhydryl complexes [41]. Nonspecific binding to thiol-SH groups of enzymes can disorder the performance of them, especially antioxidant enzymes, immune responses, protein synthesizers, and energy producers. This can be a reason for the high amount of lipid peroxidation in the kidney and liver due to the increase of mercury concentration. Furthermore, in both kidney and liver organs, the levels of antioxidant enzymes such as GPx, CAT, and SOD decreased when exposed to

mercury [42, 43]. This finding shows how the balance of the body's antioxidant system changes after the administration of mercury [44].

ALT and AST are two indicators of the proper and reliable status of liver health. If the liver is damaged, these enzymes leak from the cytosol into the bloodstream, so their concentration increased above normal levels. In this study, these two enzymes showed a significant increase in the group that received mercury. In addition, bleeding, acidophilic cytoplasm, and necrosis of hepatocytes in histological evaluation are the confirmation of this finding [45].

The use of herbal products for the detoxification of heavy metals can be one of the practical and valuable treatment strategies [46]. Alfalfa or green gold has a special place in traditional medicine due to its numerous properties and having protein, calcium, and various vitamins. This plant has the enzymes such as amylase, invertase, and pectinase, which play an important role in digestion and increase in growth. Alfalfa has a high nutritional value. It contains amino acids, namely, Arg, His, Asp, Phe, and Cys, and vitamins, niacin, pantothenic acid, biotin, folic acid, minerals, protein, and saponin [47, 48]. Our results showed that the antioxidant effects of alfalfa extract were in a dose-dependent manner. IC_{50} extract was more than vitamin C that showed the antioxidant importance of the extract compared to vitamin C. Furthermore, in this study, a dose-dependent increase in TAC concentration was observed in the serum of the treated animals with the extract. Moreover, alfalfa contains cysteine that plays an important role in enhancing the detoxification mechanisms of endogenous and heavy metals-induced damage in the body. Moreover, exposure to metals can affect the state of cysteine [49]. Cysteine and its thiol groups can absorb mercury and reduce the damage of thiol groups and proteins in the body's organs, including the liver and kidney [38]. This can be one of the possible reasons for the decrease in mercury concentration in the kidney and liver of the groups treated with alfalfa extract. Alfalfa's nonenzymatic antioxidant compounds (such as phenols and flavonoids) and phytoestrogens, can also be effective in improving liver and kidney enzymatic antioxidants, including glutathione, catalase, and SOD [17]. It could also prevent the accumulation of mercury and the production of free radicals in the liver and kidney in our study.

5. Conclusion

The results suggested that mercury chloride could damage the kidney and the liver by inducing oxidative stress. Alfalfa extract by its nutritional and antioxidative activities in a dose-dependent manner could also decrease the toxicity-induced by mercury and could improve the structure and function of the kidney and liver. This extract at a dose of 750 mg/kg showed the highest antioxidant activity against mercury chloride-induced damage in the kidney and liver. Hence, using plant compounds is one of the useful strategies in controlling and preventing heavy metal poisoning.

Data Availability

The data can be obtained upon request to the corresponding author.

Conflicts of Interest

The authors declare that there are no conflicts of interest regarding the publication of this paper.

Acknowledgments

The authors would like to sincerely appreciate the Research Vice-Chancellor at the Islamic Azad University, Sanandaj Branch. In addition, they thank Dr. Mortazavi for performing histopathological evaluations.

References

[1] I. E. Carranza-Torres, E. Viveros-Valdez, N. E. Guzmán-Delgado et al., "Protective effects of phenolic acids on mercury-induced DNA damage in precision-cut kidney slices," *Iranian Journal of Basic Medical Sciences*, vol. 22, no. 4, pp. 367–375, 2019.

[2] M. Z. Fornazier, T. B. Nascimento, V. B. Marques et al., "Mercury biodistribution in rats after chronic exposure to mercury chloride," *Journal of the Brazilian Chemical Society*, vol. 29, no. 7, pp. 1579–1584, 2018.

[3] S. Ali, S. Hussain, R. Khan et al., "Renal toxicity of heavy metals (cadmium and mercury) and their amelioration with ascorbic acid in rabbits," *Environmental Science and Pollution Research*, vol. 26, no. 4, pp. 3909–3920, 2019.

[4] S. Berenjian and M. Raeeszadeh, "Prescription of antibiotics before and after surgery at the surgical wards of isfahan amiralmomenin hospital compared with the standard guidelines," *Health Research Journal*, vol. 1, no. 3, pp. 133–140, 2016.

[5] A. Pandey, A. Singh, S. A. Holeyappa, and H. Kaur, "Enzymatic and antioxidant response of Lamellidens marginalis exposed to mercuric chloride," *Indian Journal of Animal Research*, vol. 52, no. 5, pp. 658–663, 2018.

[6] S. Ahmad and R. Mahmood, "Mercury chloride toxicity in human erythrocytes: enhanced generation of ROS and RNS, hemoglobin oxidation, impaired antioxidant power, and inhibition of plasma membrane redox system," *Environmental Science and Pollution Research*, vol. 26, no. 6, pp. 5645–5657, 2019.

[7] H. D. Li, X. M. Meng, C. Huang, L. Zhang, X. W. Lv, and J. Li, "Application of herbal traditional Chinese medicine in the treatment of acute kidney injury," *Frontiers in Pharmacology*, vol. 10, p. 376, 2019.

[8] B. A. Salih and K. O. Azeez, "Antidiabetic action of alfalfa (Medicago sativa) leaves powder on type II diabetic patients," *Polytechnic Journal*, vol. 9, no. 1, pp. 23–25, 2019.

[9] X. Liu, Y. Sun, J. Bian et al., "Phytochemical and chemotaxonomic study on Medicago sativa L. (leguminosae)," *Biochemical Systematics and Ecology*, vol. 80, pp. 55–58, 2018.

[10] M. Qaderi Forough, M. Raeeszadeh, and A. Amiri, "Dose-response changes of Brassica oleracea var. italica hydroalcholic extract in the control of oxidative stress by induction of diazinon on the cells of testicular tissue in male adult rat," *Journal of Rafsanjan University of Medical Sciences*, vol. 16, no. 7, pp. 593–604, 2017.

[11] M. S. Blois, "Antioxidant determinations by the use of a stable free radical," *Nature*, vol. 181, no. 4617, pp. 1199-1200, 1958.

[12] S. Albayrak, A. Aksoy, L. Yurtseven, and A. Yaşar, "A comparative study on phenolic components and biological activity of some senecio species in Turkey," *Journal of Pharmacy and Pharmacology*, vol. 66, no. 11, pp. 1631–1640, 2014.

[13] R. M. Lamuela-Raventós, "Folin–ciocalteu method for the measurement of total phenolic content and antioxidant capacity," *Measurement of Antioxidant Activity and Capacity: Recent Trends and Applications*, vol. 14, p. 107, 2018.

[14] G. Jagadeesan and S. S. Pillai, "Hepatoprotective effects of taurine against mercury induced toxicity in rat," *Journal of Environmental Biology*, vol. 28, no. 4, pp. 753–756, 2007.

[15] N. Ahmad, Z. Rahman, N. Akhtar, S. Ali, M. Ahmad, and I. Ahmad, "Effects of Medicago sativa on some serum biochemical metabolites in rats," *International Journal of Agriculture & Biology*, vol. 15, no. 2, pp. 297–300, 2013.

[16] K. Servatyari, A. Ahmadi, H. Kashefi, M. N. Menbari, A. Rostami, and M. R. Moloudi, "The effect of hydroalcoholic extract of Medicago sativa on liver function tests, blood biochemical factors and coagulation system in male rats," *Scientific Journal of Kurdistan University of Medical Sciences*, vol. 21, no. 6, pp. 16–26, 2017.

[17] M. Raeeszadeh, P. Mortazavi, and R. Atashin-Sadafi, "The antioxidant, anti-inflammatory, pathological, and behavioural effects of Medicago sativa L. (alfalfa) extract on brain injury caused by nicotine in male rats," *Evidence-Based Complementary and Alternative Medicine*, vol. 2021, Article ID 6694629, 9 pages, 2021.

[18] E. M. Wellington, A. B. Boxall, P. Cross et al., "The role of the natural environment in the emergence of antibiotic resistance in gram-negative bacteria," *The Lancet Infectious Diseases*, vol. 13, no. 2, pp. 155–165, 2013.

[19] R. A. Mekary, K. Wu, E. Giovannucci et al., "Total antioxidant capacity intake and colorectal cancer risk in the health professionals follow-up study," *Cancer Causes & Control*, vol. 21, no. 8, pp. 1315–1321, 2010.

[20] S. Aseyd Nezhad, A. Es-Haghi, and M. H. Tabrizi, "Green synthesis of cerium oxide nanoparticle using Origanum majorana L. leaf extract, its characterization and biological activities," *Applied Organometallic Chemistry*, vol. 34, no. 2, Article ID e5314, 2020.

[21] H. Sleven, J. E. Gibbs, S. Heales, M. Thom, and H. R. Cock, "Depletion of reduced glutathione precedes inactivation of mitochondrial enzymes following limbic status epilepticus in the rat hippocampus," *Neurochemistry International*, vol. 48, no. 2, pp. 75–82, 2006.

[22] O. Balat, E. Dikensoy, M. G. Ugur, R. Atmaca, M. Cekmen, and M. Yurekli, "Malon dialdehyde, nitrite and adrenomedullin levels in patients with premenstrual syndrome," *Archives of Gynecology and Obstetrics*, vol. 275, no. 5, pp. 361–365, 2007.

[23] W. Slavin, "[12] atomic absorption spectrometry," *Methods in Enzymology*, vol. 158, pp. 117–145, 1988.

[24] A. T. Feldman and D. Wolfe, "Tissue processing and hematoxylin and eosin staining," *Histopathology*, vol. 1180, pp. 31–43, 2014.

[25] D. Mergler, H. A. Anderson, L. H. M. Chan et al., "Methylmercury exposure and health effects in humans: a worldwide concern," *AMBIO: A Journal of the Human Environment*, vol. 36, no. 1, pp. 3–11, 2007.

[26] P. Li, X. B. Feng, G. L. Qiu, L. H. Shang, and Z. G. Li, "Mercury pollution in Asia: a review of the contaminated sites," *Journal of Hazardous Materials*, vol. 168, no. 2-3, pp. 591–601, 2009.

[27] M. Farina, D. S. Avila, J. B. T. da Rocha, and M. Aschner, "Metals, oxidative stress and neurodegeneration: a focus on iron, manganese and mercury," *Neurochemistry International*, vol. 62, no. 5, pp. 575–594, 2013.

[28] D. Krishnaiah, R. Sarbatly, and R. Nithyanandam, "A review of the antioxidant potential of medicinal plant species," *Food and Bioproducts Processing*, vol. 89, no. 3, pp. 217–233, 2011.

[29] L. Chen, H. Deng, H. Cui et al., "Inflammatory responses and inflammation-associated diseases in organs," *Oncotarget*, vol. 9, no. 6, pp. 7204–7218, 2018.

[30] M. Zaheri, S. Ebrahimi Vosta Kalai, and J. Cheraghi, "Protective effect of aerial parts extract of Scrophularia striata on cadmium and mercury-induced nephrotoxicity in rat," *Journal of Babol University of Medical Sciences*, vol. 13, no. 4, pp. 48–53, 2011.

[31] A. H. Esmaeili, R. A. Khavari-Nejad, A. Hajizadeh Moghaddam, M. J. Chaichi, and M. A. Ebrahimzadeh, "Effects of Eriobotrya japonica (Lindl.) flower extracts on mercuric chloride-induced hepatotoxicity in rats," *Chinese Science Bulletin*, vol. 57, no. 30, pp. 3891–3897, 2012.

[32] C. B. Ahn, C. H. Song, W. H. Kim, and Y. K. Kim, "Effects of Juglans sinensis dode extract and antioxidant on mercury chloride-induced acute renal failure in rabbits," *Journal of Ethnopharmacology*, vol. 82, no. 1, pp. 45–49, 2002.

[33] E. E. K. Takyi, Y. Kido, T. Rikimaru, and D. O. Kennedy, "Possible use of alfalfa (Medicago sativa) as supplement in infant nutrition: comparison of weight gained by rats fed on alfalfa and a popular weaning diet," *Journal of the Science of Food and Agriculture*, vol. 59, no. 1, pp. 109–115, 1992.

[34] E. S. Nascimento and A. A. Chasin, *Do mercúrio e seus compostos*, Serie Cadernos de Referencia Ambiental, Springer, New York, NY, USA, 2001.

[35] C. C. Bridges and R. K. Zalups, "Transport of inorganic mercury and methylmercury in target tissues and organs," *Journal of Toxicology and Environmental Health, Part B*, vol. 13, no. 5, pp. 385–410, 2010.

[36] S. Hodgson, M. J. Nieuwenhuijsen, P. Elliott, and L. Jarup, "Kidney disease mortality and environmental exposure to mercury," *American Journal of Epidemiology*, vol. 165, no. 1, pp. 72–77, 2007.

[37] M. T. Boroushaki, H. Mollazadeh, A. Rajabian et al., "Protective effect of pomegranate seed oil against mercuric chloride-induced nephrotoxicity in rat," *Renal Failure*, vol. 36, no. 10, pp. 1581–1586, 2014.

[38] M. Mesquita, T. F. Pedroso, C. S. Oliveira et al., "Effects of zinc against mercury toxicity in female rats 12 and 48 hours after $HgCl_2$ exposure," *EXCLI Journal*, vol. 15, pp. 256–267, 2016.

[39] D. Herrmann, S. Flajoulot, P. Barre, C. Huyghe, J. Ronfort, and B. Julier, "Comparison of morphological traits and molecular markers to analyse diversity and structure of alfalfa (Medicago sativa L.) cultivars," *Genetic Resources and Crop Evolution*, vol. 65, no. 2, pp. 527–540, 2018.

[40] A. Gado and B. Aldahmash, "Antioxidant effect of Arabic gum against mercuric chloride-induced nephrotoxicity," *Drug Design, Development and Therapy*, vol. 7, pp. 1245–1252, 2013.

[41] S. Asano, H. Sawada, H. Komoriya, and I. Ohya, "Effects of methylmercuric chloride intoxication on the intracellular activity of lysosomal enzymes in rat liver and brain," *Journal of Toxicological Sciences*, vol. 4, no. 3, pp. 201–210, 1979.

[42] M. Raeeszadeh, M. Rezaee, A. Akbari, and N. Khademi, "The comparison of the effect of Origanum vulgare L. extract and

vitamin C on the gentamycin-induced nephrotoxicity in rats," *Drug and Chemical Toxicology*, vol. 44, pp. 1–8, 2021.

[43] M. Raeeszadeh and M. Fallah, "The comparison of the effect of origanum vulgar aqueous extract and vitamin C on the control of cadmium chloride damage in testicular tissue in male rats," *Journal of Babol University of Medical Sciences*, vol. 20, no. 8, pp. 44–50, 2018.

[44] R. Agarwal, S. K. Goel, and J. R. Behari, "Detoxification and antioxidant effects of curcumin in rats experimentally exposed to mercury," *Journal of Applied Toxicology*, vol. 30, no. 5, pp. 457–468, 2010.

[45] M. Navarro, M. Montilla, A. Martín, J. Jiménez, and M. Utrilla, "Free radical scavenger and antihepatotoxic activity of Rosmarinus tomentosus," *Planta Medica*, vol. 59, no. 4, pp. 312–314, 1993.

[46] V. Unsal, "Natural phytotherapeutic antioxidants in the treatment of mercury intoxication-a review," *Advanced Pharmaceutical Bulletin*, vol. 8, no. 3, pp. 365–376, 2018.

[47] A. Zargari, *Therapeutic Plants*, Tehran University Press, Tehran, Iran, 1996.

[48] Y.-H. Hong, W.-W. Chao, M.-L. Chen, and B.-F. Lin, "Ethyl acetate extracts of alfalfa (Medicago sativa L.) sprouts inhibit lipopolysaccharide-induced inflammation in vitro and in vivo," *Journal of Biomedical Science*, vol. 16, no. 1, p. 64, 2009.

[49] D. Quig, "Cysteine metabolism and metal toxicity," *Alternative Medicine Review: A Journal of Clinical Therapeutic*, vol. 3, pp. 262–270, 1998.

Hindawi
Evidence-Based Complementary and Alternative Medicine
Volume 2021, Article ID 2234554, 15 pages
https://doi.org/10.1155/2021/2234554

Research Article

Integrative Bioinformatics Study of Tangeretin Potential Targets for Preventing Metastatic Breast Cancer

Adam Hermawan,[1,2] **Herwandhani Putri**,[2] **Naufa Hanif**,[2] **and Muthi Ikawati**[1,2]

[1]*Laboratory of Macromolecular Engineering, Department of Pharmaceutical Chemistry, Faculty of Pharmacy, Universitas Gadjah Mada Sekip Utara II, Yogyakarta 55281, Indonesia*
[2]*Cancer Chemoprevention Research Center, Faculty of Pharmacy, Universitas Gadjah Mada Sekip Utara II, Yogyakarta 55281, Indonesia*

Correspondence should be addressed to Adam Hermawan; adam_apt@ugm.ac.id

Received 13 May 2021; Accepted 22 June 2021; Published 14 July 2021

Academic Editor: Omayma Eldahshan

Agents that target metastasis are important to improve treatment efficacy in patients with breast cancer. Tangeretin, a citrus flavonoid, exhibits antimetastatic effects on breast cancer cells, but its molecular mechanism remains unclear. Tangeretin targets were retrieved from PubChem, whereas metastatic breast cancer regulatory genes were downloaded from PubMed. In total, 58 genes were identified as potential therapeutic target genes of tangeretin (PTs). GO and KEGG pathway enrichment analyses of PTs were performed using WebGestalt (WEB-based Gene SeT AnaLysis Toolkit). The PPI network was analyzed using STRING-DB v11.0 and visualized by Cytoscape software. Hub genes were selected on the basis of the highest degree score as calculated by the CytoHubba plugin. Genetic alterations of the PTs were analyzed using cBioPortal. The prognostic values of the PTs were evaluated with the Kaplan–Meier plot. The expression of PTs across breast cancer samples was confirmed using GEPIA. The reliability of the PTs in metastatic breast cancer cells was validated using ONCOMINE. Molecular docking was performed to foresee the binding sites of tangeretin with PIK3Cα, MMP9, PTGS2, COX-2, and IKK. GO analysis showed that PTs participate in the biological process of stimulus response, are the cellular components of the nucleus and the membrane, and play molecular roles in enzyme regulation. KEGG pathway enrichment analysis revealed that PTs regulate the PI3K/Akt pathway. Genetic alterations for each target gene were *MTOR* (3%), *NOTCH1* (4%), *TP53* (42%), *MMP9* (4%), *NFKB1* (3%), *PIK3CA* (32%), *PTGS2* (15%), and *RELA* (5%). The Kaplan–Meier plot showed that patients with low mRNA expression levels of *MTOR, TP53, MMP9, NFKB1, PTGS2,* and *RELA* and high expression of *PIK3CA* had a significantly better prognosis than their counterparts. Further validation of gene expression by using GEPIA revealed that the mRNA expression of *MMP9* was significantly higher in breast cancer tissues than in normal tissues, whereas the mRNA expression of *PTGS2* showed the opposite. Analysis with ONCOMINE demonstrated that the mRNA expression levels of *MMP9* and *NFKB1* were significantly higher in metastatic breast cancer cells than in normal tissues. The results of molecular docking analyses revealed the advantage of tangeretin as an inhibitor of PIK3CA, MMP9, PTGS2, and IKK. Tangeretin inhibits metastasis in breast cancer cells by targeting TP53, PTGS2, MMP9, and PIK3CA and regulating the PI3K/Akt signaling pathway. Further investigation is needed to validate the results of this study.

1. Introduction

Breast cancer is a common cause of death among women worldwide [1]. Breast cancer was initially considered a local disease, but it can metastasize to lymph nodes and other organs in the body, which is fatal to patients [2]. In breast cancer patients, metastases are still the leading cause of morbidity [3]. Understanding the molecular mechanisms underlying metastasis is important to improve the clinical management of breast cancer [4]. Accordingly, molecular therapeutic agents that target metastasis must be developed to enhance the effectiveness of breast cancer therapy [5].

Tangeretin, a citrus flavonoid (Figure 1(a)), may be developed as a specific molecular-targeted anticancer agent because of its antimetastatic effects [6] on cancer cells [7–9]. Specifically, this compound inhibits metastases of skin,

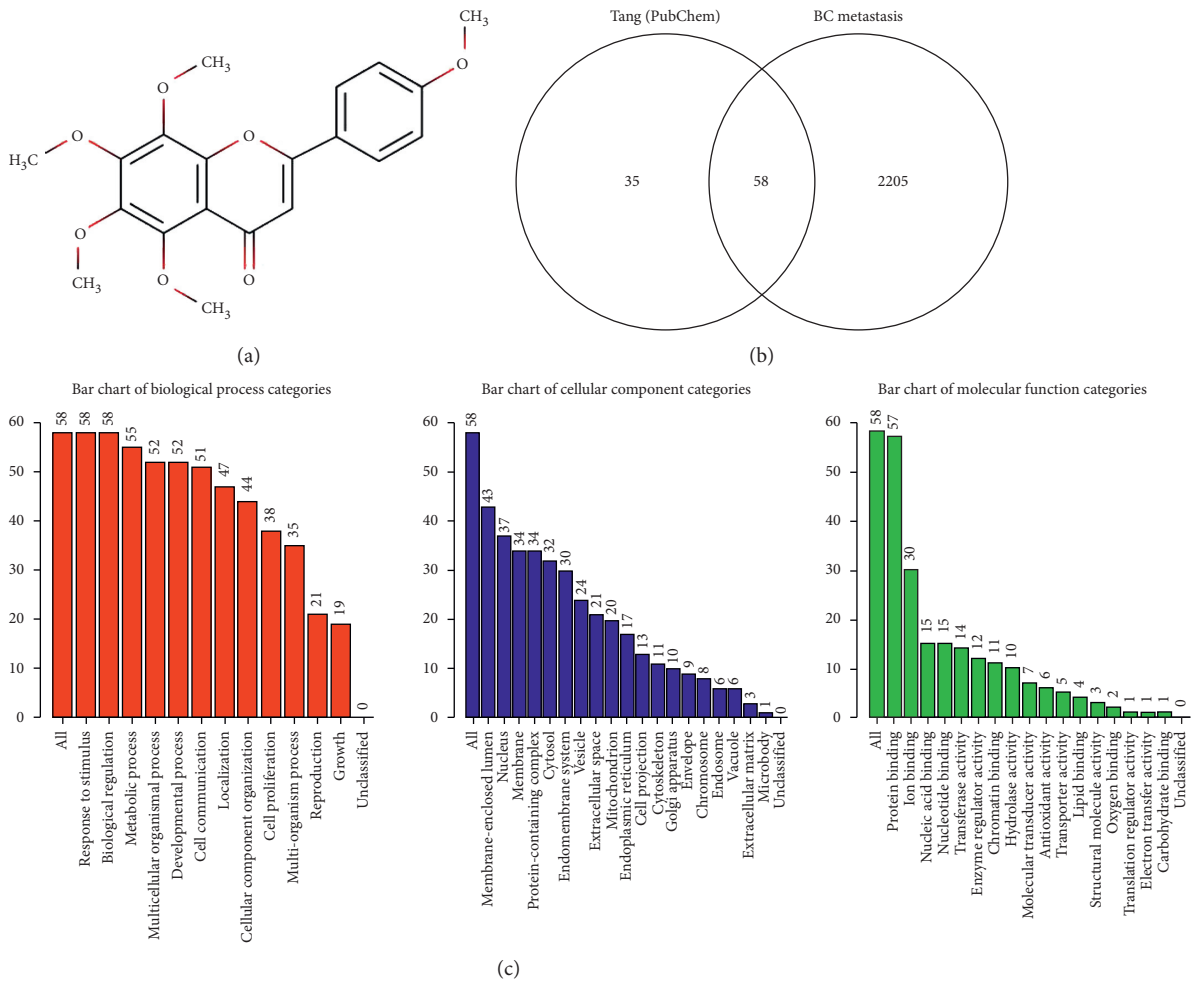

Figure 1: (a) Chemical structure of tangeretin. (b) A Venn diagram between tangeretin targets and regulatory genes of breast cancer metastasis. (c) GO enrichment, as analyzed by WebGestalt.

breast, and gastric cancer cells. Tangeretin hampers the invasion of MO4 mouse cells into the embryonic chick heart [10]. It also inhibits lung metastasis in melanoma B16F10 cell xenografts [11] and metastasis in 7,12-dimethylbenz (α) anthracene-induced rat breast cancer [12]. Moreover, tangeretin alleviates epithelial-mesenchymal transition (EMT), invasion, and migration in gastric cancer cells by down-regulating Notch-1, Jagged1/2, Hey-1, and Hes-1 [13]. Nonetheless, the molecular target of tangeretin for the metastatic inhibition of breast cancer remains unknown.

In this study, we used a bioinformatics approach to obtain tangeretin protein target data from PubChem, metastatic breast cancer regulatory genes from PubMed, and potential target genes of tangeretin against metastatic breast cancer (PT). We performed gene ontology (GO), Kyoto Encyclopedia of Genes and Genomes (KEGG) pathway enrichment, and protein-protein interaction (PPI) network analyses and selected hub genes on the basis of the highest degree score. Selected PTs were further analyzed for their prognostic values by using Kaplan–Meier survival plots and GEPIA. Corroboration of the accuracy of the selected PT in metastatic breast cancer samples was performed using ONCOMINE. Alterations in the selected genes were analyzed using the public database cBioPortal. Molecular docking studies were conducted to identify the interaction between tangeretin and PT. The results of this study emphasized the potential of tangeretin as an antimetastatic agent in breast cancer therapy.

2. Materials and Methods

2.1. Data Collection and Processing. We downloaded 95 tangeretin targets from PubChem (Supplementary Table 1) and 2263 metastatic breast cancer regulatory genes from PubMed (Supplementary Table 2). A Venn diagram was generated using the tangeretin targets from PubChem and the metastatic breast cancer regulatory genes from PubMed, which resulted in 58 genes considered potential therapeutic target genes of tangeretin (PTs) (Figure 1(b), Supplementary Table 3).

2.2. GO and KEGG Pathway Enrichment Analyses. GO and KEGG pathway enrichment analyses were performed using WebGestalt (WEB-based Gene SeT AnaLysis Toolkit) with $p < 0.05$ as the cutoff value [14].

2.3. PPI Network and Selection of Hub Genes. The PPI network was analyzed using STRING-DB v11.0 [15] with confidence scores of >0.7 and visualized by Cytoscape software [16]. Hub genes were selected on the basis of the highest degree score as calculated by the CytoHubba plugin [17].

2.4. Genetic Alteration Analysis of PTs. Genetic alterations of the PTs were analyzed using cBioPortal [18, 19]. Further connectivity analysis was performed to PTs by using the selected breast cancer study, with a cutoff value of $p < 0.05$.

2.5. Kaplan–Meier Survival Analysis. The prognostic values of the PTs were evaluated with the Kaplan–Meier plot (http://kmplot.com) by using the breast cancer database. The cutoff value was $p < 0.05$ [20], and the number of samples is displayed in each curve.

2.6. Validation of PTs in Breast Cancer and Metastatic Breast Cancer Samples. The expression of PTs across breast cancer samples from TCGA and GTEx projects was confirmed using GEPIA (http://gepia.cancer-pku.cn), with a cutoff value of $p < 0.05$ [21]. The reliability of the PTs in metastatic breast cancer cells was validated by ONCOMINE (https://www.oncomine.org) [22] using samples from some projects, including TCGA, a study by Finak et al. [23], a study by Sorlie et al. [24] and a study by Perou et al. [25].

2.7. Molecular Docking. Molecular docking was performed to foresee the binding sites of tangeretin with PIK3Cα (PDB ID: 4OVV), MMP9 (PDB ID: 2OW1), PTGS2 (PDB ID: 5F1A), COX-2 (PDB ID: 6COX), and IKK (PDB ID: 4KIK). All computational analyses were conducted using Windows 10 with an Intel Core i5-7th Gen processor and 4 GB RAM. The docking simulation, RMSD calculation, and visualization interaction were conducted using MOE 2010 (Licensed from Faculty of Pharmacy UGM). The structure of tangeretin was downloaded from PubChem (https://pubchem.ncbi.nlm.nih.gov) and sought for conformation and minimization by MOE using the energy minimization module. Docking simulations were performed on the binding side of the native ligand based on flexible ligand structures and rigid receptors. The London dG and triangle matchers were selected for the score function and placement settings, respectively, in the docking simulation. The forcefield method was used to refine the docking results of 30 settings. Docking simulation was performed using the default settings. The analysis results will conclude in which conformations generate the lowest energy when tangeretin binds to the target protein.

3. Results

3.1. GO and KEGG Pathway Enrichment Analyses. Metastasis is the main cause of death in patients with breast cancer. Utilizing the bioinformatics approach, we identified the PTs and mechanisms of tangeretin in inhibiting metastatic breast cancer. GO analysis was conducted with WebGestalt on the basis of three criteria, namely, biological process, cellular component, and molecular function (Figure 1(c)). PTs participate in the biological processes of stimulus response, metabolic process, and cell proliferation. In addition, PTs are cellular components of the nucleus and the membrane. PTs also play a molecular role in protein binding, ion binding, and enzyme regulator activity. Pathway enrichment by KEGG of the PTs (Supplementary Table 3) showed the regulation of ~106 pathways, including the PI3K-Akt, breast cancer, and TNF signaling pathways (Supplementary Table 4), three main pathways that are regulated by tangeretin in metastasis signaling, based on the literature study. Several PTs were involved in PI3K-Akt signaling (e.g., PIK3CA, PRKAA2, RELA, and TP53), the breast cancer pathway (e.g., AKT1, MTOR, NOTCH1, PIK3CA, and TP53), and the TNF signaling pathway (e.g., MMP9, NFKB1, PIK3CA, PTGS2, and RELA) (Supplementary Table 5).

3.2. Analysis of the PPI Network and Selection of Hub Genes. A PPI network was constructed from 58 proteins (confidence level of 0.4) consisting of 58 nodes, 409 edges, PPI enrichment value of $<1.10e-16$, and average local clustering coefficient of 0.62 (Figure 2(a)). The top 20 highest degree score genes, also known as hub genes, were identified, including TP53, AKT1, STAT3, IL6, and MAPK1 (Figure 2(b), Table 1).

3.3. Analysis of Genetic Alterations of Potential Target Genes. Eight PTs were analyzed using cBioportal to explore their genomic alterations across breast cancer studies. *MTOR*, *NOTCH1, PIK3CA, TP53, MMP9, NFKB1, PTGS2,* and *RELA* were selected from KEGG pathway enrichment (Supplementary Table 5), whereas *TP53, MTOR, MMP9, RELA,* and *PTGS2* were selected based on the highest degree score using CytoHubba. The study BRCA INSERM 2016 [26] was selected for further analysis (Figure 3(a)). Genetic alterations for each target gene ranged from 3% to 42% of samples, including *MTOR* (3%), *NOTCH1* (4%), *TP53* (42%), *MMP9* (4%), *NFKB1* (3%), *PIK3CA* (32%), *PTGS2* (15%), and *RELA* (5%) (Figure 3(b)). Moreover, most gene alterations belonged to amplification, missense mutation, and truncating mutation (Figure 3(b)). Further analysis of mutual exclusivity showed that only one gene pair (*NOTCH1-RELA*) exhibited significant co-occurrence ($p < 0.05$) in the breast cancer study by the INSERM 2016 project (Table 2), which indicated the pivotal role of NOTCH1 and RELA under tangeretin treatment.

3.4. Kaplan–Meier Survival Analysis. The Kaplan–Meier plot showed that patients with low mRNA expression levels of *MTOR* ($p = 3.95 \times 10^{-5}$), *TP53* ($p = 0.00054$), *MMP9* ($p = 0.0065$), *NFKB1* ($p = 3.3 \times 10^{-16}$), *PTGS2* ($p = 0.0019$), and *RELA* ($p = 0.00088$) had significantly better overall survival rates than the opposite group (Figure 4). In addition, patients with a low mRNA level of

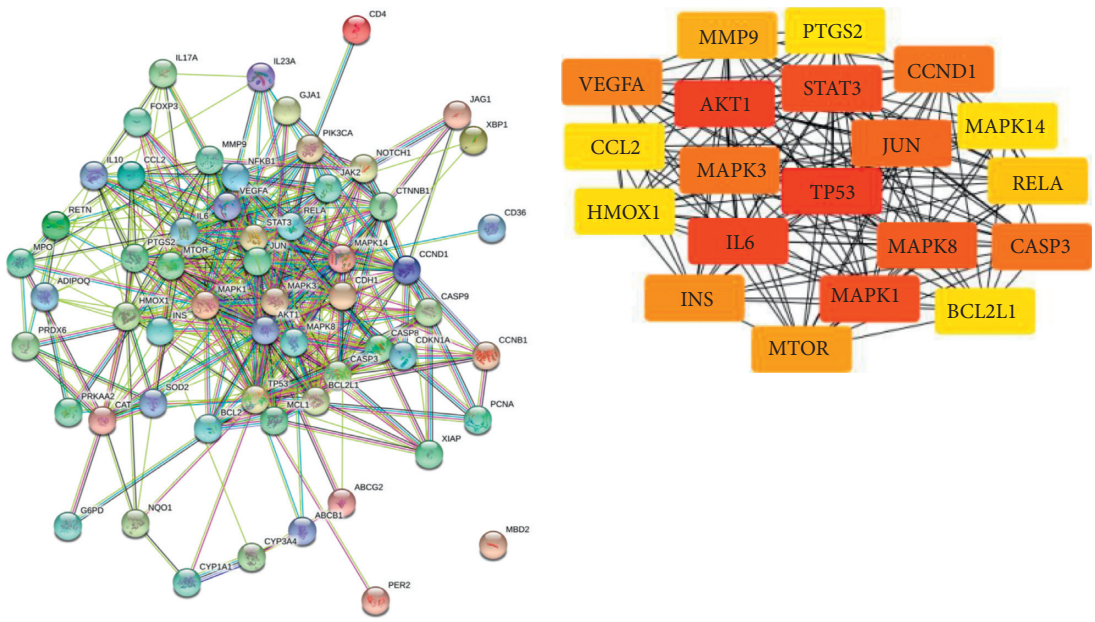

(a) (b)

Figure 2: (a) Protein-protein interaction network of potential target genes of tangeretin against metastatic breast cancer, analyzed by STRING. (b) Top 20 hub genes based on the highest degree score, analyzed by CytoHubba.

Table 1: Top 20 hub genes ranked by degree method, analyzed by CytoHubba.

Rank	Gene symbol	Gene name	Score
1	TP53	Cellular tumor antigen p53	40
2	AKT1	RAC-alpha serine/threonine-protein kinase	37
3	IL6	Interleukin-6	33
4	STAT3	Signal transducer and activator of transcription 3	31
4	MAPK1	Mitogen-activated protein kinase 1	31
6	MAPK8	Mitogen-activated protein kinase 8	29
7	JUN	Transcription factor AP-1	27
8	CCND1	G1/S-specific cyclin-D1	26
8	CASP3	Caspase-3	26
8	MAPK3	Mitogen-activated protein kinase 3	26
11	VEGFA	Vascular endothelial growth factor A	24
12	INS	Insulin	23
13	MTOR	Serine/threonine-protein kinase mTOR	22
14	MMP9	Matrix metalloproteinase-9	21
15	RELA	Transcription factor p65	20
16	BCL2L1	Bcl-2-like protein 1	19
16	CCL2	C-C motif chemokine 2	19
16	MAPK14	Mitogen-activated protein kinase 14	19
16	PTGS2	Prostaglandin G/H synthase 2	19
16	HMOX1	Heme oxygenase 1	19

NOTCH1 had better overall survival rates than those with a high mRNA level of *NOTCH1*, but the difference was not significant ($p = 0.91$). Moreover, patients with a low mRNA expression of *PIK3CA* showed significantly worse overall survival than the opposite group ($p = 2 \times 10^{-7}$).

3.5. Validation of PTs in Breast Cancer and Metastatic Breast Cancer Samples. Validation of PTs in TCGA and GTEx samples using GEPIA demonstrated that the mRNA expression of *MMP9* was significantly higher in breast cancer tissues than in normal tissues (Figure 5). In addition, the mRNA expression of *PTGS2* was significantly lower in breast cancer tissues than in normal tissues. Furthermore, no significant difference in the mRNA expression levels of *MTOR, NOTCH1, TP53, NFKB1, PIK3CA,* and *RELA* was observed between breast cancer and normal tissue samples. The validation of target genes by using ONCOMINE showed that, in samples from a TCGA study, the mRNA level of *MMP9* was significantly higher in metastatic breast cancer cells than in normal breast cells with $p = 2.97 \times 10^{-16}$ (Figure 6). In addition, samples from a study by Finak et al.

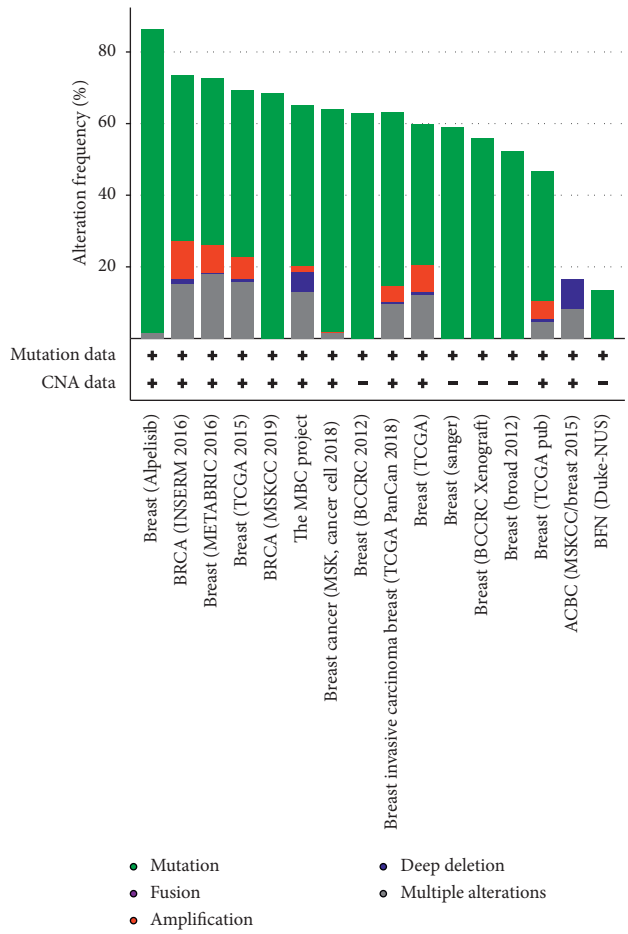

(a)

(b)

Figure 3: (a) Overview of genetic changes in *MTOR, NOTCH1, TP53, MMP9, NFKB1, PIK3CA, PTGS2,* and *RELA* across 16 breast cancer studies, as analyzed by cBioportal. (b) Summary of alterations in *MTOR, NOTCH1, TP53, MMP9, NFKB1, PIK3CA, PTGS2,* and *RELA* across breast cancer patients using a study from Lefebvre et al. [26]

Table 2: Mutual exclusivity analysis of selected genes.

A	B	Log2 odds ratio	*p* value	Tendency
NOTCH1	RELA	>3	<0.001	Co-occurrence

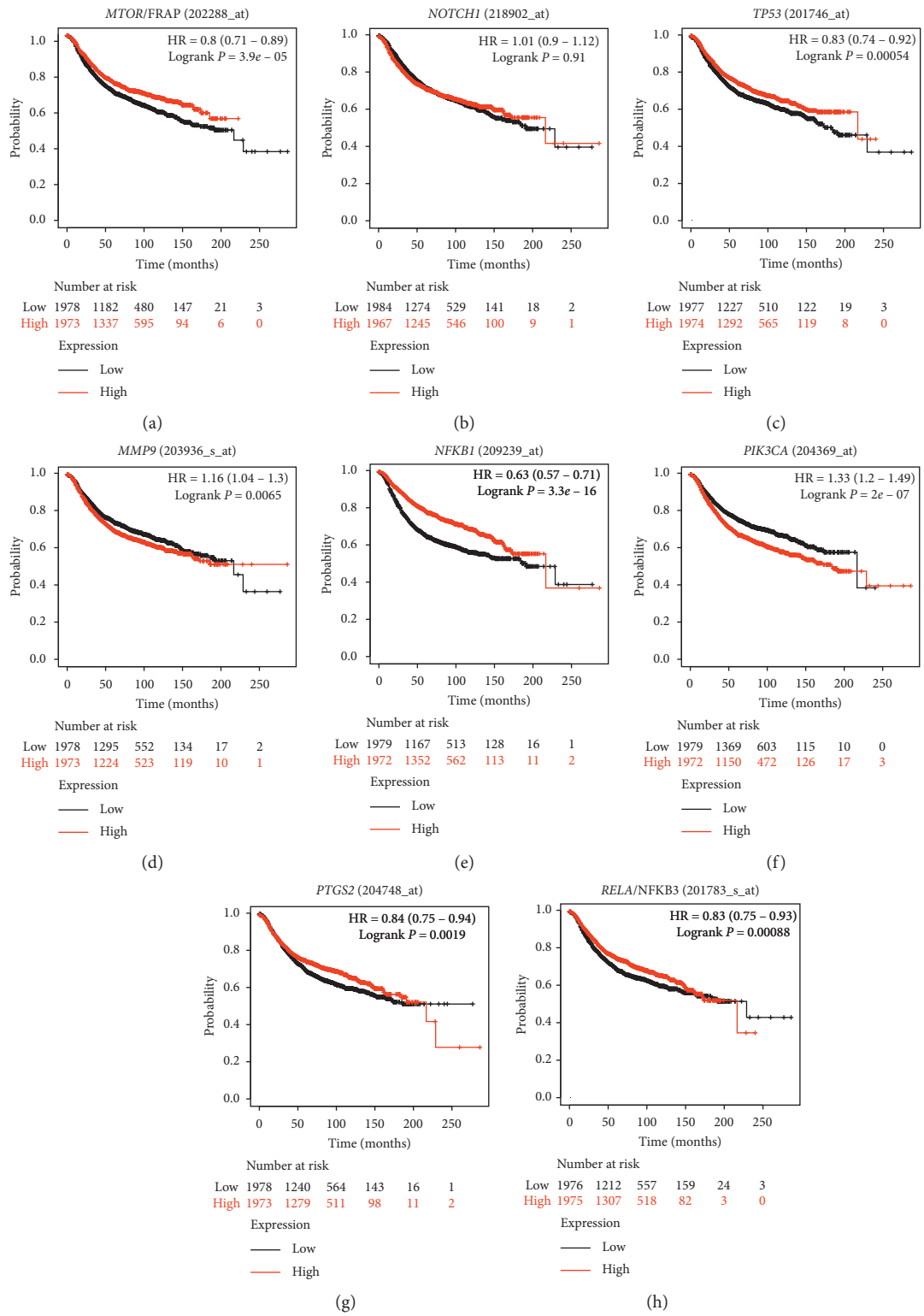

Figure 4: Overall survival of patients with breast cancer related to the mRNA levels of *MTOR*, *NOTCH1*, *TP53*, *MMP9*, *NFKB1*, *PIK3CA*, *PTGS2*, and *RELA*, as analyzed by GEPIA. (a) *MTOR*/FRAP (202288_at). (b) *NOTCH1* (218902_at). (c) *TP53* (201746_at). (d) *MMP9* (203936_s_at). (e) *NFKB1* (209239_at). (f) *PIK3CA* (204369_at). (g) *PTGS2* (204748_at). (h) *RELA*/NFKB3 (201783_s_at).

showed that the mRNA level of *NFKB1* was significantly higher in metastatic breast cancer cells than in normal breast cells ($p = 3.66 \times 10^{-14}$) [23]. Moreover, the mRNA levels of *MTOR*, *NOTCH1*, *TP53*, *PIK3CA*, *PTGS2*, and *RELA* were not different between metastatic breast cancer cells and normal breast cells.

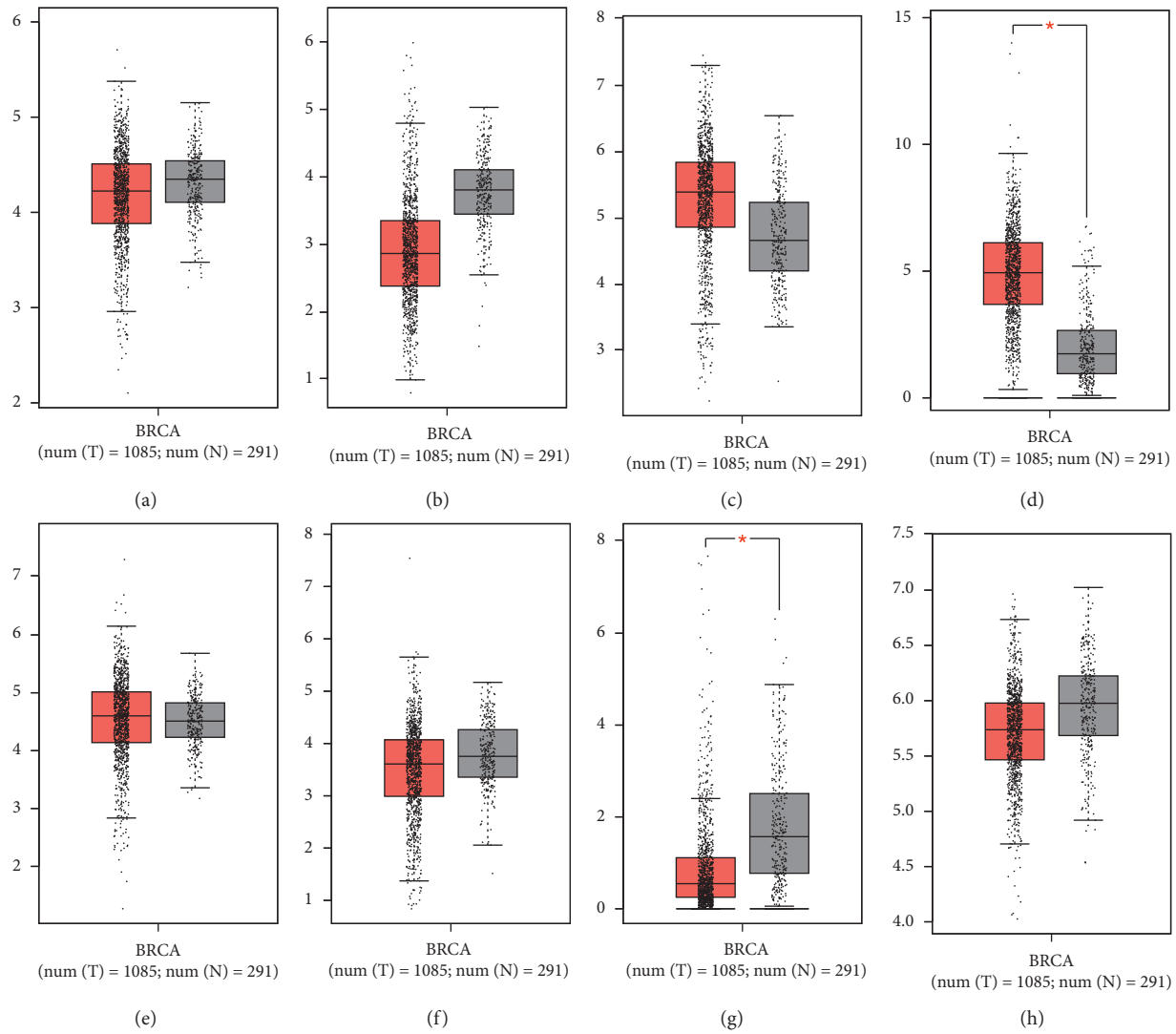

Figure 5: mRNA levels of (a) *MTOR*, (b) *NOTCH1*, (c) *TP53*, (d) *MMP9*, (e) *NFKB1*, (f) *PIK3CA*, (g) *PTGS2*, and (h) *RELA* in patients with breast cancer, as analyzed by GEPIA.

3.6. Molecular Docking. Simulation of molecular docking and visualization of ligand-protein binding were conducted with MOE software. The protein targets, including PIK3Cα, MMP9, PTGS2, COX-2, and IKK, were selected on the basis of KEGG pathway enrichment analysis, hub gene selection, survival analysis, PT validation, and uniqueness as drug targets through literature research. Native ligands of each protein consist of PIK3Cα, MMP9, PTGS2, COX-2, and IKK complexes comprising ML9 (2-amino-8-[trans-4-(2-hydroxyethoxy)cyclohexyl]-6-(6-methoxypyridin-3-yl)-4-methylpyrido[2,3-d]pyrimidin-7(8H)-one), 7 MR ((2R)-2-amino-3,3,3-trifluoro-n-hydroxy-2-{[(4-phenoxyphenyl) sulfonyl] methyl}propanamide), COH (protoporphyrin IX containing CO), HEM (protoporphyrin IX containing Fe), and KSA (K-252A). PIK3Cα and MMP9 showed slightly lower docking scores than native ligands (ML9 and 7 MR) (Table 3). The lower the docking score, the more potent the binding affinity of the ligand, implying that PIK3Cα and MMP9 tend to bend and react with tangeretin. Furthermore, tangeretin formed arene-H between Ile932 and the compound with a bonding distance of 4.07, which was shorter than the arene-H distance of ML9 with Ile932 (4.22) (Figure 7). The higher docking score of tangeretin on PTGS2, COX-2, and IKK indicated lower binding affinity compared with native ligands (3X). This phenomenon can be ascribed to the fact that only one amino acid, Gln203, interacted with tangeretin on PTGS2 by an arene-H bond (Table 3). Otherwise, the native ligand of PTGS2 (COH) had four amino acids, which interacted through arene-H (Gln203, Leu391), arene-cation (His207), and metal (His214) (Table 3). A similar phenomenon occurred for 6COX and IKK; the amino acid that interacted with tangeretin was fewer than the native ligands (Table 3).

4. Discussion

Metastasis is the main cause of death in patients with breast cancer. Utilizing a bioinformatics approach, we identified the PTs and mechanisms of tangeretin in inhibiting metastatic

Figure 6: mRNA levels of (a) *MTOR*, (b) *NOTCH1*, (c) *TP53*, (d) *MMP9*, (e) *NFKB1*, (f) *PIK3CA*, (g) *PTGS2*, and (h) *RELA* in patients with metastatic breast cancer, as analyzed by ONCOMINE.

Table 3: Molecular docking results of tangeretin against the protein targets of PIK3Cα, MMP9, PTGS2, COX-2, and IKK.

Protein	Docking score	RMSD (Å)	Ligand native				Tangeretin				
			Ligand atom	Amino acid	Binding type	Distance	Docking score	Ligand atom	Amino acid	Binding type	Distance
PIK3Cα (4TV3)	−12.3229	1.9820	C	Ile848	Arene-H	4.81	−13.0943	C	Ile932	Arene-H	4.07
			C	Ile932	Arene-H	4.22		C	Trp780	Arene-H	7.51
			N	Val851	Backbone donor-acceptor	4.10		O	Lys802	Sidechain donor	5.20

Table 3: Continued.

Protein	Docking score	RMSD (Å)	Ligand native				Tangeretin				
			Ligand atom	Amino acid	Binding type	Distance	Docking score	Ligand atom	Amino acid	Binding type	Distance
MMP9 (2OW1)	−11.4732	1.7393	C	Leu188	Arene-H	5.02	−11.5442	C	Arg424	Arene-H	6.41
			C	Tyr423	Arene-H	4.66		O	Tyr423	Backbone donor	5.82
			C	Leu418	Arene-H	4.10		C	Leu418	Arene-H	4.42
			C	7MR502	Arene-arene			O	Gln402	Sidechain donor	4.16
PTGS2 (5F1A)	−14.8424	1.2559	C	Gln203	Arene-H	3.61	−11.8904	C	Gln203	Arene-H	4.39
			C	Leu391	Arene-H	6.85					
			O-	His207	Arene-cation	4.37					
			O	His214	Metal contact	5.61					
COX-2 (6COX)	−15.6490	1.0546	O	Asn382	Sidechain donor	5.26	−12.0495	C	His386	Arene-H	5.12
			O	Thr212	Backbone donor	3.52		O	Gln203	Arene-H	4.73
			O-<	Gln454	Sidechain donor	5.73		C	Leu391	Arene-H	6.40
			O	His214	Metal contact	5.00					
IKK (4KIK)	−14.0211	0.8232	C	Ile165	Arene-H	3.89	−10.4698	C	Ile165	Arene-H	4.67
			C	Leu21	Arene-H	3.72		O	Leu21	Arene-H	6.94
			O	Cys99	Backbone donor	3.66		O	Cys99	Backbone donor	4.00
			C	Val152	Arene-H	6.07		O	Val152	Arene-H	6.05
			C	Val29	Arene-H	5.80					
			N	Glu97	Backbone acceptor	6.18		C	Asp103	Arene-H	4.40

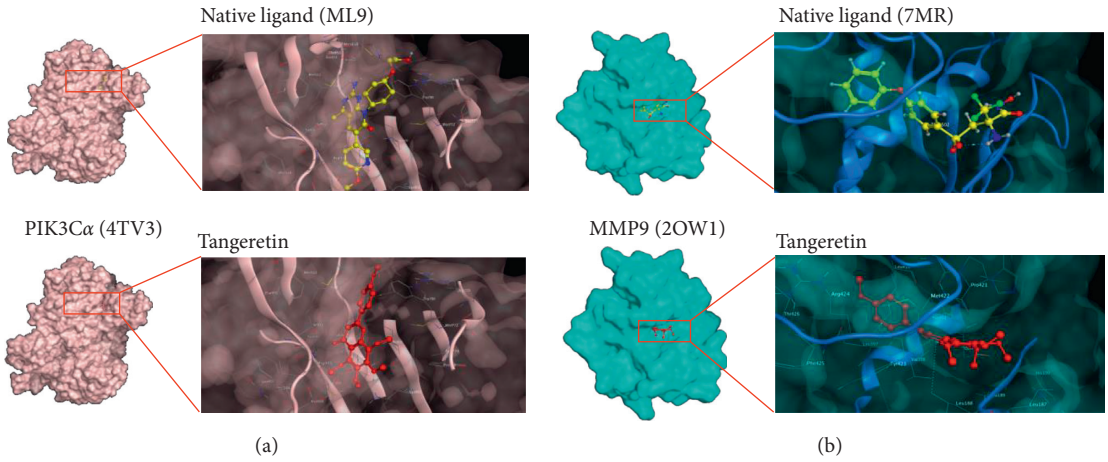

Figure 7: Continued.

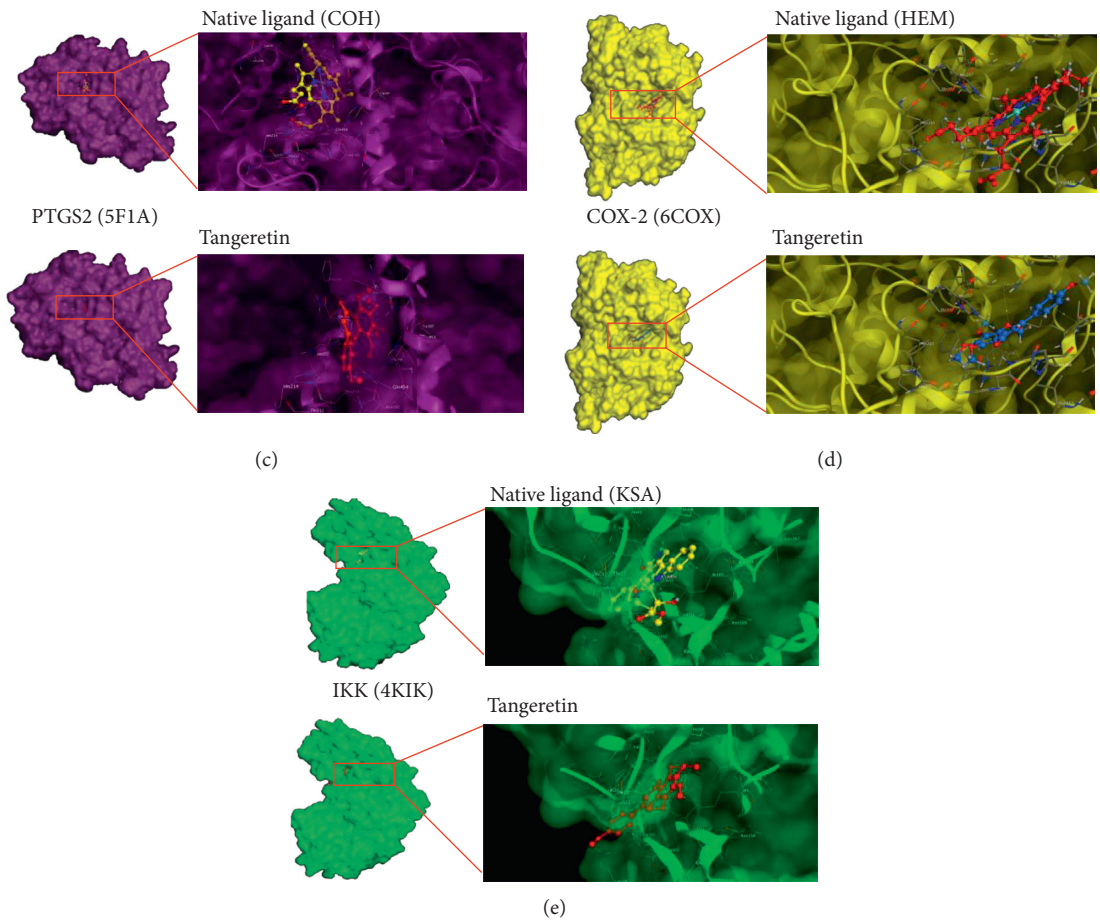

Figure 7: Visualization of ligand interaction to PIK3Cα, MMP9, PTGS2, and IKK using MOE.

breast cancer. This study emphasized the important role of the PI3K/Akt pathway and related genes (*TP53, PTGS2, NFKB1,* and *PIK3CA*) in the antimetastatic effects of tangeretin on metastatic breast cancer cells. Here, we discussed the important roles of those genes and their potential as tangeretin targets against metastatic breast cancer cells. *TP53* encodes the tumor protein p53, a tumor suppressor gene [27]. Mutations in *TP53* occur in human epidermal growth factor receptor 2-positive [27], estrogen receptor-positive, and progesterone-positive breast cancer subtypes [28]. In addition, the *TP53* gene is mutated in 80% of patients with triple-negative breast cancer [29]. Loss of *p53* or gain of mutant *p53* promotes tumor progression and metastasis [30]. In addition, loss of *p53* induces metastasis via activation of Wnt signaling [31]. Moreover, the mutation in *TP53* can promote immunogenic activity in breast cancer [32].

Tangeretin regulates *p53* expression. Tangeretin increases *p53* expression in AGS human gastric cancer cells [33]. In addition, tangeretin treatment induces the upregulation of *p53* and inhibits metastasis in 7,12-dimethylbenz (α) anthracene-induced rat breast tumors [12]. However, the study of *TP53* mutation, metastasis, and tangeretin treatment remains elusive.

MMP9 encodes matrix metalloproteinase 9 *(MMP9),* a protease that cleaves the extracellular matrix and is involved in angiogenesis, invasion, and metastasis [34]. *MMP9* is dominantly synthesized by tumor cells [35]. *MMP9* is upregulated in breast cancer cells compared with normal tissue and is correlated with metastasis and recurrence in breast cancer [36]. Thus, inhibition of MMP activity is an effective way of preventing metastasis in patients with breast cancer [37]. A previous study demonstrated that tangeretin inhibits metastasis in rat mammary carcinoma induced by 7,12-dimethylbenz (α) anthracene by downregulating *MMP2, MMP9,* and *VEGF* [12]. In addition, tangeretin inhibits the expression and activity of MMP9 in rats with pilocarpine-induced seizures [38]. Future studies of the effect of tangeretin on *MMP9* activity in metastatic breast cancer are warranted.

PTGS2 encodes prostaglandin-endoperoxide synthase 2, also known as cyclooxygenase-2 (COX-2), which participates in prostaglandin synthesis, regulates inflammation, and promotes cancer progression, invasion, and migration [39,40]. COX-2 is expressed in 40% of human metastatic breast cancers. [41]. A previous study showed that tangeretin inhibits COX-2 expression induced by IL-1beta in A549 lung cancer cells by inhibiting NF-kB, p38 MAPK, JNK, and PI3K signaling [42]. Moreover, tangeretin inhibits UVB-induced COX-2 expression by inhibiting MAPK activation and reactive oxygen species elevation [43]. Recently, an in silico

study demonstrated that tangeretin can inhibit C0X-2 [44]. Nevertheless, the effects of tangeretin on COX-2 activity and expression in metastatic breast cancer cells need further exploration.

NFKB1 encodes the nuclear factor of kappa light polypeptide gene enhancer in B-cells 1, a member subunit of NKFB [45]. NFKB1 forms various dimeric complexes with other subunits to activate NFkB signaling that regulates several biological processes, including inflammation, senescence, apoptosis, cell survival, and cancer progression [45]. NFKB1 plays a role in cancer progression and is a potential target for cancer therapy [46]. NFkB signaling is important in the invasiveness of inflammatory breast cancer [47], as well as in chemoresistance mechanisms and invasive breast cancer [48]. Moreover, NFKB1/RELA induces breast cancer progression by upregulating ETS1 [49]. A previous study showed that tangeretin treatment reduces the phosphorylation of IκB-α and IKK-β, as well as the nuclear translocation of the p65 subunit of NF-κB in lipopolysaccharide-stimulated microglial cells [50]. Hence, the inhibitory effect of tangeretin on invasion and metastasis by targeting NFkB signaling needs to be explored in future studies.

PIK3CA encodes phosphatidylinositol-4,5-bisphosphate 3-kinase catalytic subunit alpha (PIK3CA), also known as p110α, a member of the phosphoinositide 3-kinase (PI3K) family [51]. The PI3K signaling pathway is involved in the biological processes of cellular proliferation, apoptosis, survival, motility, and metastasis [52,53]. Mutation in PIK3CA is present in most solid tumors [54] and is found in 12%–15% of patients with breast cancers [55]. A recent study has shown that mutation in PIK3CA corresponds to a poor prognosis in patients with hormone receptor-positive metastatic breast cancer but a good prognosis in patients with triple-negative breast cancer [56].

Tangeretin inhibits the PI3K signaling pathway. Tangeretin enhances the sensitivity of human ovarian cancer cells to cisplatin by downregulating the PI3K/Akt signaling pathway [57]. Tangeretin also inhibits the proliferation and migration of aortic smooth muscle cells by suppressing the PI3K/AKT signaling pathway [58]. Another study showed that tangeretin poses potent neuroprotective activity by triggering the PI3K/Akt signaling pathway in pilocarpine-induced seizures rats [38]. Tangeretin also inhibits PI3K and Notch signaling in neonatal asthmatic mice [59]. Moreover, tangeretin inhibits EMT in PC-3 prostate cancer cells by downregulating the PI3K/Akt/mTOR pathway [60]. However, the effects of tangeretin on PI3K signaling and PIK3CA mutation on metastatic breast cancer cells need to be clarified in future studies.

KEGG pathway enrichment analysis indicated that PTs regulate the PI3K/Akt signaling pathway. In this study, we discussed the cross-talk between PTs in the regulation of the PI3K/Akt pathway. COX2 promotes cell survival by activating the PI3K/Akt pathway in human lung cancer cells [61]. Inhibition of COX2 blocks PI3K/AKT kinase activity in ovarian cancer [62] and hepatocellular carcinoma cells [63]. In addition, PI3K/Akt kinase activity induces COX2 expression in lipopolysaccharide-induced murine adrenocortical cells [64]. Furthermore, COX2 and PI3K are associated with the progression of colon cancer [65].

The PI3K/Akt and mTOR signaling pathways are essential for maintaining the proliferation and survival of cancer cells [66]. A recent study has shown that activation of PI3K/AKT/mTOR signaling increases hepatocellular carcinoma resistance to radiotherapy [67]. On the one hand, activation of the PI3K/Akt pathway leads to the transcriptional activity of NFκB [68]. On the other hand, NFκB activity is important for oncogenic transformation induced by PI3K/Akt signaling [68]. Mutations in PI3K signaling regulators, including PIK3CA, lead to cytokine expression upon growth factor deprivation in an NFκB-dependent manner [69]. Furthermore, PI3K/Akt/JNK/NFκB signaling plays a pivotal role in the expression of MMP-9 and enlargement in human limbal epithelial cells [70].

Activation of the PI3K/PTEN/AKT/mTOR pathway promotes invasion and metastasis by increasing the expression of MMP9 in hepatocellular carcinoma cells [71] and human breast cancer cells [72]. Furthermore, inhibition of Notch1 signaling reduces the proliferation, migration, and invasion of human breast cancer cells by decreasing PI3K/Akt activity (Li et al.). p53 participates in the regulation of cell survival by blocking the PI3K/AKT signaling pathway in cancer cells [73]. Moreover, activating mutations in PIK3CA promote the stimulation of p53 signaling [74]. A previous study showed that PI3K/Akt promotes p53 translation in cancer development [75]. Inhibition of PI3K/Akt signaling leads to p53 upregulation in leukemic cancer cells [76]. A recent study reported p53 upregulation due to PI3K/Akt signaling inhibition in EMT inhibition in liver cancer cells [77].

In this study, molecular docking analysis emphasized the potential target of tangeretin in inhibiting metastatic breast cancer cells. Tangeretin was shown to inhibit PIK3CA, MMP9, COX2, and IKK. One of the unique targets for cancer drug discovery is PIK3Cα because of the high prevalence of its mutations in various human tumors and the progression in the development of personalized cancer medicines [78]. The docking results on PIK3CA showed that the docking score of tangeretin was slightly lower than that of the native ligand ML9 ((2-amino-8-[trans-4-(2-hydroxyethoxy) cyclohexyl]-6-(6-methoxypyridin-3-yl)-4-methylpyrido [2,3-d]pyrimidin-7(8H)-one)). A low docking score represents a potent affinity of binding of the ligand, indicating that PIK3Cα tends to bend and react with tangeretin instead of the native ligand. The docking results of tangeretin on PIK3CA formed arene-H between Ile932 and the compound with a bonding distance of 4.07, which was shorter than the arene-H distance of ML9 with Ile932 (4.22) (Table 3). Furthermore, tangeretin has donor sidechains, whereas native ligands have donor-acceptor backbones. Hence, this donor sidechain is useful in increasing tangeretin binding to PIK3CA. The docking results on MMP9 showed that the docking score of tangeretin was lower than that of the native ligand 7 MR ((2R)-2-amino-3,3,3-trifluoro-n-hydroxy-2-{[(4-phenoxyphenyl) sulfonyl] methyl}propanamide)). This result is due to the differences in bond types. Specifically, the native ligand has a type of arene-arene bond, whereas tangeretin has backbone and sidechain donors. This

result is in line with the findings of Roshini et al. that tangeretin, when combined with zinc oxide (Tan-ZnO QDs), can downregulate the expression of metastasis markers, such as MMP2, MMP9, and VEGF [79]. Tangeretin showed a higher docking score than native ligands on PTGS2, COX-2, and IKK, suggesting that tangeretin has a lower binding affinity than the native ligands COH (protoporphyrin IX containing CO), HEM (protoporphyrin IX containing Fe), and KSA (K-252A) (Table 3).

Molecular docking results on PTGS2 showed that only one amino acid, Gln203, interacted with tangeretin by an arene-H bond (Table 3). Otherwise, the native ligand of PTGS2 (COH) had four amino acids, which are interacted by arene-H (Gln203, Leu391), arene-cation (His207), and metal contact (His214) (Table 3). The results of molecular docking on COX2 showed a lower docking score of tangeretin than native ligands because fewer amino acids on 6COX interacted with tangeretin than native ligands.

The IKK complex plays a pivotal role in NFkB signaling and is an important target for cancer therapy [80, 81]. Molecular docking results on IKK with the PDB code 4KIK showed that the docking scores of tangeretin were lower than those of native ligands because of the lack of one type of bonding, namely, backbone acceptor. However, tangeretin still inhibited COX2 and IKK activities. These results are supported by the previous finding of Chen et al. that tangeretin inhibits IL-1β-induced COX-2 protein expression by suppressing COX-2 gene expression [42]. Another study also showed that tangeretin significantly inhibits the activation of IKK-β induced by LPS [50]. Altogether, although the binding affinity of tangeretin is not much more robust than native ligands, it still has the potency to inhibit PTGS2, COX2, and IKK activities. Collectively, the PI3K/Akt signaling pathway is important for the regulation of metastatic breast cancer and is a potential target of tangeretin in inhibiting metastasis. However, whether the inhibitory effect of tangeretin on PI3K/Akt signaling is related to metastatic breast cancer requires further exploration.

5. Conclusions

Tangeretin inhibits metastasis in breast cancer cells by targeting TP53, PTGS2, MMP9, and PIK3CA. Molecular docking studies revealed the potential of tangeretin as an inhibitor of MMP9 and PTGS2. Furthermore, PI3K/Akt signaling is a potential target of tangeretin in inhibiting breast cancer metastasis. Future *in vitro* and *in vivo* investigations are needed to validate the results of this study.

Abbreviations

COX2: Cyclooxygenase 2
EMT: Epithelial-to-mesenchymal transition
GO: Gene Ontology
KEGG: Kyoto Encyclopedia of Genes and Genomes
MMP9: Matrix metalloproteinase 9
NFkB1: Nuclear factor of kappa light polypeptide gene enhancer in B-cells 1
PIK3CA: Phosphatidylinositol-4,5-bisphosphate 3-kinase catalytic subunit alpha
PPI: Protein-protein interaction
PT: Potential therapeutic target genes of tangeretin
PTGS2: Prostaglandin-endoperoxide synthase 2.

Data Availability

All data produced by the study are included within the manuscript and supplementary information files.

Ethical Approval

This article does not contain any studies with human participants or animals performed by any of the authors.

Conflicts of Interest

The authors declare that they have no conflicts of interest.

Authors' Contributions

AH conceptualized and designed the study; acquired, analyzed, and interpreted the data; and drafted and revised the article. HP, NH, and MI acquired and analyzed the data. NH drafted the article. All authors had final approval of the submitted manuscript.

Acknowledgments

The authors thank Badan Penerbit dan Publikasi Universitas Gadjah Mada for assistance in writing. The authors have registered their article as a preprint online as follows: https://www.researchsquare.com/article/rs-55381/v1. This work was supported by the Penelitian Dasar Unggulan Perguruan Tinggi 2020 from the Ministry of Research and Technology, National Agency for Research and Innovation, Republic of Indonesia (contract nos. 1669/UN1/DITLIT/DIT-LIT/PT/2020 and 1619/UN1/DITLIT/DIT-LIT/PT/2021).

Supplementary Materials

Supplementary Table 1. Tangeretin targets in human, as retrieved from PubChem. Supplementary Table 2. Genes related to metastatic breast cancer, as retrieved from PubMed. Supplementary Table 3. Potential therapeutic target genes of tangeretin (PTs). Supplementary Table 4. KEGG pathway enrichment analysis of the PTs. Supplementary Table 5. Gene list enriched in breast cancer, TNF, and PI3K signaling pathway. (*Supplementary Materials*)

References

[1] R. Sharma, "Breast cancer incidence, mortality and mortality-to-incidence ratio (MIR) are associated with human development, 1990-2016: evidence from global burden of disease study," *Breast Cancer*, vol. 26, no. 4, pp. 428–445, 2016.

[2] S. D. Nathanson, D. Krag, H. M. Kuerer et al., "Breast cancer metastasis through the lympho-vascular system," *Clinical & Experimental Metastasis*, vol. 35, no. 5-6, pp. 443–454, 2018.

[3] A. Bongiovanni, F. Foca, M. Fantini et al., "First prospective data on breast cancer patients from the multicentre Italian bone metastasis database," *Scientific Reports*, vol. 11, no. 1, p. 4329, 2021.

[4] Q. Liu, H. Zhang, X. Jiang, C. Qian, Z. Liu, and D. Luo, "Factors involved in cancer metastasis: a better understanding to "seed and soil" hypothesis," *Molecular Cancer*, vol. 16, no. 1, p. 176, 2017.

[5] S. Tungsukruthai, N. Petpiroon, and P. Chanvorachote, "Molecular mechanisms of breast cancer metastasis and potential anti-metastatic compounds," *Anticancer Research*, vol. 38, no. 5, pp. 2607–2618, 2018.

[6] M. E. Brack, T. Boterberg, H. T. Depypere, C. Stove, G. Leclercq, and M. M. Mareel, "The citrus methoxyflavone tangeretin affects human cell-cell interactions," *Advances in Experimental Medicine and Biology*, vol. 505, pp. 135–139, 2002.

[7] Y. P. Cheng, S. Li, W. L. Chuang et al., "Blockade of STAT3 signaling contributes to anticancer effect of 5-acetyloxy-6,7,8,4'-tetra-methoxyflavone, a tangeretin derivative, on human glioblastoma multiforme cells," *International Journal of Molecular Sciences*, vol. 2013 pages, 2019.

[8] K. L. Morley, P. J. Ferguson, and J. Koropatnick, "Tangeretin and nobiletin induce G1 cell cycle arrest but not apoptosis in human breast and colon cancer cells," *Cancer Letters*, vol. 251, no. 1, pp. 168–178, 2007.

[9] S. Surichan, R. R. Arroo, A. M. Tsatsakis, and V. P. Androutsopoulos, "Tangeretin inhibits the proliferation of human breast cancer cells via CYP1A1/CYP1B1 enzyme induction and CYP1A1/CYP1B1-mediated metabolism to the product 4' hydroxy tangeretin," *Toxicol In Vitro*, vol. 50, pp. 274–284, 2018.

[10] M. E. Bracke, B. M. Vyncke, N. A. Van Larebeke et al., "The flavonoid tangeretin inhibits invasion of MO4 mouse cells into embryonic chick heart in vitro," *Clinical and Experimental Metastasi*, vol. 7, no. 3, pp. 283–300, 1989.

[11] C. Martinez Conesa, V. Vicente Ortega, M. J. Yanez Gascon et al., "Treatment of metastatic melanoma B16F10 by the flavonoids tangeretin, rutin, and diosmin," *Journal of Agricultural and Food Chemistry*, vol. 53, no. 17, pp. 6791–6797, 2005.

[12] L. Arivazhagan and S. Sorimuthu Pillai, "Tangeretin, a citrus pentamethoxyflavone, exerts cytostatic effect via p53/p21 up-regulation and suppresses metastasis in 7,12-dimethylbenz (α) anthracene-induced rat mammary carcinoma," *Journal of Nutritional Biochemistry*, vol. 25, no. 11, pp. 1140–1153, 2014.

[13] X. Zhang, L. Zheng, Y. Sun, T. Wang, and B. Wang, "Tangeretin enhances radiosensitivity and inhibits the radiation-induced epithelial-mesenchymal transition of gastric cancer cells," *Oncology Report*, vol. 34, no. 1, pp. 302–310, 2015.

[14] J. Wang, S. Vasaikar, Z. Shi, M. Greer, and B. Zhang, "WebGestalt 2017: a more comprehensive, powerful, flexible and interactive gene set enrichment analysis toolkit," *Nucleic Acids Research*, vol. 45, no. 1, pp. W130–W137, 2017.

[15] D. Szklarczyk, A. Franceschini, S. Wyder et al., "STRING v10: protein-protein interaction networks, integrated over the tree of life," *Nucleic Acids Research*, vol. 43, pp. D447–452, 2015.

[16] P. Shannon, A. Markiel, O. Ozier et al., "Cytoscape: a software environment for integrated models of biomolecular interaction networks," *Genome Research*, vol. 13, no. 11, pp. 2498–2504, 2003.

[17] C. H. Chin, S. H. Chen, H. H. Wu, C. W. Ho, M. T. Ko, and C. Y. Lin, "cytoHubba: identifying hub objects and sub-networks from complex interactome," *BMC Systems Biology*, vol. 8, no. 4, p. S11, 2014.

[18] E. Cerami, J. Gao, U. Dogrusoz et al., "The cBio cancer genomics portal: an open platform for exploring multidimensional cancer genomics data," *Cancer Discovery*, vol. 2, no. 5, pp. 401–404, 2012.

[19] J. Gao, B. A. Aksoy, U. Dogrusoz et al., "Integrative analysis of complex cancer genomics and clinical profiles using the cBioPortal," *Science Signaling*, vol. 6, no. 269, p. pl1, 2013.

[20] B. Györffy, A. Lanczky, A. C. Eklund et al., "An online survival analysis tool to rapidly assess the effect of 22,277 genes on breast cancer prognosis using microarray data of 1,809 patients," *Breast Cancer Research Treat*, vol. 123, no. 3, pp. 725–731, 2010.

[21] Z. Tang, C. Li, B. Kang, G. Gao, C. Li, and Z. Zhang, "GEPIA: a web server for cancer and normal gene expression profiling and interactive analyses," *Nucleic Acids Research*, vol. 45, no. W1, pp. W98–W102, 2017.

[22] D. R. Rhodes, J. Yu, K. Shanker et al., "ONCOMINE: a cancer microarray database and integrated data-mining platform," *Neoplasia*, vol. 6, no. 1, pp. 1–6, 2004.

[23] G. Finak, N. Bertos, F. Pepin et al., "Stromal gene expression predicts clinical outcome in breast cancer," *Nature Medicine*, vol. 14, no. 5, pp. 518–527, 2008.

[24] T. Sorlie, R. Tibshirani, J. Parker et al., "Repeated observation of breast tumor subtypes in independent gene expression data sets," *Proceedings of the National Academy of Sciences of the United States of America*, vol. 100, no. 14, pp. 8418–8423, 2003.

[25] C. M. Perou, T. Sørlie, M. B. Eisen et al., "Molecular portraits of human breast tumours," *Nature*, vol. 406, no. 6797, pp. 747–752, 2000.

[26] C. Lefebvre, T. Bachelot, T. Filleron et al., "Mutational profile of metastatic breast cancers: a retrospective analysis," *PLoS Medicine*, vol. 13, no. 12, Article ID e1002201, 2016.

[27] J. Huszno and E. Grzybowska, "TP53 mutations and SNPs as prognostic and predictive factors in patients with breast cancer," *Oncology Letters*, vol. 16, no. 1, pp. 34–40, 2018.

[28] F. Meric-Bernstam, X. Zheng, M. Shariati et al., "Survival outcomes by TP53 mutation status in metastatic breast cancer," *JCO Precision Oncology*, vol. 2, 2018.

[29] J. P. Li, X. M. Zhang, Z. Zhang, L. H. Zheng, S. Jindal, and Y. J. Liu, "Association of p53 expression with poor prognosis in patients with triple-negative breast invasive ductal carcinoma," *Medicine (Baltimore)*, vol. 98, no. 18, Article ID e15449, 2019.

[30] E. Powell, D. Piwnica-Worms, and H. Piwnica-Worms, "Contribution of p53 to metastasis," *Cancer Discov*, vol. 4, no. 4, pp. 405–414, 2014.

[31] M. D. Wellenstein, S. B. Coffelt, D. E. M. Duits et al., "Loss of p53 triggers WNT-dependent systemic inflammation to drive breast cancer metastasis," *Nature*, vol. 572, no. 7770, pp. 538–542, 2019.

[32] Z. Liu, Z. Jiang, Y. Gao, L. Wang, C. Chen, and X. Wang, "TP53 mutations promote immunogenic activity in breast cancer," *Journal of Oncology*, vol. 2019, Article ID 5952836, 19 pages, 2019.

[33] Y. Dong, A. Cao, J. Shi et al., "Tangeretin, a citrus polymethoxyflavonoid, induces apoptosis of human gastric cancer AGS cells through extrinsic and intrinsic signaling pathways," *Oncology Reports*, vol. 31, no. 4, pp. 1788–1794, 2014.

[34] H. Huang, "Matrix metalloproteinase-9 (MMP-9) as a cancer biomarker and MMP-9 biosensors: recent advances," *Sensors (Basel)*, vol. 18, no. 10, 2018.

[35] C. Mehner, A. Hockla, E. Miller, S. Ran, D. C. Radisky, and E. S. Radisky, "Tumor cell-produced matrix metalloproteinase 9 (MMP-9) drives malignant progression and metastasis of basal-like triple negative breast cancer," *Oncotarget*, vol. 5, no. 9, pp. 2736–2749, 2014.

[36] E. M. Yousef, M. R. Tahir, Y. St-Pierre, and L. A. Gaboury, "MMP-9 expression varies according to molecular subtypes of breast cancer," *BMC Cancer*, vol. 14, no. 609, 2014.

[37] G. Shay, C. C. Lynch, and B. Fingleton, "Moving targets: emerging roles for MMPs in cancer progression and metastasis," *Matrix Biology*, vol. 44–46, pp. 200–206, 2015.

[38] X. Q. Guo, Y. L. Cao, F. Hao, Z. R. Yan, M. L. Wang, and X. W. Liu, "Tangeretin alters neuronal apoptosis and ameliorates the severity of seizures in experimental epilepsy-induced rats by modulating apoptotic protein expressions, regulating matrix metalloproteinases, and activating the PI3K/Akt cell survival pathway," *Advances in Medical Sciences*, vol. 62, no. 2, pp. 246–253, 2017.

[39] F. Khorshidi, M. M. Haghighi, E. Nazemalhosseini Mojarad et al., "The prostaglandin synthase 2/cyclooxygenase 2 (PTGS2/COX2) rs5277 polymorphism does not influence risk of colorectal cancer in an Iranian population," *Asian Pacific Journal of Cancer Prevention*, vol. 15, no. 8, pp. 3507–3511, 2014.

[40] T. L. Larkins, M. Nowell, S. Singh, and G. L. Sanford, "Inhibition of cyclooxygenase-2 decreases breast cancer cell motility, invasion and matrix metalloproteinase expression," *BMC Cancer*, vol. 6, no. 181, 2006.

[41] B. Singh, J. A. Berry, A. Shoher, G. D. Ayers, C. Wei, and A. Lucci, "COX-2 involvement in breast cancer metastasis to bone," *Oncogene*, vol. 26, no. 26, pp. 3789–3796, 2007.

[42] K. H. Chen, M. S. Weng, and J. K. Lin, "Tangeretin suppresses IL-1beta-induced cyclooxygenase (COX)-2 expression through inhibition of p38 MAPK, JNK, and AKT activation in human lung carcinoma cells," *Biochem Pharmacol*, vol. 73, no. 2, pp. 215–227, 2007.

[43] J. H. Yoon, T. G. Lim, K. M. Lee, A. J. Jeon, S. Y. Kim, and K. W. Lee, "Tangeretin reduces ultraviolet B (UVB)-induced cyclooxygenase-2 expression in mouse epidermal cells by blocking mitogen-activated protein kinase (MAPK) activation and reactive oxygen species (ROS) generation," *Journal of Agricultural and Food Chemistry*, vol. 59, no. 1, pp. 222–228, 2011.

[44] P. Sangavi and K. Langeswaran, "Anti-tumorigenic efficacy of tangeretin in liver cancer - an in-silico approach," *Current Computer-Aided Drug Design*, vol. 16, 2020.

[45] T. Cartwright and N. D. Perkins, "NFKB1: a suppressor of inflammation, ageing and cancer," *The FEBS Journal*, vol. 283, no. 10, pp. 1812–1822, 2016.

[46] J. Concetti and C. L. Wilson, "NFKB1 and cancer: friend or foe?" *Cells*, vol. 7, no. 9, 2018.

[47] F. Lerebours, S. Vacher, C. Andrieu et al., "NF-kappa B genes have a major role in inflammatory breast cancer," *BMC Cancer*, vol. 8, no. 41, 2008.

[48] W. Wang, S. A. Nag, and R. Zhang, "Targeting the NFkappaB signaling pathways for breast cancer prevention and therapy," *Current Medicinal Chemistry*, vol. 22, no. 2, pp. 264–289, 2015.

[49] G. C. Kim, H. K. Kwon, C. G. Lee et al., "Upregulation of Ets1 expression by NFATc2 and NFKB1/RELA promotes breast cancer cell invasiveness," *Oncogenesis*, vol. 7, no. 11, p. 91, 2018.

[50] Z. Shu, B. Yang, H. Zhao et al., "Tangeretin exerts anti-neuroinflammatory effects via NF-kappaB modulation in lipopolysaccharide-stimulated microglial cells," *International Immunopharmacology*, vol. 19, no. 2, pp. 275–282, 2014.

[51] P. Liu, H. Cheng, T. M. Roberts, and J. J. Zhao, "Targeting the phosphoinositide 3-kinase pathway in cancer," *Nature Reviews Drug Discovery*, vol. 8, no. 8, pp. 627–644, 2009.

[52] V. Asati, S. K. Bharti, D. K. Mahapatra, V. Asati, and A. K. Budhwani, "Triggering PIK3CA mutations in PI3K/Akt/mTOR axis: exploration of newer inhibitors and rational preventive strategies," *Current Pharmaceutical Design*, vol. 22, no. 39, pp. 6039–6054, 2016.

[53] B. Li, W. W. Xu, A. K. Y. Lam et al., "Significance of PI3K/AKT signaling pathway in metastasis of esophageal squamous cell carcinoma and its potential as a target for anti-metastasis therapy," *Oncotarget*, vol. 8, no. 24, pp. 38755–38766, 2017.

[54] R. R. Madsen, B. Vanhaesebroeck, and R. K. Semple, "Cancer-associated PIK3CA mutations in overgrowth disorders," *Trends in Molecular Medicine*, vol. 24, no. 10, pp. 856–870, 2018.

[55] N. Vasan, P. Razavi, J. L. Johnson et al., "Double PIK3CA mutations in cis increase oncogenicity and sensitivity to PI3Kalpha inhibitors," *Science*, vol. 366, no. 6466, pp. 714–723, 2019.

[56] F. Mosele, B. Stefanovska, A. Lusque et al., "Outcome and molecular landscape of patients with PIK3CA-mutated metastatic breast cancer," *Annals of Oncology*, vol. 31, no. 3, pp. 377–386, 2020.

[57] S. A. Arafa el, Q. Zhu, B. M. Barakat et al., "Tangeretin sensitizes cisplatin-resistant human ovarian cancer cells through downregulation of phosphoinositide 3-kinase/Akt signaling pathway," *Cancer Research*, vol. 69, no. 23, pp. 8910–8917, 2009.

[58] J. Seo, H. S. Lee, S. Ryoo, J. H. Seo, B. S. Min, and J. H. Lee, "Tangeretin, a citrus flavonoid, inhibits PGDF-BB-induced proliferation and migration of aortic smooth muscle cells by blocking AKT activation," *European Journal of Pharmacology*, vol. 673, no. 1-3, pp. 56–64, 2011.

[59] L. L. Liu, F. H. Li, Y. Zhang, X. F. Zhang, and J. Yang, "Tangeretin has anti-asthmatic effects via regulating PI3K and Notch signaling and modulating Th1/Th2/Th17 cytokine balance in neonatal asthmatic mice," *The Brazilian Journal of Medical and Biological Research*, vol. 50, no. 8, Article ID e599, 2017.

[60] W. B. Zhu, N. Xiao, and X. J. Liu, "Dietary flavonoid tangeretin induces reprogramming of epithelial to mesenchymal transition in prostate cancer cells by targeting the PI3K/Akt/mTOR signaling pathway," *Oncology Letters*, vol. 15, no. 1, pp. 433–440, 2018.

[61] M. T. Lin, R. C. Lee, P. C. Yang, F. M. Ho, and M. L. Kuo, "Cyclooxygenase-2 inducing Mcl-1-dependent survival mechanism in human lung adenocarcinoma CL1.0 cells. Involvement of phosphatidylinositol 3-kinase/Akt pathway," *Journal of Biological Chemistry*, vol. 276, no. 52, pp. 48997–49002, 2001.

[62] S. Uddin, M. Ahmed, A. Hussain et al., "Cyclooxygenase-2 inhibition inhibits PI3K/AKT kinase activity in epithelial ovarian cancer," *International Journal of Cancer*, vol. 126, no. 2, pp. 382–394, 2010.

[63] S.-S. LI and S. Jun, "Role of PI3K/AKT/mTOR pathway in the expression of Cox-2 in inhibition of human hepatocellular carcinoma cells by curcumin," *Medical Journal of Chinese People's Liberation Army*, vol. 39, no. 1, pp. 30–34, 2014.

[64] M. E. Mercau, F. Astort, E. F. Giordanino et al., "Involvement of PI3K/Akt and p38 MAPK in the induction of COX-2 expression by bacterial lipopolysaccharide in murine adrenocortical cells," *Molecular and Cellular Endocrinology*, vol. 384, no. 1-2, pp. 43–51, 2014.

[65] R. A. Anselmi Júnior, C. M. D. Souza, M. L. V. D. Azevedo et al., "The role of Phosphatidylinositol 3 kinase (PI3K) and Cycloxygenase-2 (COX2) in carcinogenesis of colorectal polyps," *Journal of Coloproctology*, vol. 38, no. 1, pp. 1–8, 2018.
[66] C. Porta, C. Paglino, and A. Mosca, "Targeting PI3K/Akt/mTOR signaling in cancer," *Frontiers in Oncology*, vol. 4, no. 64, 2014.
[67] O. A. Bamodu, H. L. Chang, J. R. Ong, W. H. Lee, C. T. Yeh, and J. T. Tsai, "Elevated PDK1 expression drives PI3K/AKT/MTOR signaling promotes radiation-resistant and dedifferentiated phenotype of hepatocellular carcinoma," *Cells*, vol. 9, no. 3, 2020.
[68] D. Bai, L. Ueno, and P. K. Vogt, "Akt-mediated regulation of NFkappaB and the essentialness of NFkappaB for the oncogenicity of PI3K and Akt," *International Journal of Cancer*, vol. 125, no. 12, pp. 2863–2870, 2009.
[69] J. E. Hutti, A. D. Pfefferle, S. C. Russell, M. Sircar, C. M. Perou, and A. S. Baldwin, "Oncogenic PI3K mutations lead to NF-kappaB-dependent cytokine expression following growth factor deprivation," *Cancer Research*, vol. 72, no. 13, pp. 3260–3269, 2012.
[70] C.-Y. Cheng, H.-L. Hsieh, L.-D. Hsiao, and C.-M. Yang, "PI3-K/Akt/JNK/NF-κB is essential for MMP-9 expression and outgrowth in human limbal epithelial cells on intact amniotic membrane," *Stem Cell Research*, vol. 9, no. 1, pp. 9–23, 2012.
[71] J. S. Chen, Q. Wang, X. H. Fu et al., "Involvement of PI3K/PTEN/AKT/mTOR pathway in invasion and metastasis in hepatocellular carcinoma: association with MMP-9," *Hepatology Research*, vol. 39, no. 2, pp. 177–186, 2009.
[72] J. H. Park, Y. Y. Cho, S. W. Yoon, and B. Park, "Suppression of MMP-9 and FAK expression by pomolic acid via blocking of NF-kappaB/ERK/mTOR signaling pathways in growth factor-stimulated human breast cancer cells," *International Journal of Oncology*, vol. 49, no. 3, pp. 1230–1240, 2021.
[73] B. Singh, P. G. Reddy, A. Goberdhan et al., "p53 regulates cell survival by inhibiting PIK3CA in squamous cell carcinomas," *Genes & Development*, vol. 16, no. 8, pp. 984–993, 2002.
[74] C. Lee, J. S. Kim, and T. Waldman, "Activated PI3K signaling as an endogenous inducer of p53 in human cancer," *Cell Cycle*, vol. 6, no. 4, pp. 394–396, 2007.
[75] A. G. Abraham and E. O'Neill, "PI3K/Akt-mediated regulation of p53 in cancer," *Biochemical Society Transactions*, vol. 42, no. 4, pp. 798–803, 2014.
[76] E. Naderali, B. Valipour, A. A. Khaki et al., "Positive effects of PI3K/akt signaling inhibition on PTEN and P53 in prevention of acute lymphoblastic leukemia tumor cells," *Advanced Pharmaceutical Bulletin*, vol. 9, no. 3, pp. 470–480, 2019.
[77] Y. Li, T. Wang, Y. Sun et al., "p53-Mediated PI3K/AKT/mTOR pathway played a role in ptox(dpt)-induced EMT inhibition in liver cancer cell lines," *Oxid Med Cell Longev*, vol. 2019, Article ID 2531493, 15 pages, 2019.
[78] P. Chen, Y. L. Deng, S. Bergqvist et al., "Engineering of an isolated p110α subunit of PI3Kα permits crystallization and provides a platform for structure-based drug design," *Protein Science*, vol. 23, no. 10, pp. 1332–1340, 2014.
[79] A. Roshini, S. Jagadeesan, L. Arivazhagan et al., "pH-sensitive tangeretin-ZnO quantum dots exert apoptotic and anti-metastatic effects in metastatic lung cancer cell line," *Materials Science and Engineering: C*, vol. 92, pp. 477–488, 2018.
[80] A. Israël, "The IKK complex, a central regulator of NF-kappaB activation," *Cold Spring Harbor Perspectives in Biology*, vol. 2, no. 3, Article ID a000158, 2010.
[81] J.-L. Luo, H. Kamata, and M. Karin, "IKK/NF-kappaB signaling: balancing life and death--a new approach to cancer therapy," *Journal of Clinical Investigation*, vol. 115, no. 10, pp. 2625–2632, 2005.

Hindawi
Evidence-Based Complementary and Alternative Medicine
Volume 2021, Article ID 9952578, 9 pages
https://doi.org/10.1155/2021/9952578

Review Article

Pharmaceutical Values of Calycosin: One Type of Flavonoid Isolated from *Astragalus*

Guowei Gong,[1] Yuzhong Zheng,[2] Yang Yang,[1] Yixuan Sui,[3] and Zhen Wen[4]

[1]*Department of Bioengineering, Zunyi Medical University, Zhuhai Campus, Zhuhai, Guangdong 519041, China*
[2]*Guangdong Key Laboratory for Functional Substances in Medicinal Edible Resources and Healthcare Products, School of Life Sciences and Food Engineering, Hanshan Normal University, Chaozhou, Guangdong 521041, China*
[3]*Department of Neuroscience, City University of Hong Kong, Hong Kong 999077, China*
[4]*College of Chemistry and Environmental Engineering, Shenzhen University, Shenzhen 518060, China*

Correspondence should be addressed to Yuzhong Zheng; zhengyuzhong@gmail.com

Received 19 March 2021; Revised 21 April 2021; Accepted 29 April 2021; Published 7 May 2021

Academic Editor: Oana Cioanca

Astragalus is a popular *Materia Medica* in China, and it could be applied in the treatment of various diseases. It contains a variety of chemically active ingredients, such as saponins, flavonoids, and polysaccharides. Plant-derived bioactive chemicals are considered natural, safe, and beneficial. Among the infinite plant-identified and isolated molecules, flavonoids have been reported to have positive effects on human health. Calycosin is the most important active flavonoid substance identified predominantly within this medicinal plant. In recent years, calycosin has been reported to have anticancer, antioxidative, immune-modulatory, and estrogenic-like properties. This review collected recent relevant literatures on calycosin and summarized its potential pharmaceutical properties and working mechanism involved, which provided solid basis for future clinical research.

1. Introduction

The development of traditional Chinese medicine (TCM) has a history of thousands of years, and it has accumulated myriad medical experience and summarized pharmacological effects of *Materia Medica* playing a pivotal role in modernization of TCM [1, 2]. With the development of modern medicine, the pharmaceutical properties of raw herbal extract can no longer satisfy today's sophisticated biomedical research. The bioactive molecules selected and isolated from plant are more suitable as potential medicine [3, 4]. In fact, plant-derived chemicals are associated with drug development, such as Taxol isolated from *Taxus chinensis* and camptothecin identified and enriched from *Camptotheca acuminata.*

Astragalus membranaceus, Huangqi in Chinese, as a classic traditional herbal medicine, is commonly used in a variety of traditional Chinese medicine prescriptions [5, 6]. The major pharmaceutical functions of this *Materia Medica* are boosting immune and hematopoietic systems [7, 8]. Previous studies have reported that a plethora of flavonoids have been identified and isolated from *Astragalus.* Flavonoids are classified as polyphenolic compounds and they are ubiquitously enriched in the plant kingdom [9, 10]. It is estimated that over 4000 flavonoids have been reported and identified, and they could be clustered into 8 subclasses, that is, flavanole, flavanonole, chalkone, anthocyanidine, aurone, flavone, flavanone, and isoflavone [9, 10]. Calycosin is the most enriched isoflavone found abundantly in *Astragalus.* This molecule has gained attention for its myriad medical functions both *in vitro* and *in vivo* [2, 5, 6, 11]. Hence, this review emphasizes the effects of calycosin on anticancer, antioxidative, immune-modulatory, and estrogenic-like properties.

2. Pharmacological Activities of Calycosin

2.1. Anticancer Functions. Breast cancer is one of the most common cancers threatening women globally and it accounts for approximately 15% of female cancer-related

deaths in the United States [12, 13]. Human breast cancer is classified into estrogen receptor-positive (ER+) and estrogen receptor-negative (ER−) subtypes. Tian et al. have reported that calycosin was able to inhibit both ER− and ER+ breast cancer cell proliferation in a dose-dependent manner and the inhibitory effects were associated with noncoding RNA WDR7-7 expression level by inducing G-protein coupled estrogen receptor 30 (GPR30) and RASD1 via Erk1/2 and Akt transduction pathway [14, 15]. The apoptosis-related protein, cleaved caspase 3/9, and Bax were significantly stimulated under the treatment of calycosin in ER + cancer cell type MCF-7 [14]. Li group published similar data and confirmed that calycosin at 150 μM was capable of blocking MCF-7 and T47D cells migration and invasion by wound healing and Transwell assays [16]. Interestingly, calycosin at 2 μmol/L already triggered MCF-7 cell apoptosis by flow cytometry analysis [17]. Additionally, treatment of calycosin could downregulate forkhead box P3, vascular endothelial growth factor (VEGF), and matrix metalloproteinase 9 (MMP9) in MCF-7 and T47D [17]. Furthermore, Chen group (2014) confirmed that calycosin induced ER+ MCF-7 cell apoptosis via the blocking insulin-like growth factor 1 receptor (IGF-1R) pathway after 48-hour treatment [18]. On the other hand, Wu et al. (2019) found that the application of calycosin decreased invasive and migratory effects in ER- breast cancer MDA-MB231 cells by suppressing Rab27B, ß-catenin, and VEGF levels. More importantly, the inhibitory activities under the challenge of calycosin were recovered by the overexpression of Rab27B [19].

Colorectal cancer has a high mortality rate, which is also named as bowel cancer, colon cancer, or rectal cancer, claiming at least 500 thousand lives every year globally [20, 21]. Colorectal cancer is the third highest incidence of all cancers worldwide. The early symptoms of colorectal cancer are hard to detect, and the terminal stage of colorectal cancer is barely treated due to lack of effective biomarkers for clinical screening [22]. The study found that the potential targets of calycosin on colorectal cancer were ERα, ERβ, ATP-binding cassette subfamily G member 2, breast cancer type 1 susceptibility protein, CYP19A1, and epidermal growth factor receptor (EGFR) [22]. Therefore, these targets could be used as monitor for colorectal cancer treatment. Besides, the *in vitro* and *in vivo* against colorectal properties of calycosin have been widely documented [23–25]. Zhao et al. have published that calycosin suppressed colorectal cancer cell line SW480 dose-dependently by Hoechst 33258 assay [25]. Furthermore, the xenograft tumor size in nude mice was decreased by the calycosin treatment [25]. Impressively, calycosin significantly enhanced autophagy specific protein expressions, that is, Beclin-1 and LC-3II, after 48-hour incubation in cultured HT-29 cells [26]. However, cotreatment of HT-29 with IGF-1 could recover calycosin-induced cell autophagy. Wang found that calycosin inhibited colorectal cancer proliferation and migration by enhancing BATF2 to target plasminogen activator inhibitor-1 [27]. Moreover, this molecule was able to abolish transforming growth factor ß-(TGF-β-) induced epithelial-to-mesenchymal transition via altering Wnt mechanism [27]. In addition, calycosin robustly restricted HCT-116 cells viability and invasiveness by enhancing ERβ and phosphatase and tensin homolog (PTEN) expressions [28].

Osteosarcoma is the most common malignant bone tumor with potential for invasion and metastasis; however, the current chemotherapy for osteosarcoma is not yet perfect [29, 30]. Calycosin is evidenced to induce MG-63 apoptosis, reduce cell proliferation, and decrease matrix metalloproteinase 2 (MMP2) and proliferating cell nuclear antigen expression after 48-hour incubation [31]. In tumor-bearing nude mice study, the tumor size and weight were reduced in calycosin-treated group [31]. Protein expression levels of IκBα and interleukin-6 (IL-6) were attenuated after calycosin interference for 3 weeks [31]. The data was in line with Wang et al.'s work published in 2018; they found that calycosin suppressed PI3K/AKT/mTOR pathway. In the MG-63 xenografts nude mice, calycosin inhibited tumor growth and also regulated phosphorylations of PI3K/Akt [31–33]. Hence, Table 1 summarizes the anticancer functions of calycosin.

2.2. Antioxidative Properties. Oxidative stress is a phenomenon triggered by the excessive production and accumulation of reactive oxygen species (ROS) in cells and finally leads to dysfunction of tissues [34, 35]. Calycosin has been evidenced to protect doxorubicin-induced oxidative stress in cultured cardiomyocyte by inhibiting ROS generation via enhancing antioxidant enzymatic activities, that is, glutathione peroxidase, catalase, and superoxide dismutase (SOD) (Table 2) [36]. Moreover, the levels of sirtuin 1-NOD-like receptor protein 3 and related proteins were elevated after calycosin was incubated for 24 hours both *in vitro* and *in vivo* [36]. Liu found that calycosin could also attenuate H_2O_2-induced H9C2 cell apoptosis rate in a dose-dependent manner [38]. Pretreatment with ER antagonist, ICI 182,780, negated the protective effect of calycosin against H_2O_2-induced apoptosis [37, 38]. Elsherbiny et al. (2020) have reported that calycosin showed potential effects on type 2 diabetes mellitus treatment after 4-week administration [40]. The contents of IL33/ST2 mRNA were enhanced and levels of p65, tumor necrosis factor α (TNF-α), interleukin-1β (IL-1β) and TGF-β were downregulated in calycosin treatment mice (Table 2) [39, 40]. Interestingly, calycosin reduced oxidative stress in intracerebral hemorrhage mouse model by stimulating Nrf-2 protein expression [42]. Oral administration of calycosin at 25 or 50 mg/kg/day was able to enhance amylase and lipase levels in serum in acute pancreatitis rat model [41]. The cytokine levels after calycosin treatment were mitigated [41]. Additionally, calycosin was able to decrease cerulein-induced pancreatic edema, inhibiting myeloperoxidase activity and stimulating SOD activity [41]. Studies have shown that calycosin can extend the lifespan of *C. elegans*, and this extension is related to the antioxidant capacity by enhancing stress resistance capacity and reducing the accumulation of ROS [43]. Lu group (2017) published that calycosin required insulin signaling involvement to promote lifespan extension [43]. On the other hand, they observed that calycosin can enhance the nuclear translocation of the core transcription factor DAF-16/

Table 1: Anticancer functions of calycosin

Biomarkers	Model	Reference
Cleaved caspase 3/9 upregulation; enhanced Bax/Bcl-2 ratio	MCF-7 cells; MDA-MB231 cells	Tian et al. [14]; Tian et al. [15]
Reduced cell migration and invasion; enhanced apoptosis rate via blocking IGF-1R pathway; downregulated VEGF and MMP	MCF-7 cells; T47D cells	Li et al. [16]; Chen et al. [17]; Chen et al. [18]
Downregulation of Rab27B and β-catenin	MDA-MB-231 cells	Wu et al. [19]
Abnormal expression levels of ERα, ERβ, ATP-binding cassette subfamily G member 2, breast cancer type 1 susceptibility protein, p450, and EGFR	OMIM data	Huang et al. [22]
Colorectal cancer proliferation	SW480 cells	Zhao et al. [25]
Beclin-1 and LC-3II overexpression	HT-29 cells	EI-kott et al. [26]
Upregulation of ERβ and PTEN	HCT-116 cells	Chen et al. [28]
Induced osteosarcoma apoptosis and decrease MMP2	MG-63 cells	Qiu et al. [31]
Reduced tumor size and PI3K/Akt phosphorylation	Nude mice	Wang et al. [32]; Qiu et al. [31]; Tian et al. [33]

Table 2: Antioxidative functions.

Biomarkers	Model	Reference
Enhance glutathione peroxidase, catalase, and superoxide dismutase enzymatic activities	H9C2 cells and male Kunming mice	Zhai et al. [36]
Reduced H_2O_2-induced cell apoptosis rate	H9C2	Chen et al. [37]; Liu et al. [38]
Downregulation of cytokine levels and IL33/ST2 mRNA level	Type 2 diabetes mellitus rat model	Wang & Zhao [39]; EIsherbiny et al. [40]
Stimulating Nrf2 expression and SOD levels	Intracerebral hemorrhage mouse	Ma et al. [41]; Chen et al. [42]
Prolong lifespan and stimulate SOD levels	*C. elegans*	Lu et al. [43]

FOXO, rather than the conservative stress response transcription factor SKN-1/Nrf-2 [43].

2.3. Anti-Inflammatory Functions. The anti-inflammatory properties of calycosin were widely documented on lipopolysaccharide- (LPS-) induced RAW 264.7 cells [41, 44]. Calycosin significantly attenuated nitric oxide (NO), prostaglandin E2 (PGE2), TNF-α, IL-1β, and IL-6 releases, and the anti-inflammatory properties had been confirmed by NF-κB and MAPK signal pathways [44]. The effective dosage was from 30 nM to 5 μM, and the inhibitory function was dose-dependent. Besides, calycosin could also diminish inflammatory cell markers CD68 and F4/80 mRNA levels in a dose-dependent manner [45].

Calycosin was reported to possess renal protective functions in high-fat diet-induced type 2 diabetes mellitus rat model by altering SOD and TGF-β content in renal tissues as compared to the sham group [40]. Zhang et al. published similar data and reported that this molecule was able to effectively alleviate kidney injury in diabetic kidneys of db/db mice after treatment for 28 days (Table 3) [50]. The serum contents of inflammatory cytokines were reduced via suppressing IκBα and NF-κB p65 [50]. Additionally, fed glucose level in db/db obese mice was declined after calycosin administration which was proposed to be related to the anti-inflammatory effects [45]. Reduced serum triglyceride levels, alleviated insulin resistance, and glucose intolerance were observed in calycosin-treated mice compared with the vehicle-treated controls [45].

Xu et al. found that calycosin was able to relieve advanced glycation end products- (AGE-) induced inflammation both *in vitro* and *in vivo* [49]. AGEs act as the central role in vasculitis development by recruiting the receptor for AGE overexpression (Table 3) [49]. Calycosin was able to diminish vasculitis development by downregulating the AGEs-induced overexpression of receptor for advanced glycation end products (RAGE) and proinflammatory cytokines in both rat and HUVECs [46]. ERK1/2 and NF-κB pathways were involved and evidenced by Kim et al. and Cheng et al. after calycosin presence for 4 hours [47, 48].

2.4. Estrogenic-Like Properties

2.4.1. Osteogenic Functions of Calycosin. Women suffering from menopause have higher risk of getting osteoporosis. The role of calycosin in preventing osteoporosis is widely reported [51, 52]. The proliferation and differentiation capacities of MG-63 were determined with and without calycosin presence [52]. From the results, calycosin was able to stimulate osteoblast differentiation dose-dependently [52]. The data was further confirmed in the rat primary cultured osteoblast. Data implied that the alkaline phosphatase (ALP) level and Runx2 were significantly enhanced after exposure of calycosin for 48 hours [52, 53]. Fang group found that calycosin could also modulate GSK-3β pathway for stimulating osteoblast differentiation which was further confirmed by its specific inhibitor GSK1904529A after revealing ALP, Col1a1, and Runx2 expression levels [54]. Bone mineral density was robustly enhanced in ovariectomized

Table 3: Anti-inflammatory functions.

Biomarkers	Model	Reference
Declined NO, PGE2, TNF-α, and other cytokine release activities	RAW 264.7 cells	Dong et al. [44]; Ma et al. [41]
Reduced CD68 and F4/80 mRNA levels	Raw 264.7	Hoo et al. [45]
Enhanced SOD and TGF-β contents	Type 2 diabetes mellitus rat model	EIsherbiny et al. [40]
Reduced IκBα and NF-κB p65 protein translational levels and alleviated insulin resistance	db/db obese mice	Hoo et al. [45]
Alleviated inflammatory responses and cytokine levels via attenuating Erk1/2 and NF-κB pathways	Hepatocyte cell line; HUVEC	Figarola et al. [46]; Kim et al. [47]; Cheng et al. [48]; Xu et al. [49]

(OVX) rats after administration of calycosin for 12 weeks [51]. Elevated serum level of ALP and declined tartrate-resistant acid phosphatase (TRAP) level were observed [51]. Calycosin could also stimulate osteoprotegerin transcriptional and translational activities and downregulate RANKL expression level in calycosin group as compared with OVX group, and these alternations were proposed to be correlated with MAPK pathway. On the other hand, calycosin was able to abolish RANKL-induced osteoclast formation from primary bone marrow macrophages dose-dependently after 24-hour incubation [55]. Therefore, calycosin may be useful as a therapeutic agent for bone loss-associated diseases.

2.4.2. Hematopoietic Functions of Calycosin. One symptom of estrogen deficiency is anemia [7]. Several lines of evidence suggested that calycosin could stimulate the expression of erythropoietin (EPO), the central regulator of red blood cell mass, in cultured human embryonic kidney fibroblasts (HEK293T) after exposure of calycosin for 24 hours [7, 8, 11, 35]. The calycosin-induced EPO expression was mediated by HIF-1α from western blotting results [56]. The *in vivo* experiments showed that calycosin could enhance the number of RBCs, WBCs, PLTs, and content of Hb in peripheral blood and the area of bone marrow hematopoietic tissue [57]. The serum contents of thrombopoietin, EPO, granulocyte-macrophage colony stimulating factor, colony of CFU-GM, CFU-MK, CFU-E, and BFU-E were also enriched after calycosin treatment [57]. The animal experiments showed that this agent reduced G0/G1 cells and increased G2/M cells in hematopoietic stem cells.

2.5. Neuroprotective Functions. The neuroprotective functions of calycosin were determined both *in vitro* and *in vivo*. Administered with different concentration of calycosin from 7.5 mg/kg/day to 30 mg/kg/day, reduced malondialdehyde (MDA) and ROS contents were observed in calycosin-treated ischemia reperfusion rats [58]. However, the SOD activity was induced in the calycosin-treated ischemia reperfusion rats [58]. Calycosin could also stimulate ERβ, miR-374, and Bcl-2 protein expression levels in middle cerebral artery occlusion rats from western blotting data [59]. Similar protective effects of calycosin were evidenced *in vitro* by utilizing PC12 neuronal cell line with pretreatment of l-glutamate or xanthine (XA)/xanthine oxidase (XO) [60, 61]. Calycosin showed potential neuroprotective functions by blocking XA/XO-induced cell apoptosis at ~50% and the EC50 of 0.05 mg/L and an IC50 of approximately 50 mg/L [60–62]. Interestingly, calycosin shows promising therapeutic value on Alzheimer's disease in APP/PS1 transgenic mice [63]. Intraperitoneally injected calycosin, the diminished hippocampal beta amyloid, Tau protein, IL-1β, TNF-α, acetylcholinesterase, and MDA levels were observed and the inhibitory effects were in a dose-dependent manner [63]. The maximal blockage concentration was revealed at 40 mg/kg/day. Yang found that calycosin could also mitigate Parkinson's disease in 1-methyl-4-phenyl-1,2,3,6-tetrahydropyridine- (MPTP-) induced Parkinson's disease mice [64]. From the results, Yang et al. confirmed that calycosin treatment mitigated the behavioral dysfunctions and inflammatory responses in MPTP-induced PD mice via NF-κB/MAPK pathways [64].

3. Pharmacokinetics of Calycosin

Because of hydroxyl groups found within the chemical structure of calycosin, they are metabolized to glucuronide by phase II metabolic enzymes such as UDP-glucuronosyltransferases from the intestine and liver after oral administration [65]. In addition to the role of metabolism, absorption, hydrolysis, efflux, and intestinal circulation in the intestinal tract also participate in the disposal of calycosin in the body, affecting their systemic and local bioavailability [66].

Studies have shown that, after oral administration of *Astragalus* water extract, the enriched content of calycosin-7-O-β-glucoside is detected in plasma, indicating that calycosin-7-O-β-glucoside can enter the intestinal cells in a prototype form and be metabolized [66, 67]. In the study, it was found that, after administration of calycosin by oral gavage, calycosin-7-O-β-glucoside can be detected in the plasma, which shows that calycosin-7-O-β-glucoside can penetrate the cell membrane in a prototype form and undergo further metabolism [68]. This indicates that calycosin-7-O-β-glucoside may directly pass through the cell membrane in a prototype form without hydrolysis [69]. Using Caco-2 cells to study the absorption and transport characteristics of calycosin and its glucoside, it was found that calycosin and calycosin-7-O-β-glucoside are mainly absorbed in the form of passive diffusion, and the absorption process will not be affected by inhibitors of MATEs such as P-gp and MRP2 [69, 70]. Calycosin can be metabolized in human liver microsomes to generate two glucuronides. UGT1A1 and UGT1A9 are the major metabolic enzyme

subtypes that generate these two glucuronides, respectively [71]. On the other hand, after oral administration of calycosin, the calculated bioavailability of calycosin-7-O-β-glucoside was only 0.304%, indicating that hydrolyzing is an important process of metabolism *in vivo* [72, 73]. However, glucoside hydrolase is solely present in the intestine and liver of rats. In order to confirm the hydrolysis site of calycosin-7-O-β-glucoside, the pharmacokinetics of calycosin-7-O-β-glucoside injection in rats were investigated because the drug was directly absorbed by the hepatic portal vein after intraperitoneal injection [74]. The drug will not be processed through the intestine, so as to exclude the effect of the intestine on the calycosin-7-O-β-glucoside treatment in the body [75]. The results show that the drug time curve of calycosin-7-O-β-glucoside and its metabolites is completely different from that of calycosin-7-O-β-glucoside after oral administration.

4. Chemical Interactions

As the main bioactive molecule isolated from Astragali Radix, the pharmacological activity of calycosin is not performed alone but by the joint action of multiple chemical substances. Cotreatment of calycosin with other biochemicals identified from Astragali Radix, that is, formononetin, ononin and astragaloside, showed effective therapeutic functions as compared to single compound. The study found that the expression levels of drug-metabolizing enzymes, such as CYP3A4, CYP2B6, CYP2E1, UGT1A, and efflux transporters, that is, P-gp, MRP2, BCRP, and MRP3, were increased in a dose-dependent manner in the drug combination group [76]. Zheng et al. found that cotreatment of calycosin with formononetin stimulated EPO expression in a dose- and concentration-dependent manner in cultured HEK 293 cells. The hematopoietic functions of these combinations were even stronger than the positive control [77, 78]. Furthermore, Zhang et al. reported that flavonoid combination containing formononetin and calycosin at weight ratio of 1 : 5 showed the best hematological functions on anemic rat after drug treatment [79].

The research of calycosin in modern medicine is no longer confined to a single compound or Astragali Radix. More and more scientists have discovered the combination of multiple substances enjoying a broad spectrum in disease treatment by "Fu Fang." Astragali Radix and Angelicae Sinensis Radix are usually combined together clinically [35, 52]. Cotreatment of calycosin and Astragali Sinensis Radix-derived ferulic acid protected bleomycin-induced pulmonary fibrosis in rats, and this action was believed via blocking NOX4 expression [80]. Furthermore, combination of calycosin and ferulic acid showed better immune-modulatory pharmaceutical activities in Raw 264.7 and inducing blood vessels in HUVECs and Zebra fish [81–85]. Administration of calycosin and ferulic acid attenuates cytokine and inflammatory mediators' releases in atopic dermatitis-like mouse [85].

5. Conclusion

Calycosin serves as a common dietary flavonoid and is consumed in daily cuisine and/or TCM decoction. Additionally, there are myriad of formulae containing calycosin at different dosage forms either alone or in combination with other bioactive molecules in market. The pharmaceutical functions of calycosin on anticancer, antioxidative, immune-modulatory, and estrogenic-like properties were summarized. We believe the potential pharmaceutical value of calycosin is still behind the veil, and which motivating us to discover more in the future. The *in vitro* and *in vivo* pharmaceutical functions do not directly translate into the clinic because of bioavailability and biotransformation influenced by gut microbiota. Considering various compositions of microbiota between individuals, the fluctuating process of bioavailability and biotransformation mediated by gut microbiota could have a consequential effect of calycosin and its metabolites in plasma, finally leading to diverse clinic functions. Hence, gut microbiota-induced bioavailability and biotransformation of calycosin and its metabolites should be taken into consideration before clinical application.

Abbreviations

ALP: Alkaline phosphatase
EGFR: Epidermal growth factor receptor
EPO: Erythropoietin
ER−: Estrogen receptor-negative
ER+: Estrogen receptor-positive
GPR30: G-protein coupled estrogen receptor 30
IGF-1R: Insulin-like growth factor 1 receptor
IL-1β: Interleukin-1β
IL-6: Interleukin-6
LPS: Lipopolysaccharide
MMP2: Matrix metalloproteinase 2
MMP9: Matrix metalloproteinase 9
NO: Nitric oxide
OVX: Ovariectomized
PGE2: Prostaglandin E2
PTEN: Phosphatase and tensin homolog
RAGE: Receptor for advanced glycation end products
ROS: Reactive oxygen species
SOD: Superoxide dismutase
TCM: Traditional Chinese medicine
TGF-β: Transforming growth factor β
TNF-α: Tumor necrosis factor α
TRAP: Tartrate-resistant acid phosphatase
VEGF: Vascular endothelial growth factor
MDA: Malondialdehyde
XA/XO: Xanthine/xanthine oxidase
MPTP: 1-Methyl-4-phenyl-1,2,3,6-tetrahydropyridine.

Data Availability

The data used in this paper are available upon request.

Conflicts of Interest

The authors declare that there are no conflicts of interest regarding the publication of this paper.

Authors' Contributions

Guowei Gong and Yang Yang wrote the main text. Yuzhong Zheng and Zhen Wen were responsible for polishing the manuscript. Yang Yang and Yixuan Sui formatted the references. All authors read and approved the final version of manuscript.

Acknowledgments

This work was supported by the Guizhou Provincial Natural Science Foundation (QKH-J [2020] 1Y377), Zunyi Science and Technology Project (ZSKHHZZ(2020)85), Science and Technology Program of Guizhou Province (QKPTRC [2019]-024), Zunyi Medical University for the Doctoral Program (F-937), Guangdong Key Laboratory for Functional Substances in Medicinal Edible Resources and Healthcare Products (2021B1212040015), Science and Technology Program of Guangdong Province (2018A030307074), and National Natural Science Foundation of China (22078198).

References

[1] H. Q. Lin, A. G. W. Gong, H. Y. Wang et al., "Danggui buxue tang (astragali Radix and Angelicae sinensis Radix) for menopausal symptoms: a review," *Journal of Ethnopharmacology*, vol. 199, pp. 205–210, 2017.

[2] A. G. Gong, R. Duan, H. Y. Wang et al., "Evaluation of the pharmaceutical properties and value of Astragali Radix," *Medicines*, vol. 5, no. 2, 2018.

[3] C. A. Espinosa-Leal, C. A. Puente-Garza, and S. García-Lara, "In vitro plant tissue culture: means for production of biological active compounds," *Planta*, vol. 248, no. 1, pp. 1–18, 2018.

[4] E. Lautié, O. Russo, P. Ducrot et al., "Unraveling plant natural chemical diversity for drug discovery purposes," *Front Pharmacol*, vol. 11, 2020.

[5] A. G.-W. Gong, N. Li, K.-M. Lau et al., "Calycosin orchestrates the functions of Danggui Buxue Tang, a Chinese herbal decoction composing of Astragali Radix and Angelica Sinensis Radix: an evaluation by using calycosin-knock out herbal extract," *Journal of Ethnopharmacology*, vol. 168, pp. 150–157, 2015.

[6] A. G. W. Gong, K. M. Lau, M. L. Xu et al., "The estrogenic properties of Danggui Buxue Tang, a Chinese herbal decoction, are triggered predominantly by calycosin in MCF-7 cells," *Journal of Ethnopharmacology*, vol. 189, pp. 81–89, 2016.

[7] W. L. Zhang, R. C.-Y. Choi, J. Y.-X. Zhan et al., "Can hedysari Radix replace astragali Radix in danggui buxue tang, a Chinese herbal decoction for woman aliment?" *Phytomedicine*, vol. 20, no. 12, pp. 1076–1081, 2013.

[8] W. L. Zhang, K. Y.-Z. Zheng, K. Y. Zhu et al., "Chemical and biological assessment of Angelica herbal decoction: comparison of different preparations during historical applications," *Phytomedicine*, vol. 19, no. 11, pp. 1042–1048, 2012.

[9] M. R. Akanda, M. N. Uddin, I.-S. Kim, D. Ahn, H.-J. Tae, and B.-Y. Park, "The biological and pharmacological roles of polyphenol flavonoid tilianin," *European Journal of Pharmacology*, vol. 842, pp. 291–297, 2019.

[10] X. Zeng, Y. Xi, and W. Jiang, "Protective roles of flavonoids and flavonoid-rich plant extracts against urolithiasis: a review," *Critical Reviews in Food Science and Nutrition*, vol. 59, no. 13, pp. 2125–2135, 2019.

[11] A. G. Gong, L. M. Zhang, C. T. Lam et al., "Polysaccharide of danggui buxue tang, an ancient Chinese herbal decoction, induces expression of pro-inflammatory cytokines possibly via activation of NFκB signaling in cultured RAW 264.7 cells," *Phytotherapy Research*, vol. 31, no. 2, pp. 274–283, 2017.

[12] L. Hilakivi-Clarke, C. Wang, M. Kalil, R. Riggins, and R. G. Pestell, "Nutritional modulation of the cell cycle and breast cancer," *Endocrine-Related Cancer*, vol. 11, no. 4, pp. 603–622, 2004.

[13] N. Harbeck and M. Gnant, "Breast cancer," *Lancet*, vol. 389, pp. 1134–1150, 2017.

[14] J. Tian, Y. Duan, C. Bei, and J. Chen, "Calycosin induces apoptosis by upregulation of RASD1 in human breast cancer cells MCF-7," *Hormone and Metabolic Research*, vol. 45, no. 08, pp. 593–598, 2013.

[15] J. Tian, Y. Wang, X. Zhang et al., "Correction to: calycosin inhibits the *in vitro* and *in vivo* growth of breast cancer cells through WDR7-7-GPR30 signaling," *Journal of Experimental & Clinical Cancer Research*, vol. 36, no. 1, 2017.

[16] S. Li, Y. Wang, C. Feng, G. Wu, Y. Ye, and J. Tian, "Calycosin inhibits the migration and invasion of human breast cancer cells by down-regulation of Foxp3 expression," *Cellular Physiology and Biochemistry*, vol. 44, no. 5, pp. 1775–1784, 2017.

[17] J. Chen, W.-B. Xiong, Y. Xiong et al., "Calycosin stimulates proliferation of estrogen receptor-positive human breast cancer cells through downregulation of Bax gene expression and upregulation of Bcl-2 gene expression at low concentrations," *Journal of Parenteral and Enteral Nutrition*, vol. 35, no. 6, pp. 763–769, 2011.

[18] J. Chen, R. Hou, X. Zhang et al., "Calycosin suppresses breast cancer cell growth via ERβ-dependent regulation of IGF-1R, p38 MAPK and PI3K/Akt pathways," *PLoS One*, vol. 9, no. 3, 2014.

[19] G. Wu, M. Niu, J. Qin, Y. Wang, and J. Tian, "Inactivation of Rab27B-dependent signaling pathway by calycosin inhibits migration and invasion of ER-negative breast cancer cells," *Gene*, vol. 709, pp. 48–55, 2019.

[20] M. S. Cappell, "Pathophysiology, clinical presentation, and management of colon cancer," *Gastroenterology Clinics of North America*, vol. 37, no. 1, pp. 1–24, 2008.

[21] H. J. Freeman, "Early stage colon cancer," *World Journal of Gastroenterology*, vol. 19, no. 46, pp. 8468–8473, 2013.

[22] C. Huang, R. Li, W. Shi, and Z. Huang, "Discovery of the antitumor mechanism of calycosin against colorectal cancer by using system pharmacology approach," *Medical Science Monitor*, vol. 25, pp. 5589–5593, 2019.

[23] J. Gao, Z. J. Liu, T. Chen, and D. Zhao, "Pharmaceutical properties of calycosin, the major bioactive isoflavonoid in the dry root extract of Radix astragali," *Pharmaceutical Biology*, vol. 52, no. 9, pp. 1217–1222, 2014.

[24] X. J. Hu, M. Y. Xie, F. M. Kluxen, and P. Diel, "Genistein modulates the anti-tumor activity of cisplatin in MCF-7 breast and HT-29 colon cancer cells," *Archives of Toxicology*, vol. 88, no. 3, pp. 625–635, 2014.

[25] X. Zhao, X. Li, Q. Ren, J. Tian, and J. Chen, "Calycosin induces apoptosis in colorectal cancer cells, through modulating the ERβ/MiR-95 and IGF-1R, PI3K/Akt signaling pathways," *Gene*, vol. 591, no. 1, pp. 123–128, 2016.

[26] A. F. El-Kott, M. A. Al-Kahtani, and A. A. Shati, "Calycosin induces apoptosis in adenocarcinoma HT29 cells by inducing cytotoxic autophagy mediated by SIRT1/AMPK-induced

inhibition of Akt/mTOR," *Clinical and Experimental Pharmacology and Physiology*, vol. 46, no. 10, pp. 944–954, 2019.

[27] Q. Wang, W. Lu, T. Yin et al., "Correction to: calycosin suppresses TGF-β-induced epithelial-to-mesenchymal transition and migration by upregulating BATF2 to target PAI-1 via the Wnt and PI3K/Akt signaling pathways in colorectal cancer cells," *Journal of Experimental & Clinical Cancer Research*, vol. 38, no. 1, 2019.

[28] J. Chen, X. Zhao, X. Li et al., "Calycosin induces apoptosis by the regulation of ERβ/miR-17 signaling pathway in human colorectal cancer cells," *Food Funct*, vol. 6, no. 7, pp. 3091–3097, 2015.

[29] M. F. Wedekind, L. M. Wagner, and T. P. Cripe, "Immunotherapy for osteosarcoma: where do we go from here?" *Pediatr Blood Cancer*, vol. 65, no. 9, 2018.

[30] S. Miwa, T. Shirai, N. Yamamoto et al., "Current and emerging targets in immunotherapy for osteosarcoma," *Journal of Oncology*, vol. 2019, Article ID 7035045, 8 pages, 2019.

[31] R. Qiu, X. Li, K. Qin et al., "Antimetastatic effects of calycosin on osteosarcoma and the underlying mechanism," *Biofactors*, vol. 45, no. 6, pp. 975–982, 2019.

[32] Y. Wang, Q. Ren, X. Zhang, H. Lu, and J. Chen, "Neuroprotective mechanisms of calycosin against focal cerebral ischemia and reperfusion injury in rats," *Cellular Physiology and Biochemistry*, vol. 45, no. 2, pp. 537–546, 2018.

[33] W. Tian, Z. W. Wang, B. M. Yuan et al., "Calycosin induces apoptosis in osteosarcoma cell line via ERβ-mediated PI3K/Akt signaling pathways," *Molecular Medicine Reports*, vol. 21, no. 6, pp. 2349–2356, 2020.

[34] J. S. Lou, L. Yan, C. W. Bi et al., "Yu Ping Feng San reverses cisplatin-induced multi-drug resistance in lung cancer cells via regulating drug transporters and p62/TRAF6 signalling," *Scientific Report*, vol. 6, 2016.

[35] G. Gong, H. Wang, X. Kong et al., "Flavonoids are identified from the extract of Scutellariae Radix to suppress inflammatory-induced angiogenic responses in cultured RAW 264.7 macrophages," *Scientific Report*, vol. 8, 2018.

[36] J. Zhai, L. Tao, S. Zhang et al., "Calycosin ameliorates doxorubicin-induced cardiotoxicity by suppressing oxidative stress and inflammation via the sirtuin 1-NOD-like receptor protein 3 pathway," *Phytotherapy Research*, vol. 34, no. 3, pp. 649–659, 2020.

[37] C.-Y. Chen, Y.-G. Zu, Y.-J. Fu et al., "Preparation and antioxidant activity of Radix Astragali residues extracts rich in calycosin and formononetin," *Biochemical Engineering Journal*, vol. 56, no. 1-2, pp. 84–93, 2011.

[38] B. Liu, J. Zhang, W. Liu et al., "Calycosin inhibits oxidative stress-induced cardiomyocyte apoptosis via activating estrogen receptor-α/β," *Bioorganic & Medicinal Chemistry Letters*, vol. 26, no. 1, pp. 181–185, 2016.

[39] X. Wang and L. Zhao, "Calycosin ameliorates diabetes-induced cognitive impairments in rats by reducing oxidative stress via the PI3K/Akt/GSK-3β signaling pathway," *Biochemical and Biophysical Research Communications*, vol. 473, no. 2, pp. 428–434, 2016.

[40] N. M. Elsherbiny, E. Said, H. Atef et al., "Renoprotective effect of calycosin in high fat diet-fed/STZ injected rats: effect on IL-33/ST2 signaling, oxidative stress and fibrosis suppression," *Chemico-Biological Interactions*, vol. 315, 2020.

[41] R. Ma, F. Yuan, S. Wang, Y. Liu, T. Fan, and F. Wang, "Calycosin alleviates cerulein-induced acute pancreatitis by inhibiting the inflammatory response and oxidative stress via the p38 MAPK and NF-κB signal pathways in mice," *Biomedicine & Pharmacotherapy*, vol. 105, pp. 599–605, 2018.

[42] C. Chen, J. Cui, X. Ji, and L. Yao, "Neuroprotective functions of calycosin against intracerebral hemorrhage-induced oxidative stress and neuroinflammation," *Future Medicinal Chemistry*, vol. 12, no. 7, pp. 583–592, 2020.

[43] L. Lu, X. Zhao, J. Zhang, M. Li, Y. Qi, and L. Zhou, "Calycosin promotes lifespan in *Caenorhabditis elegans* through insulin signaling pathway via daf-16, age-1 and daf-2," *Journal of Bioscience and Bioengineering*, vol. 124, no. 1, pp. 1–7, 2017.

[44] L. Dong, L. Yin, R. Chen et al., "Anti-inflammatory effect of calycosin glycoside on lipopolysaccharide-induced inflammatory responses in RAW 264.7 cells," *Gene*, vol. 675, pp. 94–101, 2018.

[45] R. L. Hoo, J. Y. Wong, C. Qiao et al., "The effective fraction isolated from Radix Astragali alleviates glucose intolerance, insulin resistance and hypertriglyceridemia in db/db diabetic mice through its anti-inflammatory activity," *Nutrition & Metabolism (London)*, vol. 7, 2010.

[46] J. L. Figarola, N. Shanmugam, R. Natarajan, and S. Rahbar, "Anti-inflammatory effects of the advanced glycation end product inhibitor LR-90 in human monocytes," *Diabetes*, vol. 56, no. 3, pp. 647–655, 2007.

[47] J. W. Kim, Y. C. Jin, Y. M. Kim et al., "Daidzein administration *in vivo* reduces myocardial injury in a rat ischemia/reperfusion model by inhibiting NF-kappaB activation," *Life Sci*, vol. 84, no. 7, pp. 227–234, 2009.

[48] C. C. Cheng, Y. H. Chen, W. L. Chang et al., "Phytoestrogen bavachin mediates anti-inflammation targeting Ikappa B kinase-IkappaB alpha-NF-kappaB signaling pathway in chondrocytes *in vitro*," *European Journal of Pharmacology*, vol. 636, pp. 181–188, 2010.

[49] Y. Xu, J. Xiong, Y. Zhao et al., "Calycosin rebalances advanced glycation end products-induced glucose uptake dysfunction of hepatocyte *in vitro*," *The American Journal of Chinese Medicine*, vol. 43, no. 06, pp. 1191–1210, 2015.

[50] Y.-Y. Zhang, R.-Z. Tan, X.-Q. Zhang, Y. Yu, and C. Yu, "Calycosin ameliorates diabetes-induced renal inflammation via the NF-κB pathway in vitro and in vivo," *Medical Science Monitor*, vol. 25, pp. 1671–1678, 2019.

[51] N. Li, Y. Tu, Y. Shen, Y. Qin, C. Lei, and X. Liu, "Calycosin attenuates osteoporosis and regulates the expression of OPG/RANKL in ovariectomized rats via MAPK signaling," *Die Pharmazie*, vol. 71, no. 10, pp. 607–612, 2016.

[52] A. G. Gong, R. Duan, H. Y. Wang et al., "Calycosin orchestrates osteogenesis of Danggui Buxue Tang in cultured osteoblasts: evaluating the mechanism of action by omics and chemical knock-out methodologies," *Frontiers in Pharmacology*, vol. 9, 2018.

[53] X. Kong, F. Wang, Y. Niu, X. Wu, and Y. Pan, "A comparative study on the effect of promoting the osteogenic function of osteoblasts using isoflavones from Radix *Astragalus*," *Phytotherapy Research*, vol. 32, no. 1, pp. 115–124, 2018.

[54] Y. Fang, Z. Xue, L. Zhao et al., "Calycosin stimulates the osteogenic differentiation of rat calvarial osteoblasts by activating the IGF1R/PI3K/Akt signaling pathway," *Cell Biology International*, vol. 43, no. 3, pp. 323–332, 2019.

[55] G.-H. Quan, H. Wang, J. Cao et al., "Calycosin suppresses RANKL-mediated osteoclastogenesis through inhibition of MAPKs and NF-κB," *International Journal of Molecular Sciences*, vol. 16, no. 12, pp. 29496–29507, 2015.

[56] K. Y. Z. Zheng, R. C. Y. Choi, A. W. H. Cheung et al., "Flavonoids from Radix astragali induce the expression of erythropoietin in cultured cells: a signaling mediated via the

accumulation of hypoxia-inducible factor-1α," *Journal of Agricultural and Food Chemistry*, vol. 59, no. 5, pp. 1697–1704, 2011.

[57] W. Zhang, J. H. Zhu, H. Xu et al., "Five active components compatibility of Astragali Radix and Angelicae Sinensis Radix protect hematopoietic function against cyclophosphamide-induced injury in mice and t-BHP-induced injury in HSCs," *Frontiers in Pharmacology*, vol. 10, 2019.

[58] C. Guo, L. Tong, M. Xi, H. Yang, H. Dong, and A. Wen, "Neuroprotective effect of calycosin on cerebral ischemia and reperfusion injury in rats," *Journal of Ethnopharmacology*, vol. 144, no. 3, pp. 768–774, 2012.

[59] Y. Wang, X. Dong, Z. Li et al., "Downregulated RASD1 and upregulated miR-375 are involved in protective effects of calycosin on cerebral ischemia/reperfusion rats," *Journal of the Neurological Sciences*, vol. 339, pp. 144–148, 2014.

[60] C.-C. Hsu, T.-W. Kuo, W.-P. Liu, C.-P. Chang, and H.-J. Lin, "Calycosin preserves BDNF/TrkB signaling and reduces post-stroke neurological injury after cerebral ischemia by reducing accumulation of hypertrophic and TNF-α-containing microglia in rats," *Journal of Neuroimmune Pharmacology*, vol. 15, no. 2, pp. 326–339, 2020.

[61] D.-H. Yu, Y.-M. Bao, L.-J. An, and M. Yang, "Protection of PC12 cells against superoxide-induced damage by isoflavonoids from *Astragalus mongholicus*," *Biomedical and Environmental Sciences*, vol. 22, no. 1, pp. 50–54, 2009.

[62] D. H. Yu, Y. L. Duan, Y. M. Bao et al., "Isoflavonoids from *Astragalus mongholicus* protect PC12 cells from toxicity induced by L-glutamate," *Journal of Ethnopharmacology*, vol. 98, no. 1-2, pp. 89–94, 2005.

[63] L. Song, X. Li, X. X. Bai, J. Gao, and C. Y. Wang, "Calycosin Improves cognitive function in a transgenic mouse model of Alzheimer's disease by activating the protein kinase C pathway," *Neural Regeneration Research*, vol. 12, no. 11, pp. 1870–1876, 2017.

[64] J. Yang, M. Jia, X. Zhang, and P. Wang, "Calycosin attenuates MPTP-induced Parkinson's disease by suppressing the activation of TLR/NF-κB and MAPK pathways," *Phytotherapy Research*, vol. 33, no. 2, pp. 309–318, 2019.

[65] Y. Wang, P. Wang, J. Xie et al., "Pharmacokinetic comparisons of different combinations of Yigan Jiangzhi formula in rats: simultaneous determination of fourteen components by UPLC-MS/MS," *Journal of Analytical Methods in Chemistry*, vol. 2020, Article ID 9353975, 16 pages, 2020.

[66] R. Liu, R. Ma, C. Yu et al., "Quantitation of eleven active compounds of Aidi injection in rat plasma and its application to comparative pharmacokinetic study," *Journal of Chromatography B*, vol. 1026, pp. 105–113, 2016.

[67] M. Liu, P. Li, X. Zeng et al., "Identification and pharmacokinetics of multiple potential bioactive constituents after oral administration of Radix Astragali on cyclophosphamide-induced immunosuppression in Balb/c mice," *International Journal of Molecular Sciences*, vol. 16, no. 3, pp. 5047–5071, 2015.

[68] H. Zhao, Y. Zhang, Y. Guo, and S. Shi, "Identification of major α-glucosidase inhibitors in Radix Astragali and its human microsomal metabolites using ultrafiltration HPLC-DAD-MS(n)," *Journal of Pharmaceutical and Biomedical Analysis*, vol. 104, pp. 31–37, 2015.

[69] X.-D. Wen, L.-W. Qi, B. Li et al., "Microsomal metabolism of calycosin, formononetin and drug-drug interactions by dynamic microdialysis sampling and HPLC-DAD-MS analysis," *Journal of Pharmaceutical and Biomedical Analysis*, vol. 50, no. 1, pp. 100–105, 2009.

[70] X. Tian, S. Chen, Y. Zhang et al., "Absorption, liver first-pass effect, pharmacokinetics and tissue distribution of calycosin-7-O-ß-d-glucopyranoside (C7G) and its major active metabolite, calycosin, following oral administration of C7G in rats by LC-MS/MS," *Journal of Pharmaceutical and Biomedical Analysis*, vol. 148, pp. 350–354, 2018.

[71] J. Guan, L. Wang, J. Jin et al., "Simultaneous determination of calycosin-7-O-β-D-glucoside, cinnamic acid, paeoniflorin and albiflorin in rat plasma by UHPLC-MS/MS and its application to a pharmacokinetic study of Huangqi Guizhi Wuwu decoction," *Journal of Pharmaceutical and Biomedical Analysis*, vol. 170, pp. 1–7, 2019.

[72] Y.-Z. Zhang, F. Xu, J. Dong et al., "Profiling and identification of the metabolites of calycosin in rat hepatic $9000 \times g$ supernatant incubation system and the metabolites of calycosin-7-O-β-D-glucoside in rat urine by HPLC-DAD-ESI-IT-TOF-MS(n) technique," *Journal of Pharmaceutical and Biomedical Analysis*, vol. 70, pp. 425–439, 2012.

[73] F. Zhang, Y. Zhang, X. Li et al., "Research on Q-markers of Qiliqiangxin capsule for chronic heart failure treatment based on pharmacokinetics and pharmacodynamics association," *Phytomedicine*, vol. 44, pp. 220–230, 2018.

[74] Q. Lin, Y. Li, X. M. Tan et al., "Simultaneous determination of formononetin, calycosin and isorhamnetin from *Astragalus mongholicus* in rat plasma by LC-MS/MS and application to pharmacokinetic study," *Zhong Yao Cai*, vol. 36, no. 4, pp. 589–593, 2013.

[75] L. Chen, Z. Li, Y. Tang et al., "Isolation, identification and antiviral activities of metabolites of calycosin-7-O-β-d-glucopyranoside," *Journal of Pharmaceutical and Biomedical Analysis*, vol. 56, no. 2, pp. 382–389, 2011.

[76] G. Zhang, R. Ou, F. Li et al., "Regulation of drug-metabolizing enzymes and efflux transporters by Astragali radix decoction and its main bioactive compounds: implication for clinical drug-drug interactions," *Journal of Ethnopharmacology*, vol. 180, pp. 104–113, 2016.

[77] K. Y. Z. Zheng, R. C. Y. Choi, H. Q. H. Xie et al., "The expression of erythropoietin triggered by Danggui Buxue Tang, a Chinese herbal decoction prepared from Radix Astragali and Radix Angelicae Sinensis, is mediated by the hypoxia-inducible factor in cultured HEK293T," *Journal of Ethnopharmacology*, vol. 132, no. 1, pp. 259–267, 2010.

[78] K. Y.-Z. Zheng, R. C.-Y. Choi, A. J.-Y. Guo et al., "The membrane permeability of Astragali Radix-derived formononetin and calycosin is increased by Angelicae Sinensis Radix in Caco-2 cells: a synergistic action of an ancient herbal decoction Danggui Buxue Tang," *Journal of Pharmaceutical and Biomedical Analysis*, vol. 70, pp. 671–679, 2012.

[79] L. Zhang, A. G. W. Gong, K. Riaz et al., "A novel combination of four flavonoids derived from Astragali Radix relieves the symptoms of cyclophosphamide-induced anemic rats," *FEBS Open Bio*, vol. 7, no. 3, pp. 318–323, 2017.

[80] P. Zhao, W. C. Zhou, D. L. Li et al., "Total glucosides of Danggui Buxue Tang attenuate BLM-induced pulmonary fibrosis via regulating oxidative stress by inhibiting NOX4," *Oxidative Medicine and Cellular Longevity*, vol. 2015, Article ID 645814, 10 pages, 2015.

[81] B. Wu, X. F. Sun, and G. Y. Yang, "Studies on different combination of the dang gui buxue decoction," *Chinese Medicine Material*, vol. 4, pp. 41–45, 1989.

[82] Y. Lei and K. J. Chen, "Study on angiogenesis effect of Radix astragali, Radix Angelicae sinensis & their combination," *Chinese Medical Sciences*, vol. 4, pp. 110–117, 2003.

[83] X. Yang, C.-G. Huang, S.-Y. Du et al., "Effect of Danggui Buxue Tang on immune-mediated aplastic anemia bone marrow proliferation mice," *Phytomedicine*, vol. 21, no. 5, pp. 640–646, 2014.

[84] J.-H. Xie, Z.-W. Chen, Y.-W. Pan et al., "Evaluation of safety of modified-Danggui Buxue Tang in rodents:immunological, toxicity and hormonal aspects," *Journal of Ethnopharmacology*, vol. 183, pp. 59–70, 2016.

[85] Y. Y. Choi, M. H. Kim, J. Hong et al., "Effect of Danggui-bohyul-Tang, a mixed extract of *Astragalus membranaceus* and *Angelica sinensis*, on allergic and inflammatory skin reaction compared with single extracts of *Astragalus membranaceus* or *Angelica sinensis*," *Evid Based Complement Altern Med*, vol. 2016, Article ID 5936354, 9 pages, 2016.

Hindawi
Evidence-Based Complementary and Alternative Medicine
Volume 2021, Article ID 6661373, 11 pages
https://doi.org/10.1155/2021/6661373

Research Article

Hair Growth Promotion Effect of Nelumbinis Semen Extract with High Antioxidant Activity

Hyeon Ju Park, Guang-Ri Jin, Jae Hyun Jung, Su Bin Hwang, Su Hyun Lee, and Bog-Hieu Lee

Department of Food and Nutrition, Chung-Ang University, Anseong, Gyeonggi-do 17546, Republic of Korea

Correspondence should be addressed to Bog-Hieu Lee; lbheelb@cau.ac.kr

Received 31 December 2020; Revised 24 February 2021; Accepted 6 March 2021; Published 15 March 2021

Academic Editor: Omayma Eldahshan

This study investigated the hair regeneration promotion and hair loss prevention properties of Nelumbinis Semen (NS) extract *in vitro* and *in vivo*. The effect of NS on the proliferation and migration of human dermal papilla cells (hDPCs) was measured *in vitro* via CCK-8 and scratch migration assays, after which the antioxidant activity of NS was also quantified. NS extracts were then applied to the back of 7-week-old C57BL/6 mice for 3 weeks to monitor hair growth patterns and hair follicle (HF) histology. The mice were divided into three groups: negative control group (NC; DMSO), positive control group (PC; 3% minoxidil), and experimental group (NS extract 1,000 ppm). Moreover, to study the molecular mechanisms by which NS extract regenerates hair growth, real-time PCR was used to analyze factors related to the hair growth cycle. The NS extracts were found to possess high antioxidant properties due to their high flavonoid contents and electron-donating ability. Moreover, NS extracts enhanced hDPC proliferation and migration in a concentration-dependent manner (15.63–125 ppm). The hair growth index and growth area of the NS group (2.81 score, 81%) on day 14 were higher than those of the PC group (2.65 score, 68%) ($p < 0.05$). Additionally, the HFs of the NS group were located deep in the subcutis, similar to the PC group with developed hair roots. Moreover, the mRNA expression of VEGF and IGF-1 was higher in the NS group compared to the PC group, whereas TGF-β1 expression was lower ($p < 0.05$). Our findings indicate that NS modulates hair growth by increasing IGF-1 and VEGF expression while inhibiting that of TGF-β1. Therefore, our findings suggest that NS extract is a promising new hair loss treatment derived from a natural substance that helps promote hair growth and prevent hair loss.

1. Introduction

Alopecia is a disease characterized by progressive hair loss from the scalp and other areas of the body. Recently, there has been a rapid rise in population-wide hair loss cases. This is due to genetic factors, as well as to increased stress, dietary changes, and hormone-related problems [1, 2]. According to the Korea National Health Insurance Service's morbidity statistics, the number of patients treated for alopecia areata increased by 24.9% from 136,248 (male: 69,280; female: 66,968) in 2010 to 170,149 (male: 92,759; female: 77,390) in 2018 [3]. The types of alopecia were largely classified into the following categories: androgenetic alopecia (AGA), female pattern hair loss (FPHL), alopecia areata (AA), postpartum telogen effluvium, telogen effluvium, and traction alopecia [4].

Currently, finasteride and minoxidil are the only drugs approved by the Food and Drug Administration (FDA) for the prevention of hair loss and promotion of hair growth. Finasteride is known to improve AGA by inhibiting the activity of 5α-reductase II;, thereby inhibiting the conversion of testosterone (T) to dihydrotestosterone (DHT). On the other hand, minoxidil is a vasodilator that enhances hair growth by inhibiting hDPC apoptosis [5, 6]. However, these FDA-approved drugs have been linked to several side effects including erectile dysfunction, infertility, and allergic dermatitis. Therefore, research and development of novel therapeutic agents capable of preventing alopecia and enhancing hair growth are necessary. Moreover, these efforts should particularly focus on natural products, which may result in fewer or less severe side effects.

hDPCs, which are involved in the hair growth cycle, are located at the bottom of the HFs and are wrapped by hair matrix cells. Hair growth can be regulated by controlling the proliferation, division, and apoptosis of hDPCs through the activity of growth and inhibitory factors such as insulin-like growth factor-1 (IGF-1), vascular endothelial growth factor (VEGF), and transforming growth factor-β1 (TGF-β1). IGF-1 is considered a representative hair growth factor that promotes epithelial cell proliferation and significantly increases the length of HF tissues [7]. Importantly, this factor also inhibits anagen to catagen transition [8]. VEGF is another factor that induces growth and differentiation of hair root cells by both improving blood circulation and enhancing vascular endothelium growth [8, 9]. Therefore, VEGF prevents hair loss by increasing HF size and hair thickness [10, 11]. Conversely, TGF-β1 causes apoptosis of hair follicle matrix cells and alopecia by rapidly entering the catagen phase. Additionally, incomplete hair follicle regeneration leads to anagen to catagen transition and reduces HF sizes, resulting in thin and short hair [12, 13].

Nelumbinis Semen was dried by removing the pericarp of ripe lotus seeds. In China, NS has long been regarded (i.e., since ancient times) as an effective therapeutic agent due to its beneficial effects on the spleen, kidney, heart, and eyes [14]. According to a recent study, NS is rich in proteins, minerals, and unsaturated fatty acids, as well as various bioactive compounds that enhance human health such as alkaloids and flavonoids. Therefore, NS is widely used in the food and medicine industries [14, 15]. NS has been mainly used to treat neurological disorders, insomnia, and postmenstrual depression in women and has been reported to have antiviral properties, as well as a liver protectant, antioxidant, memory-enhancing, and anti-inflammatory effects [16–18].

Oxidative stress is among the leading causes of hair loss [19]. Previous studies have demonstrated that naturally occurring plant antioxidants can reduce oxidative stress [20], and NS has been found to possess potent antioxidant properties [14, 15]. Therefore, we hypothesized that NS would effectively promote hair regeneration and prevent hair loss. Several studies are currently assessing the nutritional properties of NS extract; however, no previous studies have systematically characterized the effect of NS extract on the hair growth cycle. Therefore, our study sought to (1) assess the effect of NS extract on hDPCs proliferation and migration *in vitro* and (2) characterize the hair growth-promoting properties of NS *in vivo* using C57BL/6 mice. Additionally, the molecular mechanisms by which NS extract induces hair regeneration were assessed by measuring the expression of various hair growth-associated cytokines.

2. Materials and Methods

2.1. Preparation of NS Extracts. NS extract was purchased from Korea Plant Extracts at the Korea Research Institute of Bioscience and Biotechnology (Daejeon, Korea). Methyl alcohol (50%) was used as the extraction solvent of the sample, which was then dissolved in dimethyl sulfoxide (DMSO).

2.2. Antioxidant Activity of NS Extracts. Total polyphenol content was determined using Folin-Ciocalteu's method [21]. Briefly, 40 μl of NS extract prepared with 50% methanol at a concentration of 0.2 mg/ml was mixed with 50 μl of Folin-Ciocalteu's phenol, which was then added to 160 μl of 10% sodium carbonate solution after 3 min at room temperature. The mixture was kept at room temperature for 30 min, after which absorbance was measured at 700 nm using a 7315 UV spectrophotometer (JENWAY, Staffordshire, United Kingdom). Total polyphenol content was expressed as mg of gallic acid equivalent (GAE)/g.

To determine the total flavonoid content, 0.5 ml of the 0.2 mg/ml dissolved in ethanolic NS extract was mixed with 5 ml of diethylene glycol (Duksan Pure Chemicals, Ansan, Korea). After 5 min at room temperature, the mixture was added to 0.5 ml of 1N NaOH (Duksan Pure Chemicals, Ansan, Korea) and incubated for 1 hour in a 37°C water bath. Absorbance was measured at 420 nm using a 7315 UV spectrophotometer (JENWAY, Staffordshire, United Kingdom). Total flavonoid content was expressed as mg of naringin (Tokyo Kasei Kogyo Co., Ltd., Tokyo, Japan) equivalent (NE)/g.

The DPPH scavenging activity of NS extract was assessed as described by Blois [22], with some modifications. Briefly, 0.5 ml of NS extract diluted to 0.2 mg/ml was mixed with 3 ml of 0.2 mM methanolic DPPH solution. After 20 min in the dark at room temperature, the absorbance of the mixture was measured at 517 nm using a 7315 UV spectrophotometer (JENWAY, Staffordshire, United Kingdom). Electron-donating ability (EDA) was calculated as described as follows:

$$\mathrm{EDA}\,(\%) = \frac{\mathrm{ABS}_{\mathrm{blank}} - \mathrm{ABS}_{\mathrm{sample}}}{\mathrm{ABS}_{\mathrm{blank}}} \times 100, \qquad (1)$$

2.3. Cell Culture. hDPCs were obtained from Cell Engineering for Origin (CEFO BIO, Seoul, Korea). The cells were grown in Dulbecco's modified Eagle's medium (DMEM) with 1% antibiotics and 10% fetal bovine serum (FBS) at 37°C in a 5% CO_2 humidified atmosphere.

2.4. CCK-8 Assay. A CCK-8 assay was used to determine cell proliferation. The hDPCs were seeded at a 3×10^3 cells/well density in 96-well microplates for 24 h at 5% CO_2 and 37°C. The NS extract was diluted to 7 different concentrations (3.91, 7.81, 15.63, 31.52, 62.5, 125, and 250 ppm), and the cells were allowed to grow in 10 μl of each NS concentration for 24 h, as described in several previous hair loss studies [10, 23, 24]. DMEM medium, minoxidil, and triton X-100 (Sigma) were used as a negative control (NC), positive control (PC), and blank, respectively. The plates were treated for 24 h at 5% CO_2 and 37°C. Then, 10 μl of CCK-8 solution (Sigma Aldrich, St. Louis, Mo., USA) was added to each well, and the cells were incubated for 4 h at 37°C. The absorbance was measured at 450 nm (test wavelength) and 650 nm (reference wavelength) with a microplate spectrophotometer (Epoch Multi-Volume Spectrophotometer System, BioTek,

VT, USA). The measured absorbances were used to determine cell proliferation as follows:

$$\text{cell proliferation}\,(\%) = \frac{\left(\text{ABS}_{\text{sample}} - \text{ABS}_{\text{blank}}\right)_{450\text{nm}} - \left(\text{ABS}_{\text{sample}} - \text{ABS}_{\text{blank}}\right)_{650\text{nm}}}{\left(\text{ABS}_{\text{control}} - \text{ABS}_{\text{blank}}\right)_{450\text{nm}} - \left(\text{ABS}_{\text{control}} - \text{ABS}_{\text{blank}}\right)_{650\text{nm}}} \times 100. \quad (2)$$

2.5. Scratch Migration Assay. A scratch migration assay was conducted as described in a previous study [25]. The hDPCs were seeded at a 4×10^4 cell/well density in 6-well plates and grown to 90% confluence in DMEM containing 10% FBS and 1% penicillin. The cells were scratched in a straight line with a 200 μl pipette tip. Cell debris was removed by washing with Dulbecco's phosphate-buffered saline (DPBS). The hDPCs were treated with DMEM (NC, negative control), minoxidil 10 μM (PC, positive control), and 15.63, 31.25, 62.5, and 125 ppm of NS extracts. After incubation for 24 h, the widths of the scratches were photographed using an optical microscope (Leica DM500, Wetzlar, Germany) (40x magnification).

2.6. Experimental Animals. Male C57BL/6 mice (4-week-old) purchased from Dae-Han Biolink Co. (Eumsung, Chungbuk, Korea) were allowed to acclimate for 3 weeks. The mice were housed in cages at $23 \pm 1^{\circ}$C and $55 \pm 5\%$ humidity, with a 12 h light and dark cycle and free access to food and water. All experimental protocols followed the guidelines established for the management and handling of laboratory animals and were approved by the Institutional Animal Ethics Committee of Chung-Ang University, Korea (registration no. 201900112). Twenty-one mice ($n = 7$/group) were randomized into the DMSO (NC), Nelumbinis Semen (NS) extract, and 3% minoxidil (PC) treatment groups. The backs of the mice were shaved with animal clippers at 7 weeks of age. Afterward, 200 μl DMSO, 200 μl of NS extract (1,000 ppm), or 3% minoxidil was administered daily on the dorsal skin for 3 weeks using a brush, as described in previous studies [23, 24, 26]. At 21 days, the mice were anesthetized via intraperitoneal injection of 1.2% avertin to obtain dorsal skin samples.

2.7. Evaluation of Hair Growth Score and Relative Area for Each Score. To compare the hair growth effect for each group, dorsal skin photographs of the mice were obtained using a digital camera on the 14th day after hair removal. The hair growth index was quantified using the ImageJ program (Broken Symmetry Software, Bethesda, USA). Hair scores were divided into 4 levels according to the differences in the dorsal skin color of the mice from 0 to 3. A score of 0 denoted no hair growth with pink skin color, 1 point indicated that the skin color was gray, 2 points indicated the appearance of some hair growth with (dark gray skin color), and 3 points denoted hair that was completely grown (black skin color). The hair growth index was calculated using equation (3) by measuring the ratio of the area of hair growth to the total area, and the sum of the area ratio multiplied by the score was averaged for each group [27]. Thus, the minimum value of the hair growth index was 0 and the maximum value was 3:

$$\text{hair growth score} = \frac{\{(\text{area of pink}) \times 0 + (\text{area of gray}) \times 1 + (\text{area of dark gray}) \times 2 + (\text{area of black}) \times 3\}}{\text{total area}}. \quad (3)$$

2.8. Histological Analysis. To observe the histological change after the application of NS extract, the tissues were stained with hematoxylin & eosin (H&E). Mice dorsal skin tissues were fixed with 10% neutral formalin and embedded in paraffin blocks using a Tissue Tek Auto TEC Automated Embedder (Sakura, San Francisco, CA, USA). All 4 μm of sections were stained with H&E using a slide stainer (Shandon Linistain GLX, Shandon Inc., Pittsburgh, PA, USA). A veterinary pathologist then examined the histopathologic lesions in the tissues.

2.9. Real-Time PCR for Cytokine Analysis of Mice Tissue. Our study assessed the relative expression levels of cytokines involved in hair growth. After 3 weeks of administering the different treatments tested herein, the mice were sacrificed and their back tissues were collected. Then, the tissues were ground in lysis buffer using a homogenizer. mRNA was extracted using the RNeasy Mini Kit (QLAGEN, Germany). Once the total mRNA was extracted from the dorsal skin tissue of each C57BL/6 mice, cDNA was synthesized via reverse transcription. Real-time polymerase chain reaction (RT-PCR) was conducted using a Piko-real 96 real-time PCR system (Thermo Fisher Scientific Inc.; Waltham, MA, USA; 45 cycles at 95°C for 15 sec, 60°C for 30 sec, and 72°C for 30 sec). Table 1 summarizes the primer sequences for IGF-1, VEGF, and TGF-β1.

2.10. Statistical Analysis. Statistical analyses were conducted using SPSS version 25 (SPSS Inc., Chicago, USA). All data are reported as mean ± standard error (SE). Statistical analyses were conducted via one-way analysis of variance (ANOVA), and mean differences were analyzed via

Table 1: Primer pairs used for quantitative real-time RT-PCR.

Target genes	Primer	Sequence
IGF-1	Forward	5′-TGCTCTTCAGTTCGTGTG-3′
	Reverse	5′-ACATCTCCAGTCTCCTCAG-3′
VEGF	Forward	5′-TCTTCAAGCCATCCTGTGTG-3′
	Reverse	5′-GCGAGTCTGTGTTTTTGCAG-3′
TGF-β1	Forward	5′-GGCGGTGCTCGCTTTGTAC-3′
	Reverse	5′-TCCCGAATGTCTGA CGTATTGA-3′
GAPDH	Forward	5′-GGGAAGCCCATCACCATCT-3′
	Reverse	5′-CGGCCTCACCCCATTTG-3′

Duncan's multiple range test. Statistical significance was defined as $p < 0.05$.

3. Results

3.1. Antioxidant Activity of NS Extract. The antioxidant activity of NS extract is shown in Table 2. The total polyphenol content of NS was 49.52 ± 4.10 mg GAE/g extract weight, and the total flavonoid content of NS was 82.80 ± 4.01 mg NE/g extract weight. The EDA of NS was 78.81%.

3.2. Effect of NS Extract on Human Dermal Papilla Cell Proliferation. Figure 1 shows the results of hDPC proliferation at various NS extract concentrations. hDPCs were treated with a range of NS extract concentrations (3.91, 7.81, 15.63, 31.25, 62.5, 125, and 250 ppm), after which cell proliferation rates were measured following incubation for 24 hours. The 3.91 ppm and 7.81 ppm NS extract exposure groups exhibited similar cell proliferation rates to the NC group (101.3% and 94.2%, respectively) when the cell proliferation rate of the NC group was adjusted to 100%. Except for the 15.63 ppm NS treatment, all NS extracts (31.25 ppm, 62.5 ppm, 125 ppm, and 250 ppm) resulted in higher cell proliferation rates than the PC group (117.4%), reaching 119.1%, 136.1%, 144.5%, and 124.0%, respectively. Particularly, the 62.5 ppm and 125 ppm NS extracts exhibited significantly higher cell proliferation rates than the PC group.

3.3. Effect of NS Extract on Human Dermal Papilla Cell Migration. The effect of NS extract on hDPCs migration was measured using a scratch migration assay, and the alteration of the scratch line width was converted into a percentage (Figure 2). All NS extract groups from 15.63 to 125 ppm increased the migration of hDPCs compared to the NC group. The migration of hDPCs was the most active at 125 ppm NS (203.8 ± 11.2%) after the PC group (253.0 ± 7.0%), which was significantly higher than the NC group. Treatment with 31.25 ppm and 62.5 ppm of NS resulted in 179.8 ± 14.6% and 173.2 ± 3.7% migration rates, respectively, and thus was found to promote hDPC migration compared with the NC group ($p < 0.05$). Moreover, the 15.63 ppm NS extract also rendered a higher migration rate (112.7 ± 10.5%) than the NC group; however, this difference was not significant. Overall, the migration of hDPCs increased as the concentration of NS extract increased, which was consistent with the cell proliferation rate of CCK-8.

3.4. Visual Observation of Hair Growth. Upon visually confirming the hair growth pattern on the dorsal skin of each mice group after hair removal, the dorsal skin was partially pale gray in all groups on the 7th day, but no significant differences between groups were observed. On the 14th day, hair growth was observed in all mice; however, both the PC and NS extract groups had a darker dorsal skin color than the NC group and exhibited more hair growth. The NS extract group was also found to have a wider area where the hair was completely grown compared to the PC group. After 21 days, hair growth was complete in all groups (Figure 3).

3.5. Effects of NS Extract on Hair Growth in C57BL/6 Mice. After calculating the hair growth of all groups on day 14 using the ImageJ program (Broken Symmetry Software, Bethesda, USA) (Figure 4), the PC group (score: 2.65 ± 0.05) and the NS extract group (score: 2.80 ± 0.03) showed a significantly higher hair growth index than the NC group (score: 1.96 ± 0.65). Particularly, the NS extract group was found to have a significantly higher hair growth index than the PC group. The PC group exhibited an approximately 35% higher hair growth effect than the NC treatment, whereas the NS extract group exhibited a 43% higher hair growth effect than the NC treatment.

Additionally, after measuring the area of the back of each mouse according to the above-described 0 to 3 hair growth score (Figure 5), the dorsal area of the NC group covered with a score of 2 (78.5%) was the highest ($p < 0.05$), whereas the NS extract group (19.2%) and PC group (30.4%) showed no significant differences. In hair growth scores of 3, where hair growth was complete, the hair growth area was the highest in the NS extract group (80.7%), followed by the PC group (67.5%) and the NC group (8.9%), with the NS extract group being significantly higher than the other groups.

3.6. Effects of NS Extract on Hair Morphology. Histological analyses of dorsal skin tissues were performed to investigate the effect of NS extract on the development of hair follicles and hair roots. After 3 weeks of topical treatment, representative longitudinal sections of dorsal skin tissue from mice were analyzed after staining with hematoxylin & eosin (Figure 6). The hair follicles of the NC group were mainly located in the dermis, and the development of hair follicles was weak. This differed from the PC group, where it was confirmed that hair follicles were located in the deep subcutis and that hair root development was accelerated. The hair follicles of the NS group were located in subcutaneous tissue (i.e., deeper than in the NC group) and appeared larger, resulting in the development of hair roots.

3.7. Effect of NS Extract on Cytokine Expression in Mice Dorsal Tissues. To confirm the hair-growth-promoting effect of NS extract, we compared the mRNA expression levels of hair

Table 2: Total polyphenol, flavonoid content, and electron-donating ability of Nelumbinis Semen extract.

	Total polyphenols (mg GAE[1]/g)	Total flavonoids (mg NE[2]/g)	EDA[3] (%)
Nelumbinis Semen	49.52 ± 4.10	82.80 ± 4.01	78.81

All data are reported as mean ± standard error (SE). [1]GAE: gallic acid equivalent. [2]NE: naringin equivalent. [3]EDA: electron-donating ability.

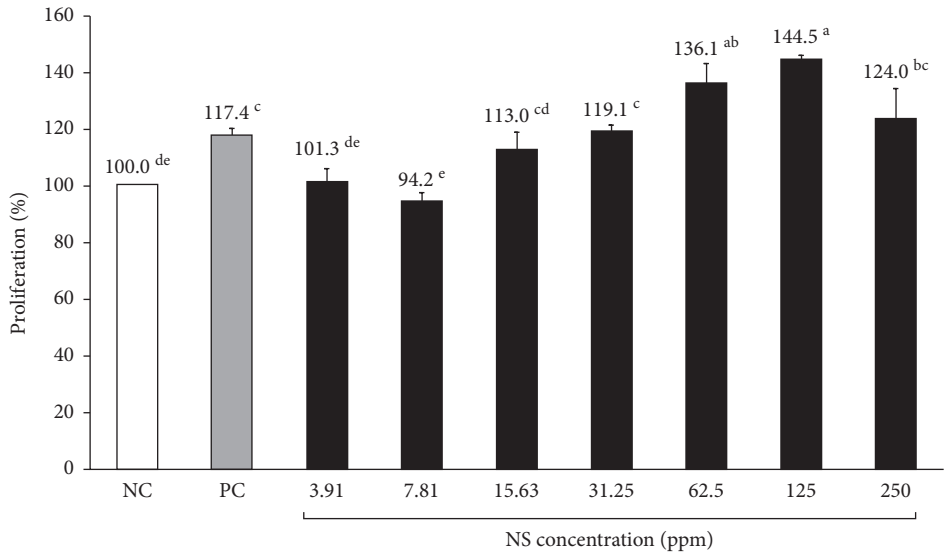

Figure 1: Proliferation of hDPC treated with various concentrations of Nelumbinis Semen extract. Effect of NS extract on hDPC proliferation, as determined by the CCK-8 assay. NC: negative control (DMEM medium), PC: positive control (10 μM minoxidil). The hDPCs were treated with various concentrations of NS extract (3.91, 7.81, 15.63, 31.25, 62.5, 125, and 250 ppm). [a-d]Values with different superscripts were found to be significantly different ($p < 0.05$), as determined by Duncan's multiple range test.

growth factors using RT-PCR (Figure 7). All gene expression levels were reported relative to the NC group, which was adjusted to 1.0 to calculate the results. The mRNA expression of VEGF, a factor that improves blood circulation by promoting the growth of the vascular endothelium and enhancing hair growth and differentiation of hair root cells, was the highest in the NS extract group (1.66 ± 0.22), which was statistically different from the NC group ($p < 0.05$). Additionally, the expression level of VEGF mRNA in the NS extract group was approximately 1.4 times higher than that in the PC group. IGF-1 is an important growth factor that regulates hair growth by promoting the proliferation of epithelial cells and increasing the length of hair follicle tissue. In this study, the mRNA expression level of IGF-1 was the highest in the NS extract group (1.28 ± 0.04), followed by the PC group (1.11 ± 0.00) and the NC group (1.00 ± 0) ($p < 0.05$). TGF-β1 accelerates the transition of the hair growth cycle from the anagen to the catagen phase and suppresses the proliferation and spread of hair follicles. The mRNA expression level of TGF-β1 was significantly lower in the PC group (0.53 ± 0.04) and the NS extract group (0.52 ± 0.09) than in the NC group (1.00 ± 0). There was no significant difference between the PC group and the NS group.

4. Discussion

In addition to genetic factors, alopecia is caused by excessive stress, malnutrition, hormonal imbalances, and aging and is accompanied by a reduction in hair follicle size and anagen follicles [28–30]. Currently, many studies have been conducted using natural materials, such as herbal medicines and biopharmaceuticals, to identify therapeutic compounds capable of promoting hair growth and reducing hair loss [31–34]. While the activity of glutathione and SOD etc. in the blood of hair loss patients has been found to be significantly low in hair loss patients, the levels of thiobarbituric acid reactive substances (TBARS) are significantly higher than those of patients without hair loss [34]. The resulting oxidative stress has been reported as the likely cause of hair loss [19]. However, these sources of oxidative stress can be reduced via the activity of natural antioxidant substances such as polyphenols, flavonoids, and phenol compounds, which are abundant in natural plant materials. Their ability to reduce oxidative stress derives from their capacity to remove free radicals and balance the reactive oxygen species metabolism [20]. NS is also thought to improve oxidative stress in the scalp of alopecia patients due to its high total polyphenol and flavonoid content, as well as its high DPPH electron radical scavenging activity [14, 15]. Dlova and Ollengo [35] reported that anthraquinone, flavonoids, tannin, saponin, chrysophanol, aloe-emodin, aloesin, and aloenin, among others, prevent hair loss and promote hair growth. Among these substances, anthraquinone, flavonoids, tannins, and saponins are the main active ingredients in NS [14]. Despite this, very few studies have assessed the hair growth and hair loss reduction potential of NS extract. Therefore, our study sought to investigate the hair-growth-

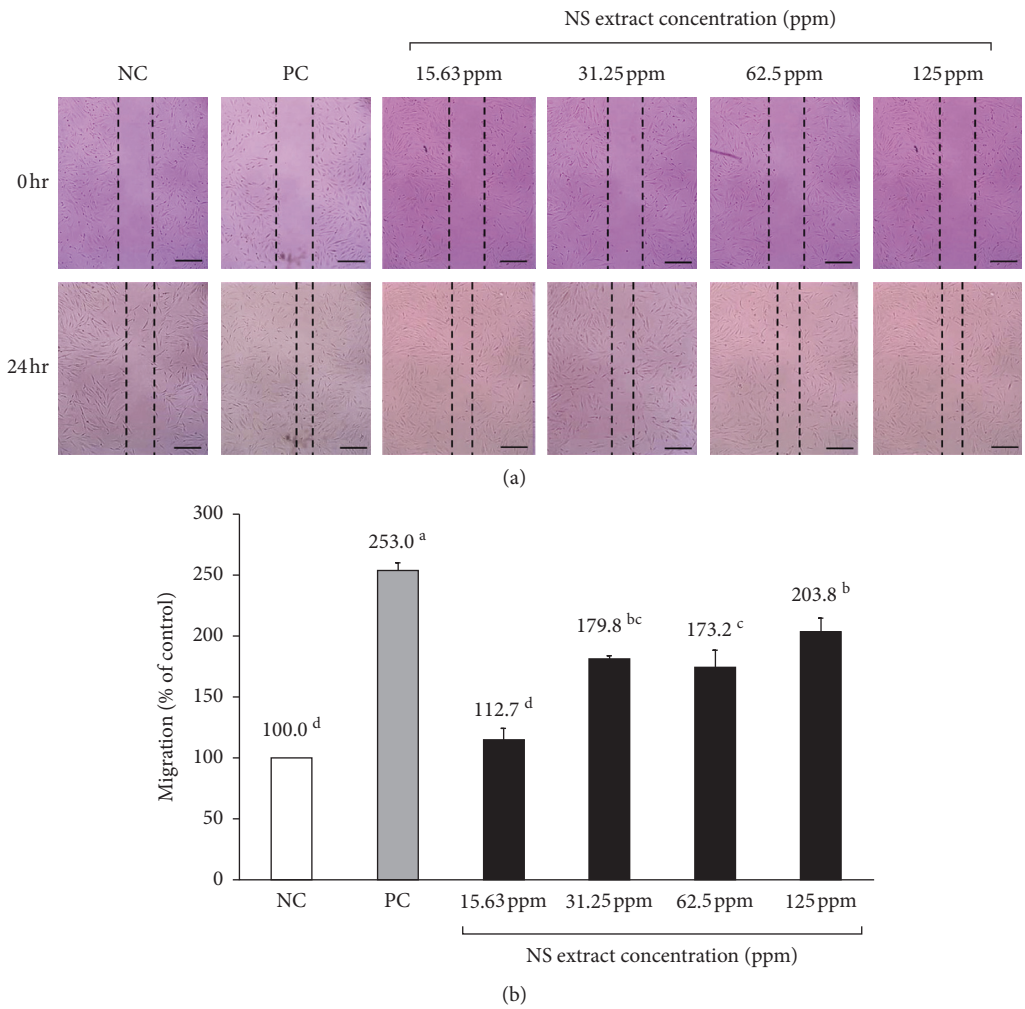

Figure 2: Migration of cells treated with various concentrations of Nelumbinis Semen extract. Effect of Nelumbinis Semen extracts on hDPC migration, as determined by the scratch assay. (a) Scratch line of each group. (b) Degree of migration of the scratch line. NC: negative control (DMEM media), PC: positive control (10 μM minoxidil). $^{a\text{-}d}$Values with different superscripts were found to be significantly different ($p < 0.05$), as determined by Duncan's multiple range test.

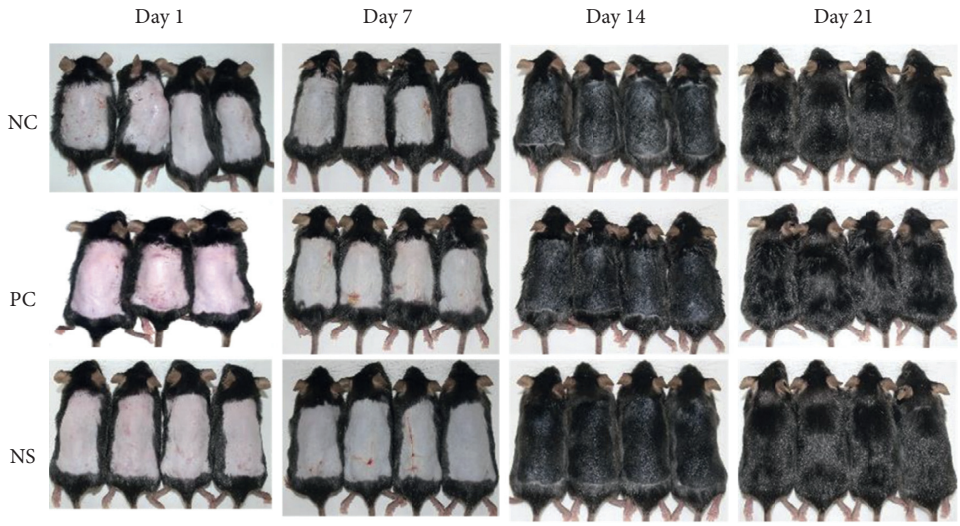

Figure 3: Effect of Nelumbinis Semen extract on anagen phase induction in 7-week-old C57BL/6 mice upon depilation. After depilation, the dorsal skin was treated with DMSO (vehicle), 3% minoxidil, or NS extract (1,000 μg/mL dissolved in DMSO) and photographed at 1, 7, 14, and 21 days (NC: dimethyl sulfoxide (DMSO); PC: 3% minoxidil; NS: Nelumbinis Semen extract with DMSO).

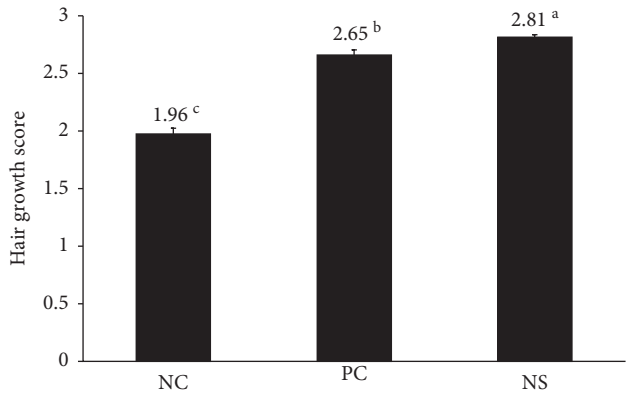

Figure 4: Effect of Nelumbinis Semen extract on hair growth score in C57BL/6 mice. Hair growth scores were calculated at 14 days. Hair growth was significantly promoted by the administration of NS extract compared to the control groups ($p < 0.05$). Differences were calculated by measuring the size of the complete black area (black skin) using ImageJ. [a-c]Values with different superscripts were found to be significantly different ($p < 0.05$), as determined by Duncan's multiple range test ($n = 7$/group). NC: dimethyl sulfoxide (DMSO); PC: 3% minoxidil; NS: Nelumbinis Semen extract with DMSO.

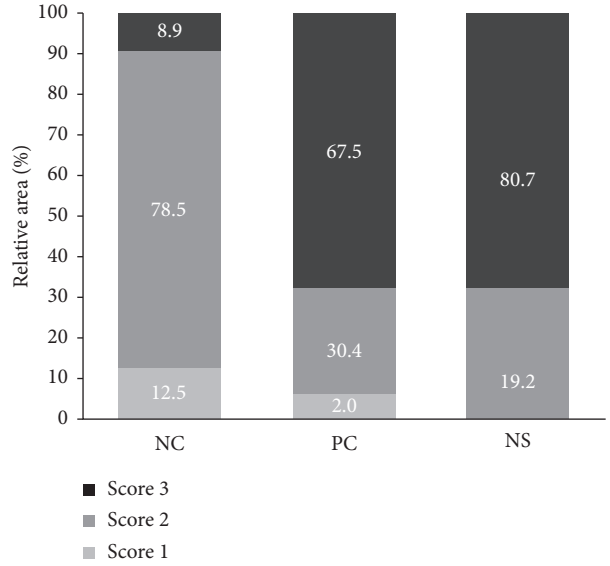

Figure 5: Effect of Nelumbinis Semen extract on relative hair growth area in C57BL/6 mice. The relative area for each score was calculated at 14 days. Differences were calculated by measuring the size of the complete black area (black skin) using the ImageJ program. Values are the percentages for each score ($n = 7$/group). NC: dimethyl sulfoxide (DMSO); PC: 3% minoxidil; NS: Nelumbinis Semen extract with DMSO.

promoting properties of NS extract through *in vitro* experiments using hDPCs and *in vivo* experiments using C57BL/6 mice.

According to previous studies, antioxidant substances suppress hair loss-promoting cytokine activity, thereby promoting hair growth [34, 36]. A study by Kim et al. [37] reported that the average flavonoid content of 40 native plants was 70 mg NE/g. The flavonoid content of NS extract is approximately 1.2 times higher. Additionally, this study found that the EDA of NS extract was approximately 1.1 times higher than the average EDA value of 74% for native plants. Asha et al. [38] found that *Rhizophora apiculata* root extract, an extract rich in flavonoids and polyphenolic compounds, effectively reduced oxidative stress in rat brains. Additionally, preclinical studies using natural extracts found that the antioxidant activity of natural substances reduces not only oxidative damage but also hair loss by promoting the expression of hair growth factors and participating in cytokine-mediated inflammation [39]. As expected, this study found that NS extract possessed a strong antioxidant capacity due to its high flavonoid content and EDA, which may reduce the oxidative damage that causes hair loss.

hDPCs make up the hair follicles and are connected to blood vessels, which supply them with nutrients, hormones, and other secreted physiological substances, such as hair growth factors. These secretory mediators affect the surrounding hair follicle cells and tissues and play an important role in hair growth and detachment [19, 40]. Driskell et al. [41] reported that hair growth could be enhanced by promoting the proliferation of hDPCs and human epidermal keratinocyte cells (HaCaT). The results of this study showed that cell proliferation and migration tend to increase as the concentration of NS extract increases. Notably, 31.25 ppm of NS extract (i.e., a relatively low concentration) resulted in a cell proliferation rate that was higher than that of minoxidil, the positive control. Previous studies have reported that plant extracts or compounds can be deemed nontoxic if cell proliferation rates exceed 85% upon their administration [23]. Both *Geranium sibiricum* extract and *Miscanthus sinensis* var. *purpurascens* extract led to cell proliferation rates below 85% at 156.3 and 62.5 ppm [24], respectively, and were, therefore, considered cytotoxic. Similarly, a *Salvia plebeia* extract substantially reduced cell proliferation rates at 125 ppm [26]. In other words, most plant extracts have been found to be toxic at high concentrations; however, the NS extracts in this study were found to be nontoxic at concentrations as high as 250 ppm, and cell proliferation rates exceeded 85% at all tested concentrations (3.91–250 ppm). Therefore, NS extracts were deemed nontoxic and likely constitute a safe hair loss treatment.

In this study, C57BL/6 mice were selected to analyze hair growth promotion and hair loss prevention. All experiments were initiated when the test mice were 7 weeks old, which is when the hair cycle enters the telogen phase. C57BL/6 mice exhibit spontaneous hair loss and are, therefore, used as representative experimental animals in alopecia research because melanocytes exist only in their hair follicles and melanin synthesis is consistent with the hair growth cycle, which can be assessed simply by observing skin color [42]. Upon measuring the hair growth index of all groups on the 14th day, it was confirmed that the NS extract group had a higher hair growth index than the PC group ($p < 0.05$). Moreover, the PC group in our study achieved a 68% hair recovery, whereas the NS extract group reached 81% within the same time. Another study reported that the

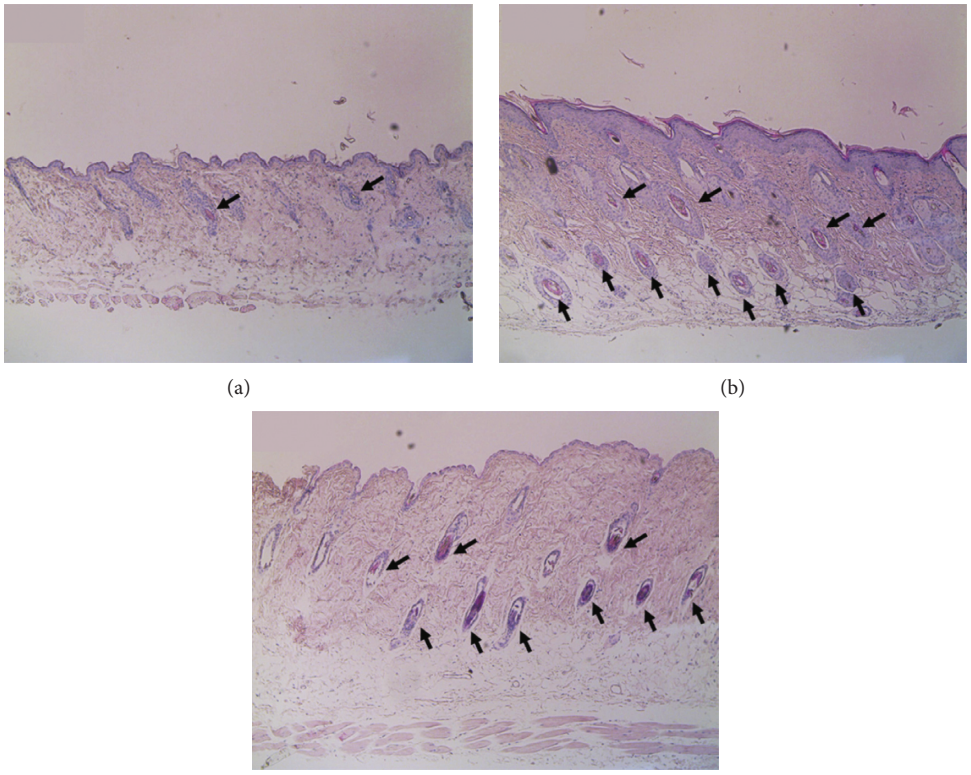

Figure 6: Histological changes in the dorsal skin of C57BL/6 mice after 21 days. (a) NC: dimethyl sulfoxide (DMSO), (b) PC: 3% minoxidil, and (c) NS: Nelumbinis Semen extract with DMSO (H&E staining, 100x magnification).

administration of a medicinal herb in C57BL/6 mice resulted in a hair growth index of 1.7 points [27]. Additionally, *Saengbal-eum-II*, a medicinal herb known to possess good hair-growth-promoting effects, had a high hair growth index of 2.28 points [43]. However, NS reached a growth index of 2.81 points, thus substantially exceeding the effects of the aforementioned herb. Therefore, these results highlight the excellent efficacy of NS extracts to promote hair growth and preventing hair loss.

HFs are composed of several layers of cells, the hair outer root sheath (ORS) and inner root sheath (IRS), hair cells, and papillary cells (DPCs), and play an important role in physiological tissue regeneration. Stem cells in the bulge region of HFs and DPCs play key roles in the regulation of successive hair cycles. These HFs undergo the anagen, catagen, and telogen phases [1, 2]. Most telogen hair follicles are located in the dermis, whereas anagen hair follicles are found only in the deep subcutis [44]. Our study also confirmed that the hair follicles and hair bulbs of the NS extract group were larger than those of the NC group. Additionally, the hair follicles of the NS extract group were found to be located in deeper subcutaneous tissue than those of the NC group. These results suggest that NS extracts promote hair growth by accelerating the telogen to anagen transition of hair follicles.

The dermal papilla cells derived from mesenchymal cells are affected by specific cytokines, and the affected dermal papilla cells regulate the growth or degeneration of hair by releasing growth factors or inhibitors of the epithelial cells of the hair follicles. Overexpression of VEGF in the outer root sheath reportedly promotes hair growth by promoting the development of blood vessels around the hair follicles [45]. In this study, VEGF mRNA expression was higher in the NS extract group than in the minoxidil group. These results are similar to those of a study that evaluated the effect of *Geranium sibiricum* extract on hair growth [23]. The mRNA expression level of IGF-1 was significantly higher in the NS extract group than in the PC group. Transgenic mice that overexpressed IGF-1 in their skin exhibited faster HF growth than the control group. This finding is supported by a study that found that the hair of patients with Laron syndrome, an IGF-1 deficiency, grows sparsely and frequently falls out in the frontal region [45]. Previous studies have shown that when the expression of TGF-β1 is increased, hair follicle proliferation is not completed and hair follicle regeneration is reduced, resulting in thin, short hair [46]. This study found that the mRNA expression of TGF-β1 was significantly lower in the NS extract group than in the NC group, which is consistent with previous studies on the hair-growth-promoting effects of *Salvia plebeian* extracts and *Laminaria japonica* extracts [26, 47]. Based on these results, we confirmed that NS extract improves hair growth by increasing the expression of hair growth-promoting cytokines such as VEGF and IGF-1, while also reducing the expression of TGF-β1, which inhibits hair growth.

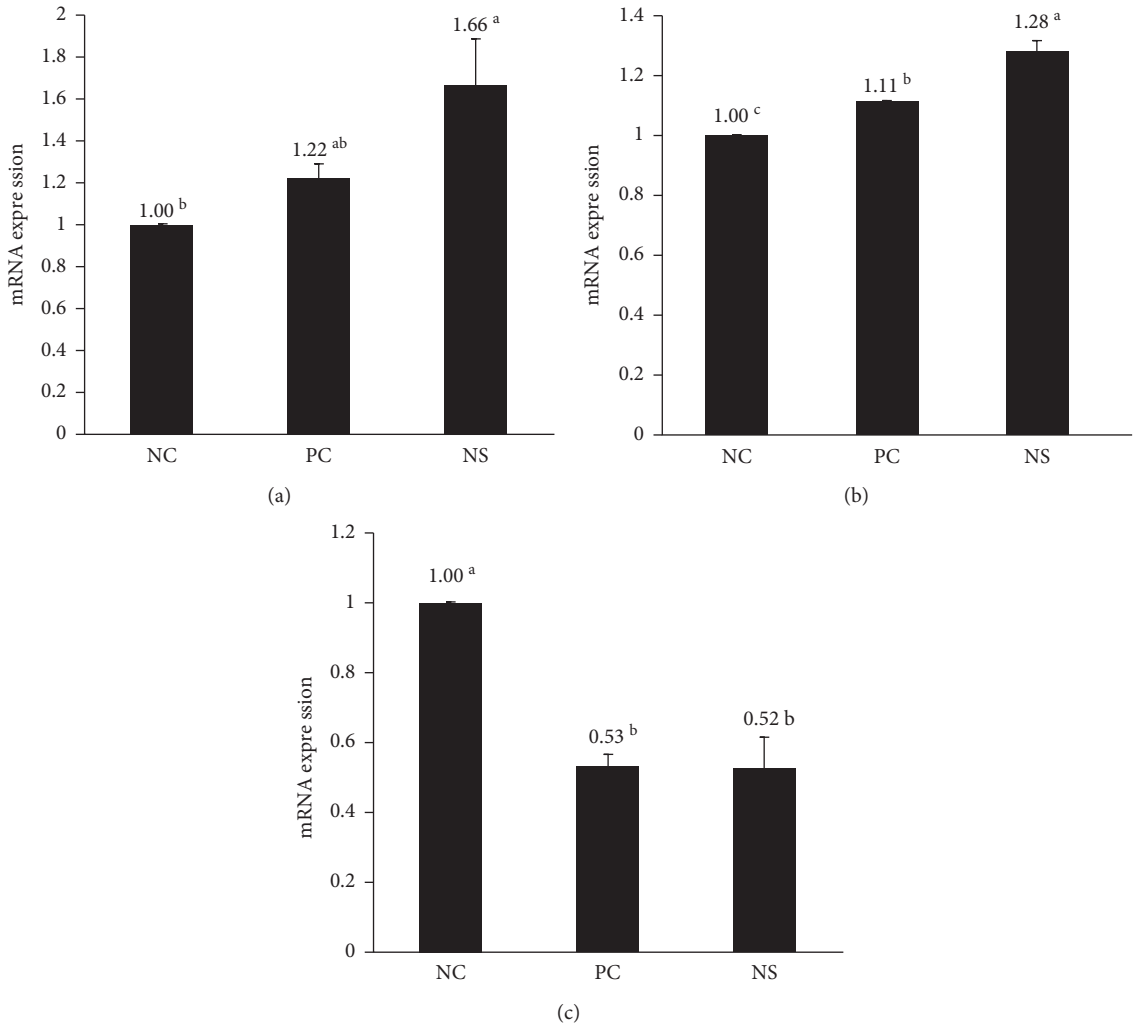

Figure 7: Effect of Nelumbinis Semen extract on the relative mRNA expression of growth factors. Relative expression of growth factors (VEGF, IGF-1, and TGF-β1) was analyzed via real-time PCR. NC: negative control (DMSO), PC: positive control (3% minoxidil), NS: Nelumbinis Semen extract. [a-c]Values with different superscripts were found to be significantly different ($p < 0.05$), as determined by Duncan's multiple range test ($n = 7$/group).

5. Conclusions

Our findings confirmed that NS extract promotes hair growth by enhancing hDPC proliferation and migration *in vitro*. Additionally, the hair growth index and hair growth area of C57BL/6 mice topically treated with NS extract for 3 weeks increased much more than in minoxidil-treated mice. Moreover, the number and location of hair follicles considered to be evidence of anagen induction were similar in the NS extract group compared to the minoxidil group. NS extract treatment also increased the mRNA expression of VEGF and IGF-1, which are cytokines involved in hair growth, and decreased the expression of TGF-β1, a hair growth inhibitor. Therefore, NS extract is a promising new hair loss treatment derived from natural substances that may be used to promote hair growth and prevent hair loss.

Abbreviations

AA: Alopecia areata
AGA: Androgenetic alopecia
DHT: Dihydrotestosterone
DMEM: Dulbecco's modified Eagle's medium
DPBS: Dulbecco's phosphate-buffered saline
EDA: Electron-donating ability
FBS: Fetal bovine serum
FPHL: Female pattern hair loss
GAE: Gallic acid equivalent
H&E: Hematoxylin and eosin
HaCaT: Human epidermal keratinocyte cells
hDPCs: Human dermal papilla cells
HFs: Hair follicles
IGF-1: Insulin-like growth factor-1
IRS: Inner root sheath
NE: Naringin equivalent
NS: Nelumbinis Semen
ORS: Outer root sheath
RT-PCR: Real-time polymerase chain reaction
T: Testosterone

TBARS: Thiobarbituric acid reactive substances
TGF-β1: Transforming growth factor-β1
VEGF: Vascular endothelial growth factor.

Data Availability

The datasets used to support the findings of this study are available from the corresponding author upon request.

Conflicts of Interest

The authors declare that there are no conflicts of interest.

Authors' Contributions

All authors conceived and designed this study. Hyeon Ju Park and Guang-Ri Jin supervised all experiments. Hyeon Ju Park, Jae Hyun Jung, and Su Bin Hwang performed the experiments. Hyeon Ju Park and Su Hyun Lee wrote the manuscript. Professor Bog-Hieu Lee carried out the final editing and proofreading of the revised manuscript. All authors read and approved the final version of this manuscript.

Acknowledgments

This work was supported by the Basic Science Research Program through the National Research Foundation of Korea (NRF) funded by the Ministry of Education, Science, and Technology (NRF-2017R1D1A1B03033507).

References

[1] M. N. Pereira, C. Y. Ushirobira, M. S. Cunha-Filho, G. M. Gelfuso, and T. Gratieri, "Nanotechnology advances for hair loss," *Therapeutic Delivery*, vol. 9, no. 8, pp. 593–603, 2018.

[2] V.-L. Truong, M. J. Bak, C. Lee, M. Jun, and W.-S. Jeong, "Hair regenerative mechanisms of red ginseng oil and its major components in the testosterone-induced delay of anagen entry in C57BL/6 mice," *Molecules*, vol. 22, no. 9, pp. 1505–1517, 2017.

[3] Korean Statistical Information Service [Internet], *National Health Insurance Service: Health Insurance Review and Assessment Service*, Korean Statistical Information Service, Republic of Korea, 2019, http://kosis.kr/statisticsList/statisticsListIndex.do?menuId=M_01_01&vwcd=MT_ZTITLE&parmTabId=M_01_01#SelectStatsBoxDiv.

[4] A. Nabahin, A. A. Eloun, and S. Samy, "Expert system for hair loss diagnosis and treatment," *IJEAIS*, vol. 4, pp. 160–169, 2017.

[5] H. Woo, S. Lee, S. Kim, D. Park, and E. Jung, "Effect of sinapic acid on hair growth promoting in human hair follicle dermal papilla cells via Akt activation," *Archives of Dermatological Research*, vol. 309, no. 5, pp. 381–388, 2017.

[6] N. Choi, S. Shin, S. Song, and J.-H. Sung, "Minoxidil promotes hair growth through stimulation of growth factor release from adipose-derived stem cells," *International Journal of Molecular Sciences*, vol. 19, no. 3, pp. 691–706, 2018.

[7] R. M. Trüeb, "Further clinical evidence for the effect of IGF-1 on hair growth and alopecia," *Skin Appendage Disorders*, vol. 4, no. 2, pp. 90–95, 2018.

[8] Y.-K. Lin, F. Sugiri, H. Ma, Y.-H. Chiu, and C.-L. Yao, "Industrial-scale processing of activated platelet-rich plasma from specific pathogen-free pigs and its effect on promoting human hair follicle dermal papilla cell cultivation," *Journal of the Taiwan Institute of Chemical Engineers*, vol. 71, pp. 28–37, 2017.

[9] T.-C. Wen, Y.-S. Li, K. Rajamani, H.-J. Harn, S.-Z. Lin, and T.-W. Chiou, "Effect of *Cinnamomum osmophloeum* Kanehira leaf aqueous extract on dermal papilla cell proliferation and hair growth," *Cell Transplantation*, vol. 27, no. 2, pp. 256–263, 2018.

[10] Y. M. Woo, O. J. Kim, E. S. Jo et al., "The effect of *Lactobacillus plantarum* hydrolysates promoting VEGF production on vascular growth and hair growth of C57BL/6 mice," *Journal of Analytical Science and Technology*, vol. 10, pp. 18–27, 2019.

[11] J. Y. Kim, Y. J. Kim, M. J. Kim, and M. R. Kim, "Ethanol extract of medicinal herbal mixture accelerates hair growth and melanogenesis *in vivo* and *in vitro*," *Korea Journal of Herbology*, vol. 33, no. 5, pp. 9–18, 2018.

[12] H. Shin, A.-R. Cho, D. Y. Kim et al., "Enhancement of human hair growth using *Ecklonia cava* polyphenols," *Annals of Dermatology*, vol. 28, no. 1, pp. 15–121, 2016.

[13] H. A. Oh, J. Kwak, B. J. Kim et al., "Migration inhibitory factor in conditioned medium from human umbilical cord blood-derived mesenchymal stromal cells stimulates hair growth," *Cells*, vol. 9, no. 6, pp. 1344–1365, 2020.

[14] Y. Zhang, X. Lu, S. Zeng et al., "Nutritional composition, physiological functions and processing of lotus (*Nelumbo nucifera Gaertn.*) seeds: a review," *Phytochemistry Reviews*, vol. 14, no. 3, pp. 321–334, 2015.

[15] I. Pal and P. Dey, "A review on lotus (*Nelumbo nucifera*) seed," *IJSR*, vol. 4, no. 7, pp. 1659–1666, 2015.

[16] H. S. Chung, H. J. Lee, and I. Shim, "Assessment of antidepressant effect of *Nelumbinis semen* on rats under chronic mild stress and its subchronic oral toxicity in rats and beagle dogs," *BMC Complementary and Alternative Medicine*, vol. 12, pp. 68–86, 2012.

[17] K. R. Paudel and N. Panth, "Phytochemical profile and biological activity of *Nelumbo nucifera*," *Evidence-Based Complementary and Alternative Medicine*, vol. 2015, Article ID 789124, 16 pages, 2015.

[18] X. Lu, S. Zeng, Y. Zhang et al., "Effects of water-soluble oligosaccharides extracted from lotus (*Nelumbo nucifera* Gaertn.) seeds on growth ability of Bifidobacterium adolescentis," *European Food Research and Technology*, vol. 241, no. 4, pp. 459–467, 2015.

[19] C. C. Yang and G. Cotsarelis, "Review of hair follicle dermal cells," *Journal of Dermatological Science*, vol. 57, pp. 2–11, 2020.

[20] F. Karahan, M. Kulak, E. Gözüacik, T. Böyümez, N. Şekeroğlu, and I. H. Doganturk, "Total phenolic content, ferric reducing and DPPH scavenging activity of *Arum dioscoridis*," *Natural Product Research*, vol. 29, no. 17, pp. 1678–1683, 2015.

[21] V. L. Singleton, R. Orthofer, and R. M. Lamuela-Raventós, "Analysis of total phenols and other oxidation substrates and antioxidants by means of folin-ciocalteu reagent," *Oxidants and Antioxidants Part A*, vol. 299, pp. 152–178, 1999.

[22] M. S. Blois, "Antioxidant determinations by the use of a stable free radical," *Nature*, vol. 181, pp. 257–268, 1958.

[23] W. A. Boisvert, M. R. Yu, Y. B. Choi et al., "Hair growth-promoting effect of *Geranium sibiricum* extract in human dermal papilla cells and C57BL/6 mice," *BMC Complementary and Alternative Medicine*, vol. 17, pp. 109–118, 2017.

[24] G. H. Jeong, W. A. Boisvert, M.-Z. Xi et al., "Effect of *Miscanthus sinensis* var. *purpurascens* flower extract on

proliferation and molecular regulation in human dermal papilla cells and stressed C57BL/6 mice," *Chinese Journal of Integrative Medicine*, vol. 24, no. 8, pp. 591–599, 2018.

[25] C.-C. Liang, A. Y. Park, and J.-L. Guan, "*In vitro* scratch assay: a convenient and inexpensive method for analysis of cell migration *in vitro*," *Nature Protocols*, vol. 2, no. 2, pp. 329–333, 2007.

[26] Y. L. Zhang, G. R. Jin, J. Yap, W. A. Boisvert, and B. H. Lee, "Hair growth potential of *Salvia plebeia* extract and its associated mechanisms," *Pharmaceutical Biology*, vol. 58, no. 1, pp. 400–409, 2020.

[27] S. Choi, N. Cho, and K. K. Kim, "Development and evaluation of the herbal medicine for hair growth-promoting activity," *KSBB Journal*, vol. 31, no. 4, pp. 237–245, 2016.

[28] M. Patel, S. Harrison, and R. Sinclair, "Drugs and hair loss," *Dermatologic Clinics*, vol. 31, no. 1, pp. 67–73, 2013.

[29] J. Y. Kim, J. Y. Shin, Y.-H. Choi et al., "Hair growth promoting effect of *Hottuynia cordata* extract in cultured human hair follicle dermal papilla cells," *Biological and Pharmaceutical Bulletin*, vol. 42, no. 10, pp. 1665–1673, 2019.

[30] J. Srivilai, N. Waranuch, A. Tangsumranjit, N. Khorana, and K. Ingkaninan, "Germacrone and sesquiterpene-enriched extracts from *Curcuma aeruginosa* Roxb. increase skin penetration of minoxidil, a hair growth promoter," *Drug Delivery and Translational Research*, vol. 8, no. 1, pp. 140–149, 2017.

[31] H. L. Zhu, Y. H. Gao, J. Q Yang, J. B. Li, and J Gao, "Serenoa repens extracts promote hair regeneration and repair of hair loss mouse models by activating TGF-β and mitochondrial signaling pathway," *European Review for Medical and Pharmacological Sciences*, vol. 22, no. 12, pp. 4000–4008, 2018.

[32] H. R. Ashtiani, F. Salehinia, H. Rastegar, A. A. Allameh, and S. Rezazadeh, "Differences in growth response human hair follicle mesenchymal stem cells to herbal extracts and a growth factor," *Journal of Medicinal Plant Research*, vol. 17, no. 65, pp. 36–46, 2018.

[33] H. C. Choi, G. W. Nam, N. H. Jeong, and B. Y. Choi, "Hair growth promotion by extracts *of Inula Helenium* and *Caesalpinia Sappan* Bark in patients with androgenetic alopecia: a pre-clinical study using phototrichogram analysis," *Cosmetics*, vol. 6, no. 4, pp. 66–74, 2019.

[34] J.-H. Kim, S.-K. Hong, S.-J. Hwang, S.-W. Son, and Y.-S. Choi, "The preclinical and clinical effects of herbal product containing *Rosa mutiflora* roots extracts as a main component on the hair growth promotion," *Korean Journal of Medicinal Crop Science*, vol. 20, no. 2, pp. 108–116, 2012.

[35] N. C. Dlova and M. A. Ollengo, "Traditional and ethnobotanical dermatology practices in Africa," *Clinics in Dermatology*, vol. 36, no. 3, pp. 353–362, 2018.

[36] H. A. Lee and J. S. Han, "Hair Growth Promoting Effect of fermented *Liriope platyphylla* on hair loss-induced C57BL/6 mice," *Journal of the Korean Society of Food Science and Nutrition*, vol. 10, pp. 347-348, 2010.

[37] E.-J. Kim, J.-Y. Choi, M.-R. Yu, M.-Y. Kim, S.-H. Lee, and B.-H. Lee, "Total polyphenols, total flavonoid contents, and antioxidant activity of Korean natural and medicinal plants," *Korean Journal of Food Science and Technology*, vol. 44, no. 3, pp. 337–342, 2012.

[38] K. K. Asha, A. K. Suseela Mathew, and P. T. Lakshmanan, "Flavonoids and phenolic compounds in two mangrove species and their antioxidant property," *Indian Journal of Geo-Marine Sciences*, vol. 41, no. 3, pp. 259–264, 2012.

[39] S.-S. Joo, "*In vitro* and *in vivo* hair growth promotion effects of *Lactobacillus plantarum*-fermented plant extracts (MBN)," *Korean Journal of Food Science and Technology*, vol. 43, no. 3, pp. 381–386, 2011.

[40] M. Ohyama, Y. Zheng, R. Paus, and K. S. Stenn, "The mesenchymal component of hair follicle neogenesis: background, methods and molecular characterization," *Experimental Dermatology*, vol. 19, pp. 89–99, 2009.

[41] R. R. Driskell, C. Clavel, M. Rendl, and F. M. Watt, "Hair follicle dermal papilla cells at a glance," *Journal of Cell Science*, vol. 124, no. 8, pp. 1179–1182, 2011.

[42] N. Kumar, W. Rungseevijitprapa, N.-A. Narkkhong, M. Suttajit, and C. Chaiyasut, "5α-reductase inhibition and hair growth promotion of some Thai plants traditionally used for hair treatment," *Journal of Ethnopharmacology*, vol. 139, no. 3, pp. 765–771, 2012.

[43] A. R. Han, N. W. Sohn, S. H. Chung, S. S. Kim, and M. Y. Song, "Study on effect of *Saengbal-eum-II* on hair regrowth promotion in C57BL/6 mice," *Journal of Oriental Rehabilitation Medicine*, vol. 19, no. 4, pp. 95–113, 2009.

[44] H.-S. Shin, J.-M. Lee, S.-Y. Park, J.-E. Yang, J.-H. Kim, and T.-H. Yi, "Hair growth activity of *Crataegus pinnatifida* on C57BL/6 mouse model," *Phytotherapy Research*, vol. 27, no. 9, pp. 1352–1357, 2013.

[45] B. H. Lee, M. J. Sim, and Y. C. Kim, "Effects of lavender oil on hair growth-relevant enzyme activity and cytokine expression in C57BL/6 mice," *Journal of Investigative Cosmetology*, vol. 12, no. 1, pp. 1–8, 2016.

[46] E. J. Kim, J. Y. Choi, B. C. Park, and B.-H. Lee, "Platycarya strobilacea S. et Z. extract has a high antioxidant capacity and exhibits hair growth-promoting effects in male C57BL/6 mice," *Preventive Nutrition and Food Science*, vol. 19, no. 3, pp. 136–144, 2014.

[47] B. M. Lee, K. S. Park, Y. J. Lee, E. S. Choi, and D. H. Park, "Hair growth effects of *Laminaria japonica* extract and growth factor mixture on a C57BL/6 mouse model," *Biotechnology and Bioprocess Engineering*, vol. 21, no. 1, pp. 175–182, 2016.